Westinghouse Non-Proprietary Class 3

WCAP-14846

Scaling Analysis for AP600 Containment Pressure During Design Basis Accidents

Westinghouse Energy Systems

9704080197 970401
PDR ADOCK 05200003
A PDR

Westinghouse Non-Proprietary Class 3

WCAP-14846

Scaling Analysis for AP600 Containment Pressure During Design Basis Accidents

Westinghouse Energy Systems

9704080197 970401
PDR ADOCK 05200003
A PDR

AP600 DOCUMENT COVER SHEET

TDC: _____ IDS: I _____ S _____

Form 58202G(5/94) [m:\3499w.non:1b] AP600 CENTRAL FILE USE ONLY:

0058.FRM RFS#: RFS ITEM #:

AP600 DOCUMENT NO.	REVISION NO.		ASSIGNED TO
PCS-GSR-020	0	Page 1 of 202	

ALTERNATE DOCUMENT NUMBER: WCAP-14846 WORK BREAKDOWN #:

DESIGN AGENT ORGANIZATION:

PROJECT: AP600

TITLE: Scaling Analysis for AP600 Containment Pressure During Design Basis Accidents

ATTACHMENTS:	DCP #/REV. INCORPORATED IN THIS DOCUMENT REVISION:
CALCULATION/ANALYSIS REFERENCE:	

ELECTRONIC FILENAME	ELECTRONIC FILE FORMAT	ELECTRONIC FILE DESCRIPTION
3499w.non	.wpf	Word Perfect 5.2 for Windows

(C) WESTINGHOUSE ELECTRIC CORPORATION 1997

☐ WESTINGHOUSE PROPRIETARY CLASS 2
This document contains information proprietary to Westinghouse Electric Corporation; it is submitted in confidence and is to be used solely for the purpose for which it is furnished and returned upon request. This document and such information is not to be reproduced, transmitted, disclosed or used otherwise in whole or in part without prior written authorization of Westinghouse Electric Corporation, Energy Systems Business Unit, subject to the legends contained hereof.

☐ WESTINGHOUSE PROPRIETARY CLASS 2C
This document is the property of and contains Proprietary Information owned by Westinghouse Electric Corporation and/or its subcontractors and suppliers. It is transmitted to you in confidence and trust, and you agree to treat this document in strict accordance with the terms and conditions of the agreement under which it was provided to you.

☒ WESTINGHOUSE CLASS 3 (NON PROPRIETARY)

COMPLETE 1 IF WORK PERFORMED UNDER DESIGN CERTIFICATION OR COMPLETE 2 IF WORK PERFORMED UNDER FOAKE.

1 ☐ **DOE DESIGN CERTIFICATION PROGRAM** – GOVERNMENT LIMITED RIGHTS STATEMENT [See page 2]

Copyright statement: A license is reserved to the U.S. Government under contract DE-AC03-90SF18495.

☐ DOE CONTRACT DELIVERABLES (DELIVERED DATA)
Subject to specified exceptions, disclosure of this data is restricted until September 30, 1995 or Design Certification under DOE contract DE-AC03-90SF18495, whichever is later.

EPRI CONFIDENTIAL: NOTICE: 1 ☐ 2 ☐ 3 ☒ 4 ☐ 5 ☐ CATEGORY: A ☒ B ☐ C ☐ D ☐ E ☐ F ☐

2 ☐ **ARC FOAKE PROGRAM** – ARC LIMITED RIGHTS STATEMENT [See page 2]

Copyright statement: A license is reserved to the U.S. Government under contract DE-FC02-NE34267 and subcontract ARC-93-3-SC-001.

☐ ARC CONTRACT DELIVERABLES (CONTRACT DATA)
Subject to specified exceptions, disclosure of this data is restricted under ARC Subcontract ARC-93-3-SC-001.

ORIGINATOR	SIGNATURE/DATE	
D. R. Spencer	Daniel R Spencer	3/17/97
AP600 RESPONSIBLE MANAGER	SIGNATURE*	APPROVAL DATE
J. A. Gresham	J A Gresham	3/17/97

*Approval of the responsible manager signifies that document is complete, all required reviews are complete, electronic file is attached and document is released for use.

Form 58202G(5/94)

LIMITED RIGHTS STATEMENTS

DOE GOVERNMENT LIMITED RIGHTS STATEMENT

(A) These data are submitted with limited rights under government contract No. DE-AC03-90SF18495. These data may be reproduced and used by the government with the express limitation that they will not, without written permission of the contractor, be used for purposes of manufacturer nor disclosed outside the government; except that the government may disclose these data outside the government for the following purposes, if any, provided that the government makes such disclosure subject to prohibition against further use and disclosure:
   (I) This "Proprietary Data" may be disclosed for evaluation purposes under the restrictions above.
   (II) The "Proprietary Data" may be disclosed to the Electric Power Research Institute (EPRI), electric utility representatives and their direct consultants, excluding direct commercial competitors, and the DOE National Laboratories under the prohibitions and restrictions above.

(B) This notice shall be marked on any reproduction of these data, in whole or in part.

ARC LIMITED RIGHTS STATEMENT:

This proprietary data, furnished under Subcontract Number ARC-93-3-SC-001 with ARC may be duplicated and used by the government and ARC, subject to the limitations of Article H-17.F. of that subcontract, with the express limitations that the proprietary data may not be disclosed outside the government or ARC, or ARC's Class 1 & 3 members or EPRI or be used for purposes of manufacture without prior permission of the Subcontractor, except that further disclosure or use may be made solely for the following purposes:

This proprietary data may be disclosed to other than commercial competitors of Subcontractor for evaluation purposes of this subcontract under the restriction that the proprietary data be retained in confidence and not be further disclosed, and subject to the terms of a non-disclosure agreement between the Subcontractor and that organization, excluding DOE and its contractors.

DEFINITIONS

CONTRACT/DELIVERED DATA — Consists of documents (e.g. specifications, drawings, reports) which are generated under the DOE or ARC contracts which contain no background proprietary data.

EPRI CONFIDENTIALITY / OBLIGATION NOTICES

NOTICE 1: The data in this document is subject to no confidentiality obligations.

NOTICE 2: The data in this document is proprietary and confidential to Westinghouse Electric Corporation and/or its Contractors. It is forwarded to recipient under an obligation of Confidence and Trust for limited purposes only. Any use, disclosure to unauthorized persons, or copying of this document or parts thereof is prohibited except as agreed to in advance by the Electric Power Research Institute (EPRI) and Westinghouse Electric Corporation. Recipient of this data has a duty to inquire of EPRI and/or Westinghouse as to the uses of the information contained herein that are permitted.

NOTICE 3: The data in this document is proprietary and confidential to Westinghouse Electric Corporation and/or its Contractors. It is forwarded to recipient under an obligation of Confidence and Trust for use only in evaluation tasks specifically authorized by the Electric Power Research Institute (EPRI). Any use, disclosure to unauthorized persons, or copying this document or parts thereof is prohibited except as agreed to in advance by EPRI and Westinghouse Electric Corporation. Recipient of this data has a duty to inquire of EPRI and/or Westinghouse as to the uses of the information contained herein that are permitted. This document and any copies or excerpts thereof that may have been generated are to be returned to Westinghouse, directly or through EPRI, when requested to do so.

NOTICE 4: The data in this document is proprietary and confidential to Westinghouse Electric Corporation and/or its Contractors. It is being revealed in confidence and trust only to Employees of EPRI and to certain contractors of EPRI for limited evaluation tasks authorized by EPRI. Any use, disclosure to unauthorized persons, or copying of this document or parts thereof is prohibited. This Document and any copies or excerpts thereof that may have been generated are to be returned to Westinghouse, directly or through EPRI, when requested to do so.

NOTICE 5: The data in this document is proprietary and confidential to Westinghouse Electric Corporation and/or its Contractors. Access to this data is given in Confidence and Trust only at Westinghouse facilities for limited evaluation tasks assigned by EPRI. Any use, disclosure to unauthorized persons, or copying of this document or parts thereof is prohibited. Neither this document nor any excerpts therefrom are to be removed from Westinghouse facilities.

EPRI CONFIDENTIALITY / OBLIGATION CATEGORIES

CATEGORY "A" — (See Delivered Data) Consists of CONTRACTOR Foreground Data that is contained in an issued reported.

CATEGORY "B" — (See Delivered Data) Consists of CONTRACTOR Foreground Data that is not contained in an issued report, except for computer programs.

CATEGORY "C" — Consists of CONTRACTOR Background Data except for computer programs.

CATEGORY "D" — Consists of computer programs developed in the course of performing the Work.

CATEGORY "E" — Consists of computer programs developed prior to the Effective Date or after the Effective Date but outside the scope of the Work.

CATEGORY "F" — Consists of administrative plans and administrative reports.

WESTINGHOUSE NON-PROPRIETARY CLASS 3

WCAP-14846

Scaling Analysis for AP600 Containment Pressure During Design Basis Accidents

D. R. Spencer

March 1997

Westinghouse Electric Corporation
Energy Systems Business Unit
P.O. Box 355
Pittsburgh, Pennsylvania 15230-0355

© 1997 Westinghouse Electric Corporation
All Rights Reserved

TABLE OF CONTENTS

TABLE OF CONTENTS (cont.)

TABLE OF CONTENTS (cont.)

TABLE OF CONTENTS (cont.)

LIST OF TABLES

LIST OF TABLES (cont.)

LIST OF FIGURES

LIST OF FIGURES (cont.)

LIST OF ACRONYMS AND ABBREVIATIONS

DBA	Design Basis Accident
DECLG	Double-Ended Cold Leg Guillotine
ECCS	Emergency Core Cooling System
IET	Integral Effects Test
IRWST	In-Containment Refueling Water Storage Tank
ISTIR	Integrated Structure for Technical Issue Resolution
LOCA	Loss-of-Coolant Accident
LST	Large-Scale Test
MSLB	Main Steamline Break
PCS	Passive Containment Cooling Accident
PIRT	Phenomena Identification Ranking Table
PWR	Pressurized Water Reactor
RPC	Rate of Pressure Change
SET	Separate Effects Test
SSAR	Standard Safety Analysis Report
STC	Westinghouse Science and Technology Center

EXECUTIVE SUMMARY

Introduction

This document presents the scaling evaluations performed to support the passive containment cooling system design basis accident (PCS DBA) evaluation model that is used to predict pressure in the AP600 containment during a DBA. The document supports design certification of the Westinghouse AP600. This document is one of the primary reports that support the PCS DBA evaluation model. The other primary reports are the SSAR[1], the PIRT report[2], the WGOTHIC code description and validation report[3], and the WGOTHIC application report[4]. Test data reports, test analysis reports, and phenomenological model reports are incorporated into the primary reports by reference.

Scaling is performed for the different time phases of the limiting large-break loss-of-coolant accident (LOCA) and the limiting main steamline break (MSLB). The double-ended cold leg guillotine (DECLG) pipe break and the MSLB initiated from 30 percent power, and the LOCA and MSLB with the limiting pressure responses are evaluated. Containment pressure, energy, mass, internal momentum, and external momentum are scaled.

The integrated structure for technical issue resolution (ISTIR), presented in NUREG/CR-5809[5], and the scaling example by Wulff[6] was used for guidance in the preparation of this document. Previous iterations on the scaling analysis were performed and documented[7,8,9]. Comments received from NRC and ACRS reviews are addressed and incorporated.

The scaling analysis satisfies the AP600 needs for containment pressure scaling which are:

- Develop dimensionless, normalized equations for the AP600 containment pressure with pi groups that represent the important effects identified in the phenomena identification ranking table (PIRT) for mass, energy, and momentum transport among components.

- Calculate the relative magnitude of the dimensionless pi groups for AP600.

- Use the quantitative evaluation to confirm the ranking of phenomena identified in the PIRT.

- Determine the range of dimensionless groups and the relevant separate effects tests (SETs) needed to validate models for the dominant phenomena in AP600.

- Confirm the use of the SETs and integral effects tests (IETs) to validate phenomenological models and the WGOTHIC computer code for use on AP600.

- Identify test distortions that limit the applicability of the tests to AP600.

The PIRT

The phenomena ranked high and medium in the PIRT are identified in Table E-1. All high and medium ranked phenomena are addressed by the scaling analysis, or references are provided showing where the phenomena are evaluated. In addition, many low ranked phenomena are also evaluated in the scaling analysis, thereby confirming their low ranking. Table E-1 is a simplification of the more detailed presentation in the PIRT. Only phenomena ranked high and medium during any time phase are listed.

Table E-1 Phenomena Identification and Ranking Table - Summary of High and Medium Ranked Phenomena

Phenomenon *	Effect on Containment	Pi Groups	Where Addressed
Break Source Mass and Energy (1A) and Liquid Flashing (1E) and Evaporation (5B)	The mass and energy source for containment pressurization	$\pi_{p,g,brk,enth}$ $\pi_{p,g,brk,work}$ $\pi_{p,work,d}$ $\pi_{p,work,p}$	Scaling Analysis
Gas Compliance (2C)	Stores mass and energy in atmosphere, increasing pressure	$\pi_{p,t}$	Scaling Analysis
Initial Conditions Inside (4A, 4B, 4C)	Temperature, humidity, pressure affect noncondensibles and energy storage	None	Initial Conditions Ref. 4, Section 5
Containment Solid Heat Sinks (3), Pool (5), Drops, and Shell (7)	Store energy (and remove mass from atmosphere) reducing pressure	$\pi_{p,g,i}$ $\pi_{p,enth,i}$ $\pi_{p,work,i}$	Scaling Analysis
Internal Heat Sink Conduction (3D, 5E, 7F) and Heat Capacity (3E, 5A, 7G, 1E)	Limits conduction heat transfer into heat sinks, shell, or pool, and through shell. Stratification in the break pool can affect the effective heat capacity of the pool.	parameter	Scaling Analysis
Heat Transfer Through Horizontal Liquid Films (3C)	Water and noncondensible layers on upward facing horizontal surfaces limit heat and mass transfer to horizontal heat sinks	parameter	Scaling Analysis
Condensation Mass Transfer (3F, 5B, 7C)	The single first order transport process that removes mass and energy from the containment gas	$\pi_{p,enth,i}$ $\pi_{p,work,i}$	Scaling Analysis
Break Source Direction and Elevation (1B), Momentum (1C), Density (1D), and Droplets (1E)	Direction, elevation, density, and momentum can dominate circulation and affect condensation rate. Existence of droplets in source during blowdown affects the effective source density.	parameter	Mixing and Stratification, Ref. 4, Section 9
Mixing and Stratification (2A)	Intercompartment Flow (Circulation) and stratification can affect the distribution of steam near heat sinks for condensation heat removal. Rising liquid level blocks lower circulation flow paths.	parameters	
Intercompartment Flow (2B)			
Break Pool Flooding Level (5F)			
Source Fog (2D)	Affects circulation and stratification via buoyancy	parameter	

Table E-1 Phenomena Identification and Ranking Table - Summary of High and Medium Ranked Phenomena (cont.)			
Phenomenon *	**Effect on Containment**	**Pi Groups**	**Where Addressed**
Evaporation Mass Transfer (7N)	The first order transport process that removes mass and energy from the evaporating external shell	$\pi_{e,fg,esx}$	Scaling Analysis
PCS Natural Circulation (9A, 13A)	Convective air flow provides heat and mass transfer from containment shell.	parameter	Scaling Analysis
Liquid Film Flow Rate (8A), Water Temperature (8B), Film Stability (8C)	Affects the upper limit for water coverage on the external shell	parameter	Film Stability Ref. 4, Section 7
Liquid Film Energy Transport (3A, 7E, 7M)	*Inside:* Carries 14% of condensation energy to the IRWST and break pool. *Outside:* Absorbs 8% of energy rejected by the external shell surface.		Scaling Analysis
Convection Heat Transfer (3G, 7A, 7H, 10A, 10B, 14A)	A second order transport process that removes energy from the containment gas, and from the external shell.	$\pi_{p,q,i}$ $\pi_{e,q,btx}$	Scaling Analysis
Radiation Heat Transfer (3H, 7B, 7I)	A second order transport process that removes energy from the containment gas and from the external shell.	$\pi_{p,q,i}$	Scaling Analysis
Baffle Conduction (10D) and Baffle Leakage paths (10G)	Conduction through the baffle into downcomer volume and leakage paths can influence the external natural circulation flow rates	None	PIRT Sections 4.4.10D and 4.4.10G

* Indicators in parentheses refer to phenomena in the "Phenomena Identification and Ranking According to Effect on Containment Pressure" table[2].

Scaling Equations

Basic Approach

The governing equations for the containment gas mass, energy, and pressure are derived by applying a simple control volume formulation, thermodynamic relationships, and an equation of state. The governing equations treat containment as a single, well-mixed control volume that is coupled to multiple heat sinks.

The above-deck region is well-mixed during and after blowdown due to the entrainment into the plume of more than 10 times its volumetric flow rate. The effect on heat sink utilization of deviations from a uniform vertical air/steam concentration distribution are shown in the

mixing and stratification report to be minor. The mixing and stratification report also examines a range of break source momenta and directions, and shows that in all cases circulation between compartments maintains all but the dead-ended compartments at or above the well-mixed steam concentration, and the above-deck region within 2 or 3 percent of the well-mixed concentration of approximately 60 percent steam. Although containment is not perfectly mixed, the deviations from well-mixed are small enough that the conclusions of the scaling analysis are valid.

For the LOCA, the heat sinks in dead-ended compartments are not included, since they are not effective heat sinks and it is conservative to ignore their heat capacity. In addition, upward facing large surfaces that may develop thick liquid films or may be blanketed with noncondensables are not included. None of the below-deck heat sinks are included for the MSLB.

Conservation of Mass - Containment

The mass conservation equation for the containment atmosphere, which consists of a constant mass of air and a varying mass of steam, can be stated as the rate of change of mass in a control volume is equal to the sum of mass flows into the control volume minus the sum of flows out of the control volume:

$$m = m_{air} + m_{stm} \quad \frac{dm}{dt} = \frac{dm_{air}}{dt} + \frac{dm_{stm}}{dt} \quad \frac{dm_{air}}{dt} = 0 \quad \text{so} \quad \frac{dm}{dt} = \frac{dm_{stm}}{dt} = \dot{m}_{brk} - \sum \dot{m}_{stm,j} \qquad (1)$$

The mass rate of change equation is made dimensionless and normalized by the reference break steam flow rate, $\dot{m}_{g,brk,o}$, resulting in the following dimensionless equation and pi groups:

$$\pi_{m,\tau} \frac{dm^*}{dt^*} = \pi_{m,brk} \dot{m}^*_{g,brk} + \sum_j \pi_{m,j} \dot{m}^*_{stm,j} \qquad m^* = \frac{m}{\dot{m}_{g,brk,o}} \qquad t^* = \frac{t}{\tau} \qquad (2)$$

where

$$\tau = \frac{V_o \rho_{g,brk,o}}{\dot{m}_{g,brk,o}} \quad \pi_{m,\tau} = \frac{\rho_o V_o \dot{m}_{g,brk,o}}{\rho_{g,brk,o} V_o \dot{m}_{g,brk,o}} = \frac{\rho_o}{\rho_{g,brk,o}} \quad \pi_{m,brk} = \frac{\dot{m}_{g,brk,o}}{\dot{m}_{g,brk,o}} = 1 \quad \pi_{m,j} = \frac{\dot{m}_{stm,j,o}}{\dot{m}_{g,brk,o}} \qquad (3)$$

Conservation of Energy - Containment

The conservation of energy equation for the containment atmosphere is as follows (note that the liquid internal energy and enthalpy of water at 120°F are used as a basis for changes in those properties):

$$\frac{d[m(u-u_{min})]}{dt} = \dot{m}_{g.brk}(h_{g.brk}-h_{f,T_o}) + \frac{P}{\rho_f}\dot{m}_f - \sum_j [\dot{m}_{stm,j}(h_{stm,j}-h_{if,j}) + \dot{m}_{m,j}(h_{if,j}-h_{f,T_o}) + h_j A_j (T-T_{if,j})] \quad (4)$$

The energy equation is made dimensionless and normalized by the break steam enthalpy flow rate, $\dot{m}_{g.brk,o}(h_{g.brk}-h_{f,To}) = \dot{m}_{g.brk,o}\Delta h_{g.brk,o}$, resulting in the following equation and pi groups:

$$\pi_{e,\tau}\frac{d(mu)^*}{dt^*} = \pi_{e.brk}\dot{m}^*_{g.brk}\Delta h^*_{brk} - \sum_j\left(\pi_{e.fg,j}\dot{m}^*_{stm,j}\Delta h^*_{stm,j} + \pi_{e.if,j}\dot{m}^*_{stm,j}\Delta h^*_{if,j} + \pi_{e.q,j}h^*_{q,j}A_j^*\Delta T^*_{if,j}\right) \quad (5)$$

where:

$$\pi_{e,\tau} = \pi_{m,\tau}\frac{\Delta u_o}{\Delta h_{g.brk.o}} \quad \pi_{e.brk} = \frac{\dot{m}_{g.brk.o}\Delta h_{g.brk.o}}{\dot{m}_{g.brk.o}\Delta h_{g.brk.o}} = 1 \quad \pi_{e.f.work} = \pi_{m.f}\frac{P_o}{\rho_{f.o}\Delta h_{g.brk.o}}$$
$$\pi_{e.fg,j} = \pi_{m,j}\frac{\Delta h_{fg,j.o}}{\Delta h_{g.brk.o}} \quad \pi_{e.if,j} = \pi_{m,j}\frac{\Delta h_{if,j.o}}{\Delta h_{g.brk.o}} \quad \pi_{e.q,j} = \frac{h_{q,j.o}A_{j.o}(T-T_{if,j.o})}{\dot{m}_{g.brk.o}\Delta h_{g.brk.o}} \quad (6)$$

Pressure Rate of Change - Containment

Combining the conservation of mass and energy equations and applying an equation of state for real gasses, PV = ZmRT, the rate of pressure change (RPC) equation is derived:

$$\frac{(1+Z^T)}{(\gamma-1)}V\frac{dP}{dt} = \dot{m}_{g.brk}\left(h_{g.brk}-h_{stm}+\frac{\gamma(1+Z^T)}{(\gamma-1)}\frac{P_{stm}}{\rho_{stm}}\right) + \dot{m}_f\frac{\gamma(1+Z^T)}{(\gamma-1)}\frac{P}{\rho_f} - \sum_j\left[\dot{m}_{stm,j}\left(h_{stm,j}-h_{stm}+\frac{\gamma(1+Z^T)}{(\gamma-1)}\frac{P_{stm}}{\rho_{stm}}\right)-h_{q,j}A_j(T-T_{if,j})\right] \quad (7)$$

The compressibility function $Z^T = (T/Z)(dZ/dT)$, where Z is the (combined air and steam) gas compressibility and T is absolute temperature. The rate of pressure change equation is made dimensionless, then normalized by dividing each term by the reference break gas work term, $\gamma_0(1+Z^T)/(\gamma-1)_o\,\dot{m}_{g.brk.o}(P_{stm}/\rho_{stm})$:

$$\pi_{p,\tau}\frac{Z^{T*}V^*}{\gamma^*}\frac{dP^*}{dt^*} = \pi_{p.g.brk.enth}\Delta h^*_{g.brk}\dot{m}^*_{g.brk} + \pi_{p.g.brk.work}\frac{\gamma^*Z^{T*}}{\gamma^*_m}\frac{P^*_{stm}}{\rho^*_{stm}}\dot{m}^*_{g.brk} + \pi_{p.f.work}\frac{\gamma^*Z^{T*}}{\gamma^*_m}\dot{m}^*_f P^* + \sum_j\left(\pi_{p.enth,j}\frac{\dot{m}^*_{stm,j}}{\dot{m}^*_{g.brk}}\Delta h^*_{stm,j} + \pi_{p.work,j}\frac{\dot{m}^*_{stm,j}}{\dot{m}^*_{g.brk}}\frac{\gamma^*Z^{T*}}{\gamma^*_m}\frac{P^*_{stm}}{\rho^*_{stm}} + \pi_{p.q,j}h^*_{q,j}A_j^*\Delta T^*_{if,j}\right) \quad (8)$$

where

$$\tau = \frac{V_o \rho_{g.brk.o}}{\dot{m}_{g.brk.o}} \qquad \pi_{p,\tau} = \pi_{m,\tau} \frac{1}{\gamma_o} \frac{P_o}{P_{stm.o}} \frac{\rho_{stm.o}}{\rho_o} \qquad \pi_{p.g.brk.enth} = \frac{(h_{g.brk} - h_{stm})_o (\gamma - 1)_o}{\gamma_o (1 + Z^T)_o} \frac{\rho_{stm.o}}{P_{stm.o}}$$

$$\pi_{p.g.brk.work} = 1 \qquad \pi_{p.f.work} = \pi_{m.f} \frac{\rho_{stm.o}}{\rho_{f.o}} \frac{P_o}{P_{stm.o}} \qquad \pi_{p.enth,j} = \pi_{m.stm,j} \frac{(\gamma - 1)_o}{\gamma_o (1 + Z^T)_o} \frac{\rho_{stm.o}}{P_{stm.o}} (h_{stm,j} - h_{stm})_o \qquad (9)$$

$$\pi_{p.work,j} = \pi_{m.stm,j} \qquad \pi_{p.q,j} = \frac{(\gamma - 1)_o}{\gamma_o (1 + Z^T)_o \dot{m}_{g.brk.o}} \frac{\rho_{stm.o}}{P_{stm.o}} h_{q,j.o} A_{j.o} (T - T_j)_o$$

Conservation of Momentum - PCS Air Flow Path

The conservation of mass, energy, and momentum equations were developed for the PCS air flow path to calculate the buoyant air flow rate that is needed to determine heat and mass transfer from the shell, and heat transfer rates between the riser and baffle, baffle and downcomer, and chimney and chimney concrete. The momentum equation was developed in vector form, following the example of Wulff[6]. The resulting momentum equation is:

$$\bar{I} \cdot \frac{d\bar{\dot{m}}}{dt} = G - \bar{R} \cdot \overline{(KE)} \qquad (10)$$

where:

$\bar{I}$ is the geometry dependent inertia vector,

$\bar{\dot{m}}$ is the mass flow rate vector,

G is the buoyancy defined by integrating the density times the dot product of the gravity and displacement vectors around a closed path,

$\bar{R}$ is the impedance vector and R_i is the sum of the form and friction resistance for each segment,

$\overline{KE}$

is the vector of kinetic energies:

The vectors are made dimensionless and the dimensionless momentum equation is normalized by the reference buoyancy, G_o:

$$\pi_{mv.in} \bar{I}^* \cdot \frac{d\bar{\dot{m}}^*}{dt^*} = \pi_{mv.buoy} G^* - \pi_{mv.res} \bar{r} \cdot \overline{KE}^* \qquad I_o = \sum I_i \qquad R_o = \frac{\sum R_i}{2 \rho_o A_o^2} \qquad (11)$$

$$\text{where} \quad \tau = \frac{V_o}{Q_o} \qquad \pi_{mv.in} = \frac{I_o \dot{m}_o / \tau}{G_o} \qquad \pi_{mv.buoy} = \frac{G_o}{G_o} = 1 \qquad \pi_{mv.res} = \frac{R_o \dot{m}_o^2}{G_o}$$

The total buoyancy can be subdivided into components corresponding to the downcomer, riser, and chimney. Defining these as pi groups, $\pi_{mv,buoy} = \pi_{mv,dc} + \pi_{mv,ri} + \pi_{mv,ch} = 1.0$, where:

$$\pi_{mv,dc} = \frac{G_{dc}}{G_o} \qquad \pi_{mv,ri} = \frac{G_{ri}}{G_o} \qquad \pi_{mv,ch} = \frac{G_{ch}}{G_o} \tag{12}$$

Constitutive Relationships

Constitutive relationships are needed to calculate heat and mass transfer to the condensing film inside containment, heat transfer through the condensed and evaporating films, evaporation and heat transfer from the external film, and heat transfer from the baffle to the riser and downcomer. Operating points for the Grashof and Reynolds numbers were calculated for the PCS air flow path downcomer, riser, and chimney and plotted on a Metais and Eckert[10] plot to determine the turbulent heat transfer mode. The results are shown in Figure E-1. The riser and downcomer operate in forced convection and the chimney operates in opposed mixed convection.

The inside of containment operates in forced convection during the large LOCA blowdown and the MSLB, and operates in free convection after the LOCA blowdown. However, free convection is assumed for the inside of containment for all analyses. This significantly underpredicts both heat and mass transfer during the MSLB and the LOCA blowdown, but is realistic for the LOCA after blowdown.

The McAdams correlation is used for free convection, the Colburn correlation for forced convection, and a combination of free and forced is used for mixed convection. Heat transfer to the small diameter liquid drops is calculated using a correlation for laminar heat transfer to small spheres from Kreith[11]. Mass transfer is calculated by the heat and mass transfer analogy. The heat and mass transfer correlations are summarized in Table E-2.

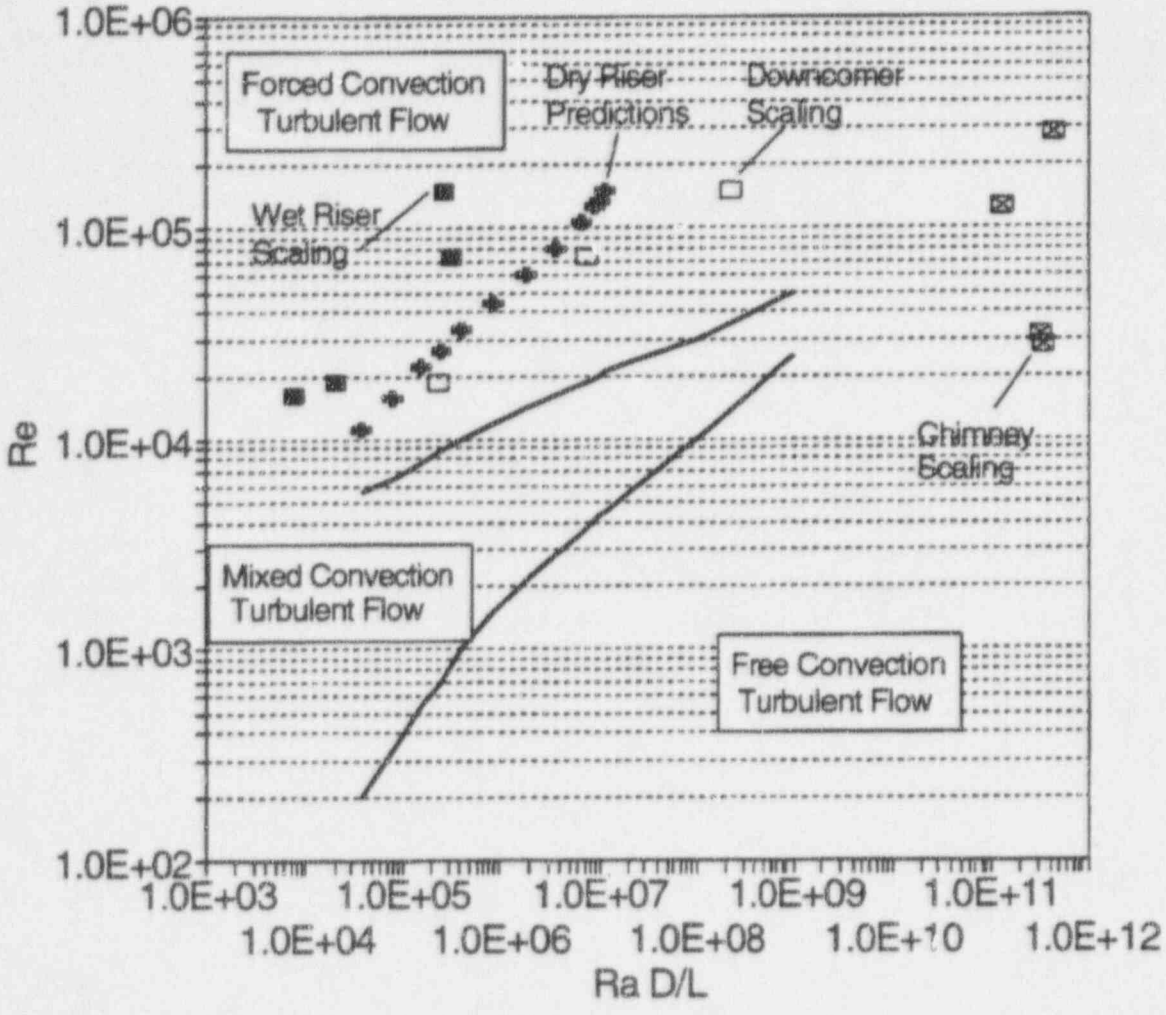

Figure E-1 **Metais and Eckert Plot Showing the Downcomer, Riser, and Chimney Heat Transfer Regimes**

Table E-2 Heat and Mass Transfer Correlations for AP600

Phenomena	Constitutive Relationship
Free Convection Heat Transfer	$Nu_{free} = 0.13(\Delta\rho/\rho)^{1/3}Pr^{1/3}$ $Nu = h(\nu^2/g)^{1/3}/k$ (13)
Forced Convection Heat Transfer	$Nu_{forc} = 0.023Re^{0.8}Pr^{1/3}$ $Nu = hd/k$ (14)
Opposed Mixed Convection Heat Transfer	$Nu_{mix} = (Nu_{forc}^3 + Nu_{free}^3)^{1/3}$ (15)
Drop Heat Transfer	$Nu = 2$ $Nu = hd/k$ (16)
Free Convection Mass Transfer	$Sh = 0.13(\Delta\rho/\rho)^{1/3}Sc^{1/3}$ $Sh = \frac{k_g \bar{R} T(\nu^2/g)^{1/3} P_{lm,air}}{D_v P}$ (17)
Forced Convection Mass Transfer	$Sh = 0.023Re^{0.8}Sc^{1/3}$ $Sh = \frac{k_g \bar{R} T(\nu^2/g)^{1/3} P_{lm,air}}{D_v P}$ (18)
Drop Mass Transfer	$Sh = 2\left(\frac{Sc}{Pr}\right)^{1/3}$ $Sh = \frac{k_g \bar{R} T(\nu^2/g)^{1/3} P_{lm,air}}{D_v P}$ (19)

Heat Sink Energy Coupling to Containment Gas

The containment gas equations are coupled by mass and energy transfer to the heat sinks and containment shell. The types of heat sinks considered for AP600 scaling are listed in Table E-3.

Table E-3 Heat Sink Energy Equation Scaling for AP600

Heat Sink	Abbreviation	Equation Solution Method
Drops	d	Exponential Approximation
Break Pool	p	Evap from a spreading layer
Internal film	if	Steady state conduction
Steel	st	Lumped parameter
Concrete	cc	Integral equation
Jacketed Concrete	jc	Bounded by steel or concrete
Shell:	sh	Integral equation
Subcooled	ss	Integral equation
Evaporating	es	Integral equation
Dry	ds	Integral equation
Baffle	bf	Lumped parameter
Chimney Concrete	ch	Integral equation

The energy equation for each heat sink was solved using the simplified technique listed in Table E-3. The internal steel and external baffle are thin enough to be modeled using a simple lumped parameter model, while the shell and concrete were modeled using integral approximations for thermally thick structures presented by Wulff[5,12]. The drop and pool required special treatment due to a singularity in the mass transfer equation when $P_{stm} = P_{total}$. Simple methods were used to overcome the singularity and calculate the mass transfer rate.

Scaling Results and Pi Group Evaluation

The simultaneous solution of the mass, energy, and momentum equations produces the values needed to solve for the mass, energy, pressure, and momentum pi groups. The equations were solved for the four LOCA time phases and the MSLB. The conclusions of those calculations follow.

Mass Scaling Results

Conclusions of the mass flow rate scaling are:

- Relative to the break gas mass flow rate pi value of 1.0, the steel, concrete, jacketed concrete, dry shell, and evaporating shell have condensation and/or evaporation mass transfer rate pi values of order 1.0 during some time phases.

- The pool, drops, subcooled shell, baffle, and chimney condensation and/or evaporation mass transfer rate pi groups are always of order 0.1 or less.

- During blowdown the break source flow rate is so high that even with significant energy absorption, the heat sink condensation mass transfer rate pi groups are all order 0.1 or less.

Since the containment gas mass rate of change responds to the sum of all the heat sink mass fluxes, it is relevant to combine all the internal heat sink mass transfer pi groups into a single value corresponding to mass transfer to a net heat sink. The result is presented in Table E-4]. The scaled mass rate of change, dm^*/dt^* is also presented.

Table E-4 Containment and Net Heat Sink Mass Scaling Pi Group Values						
Pi Group		LOCA				MSLB
		Blowdown	Refill	Peak Press	Long Term	
Containment	τ_o (sec)	31	980	908	3309	392
	$\pi_{m,s}$	1.31	1.27	1.30	1.22	1.27
	$\pi_{m,brk}$	1.00	0.00*	1.00*	1.00	1.00
	$\pi_{m,f}$	1.75	0.00	2.00	0.00	0.00
Net Heat Sink	$\pi_{m,hs}$	-0.01	-2.60	-1.37	-1.26	-1.01
	$\pi_{m,esx}$	--	--	-0.02	-0.57	--
dm*/dt*		0.76	-2.05	-0.30	-0.68	-0.01

* Refill was scaled with the same 200 lbm/sec flow rate used to normalize peak pressure.

The net heat sink shows the net blowdown mass is slightly negative (as shown by the detailed pi groups, this is due to the flashing and rapid evaporation of hot break liquid to steam). After blowdown, the condensation rate is greater than the source, indicating that dm*/dt* is negative, so the net mass of vapor in containment is decreasing. From the equation of state, since pressure is proportional to mass, it can be expected that pressure is also decreasing. Although this is contrary to predictions of the evaluation model that the pressure increases during the peak pressure time phase, the difference is due to more conservative mass transfer rate assumptions in the evaluation model.

Energy Scaling Results

Conclusions of the detailed energy scaling pi groups are:

- Sensible heat transfer related phenomena (q subscripted pi groups) are always small.
- Phenomena associated with the energy carried away by liquid films (f subscripted pi groups) are much less important than phenomena associated with energy transferred into the heat sink by condensation (fg subscripted pi groups).
- Phenomena associated with the outside shell surface energy transfer are important during long-term but not during blowdown, refill, and peak pressure. Phenomena associated with the inside of the dry shell during refill, and the inside of the evaporating shell during the peak pressure phase are very important, indicating the large shell energy storage capacity.
- Heat sink mass transfer related phenomena (fg subscripted pi groups) are important after blowdown and before the long-term phase of a large LOCA.
- Phenomena associated with the baffle and chimney are second order effects.

The detailed energy scaling results for all the internal heat sinks are combined into a few net heat sink pi groups and presented in Table E-5. The scaled rate of change of internal energy du^*/dt^* is determined according to the scaled energy equation and included in the table.

Table E-5 Containment and Net Heat Sink Energy Scaling Pi Group Values

Pi Group		LOCA				MSLB
		Blowdown	Refill	Peak Press	Long Term	
Containment	$\pi_{e,\tau}$	0.55	0.58	0.56	0.63	0.58
	$\pi_{e,brk}$	1.00	0.00*	1.00*	1.00	1.00
	$\pi_{e,f,work}$	0.00	0.00	0.00	0.00	0.00
Net Heat Sink	$\pi_{e,q,ns}$	0.00	-0.14	-0.06	-0.03	-0.07
	$\pi_{e,fg,ns}$	-0.02	-2.49	-1.30	-1.14	-0.99
	$\pi_{e,f,ns}$	0.00	-0.10	-0.09	-0.14	0.01
	$\pi_{e,q,nsx}$	0.00	0.00	0.00	-0.06	--
	$\pi_{e,q,ssx}$	--		-0.01	-0.08	--
	$\pi_{e,fg,esx}$	--	--	-0.02	-0.81	--
$d(mu)^*/dt^*$		1.78	-4.71	-0.80	-0.49	-0.12

* Refill was scaled with the same energy normalization used for peak pressure.

The net heat sink energy pi values show the heat sinks are not effective, relative to the source, during blowdown. During subsequent time phases of the LOCA, more energy is removed from the gas than added. The sensible heat transfer (q subscript) and liquid film energy transfer (f subscript) are small compared to the mass transfer (fg subscript) both inside and outside (outside has x subscript). External heat transfer is insignificant until the long-term phase.

Pressure Scaling Results

The detailed pressure scaling pi values provide the basis for the following conclusions:

- All heat sink phenomena, except those associated with the drops and pool, reduce pressure during the time phases considered.
- Drop-related phenomena produce a small pressure increase during blowdown, and thereafter are either a small pressure sink or a negligible pressure source.
- The pool is always a small pressure source.
- During the blowdown phase, phenomena associated with the internal solid heat sinks and shell reduce the RPC by 10 percent of the source work, while flashing and evaporation from the pool and drops increases the RPC by 9 percent.

- The work due to mass removal is the most significant pressure-related phenomena. Heat transfer-related phenomena (radiation plus convection) are typically much less important than flow work-related phenomena.
- Enthalpy-related phenomena for both the source and heat sinks are not important.
- Phenomena associated with mass transfer dominates the RPC after blowdown.

The detailed breakdown of heat sinks is useful for clarifying the effect of the several distinct types and locations of heat sinks. However, the RPC equation shows the same pressure response would result from considering a net source and a net sink. The pi groups resulting from this composite heat sink approach are defined by adding the values for all heat sinks. The results are presented in Table E-6.

Table E-6 Containment and Net Heat Sink Pressure Scaling Pi Group Values

Pi Group		LOCA				MSLB
		Blowdown	Refill	Peak Press	Long Term	
Containment	$\pi_{p,t}$	0.76	0.76	0.77	0.76	0.76
	$\pi_{p,g,brk,work}$	1.00	0.00*	1.00*	1.00	1.00
	$\pi_{p,g,brk,enth}$	0.03	0.00	0.03	0.02	0.03
	$\pi_{p,f,work}$	0.00	0.00	0.00	0.00	0.00
Net Heat Sinks	$\pi_{p,q,ns}$	-0.01	-0.43	-0.20	-0.12	-0.20
	$\pi_{p,enth,ns}$	0.00	0.00	0.00	0.00	0.00
	$\pi_{p,work,ns}$	-0.01	-2.60	-1.37	-1.26	-1.01
dP^*/dt^*		1.33	-3.99	-0.70	-0.47	-0.24

* Refill was scaled with the same pressure normalization used for peak pressure.

Pressure scaling with a net heat sink shows the minor effect of the heat sinks during the LOCA blowdown and the major effect thereafter. As noted for the mass and energy scaling, the pi values indicate that containment is depressurizing after blowdown, contrary to the evaluation model predictions, due primarily to mass transfer correlation conservatism in the evaluation model. Sensible heat transfer is an intermediate order ($0.1 < \pi_{p,q,ns} < 1.0$) phenomena for pressure, whereas it was order less than 0.1 for energy.

PCS Momentum Scaling Results

The PCS momentum scaling pi groups are presented in Table E-7. The Ra D/L values are the horizontal axis for the values shown on the Metais and Eckert plot, Figure E-1. PCS operation is not considered for scaling the MSLB, due to the relatively short duration of the transient.

Table E-7 PCS Air Flow Path Momentum Scaling Groups				
Group	Blowdown	Refill	Peak Press	Long Term
τ_{ri}	70	58	15	7.0
$\pi_{mv,in}$	0.13	0.13	0.13	0.11
$\pi_{mv,buoy}$	1.00	1.00	1.00	1.00
$\pi_{mv,res}$	1.00	1.00	0.97	0.86
$\pi_{mv,dc}$	0.00	-0.05	-0.03	-0.16
$\pi_{inv,ri}$	0.48	0.52	0.46	0.58
$\pi_{mv,ch}$	0.52	0.53	0.58	0.58
$Ra_dD/L)_{dc}$	--	247,000	$7.6x10^6$	$2.2x10^8$
$Re_{d,dc}$	16,100	18,500	74,000	151,000
$Ra_dD/L)_{ri}$	7,600	19,800	333,000	270,000
$Re_{d,ri}$	16,600	19,000	77,000	163,000
$Ra_dD/L)_{ch}$	$3.3x10^{11}$	$3.2x10^{11}$	$1.3x10^{11}$	$4.5x10^{11}$
$Re_{d,ch}$	27,400	31,400	128,000	282,000

The following conclusions are drawn from the momentum scaling:

- The pi groups show the inertial effect is relatively small, and the effect of the downcomer on the net buoyancy is relatively small.

- The air flow Reynolds number is high (16,100) even during blowdown due to the assumed initial condition of 120°F shell temperature and 115°F riser air. During normal operation containment temperature is expected to be higher than the outside temperature.

- The free/mixed/forced convection regime of the flow in the downcomer, riser, and chimney are determined from the Reynolds and Rayleigh (RaD/L) numbers on the Metais and Eckert plot in Figure E-1.

SETs and Constitutive Relationship Scaling

The energy and pressure pi values show the gas compliance, break source, condensation, and evaporation are the dominant order 1.0 terms. Internal sensible heat transfer is intermediate order, and external sensible heat transfer, liquid displacement, energy to the external subcooled film, energy carried by the condensed liquid, and enthalpy (of break and condensate) are order 0.1 or less terms. The conclusion is drawn that condensation and evaporation mass transfer are the dominant transport processes for containment pressurization.

This section presents summaries of constitutive relationships and scaling of phenomenological data from SETs. The summaries show the selected correlations represent the test data and the range of AP600 operation is adequately covered by the test data.

Condensation mass transfer was identified as a high importance phenomenon in the PIRT and was shown to be of order 1.0 in the scaling analysis. The dimensionless relationship for free convection condensation mass transfer, represented by the Sherwood number is presented in Figure E-2. Figure E-2 shows the range of parameters covered by the LST envelopes the operating range of AP600 and shows the test data agree well with the free convection mass transfer correlation. The data and correlation are discussed in more detail in the heat and mass transfer report[13].

Evaporation mass transfer was identified in the PIRT as a high importance phenomenon, and was verified by scaling to be of order 1.0. The forced convection evaporation mass transfer, as represented by the Sherwood number correlation, is presented in Figure E-3. The range of Sherwood and Reynolds numbers for AP600 operation are shown in Figure E-3 to be within the range covered by the LST and Gilliland and Sherwood test data. The figure also shows the data agree well with the forced convection mass transfer correlation. Note that although the Gilliland and Sherwood data range is shown on the figure, the actual data were not local, so are not included on the plot. The data and correlation are discussed in more detail in Reference 13.

Free convection heat transfer to surfaces inside containment was ranked medium in the PIRT. Scaling shows heat transfer to be of intermediate order, it accounts for approximately 10 percent as much energy and 10 to 20 percent as much dP/dt as condensation mass transfer. As second order energy transfer phenomena, heat transfer inside containment is modeled using the conventional correlations for radiation and free convection. Although the SETs and IETs included these phenomena, they were always present with condensation mass transfer, which dominated the energy transfer, and prevented measuring the second order phenomena.

Although no direct measurement of heat transfer in the presence of mass transfer is available, by the heat and mass transfer analogy it can be claimed that heat transfer is as well modeled as the mass transfer presented in Figure E-2 and Figure E-3. That is, replace $Sh\ Sc^{1/3}$ with $Nu\ Pr^{1/3}$ in Figure E-2 and Figure E-3 to estimate the agreement and uncertainty for heat transfer.

The PIRT ranked forced convection heat transfer from the shell to the riser as medium importance, and the scaling analysis showed it to be a second order phenomenon. Forced convection heat transfer from the shell to the riser in AP600 is modeled using the Colburn forced convection heat transfer correlation:

$$Nu = 0.023\,Re_D^{0.8}\,Pr^{1/3} \quad \text{where} \quad Nu = \frac{hD_h}{k} \tag{20}$$

where the length parameter is the annulus hydraulic diameter, D_h. Incropera and DeWitt[14], Table 8.4, suggests the use of Colburn, Dittus-Boelter, and Seider-Tate correlations for internal channel flows.

Figure E-2 Free Convection Condensation Data from the LST Compared to the Correlation and the AP600 Operating Range

Figure E-3 Forced Convection Evaporation Data from the STC Flat Plate Test Compared to the Correlation and the AP600 Range of Operation

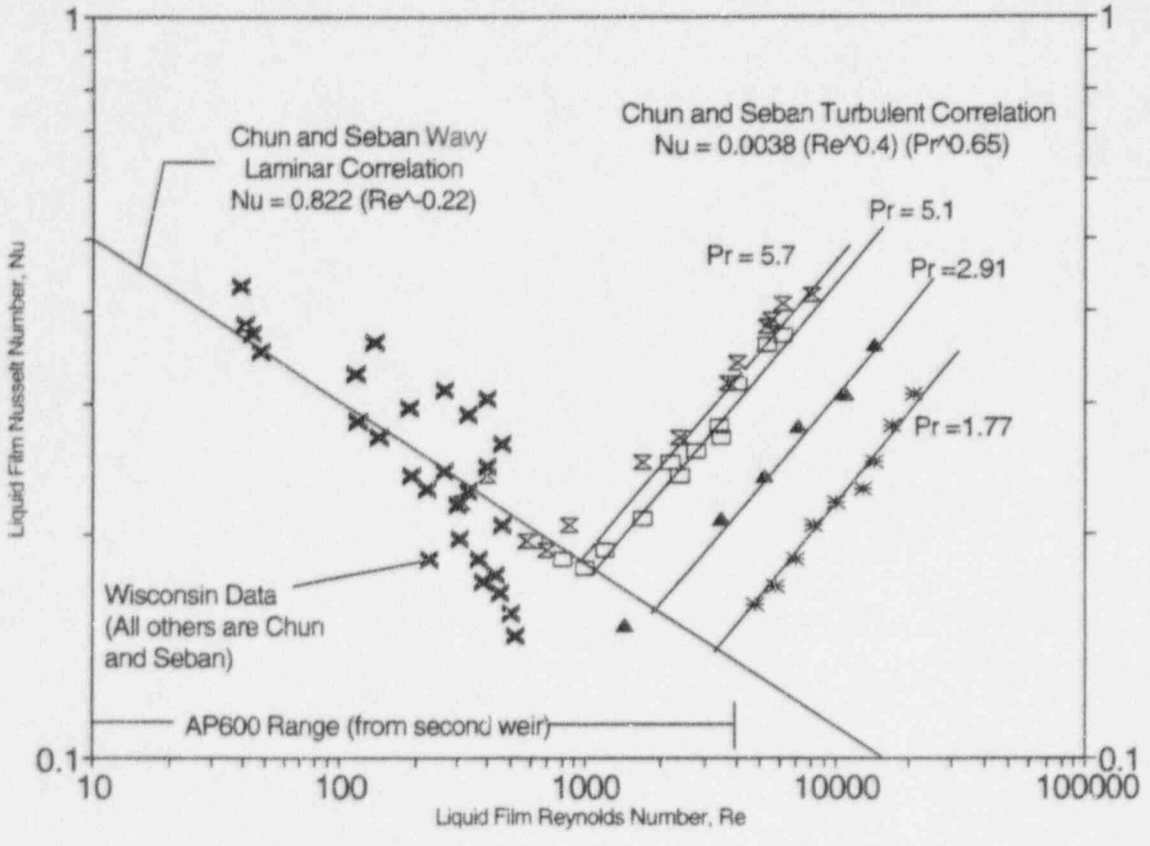

Figure E-4 **Chun and Seban Liquid Film Nusselt Number Correlation Comparison to Condensation and Evaporation Test Data**

- The Dittus-Boelter correlation differs from Colburn by a Prandtl number exponent of 0.4 instead of 1/3. For the flow in the PCS riser (approximately 90 percent air and 10 percent steam by mass), Dittus-Boelter gives results that are 2 percent less than Colburn.

- The Seider-Tate correlation adds a multiplier of $(\mu/\mu_s)^{0.14}$ to the Colburn correlation. For the PCS with air and bulk-to-surface temperature differences less than 100°F, Seider-Tate also gives results 2 percent less than Colburn.

All of these correlations are recommended for Re > 10,000, L/D > 10, and .7 < Pr < 160. The corresponding AP600 parameters are 20,000 < Re < 163,000, Pr ≈ 0.72, and L/D ≈ 60 which satisfy the criteria for use of the Colburn correlation.

The PCS flow resistance is one of the dominant terms in the PCS momentum equation. The flow resistance in the PCS air flow path was measured in the 1/6 scale air flow test[15]. Although AP600 operates in natural circulation and the test was fan forced, the buoyant pressure, G_o and the forced pressure drop, ΔP are interchangeable in the pi groups. Consequently, a fan forced test produces a flow resistance that is equally valid for a buoyancy driven system.

[

]^{a,b}

An important aspect of the AP600 design is its sensitivity to external wind. The external conditions might be postulated to affect the performance of the PCS air flow path, due to high wind speeds and turbulence induced by upwind structures or terrain.

A series of tests were conducted in wind tunnels to characterize the effect on the AP600 PCS air flow of environmental wind speeds up to the AP600 design limit of 214 mph. Since the AP600 design is wind-positive, the particular concern was the effect of upwind terrain and obstructions that could subject the PCS air flow path to pressure fluctuations that might induce reversed flow in the riser. Such fluctuations have been evaluated relative to the assumed zero environmental effect. The effect of wind tunnel model scale was evaluated to insure the appropriate flow regime was simulated in the tests. The test evaluation (Ref. 4, Section 6) showed the wind-positive characteristic of AP600 more than offset the effect of fluctuations.

The recirculation of the chimney outflow (warmer and more humid than the environment) to the downcomer inlets was evaluated (Ref. 4, Section 6) and determined to have an insignificant effect.

Liquid film stability is an important parameter in the external evaporation calculation. This was identified in the PIRT and is included in the important phenomena listed in Table E-1. The film stability is discussed in detail in Reference 4, Section 7. Heated and unheated water distribution measurements were made on tests to support the modeling of water coverage on the external shell of AP600. The dimensionless groups appropriate for scaling water

coverage are defined in the literature and those that are most significant for AP600 are the film Reynolds number, Marangoni number, and Bond number, defined respectively as:

$$Re = \frac{4\Gamma}{\mu} \qquad Ma = \frac{d\sigma}{dT}\frac{q''\delta^2\rho c_p}{2k^2\mu} \qquad B = \frac{\rho g \delta^2}{\sigma} \tag{21}$$

The range of these groups for AP600 and two of the supporting tests are presented in Table E-8. The comparisons show the range of AP600 operation is adequately covered by the test data.

Table E-8 Comparison of AP600 Operating Range to Tests for Liquid Film Stability

	AP600	Large-Scale Test	Water Distribution Test
Film Reynolds Number:	[		]a,b
Upper Sidewall			
Bottom of PCS surface			
Marangoni Number:			
Upper Sidewall			
Bottom of PCS surface			
Bond Number:			
Upper Sidewall			
Bottom of PCS surface			

Heat transfer through the draining liquid film on the inside and outside surfaces of the shell and heat sinks was ranked low importance in the PIRT. The Chun and Seban[16] correlation was selected to model the film heat transfer. The validity of the Chun and Seban correlation for evaporating turbulent and wavy laminar films on vertical surfaces was demonstrated in the original paper. Data from tests at the University of Wisconsin[17] are added to extend the validity of the Chun and Seban correlation to condensing wavy laminar flow and to surfaces that are inclined, as in the dome region of the AP600.

The Wisconsin and Chun and Seban data are compared to the Chun and Seban laminar and turbulent correlations in Figure E-4. The correlation predicts nearly best- estimate values over the full Reynolds number range of data. The range of film Reynolds numbers on the outside of AP600 is also shown in the figure and falls well within the range of the test data. Reynolds numbers on the inside of containment are less than outside due to film removal at the crane rail and stiffener ring, and the fact that the inside film flow rate starts at zero at the top of the dome and increases as the film flows down. The AP600 Prandtl number range is approximately $1.5 < Pr < 3.0$, whereas the range of the Chun and Seban data Prandtl numbers is $1.77 < Pr < 5.9$, which adequately covers the AP600 range with only a small extrapolation. Comparison of the correlation to the test data show that the Chun and Seban correlation is a reasonable, best-estimate representation of the data.

LST Scaling and Equation Validation

A scaled comparison between the large-scale (integral test) and the AP600 plant is performed. The comparison shows the scaled LST captures highly ranked phenomena associated with the AP600 containment and therefore, the data obtained from the test is adequate for code validation. The scaling equations are compared to the LST and validated for both steady-state and transient predictions.

The results for 21 steady-state LST cases show the average steady-state mass and energy transfer rates are predicted with a mean deviation of less than 0.01 and a standard deviation of 0.13. Such agreement is considered to adequately verify that the mass and energy equations accurately predict the transfer rates, thereby validating the mass and energy scaling equations. Since the RPC equation is the result of combining the mass and energy rate equations, with the equation of state, it is also true that the RPC equation is valid at steady-state.

A comparison was made between the transient RPC equation and the startup of LST 221.1. At startup there is no heat or mass transfer to the internal heat sinks or shell since there is initially no temperature or steam partial pressure differences to drive transport processes. The initial pressurization is adiabatic compression which is described by the RPC equation without heat sinks or a break liquid source. The calculated value was $dP/dt = 0.38$ psi/sec, whereas the measured transient pressure shows $dP/dt = 0.29$. The difference is likely due to the fact that the "adiabatic" assumption is not quite valid, and consequently, the source is not quite so effective. The agreement is considered to be sufficiently close to provide validation of the transient capability of the RPC equation. When combined with the steady-state comparisons, this transient comparison shows the RPC equation is valid.

The scaled comparisons between the LST and AP600 focus on the phenomena associated with the containment features that are unique to AP600, that is, the PCS. Phenomena associated with the PCS become significant during the peak pressure phase of a DECLG LOCA, become dominant as peak containment pressure is approached, and remain dominant during the long-term phase of the transient. This is supported by energy partitioning calculations that show heat sink energy removal rates for AP600. The external shell energy removal becomes important during the refill time phase (t~1000 sec) and is dominant by about 200 sec (i.e., during the peak pressure phase).

Phenomena associated with the blowdown and refill phases of a DECLG LOCA are not unique to AP600. Those phenomena exist in current pressurized water reactors (PWRs). Therefore, these scaling comparisons focus on test validation to represent the peak pressure and long-term time phases, the time when the AP600 PCS performance validation requires unique test results.

The detailed breakdown of individual pi groups shows that during all the phases of a DECLG LOCA, phenomena associated with the drops, pools, chimney, and baffle are not important and can therefore be neglected since the pi group numerical values are of order less than 0.1. The only pi groups of any significance are those associated with the solid internal heat sinks and the shell. However, these heat sinks become saturated prior to the time when the peak pressure occurs. Therefore, only the pi groups identified as containment or shell are calculated for the AP600 plant and LST.

The pi groups were calculated with the transport equations developed for scaling for both the LST and AP600. The calculation corresponded to conditions in AP600 expected at 4000 to 5000 sec. into the transient. The results of the energy scaling comparison between the LST and the AP600 plant are summarized in Table E-9. The transient pi group $\pi_{e,t} = 0$, since $d(mu)^*/dt^* = 0$; the containment atmosphere is in a quasi steady-state condition.

The dominant shell energy phenomena are condensation on the inside of the shell, $\pi_{e,fg,ns}$, and evaporation on the exterior of the shell, $\pi_{e,fg,esx}$. Table E-9 shows the dominant phenomena (condensation and evaporation) compare favorably. The shell energy phenomena for subcooled and dry shell compare well as predicted, but as actually operated, the comparisons to test date are not as close. Although the subcooled and dry pi values, $\pi_{e,q,nsx}$ and $\pi_{e,q,sex}$, do not compare quite as well as condensation and evaporation, the former are second order phenomena in both the plant and test, so do not invalidate the use of the test data.

Table E-9 Energy PI Group Comparison for AP600 and the LST

Pi Group	Predicted at 41 psia		LST Measured
	AP600	LST	
$\pi_{e,t}$	1.24	1.24	1.22
$\pi_{e,brk}$	1.00	1.00	1.00
$\pi_{e,f,wtk}$	0.00	0.00	0.00
$\pi_{e,q,ns}$	0.02	0.02	0.03
$\pi_{e,fg,ns}$	0.91	0.93	0.90
$\pi_{e,if,ns}$	0.08	0.06	0.08
$\pi_{e,q,nsx}$	0.13	0.18	0.09
$\pi_{e,q,sex}$	0.13	0.15	0.09
$\pi_{e,fg,esx}$	0.67	0.62	0.74

The scaling comparisons permit the conclusion that the scaled LST represents the dominant internal and external energy transport processes with sufficient accuracy for use to validate phenomenological models and the AP600 evaluation model during quasi-steady (long-term) operation.

Differences and Distortions between the LST and AP600

Prior to using data from the LST to represent some phenomena of AP600, it is necessary to identify the differences between the LST and AP600. Differences can be geometric or thermal-hydraulic parameters that are not prototypic. The differences are then evaluated as to whether they constitute *distortions* that must be considered when the LST data is applied to AP600. A difference becomes a distortion if it noticeably alters the phenomena in the test facility. Features of the LST that differ from AP600, the concern for each difference, and whether the difference constitutes a distortion are listed in Table E-10.

Table E-10 LST Features That Differ from AP600

Difference	Concern	Distortion
Break Source Superheat	Condensation correlation and pressurization are not prototypic because more thermal energy was input.	No
Diffuser used for break source	The actual break is a pipe break with a high velocity jet.	No
No Downcomer	Lack of downcomer may influence heat and mass transfer	No
Riser Scaled 1/4	The riser heat and evaporation mass transfer are biased because the 3-inch riser width is 1/4 scale rather then 1/8 scale, as is the remainder of the test.	Yes
Fan Forced Riser Air Flow	The fan provides a forced air flow instead of the natural circulation air flow.	Yes
No Circulation Below Deck	The above/below-deck noncondensible distribution makes the test results inapplicable.	Yes
External Water Flow too High	The external water flow rate removes too much energy by its subcooled heat capacity.	No
External Water Coverage was too high	The water coverage was controlled artificially, rather than according to stability. The excess flow rate made the water more stable than it should have been.	No
External water flow was established before break	Cold water was not applied to a hot surface.	No
Internal heat sinks not prototypic	The internal concrete, steel, and pools are not represented.	Yes
External water flow oscillation	Oscillations in the external water flow rate affected the cooling and water coverage	Yes
Crane rails not the same	Internal liquid film is different	No
External water not applied by weirs	External water coverage and stability are different	No
Condensate drained out	There was no break pool to interact with the atmosphere in the test	No

In conclusion, there are several distortions associated with the LST representation of AP600. Those distortions are recognized and taken into account. The distortions do not prevent the use of the LST results to validate the high-ranked phenomena of condensation mass transfer and liquid film stability and coverage. The temperature and concentration measurements from the LST provide data to understand and bound stratification in the AP600 evaluation model. Heat transfer measurements from tests with no external water provided data to validate dry heat transfer to the riser. In addition, the steady-state and transient LST are used to validate predictions of the scaling equations and the evaluation model, and selected segments of the LST are scaled to represent portions of the dP/dt behavior of AP600.

Executive Summary References

*1. "AP600 Standard Safety Analysis Report," Section 6.2, June 26, 1992, Westinghouse Electric Corporation.

2. M. J. Loftus, D. R. Spencer, J. Woodcock, "Accident Specification and Phenomena Evaluation for AP600 Passive Containment Cooling System," WCAP-14811, Westinghouse Electric Corporation.

*3. D. L. Paulsen, et. al., "WGOTHIC Code Description and Validation," WCAP-14382, May 1995, Westinghouse Electric Corporation.

*4. D. L. Paulsen, et. al., "WGOTHIC Application to AP600," WCAP-14407, September 1996, Westinghouse Electric Corporation.

5. NUREG/CR-5809 EGG-2659, "An Integrated Structure and Scaling Methodology for Severe Accident Technical Issue Resolution," INEL, EG&G Idaho, Inc.

6. W. Wulff, "Scaling of Thermohydraulic Systems," BNL-62325, May 1995, Brookhaven National Laboratory.

7. Letter, N. J. Liparulo (Westinghouse) to R. W. Borchardt (US NRC), "AP600 Passive Containment Cooling System Preliminary Scaling Report," NTD-NRC-94-4246, July 28, 1994. (Superceded by WCAP-14845).

8. D. R. Spencer, Scaling Analysis for AP600 Passive Containment Cooling System," WCAP-14190, October 1994, Westinghouse Electric Corporation. (Superseded by WCAP-14845).

9. Letter, B. A. McIntyre (Westinghouse) to T. R. Quay (USNRC), NSD-NRC-96-4762, July 1, 1996, D. R. Spencer, "Scaling Analysis for AP600 Containment Pressure During Design Basis Accidents," (Superseded by WCAP-14845).

10. B. Metais and E. R. G. Eckert, *Journal of Heat Transfer*, **86**:295 (1964).

11. F. Kreith, *Principles of Heat Transfer*, 1965, International Textbook Company.

12. W. Wulff, "Integral Methods for Simulating Transient Conduction in Nuclear Reactor Components," *Nuclear Engineering and Design* 151 (1994) 113-129.

*13. R. P. Ofstun, "Experimental Basis for the AP600 Containment Vessel Heat and Mass Transfer Correlations," WCAP-14326, March 31, 1995, Westinghouse Electric Corporation.

14. F. P. Incropera and D. P. DeWitt, *Fundamentals of Heat and Mass Transfer*, Second Edition, John Wiley & Sons.

15. W. A. Stewart and A. T. Pieczynski, "Tests of Air Flow Path for Cooling the AP600 Reactor Containment," WCAP - 13328, 1992, Westinghouse Electric Company.

16. K. R. Chun and R. A. Seban, "Heat Transfer to Evaporating Liquid Films," *Journal of Heat Transfer*, November 1971.

17. WCAP-13307, "Condensation in the Presence of a Noncondensible Gas - Experimental Investigation," Westinghouse Electric Corporation.

* One or more sections of report will be revised as a result of outstanding NRC open items.

PREFACE

This document presents the scaling evaluations performed to support the passive containment cooling system design basis accident (PCS DBA) evaluation model. This document is one of the primary reports (Tables 1 and 2 of Reference [1]) that support the PCS DBA evaluation model. The other primary reports are the SSAR[2], the PIRT report[3], the WGOTHIC code description and validation report[4], and the evaluation model application report[5]. Test data reports, test analysis reports, and phenomenological model reports are incorporated into the primary reports by reference. Although the focus of this report is to develop the scaling laws for AP600 PCS performance and to scale the tests, this preface describes how the scaling analysis fits into the overall program.

Background

The evaluation model for the PCS DBA has been developed using elements of scaling (top-down modeling of the integrated components), testing, and analysis (bottom-up phenomenological models and evaluations). The results have been used to identify bounding models and input values for use in the DBA evaluation model. The results of the evaluation model provide conservative predictions of design basis transient pressure and temperature response for the containment.

The PCS DBA methodology has followed an approach that can be organized into four elements as shown in Figure P-1. The elements include tasks which together provide a structured, traceable, and practical method for

- Specifying the scenario
- Identifying and ranking phenomena important to the transient
- Evaluating data and scale effects
- Documenting and validating the computer code
- Assessing margins and uncertainties
- Developing and applying the evaluation model

The process is represented as a once-through flow diagram for simplicity. The actual process followed includes iterations between the various tasks. For example, to better represent the observations of the large-scale test (LST) dome temperature distribution due to the subcooling of the liquid film applied to the LST, the initial WGOTHIC code version used in 1992 was augmented by the addition of a model for convective heat transport for the liquid film.

Review by representatives of industry, academia, and regulatory agencies were incorporated into the process. The end result is documentation that describes the PCS DBA evaluation model and its bases in an auditable, traceable manner. Following is a brief description of the four major process elements.

Element 1 Determine AP600 PCS Modelling Requirements

The PCS DBA methodology development process began with a review of the AP600 design and DBA scenarios and an identification of phenomena important for AP600 containment pressurization. This review identified several separate effects tests (SETs) to investigate specific phenomena such as the liquid flow over the outside of the containment shell, and

condensation and evaporation mass transfer. In addition, integral effects tests (IETs) at two different scales were also identified to examine the integrated heat and mass transfer behavior of the PCS. The need for such tests was recognized and testing was initiated in the late 1980's. Table P-1 was used to identify the containment phenomena unique to AP600 and the tests required to validate models of those phenomena. From this review, the Westinghouse-GOTHIC (W GOTHIC) computer code was selected as the best available tool to evaluate containment pressure.

A phenomena identification and ranking table (PIRT) is developed to identify the key thermal-hydraulic phenomena which govern the transients of interest. To allow definition of the relevant phenomena, plant design parameters and design basis scenarios are first defined. The PIRT[3] then ranks phenomena according to their relative importance to the particular transient phase of interest. The PIRT process included input and review by representatives of academia, cross-functional Westinghouse technical reviews, and regulatory authorities. The bases for high, medium, and low rankings are documented with the PIRT. From the PIRT, evaluation model requirements and approaches to address phenomena can be defined. A key result of the PIRT is that the dominant phenomenon for transferring energy from the containment is mass transfer – condensation on the inside and evaporation on the outside. Phenomena ranked high or medium during any accident phase are investigated, and methods to bound uncertainties are developed (see Element 3 below). Phenomena with a low ranking do not significantly influence the containment pressure response; thus, models which capture the gross behavior are sufficient, and where justifiable, a low ranked phenomenon may be neglected entirely. Evaluation model features are defined from the PIRT. Section 2 summarizes the PIRT high and medium ranked phenomena and the approach that is used to address each.

The WGOTHIC computer code was selected, upgraded, and frozen to allow explicit modeling of many of the phenomena identified in the initial review. As the scaling analysis and testing programs progressed, code upgrades to better model experimental results were completed according to guidelines consistent with life-cycle management identified in NQA 2a Part 2.7. Extensive hand calculations and spreadsheets were used to verify correct programming of the upgrades as documented within the Westinghouse QA program. Documentation of the code used in the evaluation model has been issued[4,6,7,8].

Table P-1 Containment Processes Used to Initially Define Test Program

Containment Process	AP600 Uniqueness with Respect to Westinghouse Plants?	Containment Validation - Does it Exist?	AP600-Specific Validation Needed?	Tests Identified
Evaporative film cooling	Yes	No	Yes	PCS tests, 1/8 scale tests, heated plate tests
Liquid film distribution on containment	Yes	No	Yes	Film flow experiments to investigate the water distribution: - heated plate tests - large-scale film flow coverage tests - 1/8 scale tests
Condensation, with noncondensibles	No	Yes, not AP600-specific	Yes	CVTR, University of Wisconsin, literature
Effect of hydrogen on containment heat transfer	No	Yes, not AP600-specific	Yes	1/8 scale test
Air cooling of steel shell, natural convection	Yes	No	Yes	A large-scale test to simulate air passage hydraulic characteristics
Internal circulation patterns in containment, Stratification	No	Yes, not AP600-specific	Yes	1/8 scale test - stratification; International tests at large scale (HDR, NUPEC) for circulation
Effects of buildings and wind velocity on air flow over steel shell	Yes	No	Yes	Wind tunnel tests with building effects and site effects. Literature for effluent recirculation

Element 2 Assess Phenomena Models and Code Capabilities with Tests

Scaling has been used to support the PCS DBA evaluation model as summarized in Figure P-2. The PCS test program includes SETs[5,9], as well as an LST[10], that provided data for simultaneous external evaporation and internal condensation in an integral setting. A scaling evaluation identifies the effects of facility scales and differences and distortions between the AP600 and tests, and provides insight into the AP600 PCS system performance. Scaling results also have been used to confirm PIRT rankings. Scaling also identified the appropriate non-dimensional parameters for phenomena and AP600 ranges. The LST was not designed to simulate a particular AP600 transient response from beginning to end. Rather, the LST varied boundary conditions over significant portions of the AP600 range to gain insight into the physics, confirm the selection of mass transfer correlations that were based on smaller scale tests, and to examine the performance of the WGOTHIC computer code in modeling AP600 phenomena.

Where the LST does not well represent the AP600, other data and scaling considerations were used together with bottom-up phenomena modelling to develop a bounding approach. Phenomena evaluations have been used to assess phenomena importance, develop correlations, and identify bounding approaches. Such phenomena evaluations include heat and mass transfer correlation development[9], water coverage on the external containment shell (Ref 5, Section 7), and mixing and stratification effects on mass transfer inside containment (Ref 5, Section 9), as well as specific phenomena evaluations used to assess PIRT phenomena such as forced convection and radiation heat transfer in the annulus. Results of phenomena reports have been factored into the PIRT.

The results from the following tests were used to assess and validate the phenomena important in the AP600 containment:

- Heated Flat Plate Test performed at Westinghouse Science and Technology Center (STC)
- Wind Tunnel Tests performed at Boundary Layer Wind Tunnel Laboratory of the University of Western Ontario
- Condensation Tests performed at University of Wisconsin
- Air Flow Path Tests performed at Westinghouse STC
- Water Film Formation Tests
- Water Distribution Tests performed at Westinghouse Waltz Mill
- Small-Scale Integral PCS Tests performed at Westinghouse STC
- Large-Scale Integral PCS Tests (LST) performed at Westinghouse STC

The first six test series represent the SETs and the last two test series represent the IETs. An overview summary of these tests and a cross-reference between phenomena and test reports may be found in Reference 3. A listing of test reports issued for AP600 Design Certification has been issued[11].

In addition to the Westinghouse-sponsored tests, the evaluation of AP600 containment phenomena was supplemented with test data available in the open literature. These included the Hugot heated, parallel, vertical, isothermal plate tests; the Eckert and Diaguila heated vertical tube tests; the Siegel and Norris heated, parallel, vertical flat plate tests; and the Gilliland and Sherwood Evaporation tests. These tests, as described in Reference 9, provided additional data to validate models for convective heat and mass transfer in AP600.

The PCS test data and other data from the literature were used to provide input to code validation[4]. The lumped parameter codes oversimplify the flow field by assuming a homogeneous mixture exists within each node. Since lumped parameter cannot resolve gradients within a node, effects such as stratification have been addressed external to the code to quantify the effects on AP600 containment pressure response. The use of the relatively large lumped parameter nodes in the AP600 evaluation model also overexpands an entering jet, leading to two competing effects on containment pressure calculation - overprediction of velocity and underprediction of steam concentration above the operating deck. The competing effects have been bounded (Reference 3, pages 8-9) by utilizing only free convection on the inside of containment, which effectively eliminates the non-conservative velocity. This leaves only the underpredicted above-deck steam concentration which is itself conservative with respect to PCS heat removal.

Comparisons with LST data were also performed with calculations using the distributed parameter WGOTHIC formulation. The more detailed distributed parameter model (Reference 4, Appendix A) better represents phenomena, more closely matches the LST data, and helped confirm that phenomena occurring in the LST had been identified.

Element 3 Assess Uncertainties and Develop Bounding Modeling Approaches

The results of scaling, testing, and code validation were used to establish a bounding analysis approach for each of the PIRT phenomena. Results of code validation and assessment of model uncertainties were used to develop a method of applying the WGOTHIC lumped parameter formulation to create a bounding DBA evaluation model using fixed noding. Sensitivity calculations were performed to gain insight into the influence of important parameters on the predicted pressure response. A key aspect of the evaluation model is that phenomena that are not part of the code calculation or are not well-represented within the code are evaluated separately and bounded by applying conservative boundary conditions or introducing biases into the evaluation model, as summarized in Section 2.

Element 4 Perform DBA Calculations and Compare to Success Criteria

The evaluation model was developed as described above to produce conservative, bounding pressure transients for each postulated accident. The acceptance criteria are that the peak pressure must remain below the design pressure of 45 psig, and the pressure at 24 hours must be less than 1/2 of the design pressure. Road maps (Ref. 5, Tables 2-3 and 2-4) that address each phenomenon identified in the PIRT show:

- Relevant model in the code
- Test basis
- Report references
- Summary report conclusions
- Applicability of LST

- Validation basis summary
- How validation results are used
- How uncertainty is bounded

This report documents the scaling evaluation performed for the AP600 DBA response, and fits within the AP600 PCS DBA licensing documentation as depicted in Figure P-3. The primary purpose of this report, as discussed in Element 2 above, is to develop scaling relations, apply the results to determine appropriate non-dimensional groups for assessing the effects of scale, and to assess the applicable test databases for application to AP600.

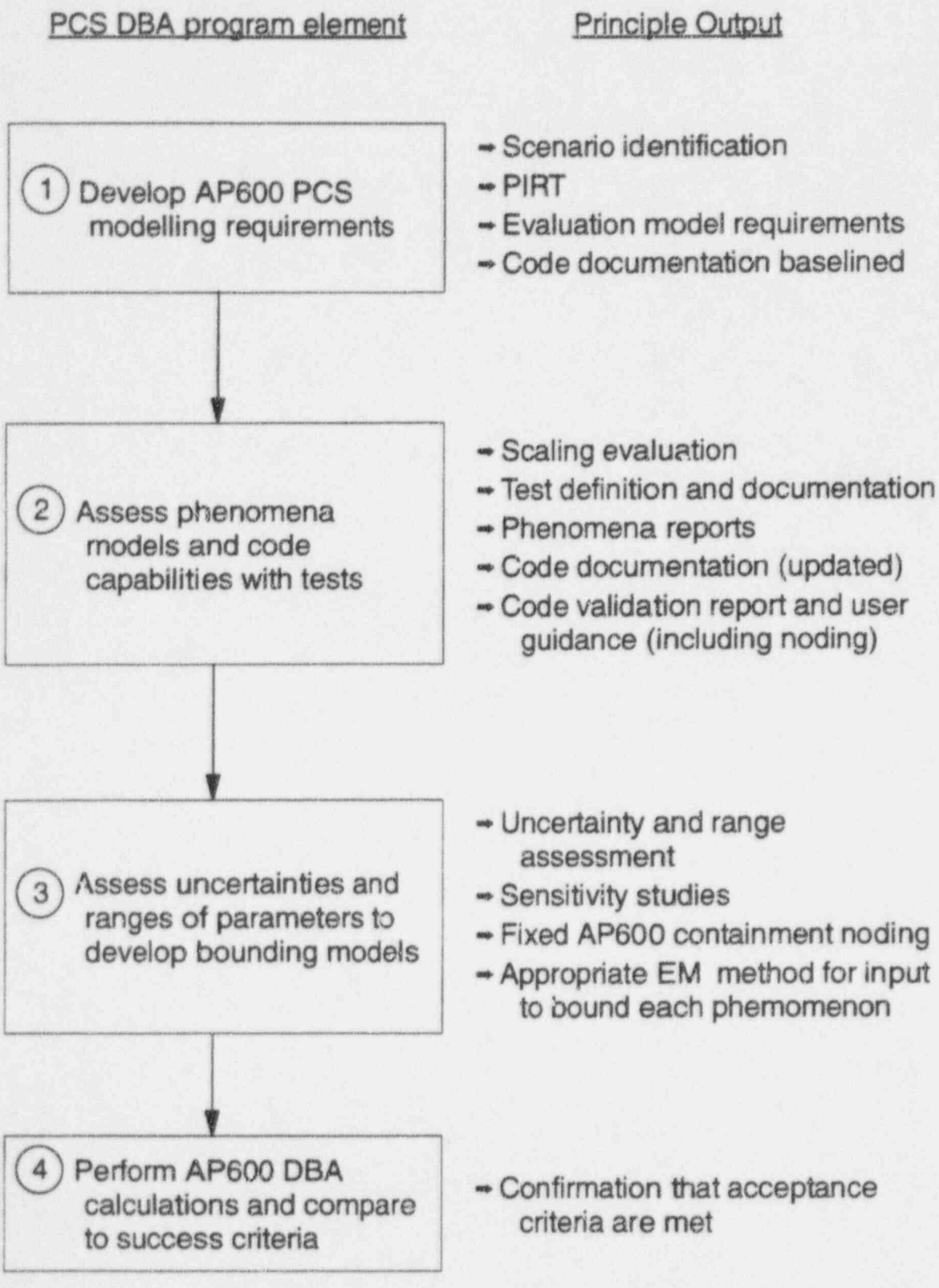

Figure P-1 PCS Test and Analysis Process Overview

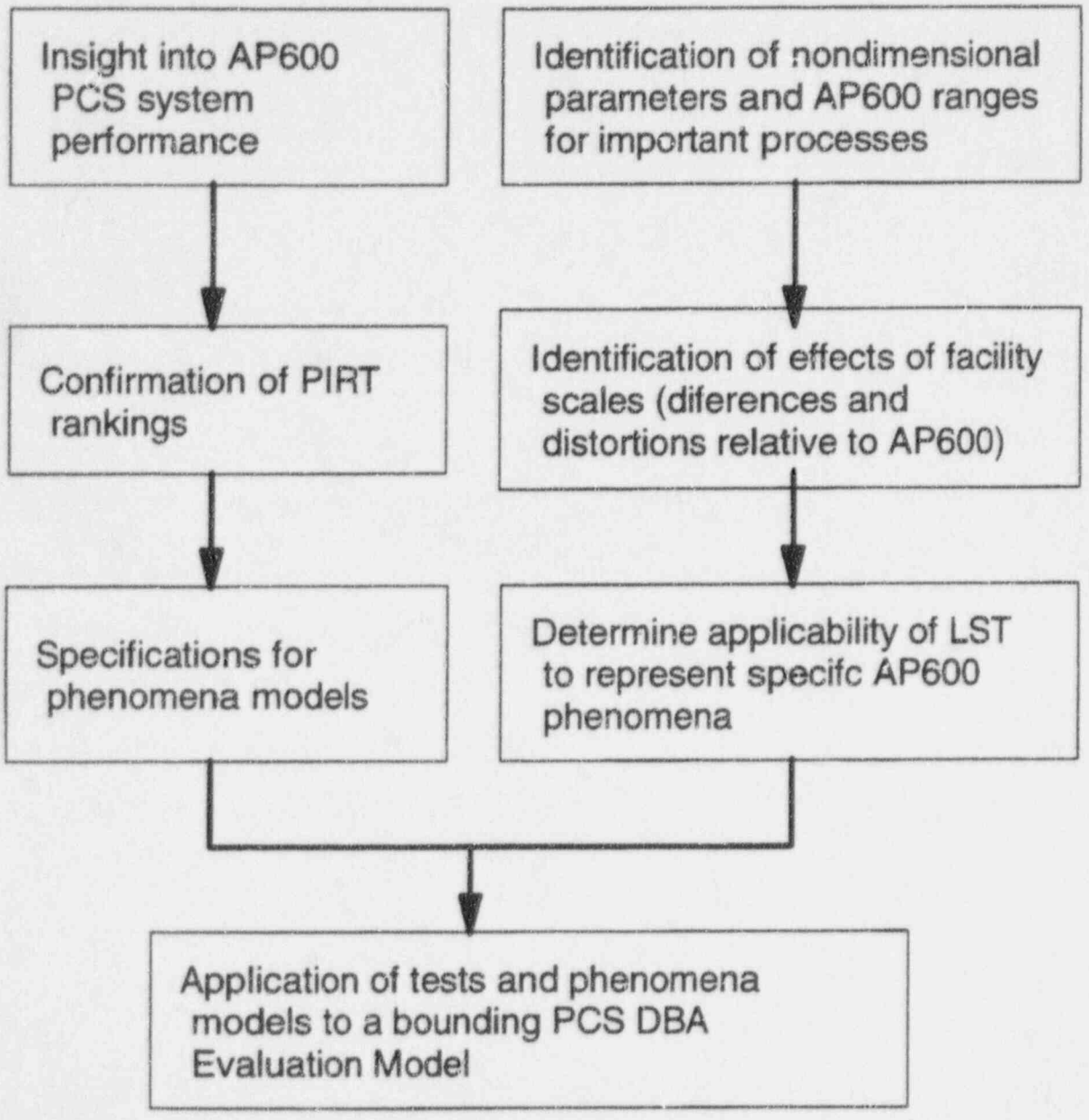

Figure P-2 PCS Scaling Role in PCS DBA

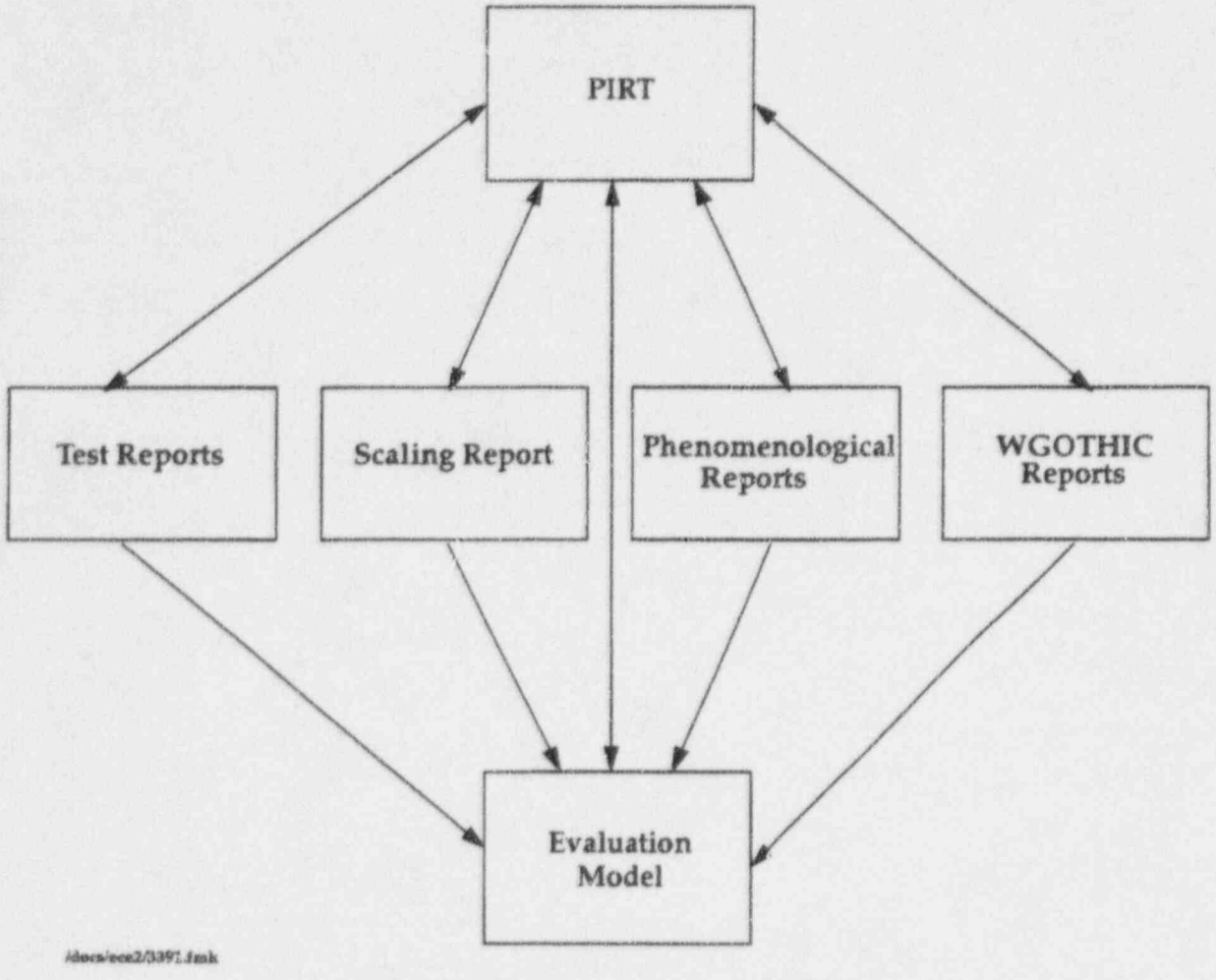

Figure P-3 **Relationship Between AP600 PCS PIRT, Testing, Scaling, Analysis, and Evaluation Model**

1 INTRODUCTION

This report was prepared to support design certification of the Westinghouse AP600. This report presents the scaling analysis for pressurization of the AP600 containment. The scaling analysis was performed to identify the phenomena necessary to be modeled for accurate predictions of pressure within the AP600 containment during a design basis accident (DBA) and to permit a scaled comparison of the supporting separate effects (SETs) and integral effects tests (IETs) to the AP600 performance.

The scaling analysis presented in this document generally follows the scaling methodology for severe accidents presented in NUREG/CR-5809[12]. The passive containment cooling system (PCS) air flow path momentum scaling is based on the example presented by W. Wulff[13] for scaling interconnected regions.

Containment pressure is the variable of primary interest for evaluating whether the PCS maintains containment pressure below the design limit during DBAs. The pressure rate of change (RPC) equation is developed by combining rate of change equations for containment gas mass and energy with the gas equation of state. The containment gas volume is coupled by energy transfer equations to internal heat sinks and the external PCS. The equations are made dimensionless, and normalized to produce the pi groups required to scale containment pressure. The variables selected for AP600 scaling and the reference normalizing parameters are presented in Table 1-1. The pi groups are one of the analytical tools used to scale SET and IET phenomena to AP600.

Table 1-1 Parameters Selected for Scaling AP600

Scaled Parameter	Location	Normalizing Parameter
Mass Flow Rate	Inside Containment	Break mass flow rate, $\dot{m}_{g,brk,o}$
Energy Transfer Rate	Inside and Outside Containment	Break enthalpy flow rate, $\dot{m}_{g,brk,o}\Delta h_{g,brk,o}$
Conductance	Inside and Outside Containment	Coated shell conductance, h_{sh}
Pressure	Inside Containment	Break flow work rate, $\gamma_o(1+Z^T)/(\gamma-1)_o\dot{m}_{g,brk,o}P_{sim}/\rho_{sim}$
Momentum	Inside Containment	Buoyancy, $\Delta\rho gH$
Momentum	PCS Air Flow Path	Buoyancy, G_o

The dimensionless groups needed to scale jet and plume momentum for their effects on stratification in the containment volumes are presented and relationships between AP600 and

the LST are discussed. The evaluation of stratification in compartments, and circulation between compartments, on AP600 are documented in Reference 5, Section 9.

The momentum equation for the air flow through the PCS air flow path (downcomer, riser, and chimney) are developed, made dimensionless, and normalized to produce the pi groups required to scale momentum in the PCS air flow path.

The pi group values for the AP600 phenomena are evaluated, thereby providing a numerical basis for the importance of the dominant phenomena (transport processes and components) and validation of the PIRT rankings.

Scaled data from the SETs and IETs are compared to the scaling and phenomenological equations. The scaled tests are compared to AP600 to justify the use of the tests for evaluation model validation.

The rate of change equations for the containment gas mass, energy, and pressure are derived based on simple assumptions, using thermodynamic relationships, equation of state, and control volume conservation equations. The rate of change equations represent a single gas volume that is coupled to multiple heat sinks. The containment volume is assumed well-mixed, except for the dead-ended compartments. The above-deck region is nearly well-mixed during and after blowdown due to the entrainment into the plume of more than 10 times its volumetric flow rate. The effect on heat sink utilization of deviations from a uniform vertical air/steam concentration distribution are shown in the mixing and stratification report to be minor.

The mixing and stratification report examines a range of break source momenta and directions and shows that in all cases circulation between compartments maintains all but the dead-ended compartments at, or above the well-mixed steam concentration, and the above-deck region within 2 or 3 percent of the well-mixed concentration of approximately 60 percent steam. Although containment is not perfectly mixed, the deviations from well-mixed are small enough that the conclusions of the scaling analysis are valid.

The Westinghouse containment scaling analysis has evolved through a series of issued documents, presentations, and reviews. Extensive input has been received from the USNRC and the ACRS Thermal Hydraulics Subcommittee.

- Westinghouse issued Passive Containment Cooling System Preliminary Scaling Report[14], July 1994.

- Westinghouse presentation to USNRC, AP600 Passive Containment Cooling System (PCS) Scaling - Iteration 1 Report Review Kickoff Meeting, July 26, 1994.

- Westinghouse issued Scaling Analysis for AP600 Passive Containment Cooling System[15], October 1994.

- Westinghouse presentation to ACRS Thermal Hydraulics Subcommittee, March 29, 1995.

- NRC presentation of (LASL) review comments on Containment Scaling, June 20-22, 1995.

- NRC issued requests for additional information that are answered in this document.

- Westinghouse issued Scaling Analysis for AP600 Containment Pressure during Design Basis Accidents[16], June 1996.

- NRC requested clarification of information contained in the June 1996 scaling report.

2 DOMINANT PHENOMENA

The transport processes and components that affect containment pressure were identified and ranked according to importance in the PIRT. The phenomena ranked high and medium are the ones that receive more detailed treatment and validation, and should be addressed in the evaluation model. The phenomena ranked high or medium importance are listed in Table 2-1. The phenomena are organized according to whether they are represented by pi groups in the scaling analysis or whether the phenomena appear as parameters in pi groups. Those that appear as parameters are indented in the first column of the table, and identified as parameters in the column headed "PI Group." The high- and medium-ranked phenomena evaluated in this scaling analysis are identified in the column headed "Where Addressed." Many low importance phenomena are also addressed in this scaling analysis. High ranked phenomena not evaluated in this scaling analysis are briefly discussed and referenced to source documents at the end of this section.

The following high ranked phenomena are addressed by separate, detailed evaluations in which AP600 parameters were ranged to derive bounding inputs for the evaluation model.

- Mixing and Stratification - Mixing in AP600 can be characterized by stratification within compartments and circulation between compartments. The scaling of jets and plumes, and the relationship of large-scale test (LST) stratification data to AP600 operation is presented in Section 6.5 of this document. The application of those data to AP600 is presented in Reference 5, Section 9. The circulation rates of air and steam between interconnected gas volumes (compartments) is addressed in Reference 5, Section 9.

- Intercompartment Flow - The mass flow rate of air and steam between interconnected gas volumes (usually referred to as circulation) affects heat sink utilization and is also addressed in the mixing and stratification report.

- Source Fog - Source droplets (fog) occur during blowdown and increase the steam source density, thereby reducing its buoyancy. However, during blowdown, mixing inside containment is momentum- and pressure-dominated, not buoyancy-dominated. After blowdown, drops do not occur in the break source, so the post-blowdown source buoyancy is not affected. The effect of blowdown-generated drops on post-blowdown circulation is addressed in the mixing and stratification report. However, the effect of droplets as heat sinks is addressed in this scaling document.

Table 2-1 Phenomena Identification and Ranking Table - Summary of High and Medium Ranked Phenomena

Phenomenon *	Effect on Containment	Pi Groups	Where Addressed
Break Source Mass and Energy (1A) and Liquid Flashing (1E) and Evaporation (5B)	The only mass and energy source for containment pressurization	$\pi_{p,g,brk,enth}$ $\pi_{p,g,brk,work}$ $\pi_{p,work,d}$ $\pi_{p,work,p}$	Scaling Analysis
Gas Compliance (2C)	Stores mass and energy in atmosphere, increasing pressure	$\pi_{p,\tau}$	Scaling Analysis
Initial Conditions Inside (4A, 4B, 4C)	Temperature, humidity, pressure affect noncondensables and energy storage	None	Initial Conditions Ref. 5, Section 5
Containment Solid Heat Sinks (3), Pool (5), Drops (1), and Shell (7)	Store energy (and remove mass from atmosphere) reducing pressure	$\pi_{p,g,i}$ $\pi_{p,work,i}$	Scaling Analysis
Internal Heat Sink Conduction (3D, 5E, 7F) and Heat Capacity (3E, 5A, 7G, 1E)	Limits conduction heat transfer into heat sinks, shell, or pool, and through shell. Stratification in the break pool can affect the effective heat capacity of the pool.	parameter	Scaling Analysis
Heat Transfer Through Horizontal Liquid Films (3C)	Water and noncondensible layers on upward facing horizontal surfaces limit heat and mass transfer to horizontal heat sinks	parameter	Scaling Analysis
Condensation Mass Transfer (3F, 5B, 7C)	The single first-order transport process that removes mass and energy from the containment gas	$\pi_{p,work,i}$	Scaling Analysis
Break Source Direction and Elevation (1B), Momentum (1C), Density (1D), and Droplets (1E)	Direction, elevation, density, and momentum can dominate circulation and affect condensation rate. Existence of droplets in source during blowdown affects the effective source density.	parameter	Mixing and Stratification, Ref. 5, Section 9
Mixing and Stratification (2A)	Intercompartment Flow (Circulation) and stratification can affect the distribution of steam near heat sinks for condensation heat removal. Rising liquid level blocks lower circulation flow paths.	parameters	
Intercompartment Flow (2B)			
Break Pool Flooding Level (5F)			
Source Fog (2D)	Affects circulation and stratification via buoyancy	parameter	

Table 2-1 Phenomena Identification and Ranking Table - Summary of High and Medium Ranked Phenomena (cont.)

Phenomenon *	Effect on Containment	Pi Groups	Where Addressed
Evaporation Mass Transfer (7N)	The first-order transport process that removes mass and energy from the evaporating external shell	$\pi_{e,fg,esx}$	Scaling Analysis
PCS Natural Circulation (9A, 13A)	Convective air flow provides convective heat and mass transfer from containment shell.	parameter	Scaling Analysis
Liquid Film Flow Rate (8A), Water Temperature (8B), Film Stability (8C)	Affects the upper limit for water coverage on the external shell	parameter	Film Stability, Ref. 5, Section 7
Liquid Film Energy Transport (3A, 7E, 7M)	*Inside:* Carries 14 percent of condensation energy to the IRWST and break pool. *Outside:* Absorbs 8 percent of energy rejected by the external shell surface.	$\pi_{e,f,if}$ $\pi_{e,q,ssx}$	Scaling Analysis
Convection Heat Transfer (3G, 7A, 7H, 10A, 10B, 14A)	A second order transport process that removes energy from the containment gas, and from the external shell.	$\pi_{p,q,i}$ $\pi_{e,c,i}$	Scaling Analysis
Radiation Heat Transfer (3H, 7B, 7I)	A second order transport process that removes energy from the containment gas and from the external shell.	$\pi_{p,q,i}$ $\pi_{c,r,i}$	Scaling Analysis
Baffle Conduction (10D) and Baffle Leakage paths (10G)	Conduction through the baffle into downcomer volume and leakage paths can influence the external natural circulation flow rates	None	PIRT Sections 4.4.10D and 4.4.10G

* Indicators in parentheses refer to phenomena in the "Phenomena Identification and Ranking According to Effect on Containment Pressure" table[3].

- Liquid Film Stability - Liquid film stability affects the amount of surface area that can be covered by the PCS cooling water. In AP600, the time constant for heat transmission through the shell is relatively long, so the external surface temperature rises slowly relative to application of cooling water. Once the PCS water supply valve is opened, the water distribution weirs begin to fill and spill, leading to a development time for flow rate, and coverage (spreading of the liquid film) develops as flow develops. Documentation of liquid film stability phenomena as they affect containment pressure performance, and a water coverage model that couples coverage to shell heat flux, is provided in the liquid film stability report (Ref. 5, Section 7). The

model shows that by the time of the peak pressure, approximately 40 lbm/sec is evaporated of the 60 lbm/sec applied.

3 DESIGN, BOUNDARY, AND INITIAL CONDITION INPUT DATA

The system to be analyzed is the AP600 containment, subjected to overpressure DBAs. Sections 1, 2, and 3 of the PIRT describe the plant geometry, the accident sequences, and the phenomena in more detail. The double-ended cold leg guillotine loss-of-coolant accident (DECLG LOCA), and the main steamline break (MSLB) from 30 percent power are the DBAs that produce the highest containment pressure and are the subject of this analysis. The design and boundary conditions for the plant and these accidents follow.

Parameter	Value	Comment
Water Capacities:		
PCS Water Flow Rate	Figure 3-1	
Cold Leg Pipe ID	[ ] a,c	
Main Steamline ID		
IRWST Liquid Volume		
Double-End Cold Leg Guillotine		
Transient Mass Flow Rate	Figure 3-2	Typical DECLG transient
Transient Energy Flow Rate	Figure 3-3	Typical DECLG transient
Transient Pressure and Temp	Figure 3-4	Typical DECLG transient
Main Steamline Break:		
Transient Mass Flow Rate	Figure 3-5	Typical MSLB transient
Transient Energy Flow Rate	Figure 3-6	Typical MSLB transient
Transient Pressure and Temp	Figure 3-7	Typical MSLB transient
Break Pool Water Level and Surface Area	Figure 3-8	Typical DECLG transient
Containment Vessel		
Shell Thickness	1.625 in.	
Externally Cooled Surface Area	52,662 $ft.^2$	
Vessel Internal Free Volume	1,740,944 $ft.^2$	
Steel Heat Sink Surface Area	142,700 $ft.^2$	
Volume	4739 $ft.^3$	
Concrete Heat Sink Surface Area	22,600 $ft.^2$	

Jacketed Concrete Surface Area	46,500 ft.^{2}	
Baffle Thickness	0.12 in.	
Chimney Height	[	a,b
Riser Height		
Downcomer Height		
Vessel Coating	]	
Material Properties	Section 4.7	

The large-scale integral test (LST) provided both SET and IET data that are used to validate phenomenological models used in the AP600 evaluation model, and to scale transient behavior in AP600. The design and test results for the LST are presented in the test data reports[10,17], and the test as-built drawings[18]. Design characteristics of the LST are summarized as follows:

LST Vessel Coating	[	a,b
LST Coating Thickness		
Shell Thickness		
Shell Thermal Conductivity[19]		
External Wetted Surface area		
Vessel Internal Free Volume	]	

Initial conditions for the inside and outside of containment follow. These were determined to be limiting in the sense of producing the highest containment pressure during transients.

Environment, shield building, baffle, chimney, and PCS cooling water temperature	115°F
Environment pressure	14.7 psia
Environment humidity	25%
Containment air, shell, and heat sink temperature	120°F
Containment pressure	15.7 psia
Containment humidity	0%

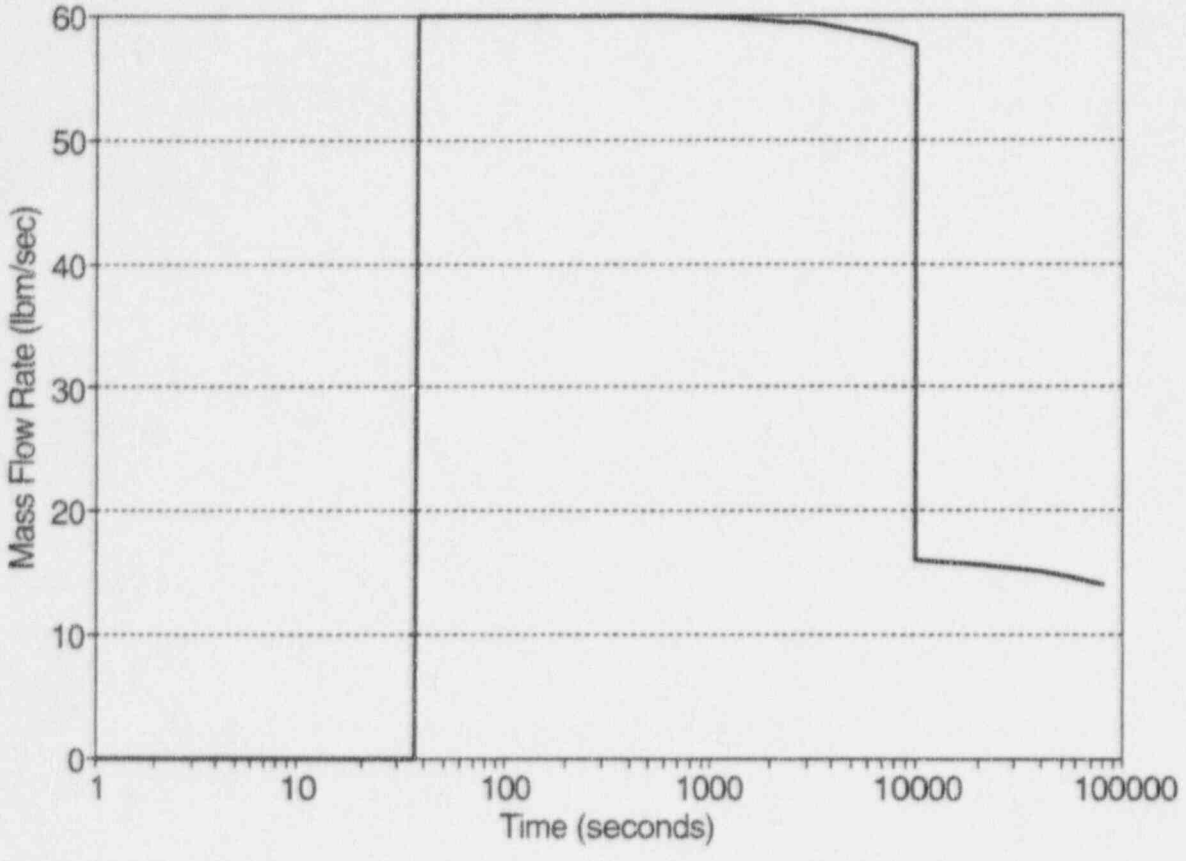

Figure 3-1 PCS Water Flow Rate after Overpressure Signal

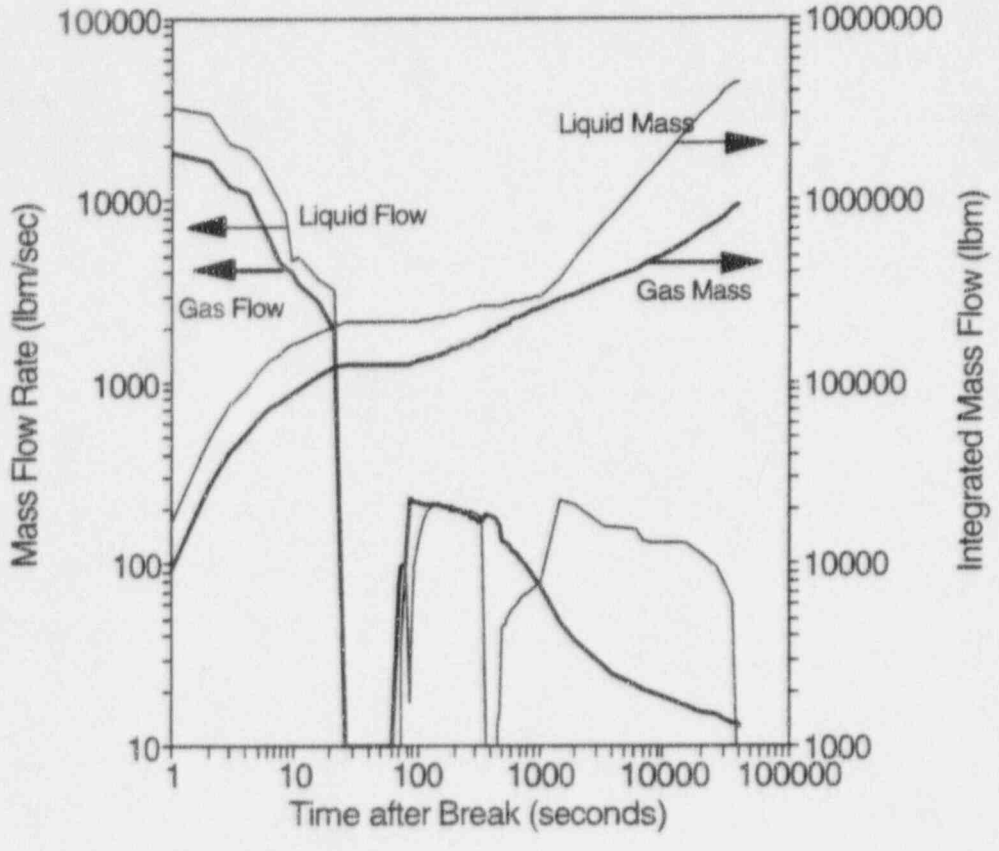

Figure 3-2 Transient Mass Release Rate in AP600 During a DECLG LOCA

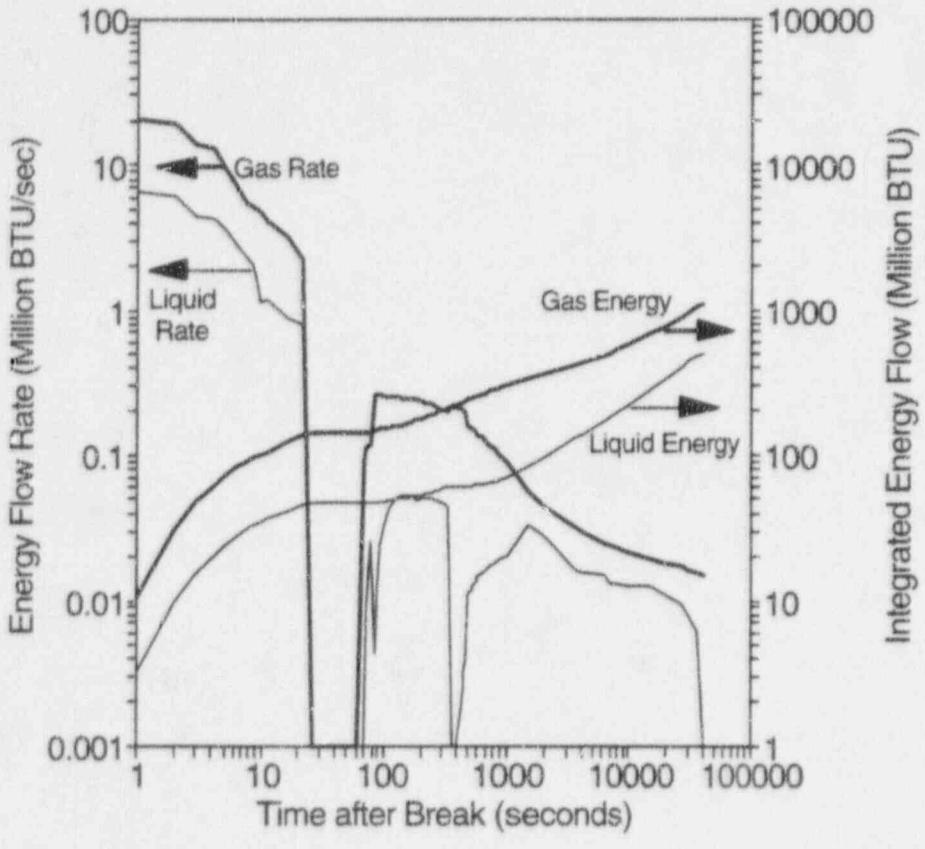

Figure 3-3 Transient Energy Release in AP600 During a DECLG LOCA

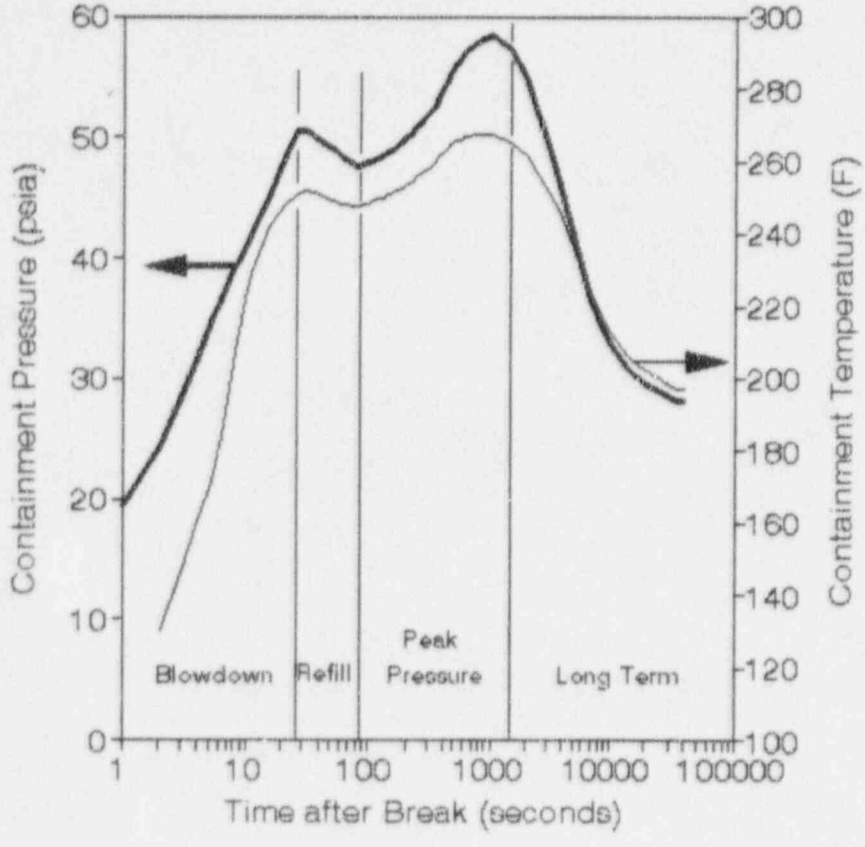

Figure 3-4 **Transient Containment Pressure, Temperature, and Time Phases for a DECLG LOCA in AP600**

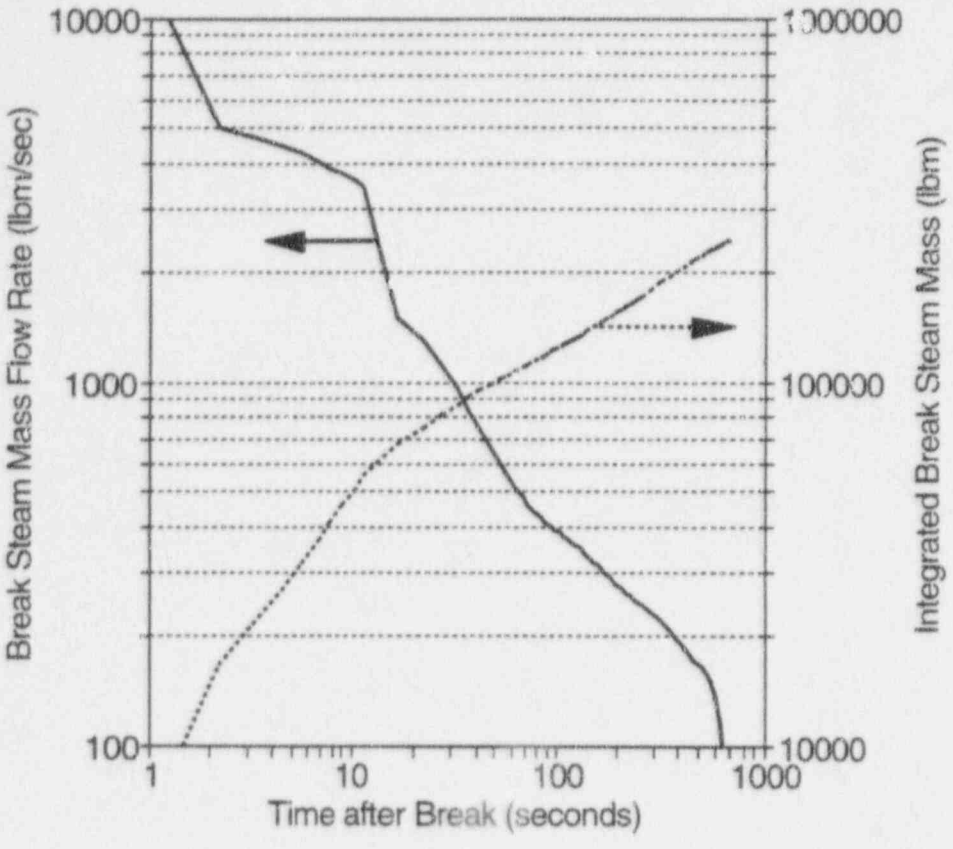

Figure 3-5 Transient Mass Release Rate in AP600 during an MSLB

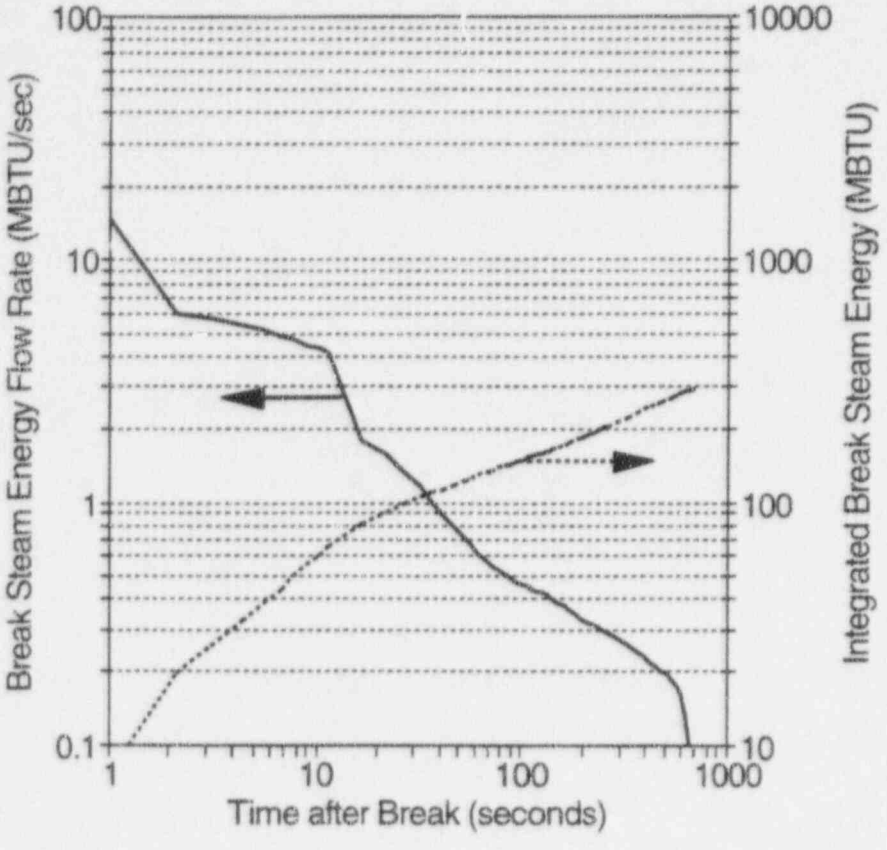

Figure 3-6 Transient Energy Release Rate in AP600 during an MSLB

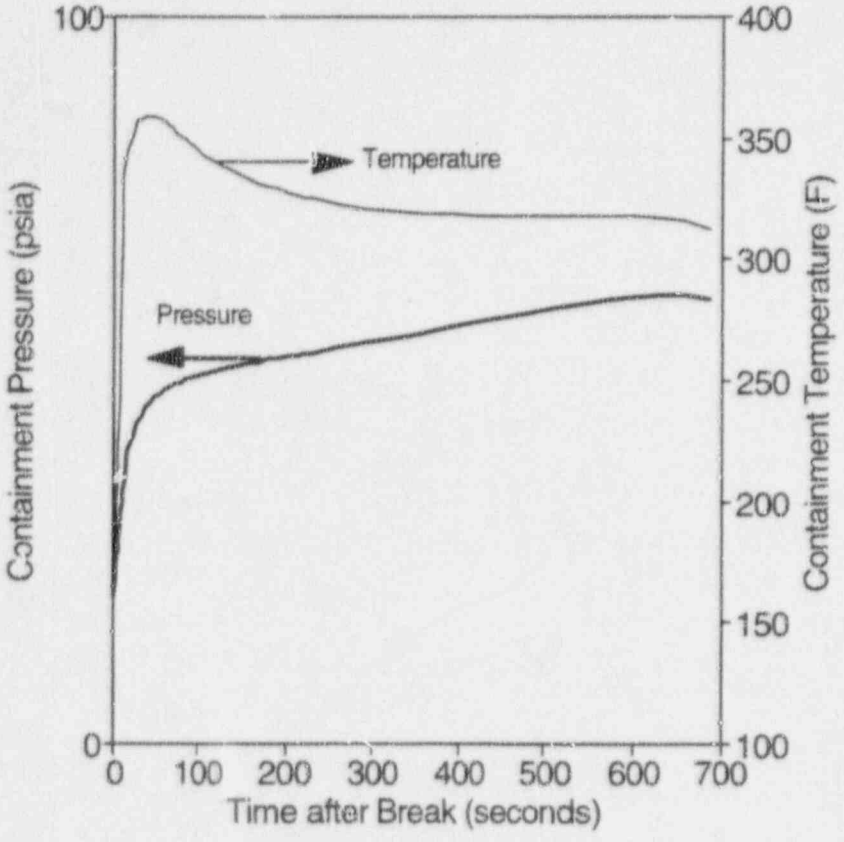

Figure 3-7 Transient Pressure, Average Pressure, and Time Phase for an MSLB Transient in AP600

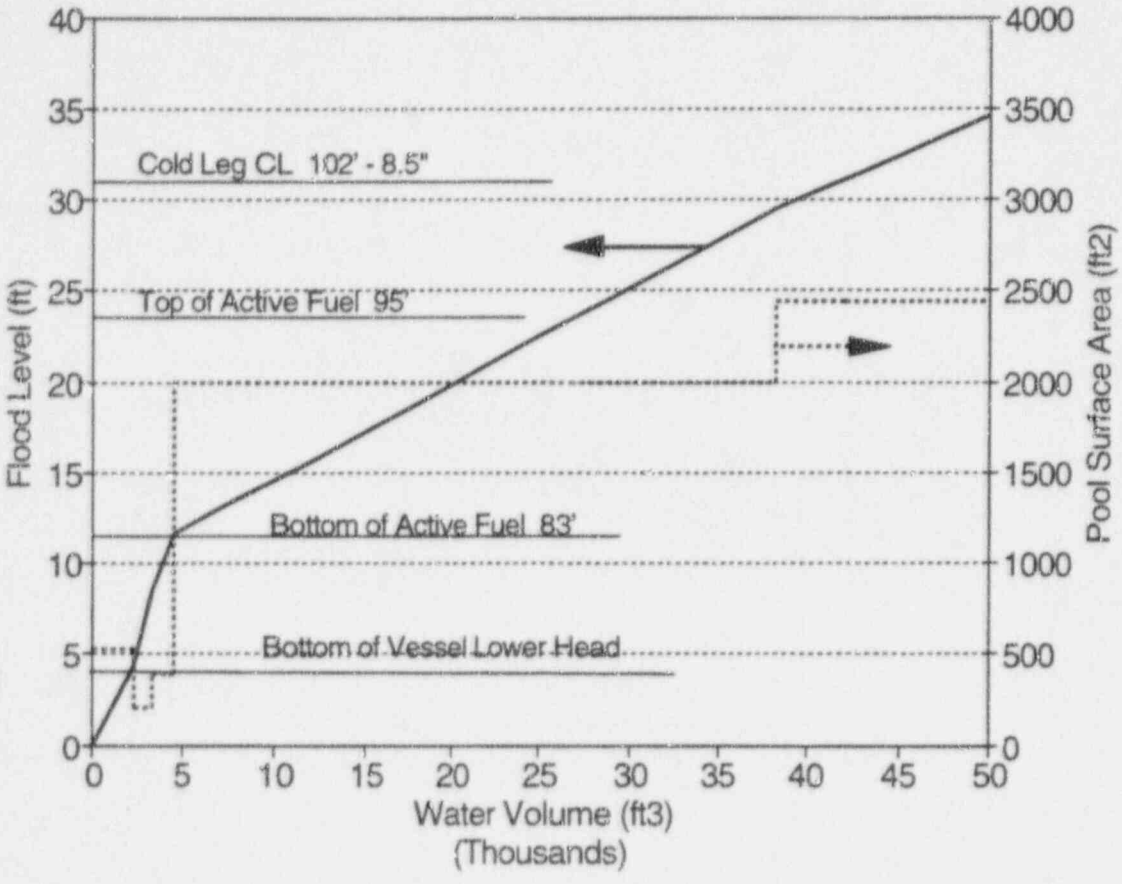

Figure 3-8 Break Pool Water Level and Surface Area in AP600 for a DECLG LOCA

4 CONSTITUTIVE EQUATIONS FOR HEAT, MASS, AND RADIATION TRANSFER

The constitutive relationships for radiation, convection, condensation, and evaporation heat transfer, and for condensation and evaporation mass transfer are presented and formulated in terms of a conductance and a temperature difference. The formulation in terms of conductance and temperature difference facilitates coupling the inside of containment through the shell to the outside, and permits direct comparisons of energy transport coefficients for mass with radiation and convection. Summary comparisons of the correlations selected for convective heat and mass transfer to data, other correlations, and the AP600 range of operation is presented in Section 10.

4.1 RADIATION HEAT TRANSFER

Radiation heat transfer can be written in terms of a conductance and a temperature difference:

$$\dot{q}_r'' = \sigma\varepsilon(T^4 - T_{srf}^4) \quad \text{or} \quad \dot{q}_r'' = h_r(T - T_{srf}) \tag{1}$$

where the conductance is $h_r = \sigma\varepsilon f(T,T_{srf})$ and $f(T,T_{srf}) = (T + T_{srf})(T^2 + T^2_{srf})$. The character ε is the surface emissivity for surface-to-surface radiation, and the product of the emissivity and beam length for radiation from the containment gas to the surface.

4.2 CONVECTION HEAT TRANSFER

The inside of containment is expected to operate in turbulent forced or mixed convection during both the LOCA and MSLB blowdown, and in turbulent free convection after blowdown. However, since insufficient data are available to validate forced or mixed convection models for the inside of containment, the inside of containment is modeled using turbulent free convection throughout the transient. This modeling approach underestimated energy transfer to the shell and heat sinks during blowdown, but is accurate after blowdown as shown by the condensation mass transfer correlation to data in Section 10.1.1.

Turbulent free convection heat transfer is expected for Grashof number (based on height) $> 10^9$. This is the case over all but 2 feet or less of height of heat sinks and the shell, after the first few seconds of the transient. The turbulent free convection correlation underestimates heat and mass transfer at Grashof numbers less than 10^9, so its use is conservative for smaller structures or early time values. The turbulent free convection correlation is shown in Section 10 in a dimensionless form compared to the LST condensation data. The correlation compares well with the data, especially considering that the LST is 1/8 geometric scale and therefore has more of its total height within the 2 to 3 foot height limit for turbulent free convection.

The PCS air flow outside of containment operates over a range of free, mixed, and forced convection heat transfer. The downcomer, riser, and chimney operating points were calculated as described in Section 9.0 and are shown on an Eckert and Metais[20] plot in Figure 4-1. The progression of calculated operating points for the downcomer, riser, and chimney is from blowdown at the lower left point, to refill, peak pressure, and to long term operation at the upper right point. The results from an alternate calculation[21] for a dry riser are also shown. That calculation concluded heat transfer in the riser is turbulent forced convection for shell surface temperatures more than 2°F above the environment air temperature. Figure 4-1 shows the downcomer and riser operate in forced convection, and chimney operation progresses from free to mixed to forced convection. The information presented in the figure supports the selection of the turbulent convection regimes specified for the downcomer, riser, and chimney.

Convection heat transfer can be written in terms of a conductance and a temperature difference:

$$q_c'' = h_c(T - T_{srf}) \tag{2}$$

where the conductance, h_c, is given by one of the following constitutive correlations.

4.2.1 Turbulent Free Convection Heat Transfer

The McAdams correlation was selected[9] for scaling turbulent free convection heat transfer for all surfaces inside containment, horizontal as well as vertical, except for drops:

$$h_c = h_{free} = 0.13\frac{k}{L}(Gr_L Pr)^{1/3} = 0.13\frac{k}{(\nu^2/g)^{1/3}}\left(\frac{\Delta\rho}{\rho}\right)^{1/3} Pr^{1/3} \tag{3}$$

The term $(\Delta\rho/\rho)$ is the difference between the bulk density and surface density, divided by the bulk density. Note that in this form the Grashof number with its length dependence no longer appears and the heat transfer coefficient is dependent only on local properties.

4.2.2 Laminar Free Convection Heat Transfer

Laminar free convection heat transfer is considered for the drops that result from the break liquid during blowdown, because their diameter is so small (~ 10^{-4} ft.) that $Gr_d << 1$. For this case, Kreith[22] presents the correlation for small spheres:

$$h_c = h_{free} = 2\frac{k}{d} \tag{4}$$

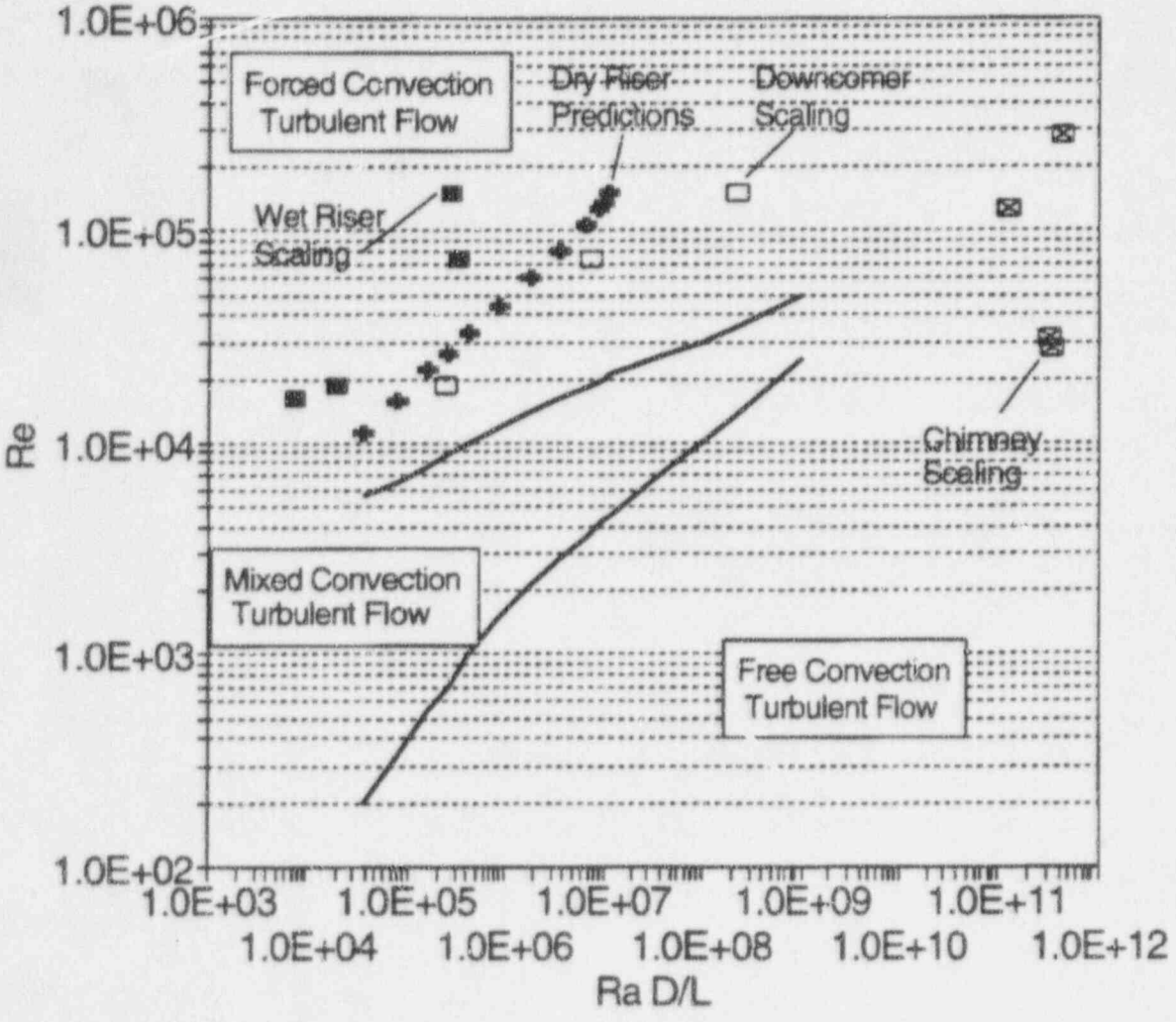

Figure 4-1 **Metais and Eckert Plot Showing the Downcomer, Riser, and Chimney Heat Transfer Regimes for the AP600 PCS**

4.2.3 Turbulent Forced Convection Heat Transfer

The Colburn correlation was selected[9] for turbulent forced convection in a channel:

$$h_c = h_{forc} = 0.023 \frac{k}{d_h} Re_d^{0.8} Pr^{1/3} \quad (5)$$

where the hydraulic diameter is two times the riser width.

On the inside of containment, turbulent forced convection is expected during blowdown, and produces heat and mass transfer rates significantly greater than free convection. However, forced convection is conservatively neglected during blowdown; free convection is assumed. This conservatism results in under-predicted heat sink energy absorption during blowdown, and a small overprediction of containment pressure. The assumption does not change the conclusions of the scaling analysis.

4.2.4 Turbulent Opposed Mixed Convection

Opposed free and forced (mixed) convection exists in the chimney where the PCS natural circulation induces a bulk upward flow that is opposed by the negatively buoyant free convection on the cooler chimney concrete. The correlation for opposed turbulent mixed convection recommended by Churchill[23] is used:

$$N_{mix} = (N_{free}^3 + N_{force}^3)^{1/3} \quad (6)$$

Using the correlations for free and forced turbulent convection, Equations (3) and (5), the mixed convection heat transfer coefficient correlation is:

$$h_{mix} = \frac{k}{D}\left(\frac{(0.13 D_o)^3}{(\nu^2/g)} \frac{\Delta\rho_o}{\rho_o} Pr_o + (0.023)^3 Re_{D,o}^{2.4} Pr_o \right)^{1/3} \quad (7)$$

4.3 CONDENSATION AND EVAPORATION MASS TRANSFER

The mass transfer rate expressions are evaluated and simplified assuming both air and steam are ideal gasses. In AP600 compressibility is limited to approximately $0.97 < Z < 1.0$, where the minimum value corresponds to 40 psia of saturated steam. The assumption that $Z = 1.0$ introduces an error of less than 3 percent and is a significant simplification over the necessary steam table look-up required to quantify Z. Although compressibility is neglected in this application of the equation of state, compressibility has been considered where it is more

significant: the evaluation of the enthalpy rate of change with pressure in the energy and pressure change equations.

Kreith defines the mass flux from the bulk gas to the condensing surface as:

$$\dot{m}'' = k_g M_{stm} \Delta P_{stm} \tag{8}$$

where $\Delta P_{stm} = (P_{stm,bulk} - P_{stm,srf})$. The mass transfer coefficient, k_g is determined from the heat and mass transfer analogy. The heat and mass transfer analogy can be expressed as $Sh/Nu = (Sc/Pr)^{1/3}$, and when rearranged in terms of the mass transfer coefficient:

$$k_g = \frac{h_c P D_v}{\bar{R} T P_{lm,air} k} \left(\frac{Sc}{Pr}\right)^{1/3} \tag{9}$$

where the log-mean air pressure is defined $P_{lm,air} = (P_{air,bulk} - P_{air,srf})/\ln(P_{air,bulk} / P_{air,srf})$. Combining these two equations gives the expression for condensation or evaporation mass flux:

$$\dot{m}'' = \frac{h_c M_{stm} P D_v \Delta P_{stm}}{\bar{R} T P_{lm,air} k} \left(\frac{Sc}{Pr}\right)^{1/3} \tag{10}$$

With the steam density defined $\rho_{stm} = M_{stm} P / \bar{R} T$ the mass flux is:

$$\dot{m}'' = \frac{h_c \rho_{stm} D_v}{k} \frac{\Delta P_{stm}}{P_{lm,air}} \left(\frac{Sc}{Pr}\right)^{1/3} \tag{11}$$

Condensation and evaporation mass transfer are calculated from Equation (11) and the appropriate heat transfer correlation from Section 4.2. Three distinct mass transfer correlations result from the turbulent free, turbulent forced, and laminar free convection heat transfer correlations. For turbulent free convection mass transfer:

$$\dot{m}''_{free} = 0.13 \frac{\rho_{stm} D_v}{(\nu^2 / g)^{1/3}} \frac{\Delta P_{stm}}{P_{lm,air}} \left(\frac{\Delta \rho}{\rho} Sc\right)^{1/3} \tag{12}$$

For turbulent forced convection mass transfer:

$$\dot{m}''_{force} = 0.023 \frac{\rho_{stm} D_v}{d_h} \frac{\Delta P_{stm}}{P_{lm,air}} Re_d^{0.8} Sc^{1/3} \quad (13)$$

For laminar free convection mass transfer to the drops:

$$\dot{m}''_{lam} = 2.0 \frac{\rho_{stm} D_v}{d} \frac{\Delta P_{stm}}{P_{lm,air}} \left(\frac{Sc}{Pr}\right)^{1/3} \quad \text{for small } \Delta T \quad = 2.0 \frac{\rho_{stm} D_v}{d} \frac{dP_{sat}}{dT} \frac{\Delta T}{P_{air}} \left(\frac{Sc}{Pr}\right)^{1/3} \quad (14)$$

The conductances, h_m and h_{mx}, are defined by the energy transfer relationships:

$$\dot{m}''_{cond}(h_g - h_f) = h_m(T - T_{srf}) \quad \dot{m}''_{evap} h_{fg} = h_{mx}(T_{srf} - T_{ri}) \quad (15)$$

4.3.1 Dimensionless Relationships for Data Evaluation

Equations (8) and (12) for free convection can be combined and rearranged in dimensionless form using the Sherwood number definition:

$$Sh_v = \frac{k_{g,o} \bar{R} T_o (\nu^2/g)^{1/3} P_{lm,air,o}}{D_{v,o} P_o} \quad \text{so} \quad Sh_v = 0.13 \left(\frac{\Delta\rho}{\rho}\right)^{1/3} Sc_o^{1/3} \quad (16)$$

The term $(\nu^2/g)^{1/3}$ has the units of length, so by defining the Sherwood number length accordingly, the simple relationship for the Sherwood number presented in Equation (16) results. Note that multiplying both sides of the equation by L, and dividing both sides by the term $(\nu^2/g)^{1/3}$ produces the more familiar form:

$$\frac{k_{g,o} \bar{R} T_o L P_{lm,air,o}}{D_{v,o} P_o} = 0.13 \left(\frac{L^3}{(\nu^2/g)^{1/3}} \frac{\Delta\rho}{\rho}\right)^{1/3} Sc_o^{1/3} \quad \text{or} \quad Sh_L = 0.13 Gr_L^{1/3} Sc^{1/3} \quad (17)$$

Similarly for forced convection, Equations (8) and (13) can be combined and rearranged as:

$$\frac{k_{g,o}\bar{R}T_o D_h P_{lm,air,o}}{D_{v,o}P_o} = 0.023 Re_D^{0.8} Sc^{1/3} \quad \text{or} \quad Sh_D = 0.023 Re_D^{0.8} Sc^{1/3} \tag{18}$$

4.3.2 Gas Mixture Property Correlations

A correlation for the air-steam diffusion coefficient is available to use in the mass transfer correlation[24]:

$$D_v = 0.892 \frac{14.2psi}{P}\left(\frac{T}{460°R}\right)^{1.81} ft^2/hr \tag{19}$$

The temperature in the diffusion coefficient is the absolute boundary layer temperature: the arithmetic mean of the bulk and surface temperatures. The correlation is believed to produce air/steam diffusion values that are approximately 10 percent too high. However, the correlation has been used consistently in the scaling analysis, in the mass transfer correlation validation, and in WGOTHIC. The validation shows the nominal mass transfer rate predictions are slightly less than the measurements, and the bias factors included in the evaluation model for condensation and evaporation further reduce the predicted mass transfer rates, accounting for the net uncertainty.

The boundary layer steam mole fraction is assumed to be the arithmetic mean of the bulk and surface values. The dynamic viscosity, thermal conductivity, Prandtl, and Schmidt numbers in the heat and mass transfer correlations are evaluated at the boundary layer steam mole fraction and the boundary layer temperature. These parameters have been evaluated over a range of temperatures and air/steam compositions and are presented in Figure 4-2, Figure 4-3, and Figure 4-4.

The mixture properties presented in Figure 4-2, Figure 4-3, and Figure 4-4 were calculated using the semi-empirical formula of Wilke[25], as presented in Bird, Stewart and Lightfoot[26], pp 24-26. The properties of steam and air were taken from Kreith, Table A-3.

Calculations for mass transfer inside containment use bulk (or system) values of $P_{air,bulk}$ and $P_{stm,bulk}$, and assume the steam pressure at the liquid (film or pool) surface is the steam saturation pressure at the surface temperature. The air partial pressure at the surface is the total pressure minus the steam partial pressure, $P_{air,srf} = P_{tot} - P_{stm,srf}$.

Calculations for mass transfer outside containment assume the riser or chimney gas is saturated. This assumption overestimates the bulk gas steam partial pressure, since it is always less than or equal to saturation. The difference is generally small because the bulk saturation pressure is much less than the surface saturation pressure. The bulk air partial

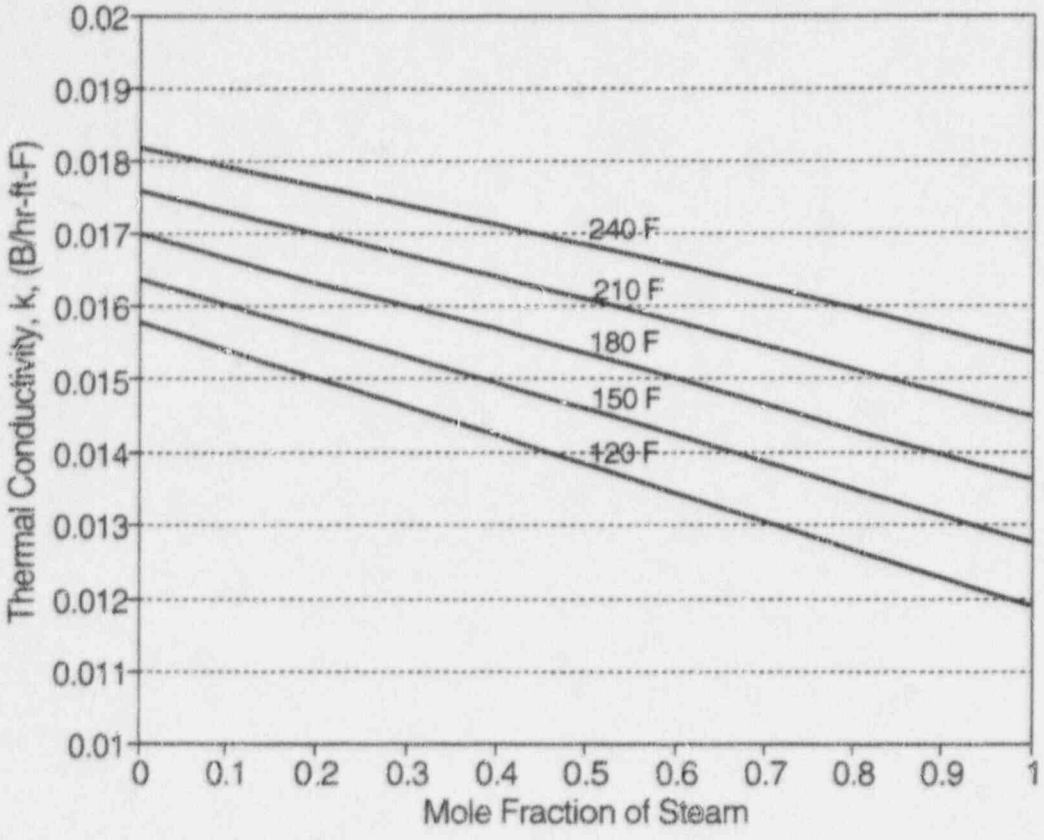

Figure 4-2 **Temperature and Concentration Dependence of the Thermal Conductivitv of an Air-Steam Mixture**

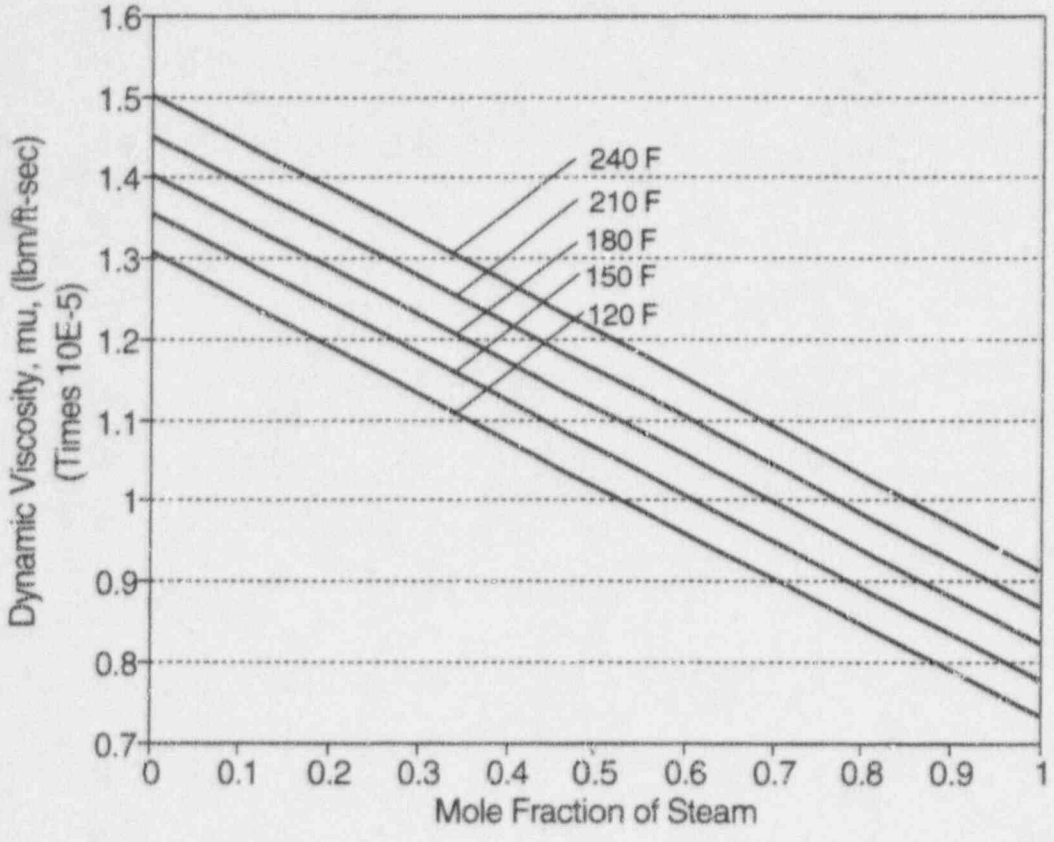

Figure 4-3 Temperature and Concentration Dependence of the Dynamic Viscosity of an Air-Steam Gas Mixture

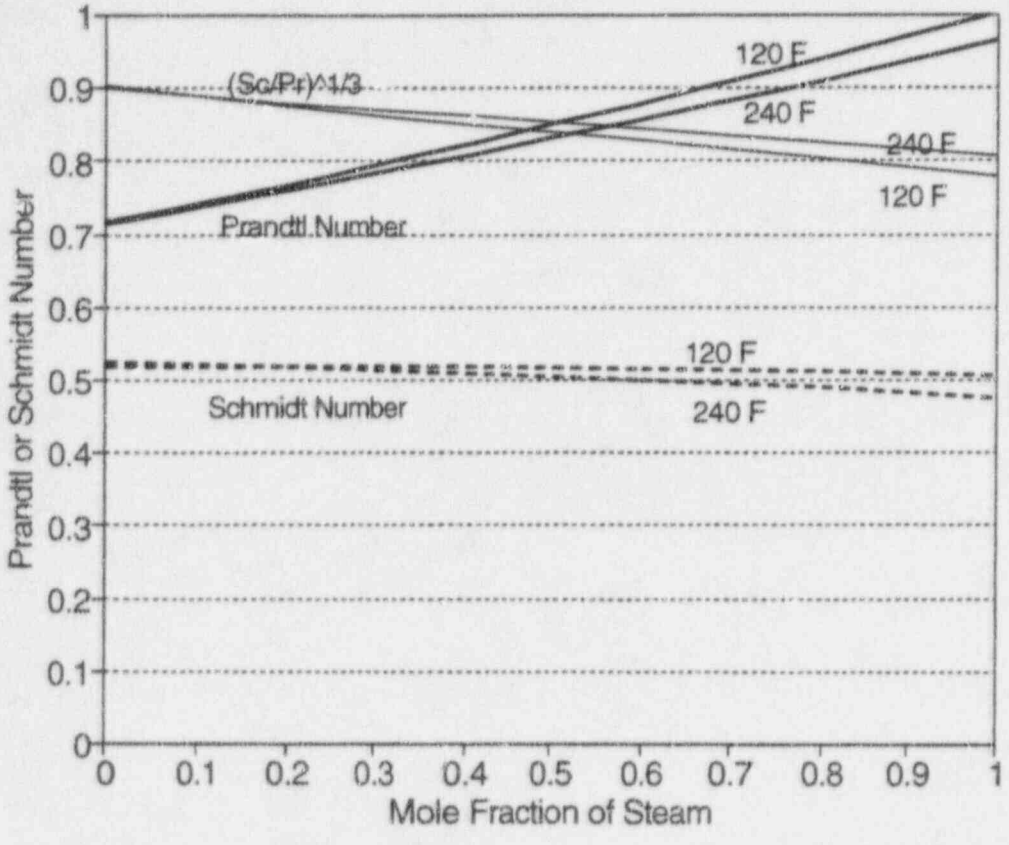

Figure 4-4 **Temperature and Concentration Dependence of the Prandtl and Schmidt Numbers for an Air-Steam Mixture**

pressure is calculated $P_{air,bulk} = P_{tot} - P_{stm,bulk}$ where P_{tot} is 14.7 psia. The partial pressure of the evaporating surface is assumed to be the saturation pressure at the liquid surface temperature, and the surface air partial pressure is calculated $P_{air,srf} = P_{tot} - P_{stm,srf}$ where P_{tot} is 14.7 psia.

4.4 CONDENSATION AND EVAPORATION ENERGY TRANSFER

The energy transferred by condensation and evaporation mass transfer is the product of the mass transfer rate and the enthalpy transported. For condensation, the condensed mass leaves the gas control volume with gas enthalpy, h_g, and the condensate retains the liquid enthalpy, h_f. The difference, $h_g - h_f$ is greater than h_{fg} since the gas temperature is generally higher than the liquid temperature. For evaporation, the evaporated mass leaves the liquid surface at the liquid surface temperature, so the enthalpy change is h_{fg}. Using the subscripts m for condensation mass transfer and mx for evaporation, the corresponding heat transfer rates in terms of conductances are:

$$\dot{q}''_m = h_m(T_{srf} - T) \quad \text{and} \quad \dot{q}''_{mx} = h_{mx}(T_{srf} - T) \tag{20}$$

Thus the conductances are defined in terms of a temperature difference and an energy flux determined from the relationship $\dot{q}'' = \dot{m}''(h_g - h_f)$, where $\dot{m}''$ is determined from the relationships in Section 4.3.

4.5 LIQUID FILM CONDUCTANCE

Although the film flow rates vary considerably both inside and outside containment, a detailed evaluation[27] showed the films quickly achieve a thickness of approximately 0.005 inches, and do not increase much thereafter due to the cube root dependence of thickness on flow rate. Therefore, the conductance through both the inner film (if), and the external film (xf) can be adequately modeled for the scaling analysis using a constant mean film thickness of 0.005 inches, and a thermal conductivity value for water of 0.38 BTU/hr-ft.-F. The conductance is determined from:

$$h_{if} = h_{xf} = k/\delta \tag{21}$$

Since the resulting conductance value is 912 B/hr-ft.^{2}-F, approximately 10 times greater than the limiting conductance from the gas to the surface, the error introduced by this approximation is not significant.

4.6 HEAT SINK CONDUCTANCES

The conductances for the heat sink energy equations presented in Section 7 are determined from the constitutive correlations presented in Sections 4.1 to 4.5. The correlations for the individual and combined conductances are presented in Section 7.2.

4.7 CONSTANT PROPERTIES

The water, steel, and concrete density, thermal conductivity, and specific heat are approximated as constants. The liquid film thickness is approximated as a constant as discussed in Section 7.4. The heat sink thickness is a constant that is defined by the total volume divided by the total surface area. The values of these and other constants are defined below.

Water density	$\rho_f =$	$\rho_{f,o} =$	60 lbm/ft.^{3}
Water thermal conductivity	$k_f =$	$k_{f,o} =$	0.38 BTU/hr-ft.-F
Water specific heat	$c_{v,f} =$	$c_{v,f,o} =$	1.0 BTU/lbm-F
Steel density	$\rho_{sh} =$	$\rho_{sh,o} =$	488 lbm/ft.^{3}
Steel thermal conductivity	$k_{st} =$	$k_{st,o} =$	26 BTU/hr-ft.-F
Steel specific heat	$c_{v,st} =$	$c_{v,st,o} =$	0.11 BTU/lbm-F
Concrete density	$\rho_{cc} =$	$\rho_{cc,o} =$	140 lbm/ft.^{3}
Concrete thermal conductivity	$k_{cc} =$	$k_{cc,o} =$	0.83 BTU/hr-ft.-F
Concrete specific heat	$c_{v,cc} =$	$c_{v,cc,o} =$	0.19 BTU/lbm-F
Water film thickness	$\delta =$	$\delta_o =$	0.005 in.
Steel shell thickness	$\delta_{sh} =$	$\delta_{sh,o} =$	1.625 in.
Steel heat sink thickness	$\delta_{st} =$	$\delta_{st,o} =$	0.40 in.
Radiation constant	$\sigma =$	$\sigma_o =$	0.1714×10^{-8} BTU/hr-ft.^{2}-°R^4
Emissivity	$\varepsilon =$	$\varepsilon_o =$	0.9
Containment volume	$V_{ct} =$	$V_{ct,o} =$	1.74×10^6 ft.^{3}

Figure 4-4 shows the Schmidt number is nearly constant at approximately 0.51 over all air-steam concentrations, so

Schmidt Number	Sc =	Sc_o =0.51

5 GENERAL RELATIONSHIPS FOR SCALING EQUATIONS

Assumptions and relationships are developed that are used in subsequent sections to develop the rate of change equations for the gas control volume mass, energy, momentum, and pressure.

5.1 ASSUMPTIONS

The following assumptions, combined with classical thermodynamic relationships, were used to develop the scaling equations:

- The mass of the gas mixture is the sum of the individual air and steam masses: $m = m_{air} + m_{stm}$.
- The gas species are in thermal and mechanical equilibrium – each volume has one temperature and total pressure.
- The internal energy of the mixture, U, is the sum of the individual air and steam internal energies, that is, there is no reaction between the two: $U = mu = m_{air}u_{air} + m_{stm}u_{stm}$. The energy reference datum for air and water, where the internal energies are zero, is 32°F. The thermodynamic properties of air and steam in the containment gas mixture are defined by the partial pressure and temperature of each gas.
- The Dalton rule for additive partial pressures: the total pressure is the sum of the air and steam partial pressures, $P = P_{air} + P_{stm}$.
- Air can be approximated as an ideal gas due to high reduced temperature and low reduced pressure ($T_r > 2$ and $P_r < 0.11$). Thus $P_{air}V = Z_{air}m_{air}R_{air}T$ where the compressibility factor $Z_{air} = 1$. (Later in this analysis the containment is assumed to be well-mixed, resulting in a maximum air partial pressure of 20.6 psi at the containment design pressure. At 20.6 psi, the air pressure ratio is 0.038).
- Steam is a real gas with equation of state $P_{stm}V = Z_{stm}m_{stm}R_{stm}T$ where the compressibility factor $Z_{stm} = Z_{stm}(P_{stm}, T)$. Steam properties are from steam tables.
- There is no liquid-vapor phase change within the gas control volume. Phase change occurs after the gas passes out of the gas control volume.

Extensive properties are defined in terms of the gas mixture P, T, m_{air}, and m_{stm}. Intensive properties are defined in terms of P, T, and the steam mass concentration, C.

5.2 GAS MIXTURE RELATIONSHIPS

The gas mixture relationships required to develop the conservation equations, and to evaluate the resulting pi groups are first defined. The gas is a mixture of air and steam with a relative concentration that may range from pure air to predominantly steam with little air present.

5.2.1 Mass

On a mass basis the mass of mixture is the sum of the masses of the individual gasses:

$$m = m_{air} + m_{stm} \tag{22}$$

On a molar basis for a non-reacting mixture, the number of moles of gas mixture is the sum of the moles of individual gasses:

$$n = n_{air} + n_{stm} \tag{23}$$

5.2.2 Molecular Weight

Because the number of moles is defined n = m/M, the mixture molecular weight can be defined from (23):

$$\frac{m}{M} = \frac{m_{air}}{M_{air}} + \frac{m_{stm}}{M_{stm}} \quad \text{so} \quad M = \frac{m_{air} + m_{stm}}{m_{air}/M_{air} + m_{stm}/M_{stm}} \tag{24}$$

5.2.3 Gas Constant

The mixture gas constant can be determined from (24) and the definition of the gas constant $R = \bar{R}/M$

$$R = \frac{\bar{R}(m_{air}/M_{air} + m_{stm}/M_{stm})}{(m_{air} + m_{stm})} \quad \text{so} \quad R = \frac{m_{air}R_{air} + m_{stm}R_{stm}}{m} \tag{25}$$

Defining the steam concentration $C = m_{stm}/m$, the air concentration is (1-C), so Equation (25) can be written:

$$R = (1-C)R_{air} + CR_{stm} \tag{26}$$

5.2.4 Enthalpy

The mixture enthalpy can be derived from the definition of enthalpy, $H = mh = mu + PV$, the internal energy of the mixture, $mu = m_{air}u_{air} + m_{stm}u_{stm}$, and the Dalton rule, $P = P_{air} + P_{stm}$:

$$\begin{aligned} mh &= m_{air}u_{air} + m_{stm}u_{stm} + P_{air}V + P_{stm}V \\ \text{so} \quad h &= \frac{m_{air}h_{air} + m_{stm}h_{stm}}{m} \quad \text{or} \quad h = (1-C)h_{air} + Ch_{stm} \end{aligned} \tag{27}$$

The gas mixture total enthalpy, $H = mh = m_{air}h_{air} + m_{stm}h_{stm}$ is a function of the four independent variables P, T, m_{air}, m_{stm}. The derivative of H can be written:

$$\begin{aligned} d(mh) &= m\frac{\partial h}{\partial T}dT + m\frac{\partial h}{\partial P}dP + h_{air}\frac{\partial m_{air}}{\partial m_{air}}dm_{air} + h_{stm}\frac{\partial m_{stm}}{\partial m_{stm}}dm_{stm} \\ \text{so} \quad d(mh) &= mc_p dT + m\frac{\partial h}{\partial P}dP + h_{air}dm_{air} + h_{stm}dm_{stm} \end{aligned} \tag{28}$$

Examination of the steam tables shows that along the saturation line from 38 to 42 psia, Δh = 1.9 B/lbm, while $c_p\Delta T$ = 3.0 B/lbm and $(\partial h/\partial P)\Delta P$ = -1.1 B/lbm. Although containment pressurization does not follow the saturation line exactly, it does follow with, at most, a modest superheat. Consequently, the rate of change of enthalpy due to pressure is approximately -1/2 of the total, while that due to temperature is 3/2 of the total. Clearly, the pressure derivative of enthalpy may be substantial, and thus may contribute to pressurization. The presence of air inside containment will somewhat reduce the magnitude of the enthalpy rate of change with pressure.

From thermodynamic relationships, the partial derivative of enthalpy with respect to pressure can be written[28] in terms of a temperature derivative:

$$\frac{\partial h}{\partial P} = v - T\frac{\partial v}{\partial T} \tag{29}$$

With the equation of state $v = ZRT/P$, and considering Z and v to be functions of the independent variables P, T, and C, the pressure derivative of enthalpy is:

$$\frac{\partial h}{\partial P} = v - T\left(\frac{RT}{P}\frac{\partial Z}{\partial T} + \frac{ZR}{P}\right) \quad \text{so} \quad \frac{\partial h}{\partial P} = -T\frac{v}{Z}\frac{\partial Z}{\partial T} \tag{30}$$

With this expression and the abbreviation $Z^T = (T/Z)(\partial Z/\partial T)$, d(mh) can also be written:

$$d(mh) = mc_p dT - VZ^T dP + h_{air}dm_{air} + h_{stm}dm_{stm} \tag{31}$$

5.2.5 Specific Heat

The mixture constant pressure specific heat can be derived by taking the partial derivative of mh with respect to temperature, and noting that the masses are not functions of temperature:

$$\frac{\partial}{\partial T}(mh) = \frac{\partial}{\partial T}(m_{air}h_{air} + m_{stm}h_{stm}) \quad \text{so} \quad m\frac{\partial h}{\partial T} = m_{air}\frac{\partial h_{air}}{\partial T} + m_{stm}\frac{\partial h_{stm}}{\partial T}$$
$$\text{and} \quad c_p = \frac{m_{air}c_{p,air} + m_{stm}c_{p,stm}}{m} \quad \text{or} \quad c_p = (1-C)c_{p,air} + Cc_{p,stm} \tag{32}$$

A similar approach can be applied to the internal energy to derive the mixture constant volume specific heat:

$$c_v = \frac{m_{air}c_{v,air} + m_{stm}c_{v,stm}}{m} \quad \text{or} \quad c_v = (1-C)C_{v,air} + Cc_{v,stm} \tag{33}$$

From the definition of the constant pressure and constant volume specific heats, and the definition of enthalpy:

$$c_p - c_v = \frac{\partial h}{\partial T} - \frac{\partial u}{\partial T} = \frac{\partial(u+Pv)}{\partial T} - \frac{\partial u}{\partial T} \quad \text{so} \quad c_p - c_v = \frac{\partial(Pv)}{\partial T} \tag{34}$$

Substituting the equation of state, Pv = ZRT:

$$c_p - c_v = \frac{\partial(ZRT)}{\partial T} = ZR\frac{\partial T}{\partial T} + RT\frac{\partial Z}{\partial T} \quad \text{so} \quad c_p - c_v = ZR\left(1 + \frac{T}{Z}\frac{\partial Z}{\partial T}\right) \tag{35}$$

With the substitution $Z^T = (T/Z)\partial Z/\partial T$

$$c_p - c_v = ZR(1+Z^T) \tag{36}$$

With the specific heat ratio $\gamma = c_p/c_v$, the ratio c_p/ZR can be expressed:

$$\frac{c_p}{ZR} = \frac{\gamma}{(\gamma-1)}(1+Z^T) \tag{37}$$

5.2.6 Gas Compressibility

The gas mixture compressibility, Z, can be derived from the Dalton rule and the equation of state:

$$P = P_{air} + P_{stm} \quad \text{and} \quad P = \frac{Zn\bar{R}T}{V} \quad \text{so} \quad Zn\frac{\bar{R}T}{V} = (Zn)_{air}\frac{\bar{R}T}{V} + (Zn)_{stm}\frac{\bar{R}T}{V} \tag{38}$$

Deleting $\bar{R}T/V$ from each term and divide by n:

$$Z = \frac{n_{air}Z_{air} + n_{stm}Z_{stm}}{n} \tag{39}$$

With $n\bar{R} = mR$, Equation (39) can be written:

$$ZmR = Z_{air}m_{air}R_{air} + Z_{stm}m_{stm}R_{stm} \quad \text{or} \quad ZR = (1-C)Z_{air}R_{air} + CZ_{stm}R_{stm} \tag{40}$$

The derivative of ZR is:

$$d(ZR) = -Z_{air}R_{air}dC + (1-C)(Z_{air}dR_{air} + R_{air}dZ_{air}) + Z_{stm}R_{stm}dC + C(Z_{stm}dR_{stm} + R_{stm}dZ_{stm}) \tag{41}$$

The values of Z_{air}, R_{air}, and R_{stm} are constants, so Equation (41) can be simplified to:

$$d(ZR) = dC(Z_{stm}R_{stm} - Z_{air}R_{air}) + CR_{stm}dZ_{stm} \tag{42}$$

Whereas the concentration, C, can range from 0 to 1, Z_{stm} is limited to the range 0.97 to 1.0. Therefore, the derivative dZ_{stm} can be neglected and dZR expressed:

$$d(ZR) = dC(Z_{stm}R_{stm} - Z_{air}R_{air}) \tag{43}$$

The property Z^T, where $Z^T = (T/Z)\partial Z/\partial T$, can be expressed in terms of Z^T_{air} and Z^T_{stm} with Equation (39):

$$\frac{T}{Z}\frac{\partial Z}{\partial T} = \frac{T}{Z}\frac{\partial\left(\frac{n_{air}}{n}Z_{air} + \frac{n_{stm}}{n}Z_{stm}\right)}{\partial T} = \frac{T}{Z}\frac{n_{stm}}{n}\frac{\partial Z_{stm}}{\partial T} \tag{44}$$

since n, n_{air}, n_{stm}, and Z_{air} are not functions of temperature. With the substitution $Z_{stm}n_{stm}/Zn = P_{stm}/P$:

$$\frac{T}{Z}\frac{n_{stm}}{n}\frac{\partial Z_{stm}}{\partial T} = \frac{Z_{stm}}{Z}\frac{n_{stm}}{n}\frac{T}{Z_{stm}}\frac{\partial Z_{stm}}{\partial T} = \frac{P_{stm}}{P}Z^T_{stm} = Z^T \tag{45}$$

For steam at 40 psi and 280°F the magnitude of Z^T_{stm} is 0.13. Consequently, the temperature derivative of the compressibility factor may be significant.

5.3 EQUATION OF STATE

Starting with the equation of state, T = PV/ZmR, and differentiating:

$$dT = T\left(\frac{d(PV)}{PV} - \frac{d(ZR)}{ZR} - \frac{dm}{m}\right) \tag{46}$$

Substituting Equation (43) for d(ZR):

$$dT = T\left(\frac{d(PV)}{PV} - \frac{(Z_{stm}R_{stm} - Z_{air}R_{air})dC}{ZR} - \frac{dm}{m}\right) \quad (47)$$

Or, in terms of the individual air and steam masses:

$$dT = T\left(\frac{d(PV)}{PV} - \frac{Z_{air}R_{air}dm_{air}}{ZRm} - \frac{Z_{stm}R_{stm}dm_{stm}}{ZRm}\right) \quad (48)$$

5.4 RATE OF CHANGE OF INTERNAL ENERGY

The total derivative of the gas mixture internal energy can be expressed in terms of enthalpy and pressure:

$$d(mu) = d(mh - PV) = d(mh) - d(PV) \quad (49)$$

Substituting Equation (31) for d(mh):

$$d(mu) = mc_p dT - VZ^T dP + h_{air}dm_{air} + h_{stm}dm_{stm} - d(PV) \quad (50)$$

Now substitute Equation (47) for dT:

$$d(mu) = mc_p T\left(\frac{d(PV)}{PV} - \frac{(Z_{stm}R_{stm} - Z_{air}R_{air})dC}{ZR} - \frac{dm}{m}\right) - VZ^T dP + h_{air}dm_{air} + h_{stm}dm_{stm} - d(PV) \quad (51)$$

Substitute PV/ZR for mT and combine coefficients on d(PV):

$$d(mu) = \left(\frac{c_p}{ZR} - 1\right)d(PV) - \frac{c_p PV}{ZR}\left(\frac{(Z_{stm}R_{stm} - Z_{air}R_{air})}{ZR}dC + \frac{dm}{m}\right) - VZ^T dP + h_{air}dm_{air} + h_{stm}dm_{stm} \quad (52)$$

Substitute Equation (37) for c_p/ZR and combine dP terms:

$$d(mu) = \frac{(1+Z^T)}{(\gamma-1)}VdP + \frac{(1+\gamma Z^T)}{(\gamma-1)}PdV - \frac{\gamma(1+Z^T)}{(\gamma-1)}PV\frac{(Z_{stm}R_{stm}-Z_{air}R_{air})}{ZR}dC - \frac{\gamma(1+Z^T)}{(\gamma-1)}PV\frac{dm}{m} + h_{air}dm_{air} + h_{stm}dm_{stm} \quad (53)$$

Or in terms of air and steam mass, instead of total mass and concentration:

$$d(mu) = \frac{(1+Z^T)}{(\gamma-1)}VdP + \frac{(1+\gamma Z^T)}{(\gamma-1)}PdV - \frac{\gamma(1+Z^T)}{(\gamma-1)}PV\frac{Z_{air}R_{air}}{ZRm}dm_{air} - \frac{\gamma(1+Z^T)}{(\gamma-1)}PV\frac{Z_{stm}R_{stm}}{ZRm}dm_{stm} + h_{air}dm_{air} + h_{stm}dm_{stm} \quad (54)$$

With the relationships $PV/ZmR = P_{air}V/Z_{air}m_{air}R_{air} = P_{stm}V/Z_{stm}m_{stm}R_{stm}$:

$$d(mu) = \frac{(1+Z^T)}{(\gamma-1)}VdP + \frac{(1+\gamma Z^T)}{(\gamma-1)}PdV - \frac{\gamma(1+Z^T)}{(\gamma-1)}P_{air}Vdm_{air} - \frac{\gamma(1+Z^T)}{(\gamma-1)}P_{stm}Vdm_{stm} + h_{air}dm_{air} + h_{stm}dm_{stm} \quad (55)$$

6 CONTAINMENT GAS ANALYSIS AND EQUATIONS FOR SCALING

The parameter of primary interest for this scaling analysis is the containment gas pressure during transients. The pressure solution requires consideration of mass, momentum, and energy transport, as well as an equation of state and constitutive relationships. Consequently, the time constant and pi groups for mass, momentum, energy, and pressure scaling are developed and quantified. The assumptions and mathematical techniques used to quantify the scaling relationships are presented.

A containment gas pressure relationship is desired that couples the gas volume to the break source and heat sinks. Because the film retains a significant fraction of the energy transferred by condensation, the liquid film must also be considered when the containment gas is coupled to the heat sinks.

The control volume equations that are used to model mass, energy, and pressure require a sign convention to distinguish between influxes and effluxes. The approach followed consistently in this analysis is to assume a flux direction and assign it a positive sign if it flows into the control volume or a negative sign if it flows out of the control volume. In most equations the direction of fluxes of mass, energy, and momentum are assumed and the assignment of a sign imparts a greater level of information to the equation. When this approach is followed consistently throughout the analysis, an incorrectly assumed flux direction does not cause an error in the solution.

6.1 MASS CONSERVATION EQUATIONS INSIDE CONTAINMENT

Conservation of mass applied to a control volume can be stated as "the rate of change of mass in a control volume is equal to the sum of the mass fluxes in and out of the control volume." The equations for conservation of mass are developed and then made dimensionless and normalized. The time constant and pi groups are defined and quantified.

Both the mass of gas (air and steam) and the mass of liquid water must be considered to develop the equations necessary to solve for the rates of change that are of interest for AP600 containment pressure scaling.

6.1.1 Containment Gas Conservation of Mass

The conservation equations inside containment are written for a gas control volume with multiple convective flows from adjacent volumes (i subscripted), multiple heat sinks (j subscripted), and a single steam break source, although flow from a sink can be considered

the same as a source. Conservation of mass can be applied to each gas species (air and steam) with the result:

$$\frac{dm_{air}}{dt} = \sum_i \dot{m}_{air,i} \quad \text{and} \quad \frac{dm_{stm}}{dt} = \dot{m}_{brk} + \sum_i \dot{m}_{stm,i} - \sum \dot{m}_{stm,j} \tag{56}$$

The index j represents condensation or evaporation steam mass transfer terms corresponding to the heat sinks listed in Table 6-1. Positive flows are into the control volume and negative flows are out. The air and gas mass equations can be added to produce the equation for conservation of the containment gas mixture mass:

$$\frac{dm}{dt} = \dot{m}_{brk} + \sum_i (\dot{m}_{air,i} + \dot{m}_{stm,i}) - \sum \dot{m}_{stm,j} \tag{57}$$

Table 6-1 Types of Heat Sinks Considered in the AP600 Containment Pressure Scaling Analysis

Index - j	Description	Abbreviation
1	Drops	d
2	Break Pool	p
3	Steel heat sinks	st
4	Concrete heat sinks	cc
5	Steel-jacketed concrete	jc
6	Subcooled shell	ss
7	Evaporating shell	es
8	Dry shell	ds
9	Baffle	bf
10	Chimney	ch

For the AP600 scaling analysis the assumption is made that containment is well-mixed, so there are no intercompartment convection terms (the i subscripted terms vanish). The basis for this assumption was discussed briefly in Section 1.0. The resulting equation is:

$$\frac{dm_{air}}{dt} = 0 \quad \text{so} \quad \frac{dm}{dt} = \frac{dm_{stm}}{dt} = \dot{m}_{brk} - \sum \dot{m}_{stm,j} \tag{58}$$

All variables are made dimensionless by dividing by the initial value of the variable for the time phase under consideration. The DECLG transient has four time phases that are shown in Figure 3-4 and discussed in more detail in the PIRT[3]. In general, the initial value of each variable differs for each time phase. Steam and air mass and flow rate dimensionless variables are defined:

Containment gas mass	m	=	$m_o m^*$
Containment gas volume	V	=	$V_o V^*$
Containment gas density	ρ	=	$\rho_o \rho^*$
Time	t	=	$\tau\, t^*$
Break steam flow rate	$\dot{m}_{g,brk}$	=	$\dot{m}_{g,brk,o} \dot{m}^*_{g,brk}$
Break steam density	$\rho_{g,brk}$	=	$\rho_{g,brk,o} \rho^*_{g,brk}$
Heat sink j steam flow rate	$\dot{m}_{stm,j}$	=	$\dot{m}_{stm,j,o} \dot{m}^*_{stm,j}$

The conservation of gas mixture mass equation, Equation (57), is made dimensionless by substituting these relationships and normalized by the reference break source term, $\dot{m}_{g,brk,o}$ as follows:

$$\frac{m_o}{\dot{m}_{g,brk,o}\tau}\frac{dm^*}{dt^*} = \frac{\dot{m}_{g,brk,o}}{\dot{m}_{g,brk,o}}\dot{m}^*_{g,brk} + \sum_j \frac{\dot{m}_{stm,j,o}}{\dot{m}_{g,brk,o}}\dot{m}^*_{stm,j}$$

$$\pi_{m,\tau}\frac{dm^*}{dt^*} = \pi_{m,brk}\dot{m}^*_{g,brk} + \sum_j \pi_{m,j}\dot{m}^*_{stm,j} \qquad (59)$$

where $\tau = \dfrac{V_o \rho_{g,brk,o}}{\dot{m}_{g,brk,o}}$ $\pi_{m,\tau} = \dfrac{\rho_o}{\rho_{g,brk,o}}$ $\pi_{m,brk} = 1$ $\pi_{m,j} = \dfrac{\dot{m}_{stm,j,o}}{\dot{m}_{g,brk,o}}$

6.1.2 Containment Liquid Conservation of Mass

Conservation of mass can also be applied to the liquid that forms part of the gas control volume boundary. The changing volume of liquid does work on the containment gas by compressing the control volume boundary. The gas control volume excludes the volume upstream of the break, so the liquid released from the break displaces gas in the control volume. Thus, the liquid stored in the piping, heat exchangers, pressurizer, reactor, pumps, accumulators, and core makeup tanks (CMTs) displaces containment volume, if released from the break as liquid. During a LOCA transient, after the passive reactor cooling system depressurizes the primary system to containment pressure, the in-containment refueling water storage tank (IRWST) drains by gravity into the reactor vessel, then out the break. Since the IRWST is open to containment, its liquid flow into the reactor is an outflow, whereas the break flow is an inflow.

The total liquid mass that displaces gas volume includes the masses of the IRWST, break pool, drops, and liquid films. These are the liquid masses that displace gas in the containment volume, and cause the containment pressure to change. The rate of change of liquid mass is the sum of the flows of break liquid to the pool, break liquid to drops, condensation on heat sinks, minus the flow out of the IRWST:

$$\frac{dm_f}{dt} = \dot{m}_{f,brk,p} + \dot{m}_{f,brk,d} + \sum \dot{m}_{stm,j} - \dot{m}_{IR} = \dot{m}_f \qquad (60)$$

Where $\dot{m}_f$ is the net liquid flow rate that displaces containment volume. The evaporation rates from the pool and drops appear as negative flow rates in the summation over the heat sinks.

The break pool, break drops, IRWST, and heat sink liquid mass flow rate terms can be quantified for each time phase of a DECLG with the following assumptions.

- The total break flow rate for each time phase is determined from the break liquid flow rate curve in Figure 3-2. The blowdown value is the time average over blowdown, while the other break flow rates are read from Figure 3-2 for the beginning of each time phase.

- The drop flow rate, as discussed in Section 7.1, is 1/2 the break gas flow rate during blowdown and zero thereafter.

- The break flow to the pool is the total break liquid flow minus the drop flow.

- During blowdown the condensation rate on all heat sinks is a small fraction of the break steam flow rate (see pi values in Section 7.10), and the break steam flow rate is less than the break liquid flow rate. Thus the condensation rates are neglected.

- The IRWST flow is zero during blowdown, refill, and the early portion of the peak pressure phase, since the RCS pressure is too high to allow the IRWST to gravity drain. By the beginning of the long-term phase, the IRWST is the only source to the break, so $\dot{m}_{IR} = \dot{m}_{f,brk} + \dot{m}_{g,brk}$, and $\dot{m}_f = 0$.

- After blowdown, the pi groups are evaluated at inflection points on the containment pressure curve, so $dm_{stm}/dt = \dot{m}_{g,brk} - \Sigma \dot{m}_{stm,j} = 0$. Thus, the break gas flow rate is approximately equal to the sum of the heat sink mass flow rates. Thus, $\dot{m}_{g,brk} = \Sigma \dot{m}_{stm,j}$.

From these considerations, the rate of change of the liquid mass is presented for each time phase in Table 6-2.

During an MSLB the total mass of gas released to containment, when condensed to liquid, has a volume of approximately 4000 ft.^{3}. Expressed as a fraction of total containment gas volume, $\Delta V/V = 0.0023$. Consequently, work due to gas volume change during an MSLB is similarly small and is neglected. The MSLB average flow rate for the first 600 sec of the transient is 367 lbm/sec, from Figure 3-5.

Table 6-2 Liquid Flow Rates Contributing to Containment Pressurization

Time Phase	Break Gas lbm/sec	Break Liquid lbm/sec	Break Pool lbm/sec	Break Drops lbm/sec	IRWST lbm/sec	Condensed lbm/sec	$\dot{m}_f$ lbm/sec	$\pi_{m,f}$
Blowdown	4444	7777	5555	2222	0	neglected	7777	1.75
Refill	200[1]	0	0	0	0	0	0	0
Peak Pres	200	200	200	0	0	200	400	2.0
Long Term	45	200	200	0	245	45	0	0

1. A value of 200 lbm/sec was assumed to provide a denominator for scaling during refill.

The net liquid mass flow rate, $\dot{m}_f$ is made dimensionless with the substitution $\dot{m}_f = \dot{m}_{f,o}\, \dot{m}_f^*$, and scaled to the mass flow rate of break gas:

$$\frac{\dot{m}_f}{\dot{m}_{g,brk,o}} = \frac{\dot{m}_{f,o}}{\dot{m}_{g,brk,o}} \dot{m}_f^* \quad \text{so} \quad \pi_{m,f} = \frac{\dot{m}_{f,o}}{\dot{m}_{g,brk,o}} \tag{61}$$

The mass pi values presented in Table 6-2 for blowdown and peak pressure are relatively large numbers, so it is reasonable to consider evaluating pi values for each of the j heat sinks and each of the mass flow rate terms comprising the net liquid flow rate. However, when the energy and pressure equations are scaled (Section 8.0), the work term associated with the liquid rate of change is shown to be very small, so it is not useful to further subdivide an already small term. Hence, only the net liquid mass flow rate term will be used to represent the liquid rate of change.

6.1.3 Inner Film Liquid Conservation of Mass

A mass conservation equation can be written for the inner liquid film that forms on structure j. The rate of change of film mass is the condensation rate minus the film drain rate:

$$\frac{dm_{if,j}}{dt} = \dot{m}_{stm,j} - \dot{m}_{drain,j} \tag{62}$$

This equation is examined further in Section 7.4.

6.2 ENERGY CONSERVATION EQUATION INSIDE CONTAINMENT

Conservation of energy for a control volume can be stated as "the rate of change of internal energy in a control volume is equal to the sum of the enthalpy fluxes and heat transfer in and out of the control volume, and the work done on the control volume." Conservation of energy for the control volume encompassing only the containment gas relates the rate of change of gas internal energy to the enthalpy of the break source, the sum of the air and steam convective flows from other volumes, the sum of the condensed steam enthalpy flows to each heat sink, the sum of the heat transferred by radiation and convection to each heat sink, and the compression work done on the gas by a change in the volume of the control volume. These terms are presented, respectively, in the containment gas energy equation, where the sign on each term represents the assumed direction of flow:

$$\frac{d(mu)_g}{dt} = \dot{m}_{g,brk} h_{g,brk} + \sum_i (\dot{m}_{air,i} h_{air,i} + \dot{m}_{stm,i} h_{stm,i}) - \sum_j (\dot{m}_{stm,j} h_{stm,j} + \dot{q}_j) - P\frac{dV}{dt} \tag{63}$$

where $h_{g,brk}$ is the total break steam enthalpy, $h_{g,brk} = h + v^2/2 + gz$. Elevation is negligible, as is $v^2/2$ for all but the break source during blowdown. (Post-blowdown, $v < 200$ ft./sec, so $v^2/2 < 0.8$ BTU/lbm.)

Since the total containment volume is constant, the sum of the rates of change of the gas and liquid volumes must be equal, or $dV/dt = -dV_f/dt$. With an approximately constant liquid ensity, $dV_f/dt = dm_f/\rho_f dt = \dot{m}_f/\rho_f$, so the term PdV/dt can be expressed as $-(P/\rho_f)\dot{m}_f$. Thus:

$$\frac{d(mu)_g}{dt} = \dot{m}_{g,brk} h_{g,brk} + \sum_i (\dot{m}_{air,i} h_{air,i} + \dot{m}_{stm,i} h_{stm,i}) - \sum_j (\dot{m}_{stm,j} h_{stm,j} + \dot{q}_j) + \frac{P}{\rho_f}\dot{m}_f \tag{64}$$

An energy equation is desired that relates the rate of change of energy stored in the gas atmosphere to the heat input to each heat sink. The heat input to the heat sink is used in Section 7 to model the individual heat sink thermal performance. However, the energy out of the gas differs from the energy into the solid by the amount of energy retained by the film. The liquid film lies outside both the gas and solid heat sink control volumes. With the substitution $h_{stm,j} = h_{stm,j} - h_{f,j} + h_{f,j}$, Equation (64) becomes:

(65)

$$\frac{d(mu)_g}{dt} = \dot{m}_{g,brk} h_{g,brk} + \sum_i (\dot{m}_{air,i} h_{air,i} + \dot{m}_{stm,i} h_{stm,i}) - \sum_j (\dot{m}_{stm,j} (h_{stm,j} - h_{f,j}) + \dot{m}_{stm,j} h_{f,j} + \dot{q}_j) + \frac{P}{\rho_f} \dot{m}_f$$

This energy equation now includes a term for the gas-to-liquid enthalpy difference that is equal to the energy transferred into the solid heat sink, and a term for the energy carried away by the liquid film that is defined by $\dot{m}_{stm,j} h_{f,j}$. When the condensation or evaporation is on a pool or drop, the liquid film is indistinguishable from the other liquid, so the terms are combined.

This equation is still not optimal for scaling, since the enthalpy and internal energy are both measured relative to the triple point of water. This bias can be eliminated as follows: The gas mass is the sum of the air, and steam masses: $m = m_{air} + m_{stm}$ and the gas specific internal energy is: $mu = m_{air} u_{air} + m_{stm} u_{stm}$. With this definition, a minimum energy reference datum, u_{min}, can be defined that corresponds to the system with the specific internal energies of water and air at the same temperature and pressure. That is, $mu_{min} = m_{air} u_{air,min} + m_{stm} u_{stm,min}$. Note that although $u_{air,min}$ and $u_{stm,min}$ are constants, u_{min} is not constant since the air and steam masses change with time. The time derivatives of the gas internal energies can be written:

$$\frac{d(mu)}{dt} = \frac{d[m(u - u_{min})]}{dt} + \frac{d(mu_{min})}{dt} = \frac{d[m(u - u_{min})]}{dt} + u_{air,min} \frac{dm_{air}}{dt} + u_{stm,min} \frac{dm_{stm}}{dt} \quad (66)$$

With these derivative expressions and the definition of enthalpy, $u = h - P/\rho$, the gas energy equation can be written:

$$\frac{d[m(u - u_{min})]}{dt} = \dot{m}_{g,brk} (h_{g,brk} - h_{stm,min}) + \sum_i [\dot{m}_{air,i} (h_{air,i} - h_{air,min}) + \dot{m}_{stm,i} (h_{stm,i} - h_{stm,min})] \quad (67)$$
$$- \sum_j [\dot{m}_{stm,j} (h_{stm,j} - h_{if,j}) + \dot{m}_{stm,j} (h_{if,j} - h_{stm,min}) + \dot{q}_j] + \frac{P_{air,min}}{\rho_{air,min}} \frac{dm_{air}}{dt} + \frac{P_{stm,min}}{\rho_{stm,min}} \frac{dm_{stm}}{dt} + \frac{P}{\rho_f} \dot{m}_f$$

In this form the energy equation represents the change in internal energy relative to a minimum energy reference condition. For AP600 scaling, a single volume is considered, so the air subscripted terms and the term dm_{air}/dt vanish. The heat transfer into the heat sink can be expressed in terms of conductance as $q_j = h_j A_j (T - T_{if,j})$, where $T_{if,j}$ is the liquid film free surface temperature on heat sink j.

The minimum energy state will be selected as the internal energy of water at the initial temperature, T_o. The internal energy and enthalpy of liquid are equal, and P_{stm} is zero for liquid, so the energy equation is:

$$\frac{d[m(u-u_{min})]}{dt} = \dot{m}_{g,brk}(h_{g,brk} - h_{f,T_o}) + \frac{P}{\rho_f}\dot{m}_f - \sum_j [\dot{m}_{stm,j}(h_{stm,j} - h_{if,j}) + \dot{m}_{stm,j}(h_{if,j} - h_{f,T_o}) + h_j A_j (T - T_{if,j})] \quad (68)$$

This equation shows the rate of change of internal energy is equal to the break steam enthalpy flowing in, plus the work done on the gas, minus the enthalpy that drains out of the films, minus the heat transfer into the heat sinks, minus the energy stored in the films. The term $\dot{q}_j = h_j A_j (T - T_{if,j})$ also appears in the heat sink energy equations, where it is further separated into terms representing convection heat transfer and radiation heat transfer as described in Section 7. Equations (65), (67), and (68) are used for all subsequent containment gas energy scaling.

Many of the mass and flow rate variables required to make the energy equation dimensionless were defined under mass scaling. Additional variables are defined:

Containment gas mass	m	$= m_o m^*$	
Containment gas volume	V	$= V_o V^*$	
Containment gas density	ρ	$= \rho_o \rho^*$	
Break steam density	$\rho_{g,brk}$	$= \rho_{g,brk,o} \rho^*_{g,brk}$	
Time	t	$= \tau\, t^*$	
Break steam flow rate	$\dot{m}_{g,brk}$	$= \dot{m}_{g,brk,o} \dot{m}^*_{g,brk}$	
Gas internal energy diff	$u - u_{min}$	$= \Delta u_o u^*$	Containment gas mixture u - $u_{f,To}$
Break steam enthalpy diff	$h_{g,brk} - h_{f,To}$	$= \Delta h_{g,brk,o} h^*_{g,brk}$	Break steam h_g - liquid h_f at T_o
Pressure	P	$= P_o P^*$	
Heat sink j:			
Steam flow rate	$\dot{m}_{stm,j}$	$= \dot{m}_{stm,j,o} \dot{m}^*_{stm,j}$	
Gas-film enthalpy diff	$h_{stm,j} - h_{if,j}$	$= \Delta h_{(g,j,o} h^*_{fg,j}$	h_g of steam j - h_f of inner film j
Film enthalpy diff	$h_{if,j} - h_{f,To}$	$= \Delta h_{if,j,o} h^*_{if,j}$	h_f of inner film j - liquid h_f at T_o
Heat trans coef	$h_{q,j}$	$= h_{q,j,o} h^*_{q,j}$	radiation + convection ($h_{r,j} + h_{c,j}$)
Heat transfer area	A_j	$= A_{j,o} A^*_j$	
Gas - liquid surf temp diff	$T - T_{if,j}$	$= (T - T_{if,j})_o \Delta T^*_{if,j}$	

Substitutions are made to the conservation of containment gas energy equation to make it dimensionless, and the equation is normalized as follows:

$$\frac{m_o \Delta u_o}{\dot{m}_{g,brk,o} \Delta h_{g,brk,o} \tau} \frac{d(mu)^*}{dt^*} = \frac{\dot{m}_{g,brk,o} \Delta h_{brk,o}}{\dot{m}_{g,brk,o} \Delta h_{g,brk,o}} \dot{m}^*_{g,brk} h^*_{brk} + \frac{P_o \dot{m}_{f,o}}{\rho_{f,o} \dot{m}_{g,brk,o} \Delta h_{g,brk,o} \tau} P^* \dot{m}^*_f$$
$$- \sum_j \left(\frac{\dot{m}_{stm,j,o} \Delta h_{stm,j,o}}{\dot{m}_{g,brk,o} \Delta h_{g,brk,o}} \dot{m}^*_{stm,j} h^*_{stm,j} + \frac{\dot{m}_{stm,j,o} \Delta h_{if,j,o}}{\dot{m}_{g,brk,o} \Delta h_{g,brk,o}} \dot{m}^*_{drain,j} h^*_{if,j} + \frac{h_{q,j,o} A_{j,o} (T - T_{if,j,o})}{\dot{m}_{g,brk,o} \Delta h_{g,brk,o}} h^*_{q,j} A^*_j \Delta T^*_{if,j} \right) \quad (69)$$

$$\pi_{e,\tau} \frac{d(mu)^*}{dt^*} = \pi_{e,brk} \dot{m}^*_{g,brk} \Delta h^*_{brk} - \sum_j \left(\pi_{e,fg,j} \dot{m}^*_{stm,j} \Delta h^*_{stm,j} + \pi_{e,if,j} \dot{m}^*_{stm,j} \Delta h^*_{if,j} + \pi_{e,q,j} h^*_{q,j} A^*_j \Delta T^*_{if,j} \right)$$

where:

$$\pi_{e,\tau} = \pi_{m,\tau} \frac{\Delta u_o}{\Delta h_{g,brk,o}} \qquad \pi_{e,brk} = 1 \qquad \pi_{e,f,work} = \pi_{m,f} \frac{P_o}{\rho_{f,o} \Delta h_{g,brk,o}}$$
$$\pi_{e,fg,j} = \pi_{m,j} \frac{\Delta h_{fg,j,o}}{\Delta h_{g,brk,o}} \qquad \pi_{e,if,j} = \pi_{m,j} \frac{\Delta h_{if,j,o}}{\Delta h_{g,brk,o}} \qquad \pi_{e,q,j} = \frac{h_{q,j,o} A_{j,o} (T - T_{if,j,o})}{\dot{m}_{g,brk,o} \Delta h_{g,brk,o}} \quad (70)$$

6.3 PRESSURE EQUATION INSIDE CONTAINMENT

Pressure scaling requires the steam partial pressure, and when heat sink transport is considered, the air partial pressure is also required. With the well-mixed assumption discussed in Section 1.0, there is only one bulk value of P_{stm}, and one value of P_{air} at any time. The air density is always constant at the initial value, so the air pressure is proportional to the absolute temperature. The steam pressure is the total pressure minus the air pressure:

$$P_{air} = \frac{T_{abs}}{T_{i,abs}} P_{air,i} \qquad P_{stm} = P_{total} - P_{air} \quad (71)$$

6.3.1 Rate of Pressure Change (RPC) Equation

An RPC equation can be written by combining the equation for the rate of change of internal energy, Equation (55) with conservation of energy, Equation (64):

$$\frac{(1+Z^T)}{(\gamma-1)} V \frac{dP}{dt} = \dot{m}_{g,brk} \left(h_{g,brk} - h_{stm} + \frac{\gamma(1+Z^T)}{(\gamma-1)} \frac{P_{stm}}{\rho_{stm}} \right) + \dot{m}_f \frac{\gamma(1+Z^T)}{(\gamma-1)} \frac{P}{\rho_f}$$
$$- \sum_j \left[\dot{m}_{stm,j} \left(h_{stm,j} - h_{stm} + \frac{\gamma(1+Z^T)}{(\gamma-1)} \frac{P_{stm}}{\rho_{stm}} \right) - h_{q,j} A_j (T - T_{if,j}) \right] \quad (72)$$

6.3.2 Normalized, Dimensionless RPC Equation

Dimensionless variables used to make the RPC equation dimensionless are:

Containment steam mass	m_{stm}	=	$m_{stm,o}m^*_{stm}$
Time	t	=	$\tau\, t^*$
Net liquid flow rate	$\dot{m}_f$	=	$\dot{m}_{f,o}\dot{m}^*_f$
Heat sink j steam flow rate	$\dot{m}_{stm,j}$	=	$\dot{m}_{stm,j,o}\dot{m}^*_{stm,j}$
Heat sink surface area	A_j	=	$A_{j,o}A_j^*$
Containment to liquid surf temp diff	$(T-T_{if,j})$	=	$(T-T_{if,j})_o\Delta T^*_{if,j}$
Combined rad + conv heat trans coef	h_q	=	$h_{q,o}h_q^*$
Cond/evap energy transfer coefficient	h_m	=	$h_{m,o}h_m^*$
Effective energy transfer coefficient	h_e	=	$h_{e,o}h_e^*$
Gas volume	V	=	V_oV^*
Break steam flow rate	$\dot{m}_{g,brk}$	=	$\dot{m}_{g,brk,o}\dot{m}^*_{g,brk}$
Break-bulk steam enthalpy difference	$(h_{g,brk} - h_{stm})$	=	$(h_{g,brk}-h_{stm})_o\Delta h^*_{brk}$
Condensate enthalpy difference	$(h_{stm,j} - h_{stm})$	=	$(h_{stm,j}-h_{stm})_o\Delta h^*_{stm,j}$
Bulk steam density	ρ_{stm}	=	$\rho_{stm,o}\rho^*_{stm}$
Compressibility function	$(1+Z^T)$	=	$(1+Z^T)_oZ^{T*}$
Specific heat ratio	γ	=	$\gamma_o\gamma^*$
Specific heat difference	$(\gamma-1)$	=	$(\gamma-1)_o\gamma^*_m$
Total pressure	P	=	P_oP^*
Steam partial pressure	P_{stm}	=	$P_{stm,o}P^*_{stm}$

The RPC is made dimensionless by substituting the expressions for the dimensioned variables defined above, and is normalized by dividing each term in the RPC by the reference break gas work term, $\gamma_0(1+Z^T)/(\gamma-1)_o\ \dot{m}_{g,brk,o}\ (P_{stm}/\rho_{stm})$. The following sections present the normalization, dimensionless substitutions, and pi groups that result for each term of the RPC.

6.3.2.1 Pressure Term

$$\frac{(\gamma-1)_o}{\gamma_o(1+Z^T)_o\dot{m}_{g,brk,o}}\frac{\rho_{stm,o}}{P_{stm,o}}\frac{(1+Z^T)}{(\gamma-1)}V\frac{dP}{dt} = \frac{(\gamma-1)_o}{\gamma_o(1+Z^T)_o\dot{m}_{g,brk,o}}\frac{\rho_{stm,o}}{P_{stm,o}}\frac{(1+Z^T)_oZ^{T*}}{(\gamma-1)_o\gamma^*_m}V_oV^*\frac{P_o\,dP^*}{\tau\,dt^*} \quad (73)$$

$$= \pi_{p,\tau}\frac{Z^{T*}V^*}{\gamma^*_m}\frac{dP^*}{dt^*}$$

where:

$$\pi_{p,\tau} = \frac{1}{\gamma_o}\frac{\rho_{stm,o}}{\rho_{g,brk,o}}\frac{P_o}{P_{stm,o}} = \pi_{m,\tau}\frac{1}{\gamma_o}\frac{P_o}{P_{stm,o}}\frac{\rho_{stm,o}}{\rho_o} \quad \text{and} \quad \tau = \frac{V_o\rho_{g,brk,o}}{\dot{m}_{g,brk,o}} \tag{74}$$

6.3.2.2 Break Source Gas Term

The first term on the right side of the RPC represents the break source steam enthalpy and work. The dimensionless substitutions and normalization give:

(75)

$$\frac{(\gamma-1)_o}{\gamma_o(1+Z^T)_o}\frac{\rho_{stm,o}}{P_{stm,o}}\dot{m}_{g,brk}\left((h_{g,brk}-h_{stm})+\frac{\gamma(1+Z^T)}{(\gamma-1)}\frac{P_{stm}}{\rho_{stm}}\right) =$$

$$\frac{\dot{m}_{g,brk,o}\dot{m}^*_{g,brk}}{\dot{m}_{g,brk,o}}\left[\frac{(\gamma-1)_o}{\gamma_o(1+Z^T)_o}\frac{\rho_{stm,o}}{P_{stm,o}}(h_{g,brk}-h_{stm})_o\Delta h^*_{g,brk}+\frac{(\gamma-1)_o}{\gamma_o(1+Z^T)_o}\frac{\rho_{stm,o}}{P_{stm,o}}\frac{\gamma_o\gamma^*(1+Z^T)_oZ^{T*}}{(\gamma-1)_o\gamma^*_m}\frac{P_{stm,o}P^*_{stm}}{\rho_{stm,o}\rho^*_{stm}}\right]$$

$$= \pi_{p,g,brk,enth}\Delta h^*_{g,brk}\dot{m}^*_{g,brk} + \pi_{p,g,brk,work}\frac{\gamma^*Z^{T*}}{\gamma^*_m}\frac{P^*_{stm}}{\rho^*_{stm}}\dot{m}^*_{g,brk}$$

where:

$$\pi_{p,g,brk,enth} = \frac{(h_{g,brk}-h_{stm})_o(\gamma-1)_o}{\gamma_o(1+Z^T)_o}\frac{\rho_{stm,o}}{P_{stm,o}} \quad \text{and} \quad \pi_{p,g,brk,work} = 1 \tag{76}$$

6.3.2.3 Net Liquid Work Term

The break source liquid displaces gas from the containment volume, and hence, does work on the containment gas. The normalized, dimensionless term is:

$$\frac{(\gamma-1)_o}{\gamma_o(1+Z^T)_o\dot{m}_{g,brk,o}}\frac{\rho_{stm,o}}{P_{stm,o}}\frac{\dot{m}_f\gamma(1+Z^T)}{(\gamma-1)}\frac{P}{\rho_f} =$$

$$\frac{\dot{m}_{f,o}\dot{m}^*_f}{\dot{m}_{g,brk,o}}\frac{(\gamma-1)_o}{\gamma_o(1+Z^T)_o}\frac{\rho_{stm,o}}{P_{stm,o}}\frac{\gamma_o(1+Z^T)_o\gamma^*Z^{T*}}{(\gamma-1)_o\gamma^*_m}\frac{P_oP^*}{\rho_{f,o}} \tag{77}$$

$$= \pi_{p,f,work}\frac{\gamma^*Z^{T*}}{\gamma^*_m}\dot{m}^*_fP^*$$

where:

$$\pi_{p,f,work} = \frac{\dot{m}_{f,o}}{\dot{m}_{g,brk,o}} \frac{\rho_{stm,o}}{\rho_{f,o}} \frac{P_o}{P_{stm,o}} = \pi_{m,f} \frac{\rho_{stm,o}}{\rho_{f,o}} \frac{P_o}{P_{stm,o}} \quad (78)$$

6.3.2.4 Condensation/Evaporation Phase Change Terms

The second line of the RPC, Equation (72), represents the energy transfer associated with the heat sinks, and, because it is unwieldy, will be separated into phase change mass transfer and convection/radiation heat transfer terms. The mass transfer (the steam that flows between the containment gas and the heat sinks) includes terms corresponding to enthalpy and gas flow work:

$$\dot{m}_{stm,j}\left[(h_{stm,j} - h_{stm}) + \frac{\gamma(1+Z^T)}{(\gamma-1)} \frac{P_{stm}}{\rho_{stm}}\right] \quad (79)$$

The enthalpy and work terms are normalized by the break enthalpy flow rate, and made dimensionless as follows:

(80)

$$\frac{(\gamma-1)_o}{\gamma_o(1+Z^T)_o \dot{m}_{g,brk,o}} \frac{\rho_{stm,o}}{P_{stm,o}} \dot{m}_{stm,j}\left[(h_{stm,j} - h_{stm}) + \frac{\gamma(1+Z^T)}{(\gamma-1)} \frac{P_{stm}}{\rho_{stm}}\right] =$$

$$\frac{\dot{m}_{stm,j,o}}{\dot{m}_{g,brk,o}} \frac{\dot{m}^*_{stm,j}}{\dot{m}^*_{g,brk}}\left[\frac{(\gamma-1)_o}{\gamma_o(1+Z^T)_o} \frac{\rho_{stm,o}}{P_{stm,o}} (h_{stm,j} - h_{stm})_o \Delta h^*_{stm,j} + \frac{(\gamma-1)_o}{\gamma_o(1+Z^T)_o} \frac{\rho_{stm,o}}{P_{stm,o}} \frac{\gamma_o \gamma^* (1+Z^T)_o Z^{T*}}{(\gamma-1)_o \gamma^*_m} \frac{P_{stm,o} P^*_{stm}}{\rho_{stm,o} \rho^*_{stm}}\right]$$

$$= \pi_{p,enth,j} \frac{\dot{m}^*_{stm,j}}{\dot{m}^*_{g,brk}} \Delta h^*_{stm,j} + \pi_{p,work,j} \frac{\dot{m}^*_{stm,j}}{\dot{m}^*_{g,brk}} \frac{\gamma^* Z^{T*}}{\gamma^*_m} \frac{P^*_{stm}}{\rho^*_{stm}}$$

where:

$$\pi_{p,enth,j} = \pi_{m,stm,j} \frac{(\gamma-1)_o}{\gamma_o(1+Z^T)_o} \frac{\rho_{stm,o}}{P_{stm,o}} (h_{stm,j} - h_{stm})_o \quad \pi_{p,work,j} = \pi_{in,stm,j} \quad (81)$$

The enthalpy to or from the heat sink, $h_{stm,j}$ and the value of $\dot{m}_{stm,j}$ needed to calculate $\pi_{m,stm,j}$ can only be determined after calculating the heat sink temperature. This evaluation is performed in Section 7 for each heat sink.

6.3.2.5 Convection and Radiation Heat Transfer Terms

The energy transferred between the gas and the heat sinks includes a convection heat transfer term and a radiation heat transfer term, $h_q = (h_r + h_c)$. The heat transfer is normalized and made dimensionless as follows:

$$\frac{(\gamma-1)_o}{\gamma_o(1+Z^T)_o \dot{m}_{g,brk,o}} \frac{\rho_{stm,o}}{P_{stm,o}} h_{q,j} A_j (T - T_j) = \frac{(\gamma-1)_o \rho_{stm,o} h_{q,j,o} h^*_{q,j} A_{j,o} A^*_j (T - T_{if,j})_o \Delta T^*_{if,j}}{\gamma_o(1+Z^T)_o \dot{m}_{g,brk,o} P_{stm,o}} = \pi_{p,q,j} h^*_{q,j} A^*_j \Delta T^*_{if,j} \quad (82)$$

where:

$$\pi_{p,q,j} = \frac{(\gamma-1)_o}{\gamma_o(1+Z^T)_o \dot{m}_{g,brk,o}} \frac{\rho_{stm,o}}{P_{stm,o}} h_{q,j,o} A_{j,o} (T - T_j)_o \quad (83)$$

6.4 INITIAL AND BOUNDARY CONDITIONS FOR CONTAINMENT MASS, ENERGY, AND PRESSURE

It is desired to scale the RPC for four LOCA time phases: blowdown, refill, peak pressure, and long-term depressurization, and for the MSLB blowdown. The dimensionless variables have different values for each time phase. Initial values are used as the reference values for each variable for each time phase except blowdown. For blowdown, the time average pressure values are used to define all dimensionless, thermodynamic properties for two reasons:

- The only non-zero pi groups at zero time are the transient and break source groups; all heat sink groups are zero. The transient and break source groups provide little useful information.

- The time constant for the steel heat sinks is on the order of 80 sec, so the heat input to the heat sinks during the 27 sec blowdown cannot be neglected. The use of the time average pressure allows the energy input to the heat sinks to be easily calculated.

The calculation of containment pi values begins with the following assumptions:

- The initial containment pressure is 15.7 psia, composition is pure air, and temperature is 120°F. The air density remains constant throughout the transient.

- The initial temperature of all structures and the IRWST is 120°F.

- An estimate of the containment pressures at the beginning of each time phase was obtained from the WGOTHIC code as a reasonable estimate. The specific pressure history does not significantly affect the results or conclusions of the scaling analysis.

  - The containment pressure during the blowdown phase of a DECLG is shown in Figure 6-1. The time averaged pressure is 44 psia.

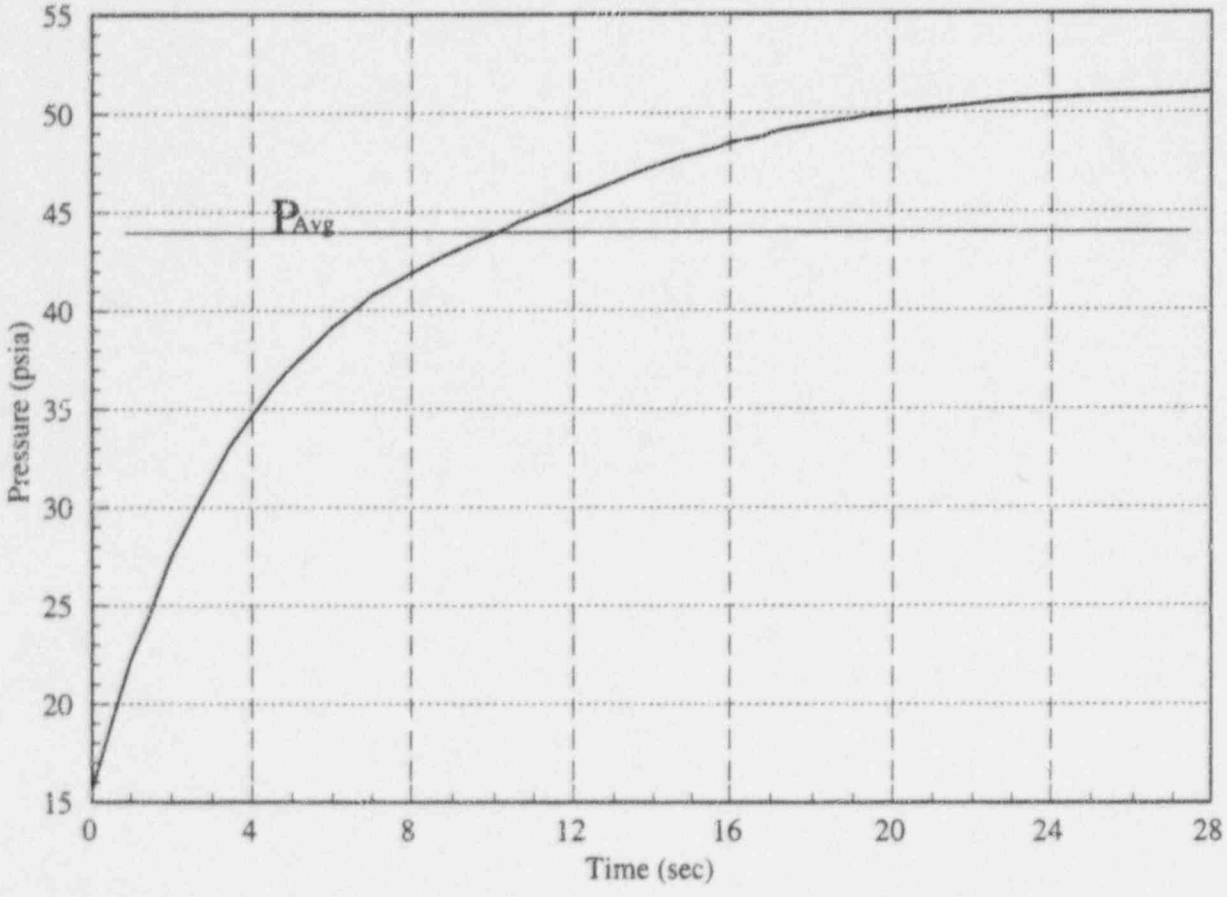

Figure 6-1 AP600 Containment Pressure During Blowdown

  - Reference pressures for the refill, peak pressure, and long-term depressurization phases of a DECLG are from Figure 3-4.

  - Reference pressure for the MSLB is from Figure 3-7.

- The basis for the mass flow rates is discussed in Section 6.1.2.

- The containment temperature is the saturation temperature at the steam partial pressure. The presence of drops in the DECLG will maintain a state near saturation. Even the MSLB is expected to operate near saturation, as shown by the superheated LST.

- The blowdown break source flow is assumed to enter containment at the saturation temperature corresponding to the total pressure. Saturation is also assumed for subsequent time phases to produce an upper bound on the drop and pool evaporation (Sections 7.1 and 7.2).

Given these assumptions, the reference values used to scale the containment gas are calculated and presented in Table 6-3.

The containment gas pi groups for mass, energy, and pressure are presented in Section 8.

6.5 MOMENTUM EQUATIONS INSIDE CONTAINMENT

Mixing within and between the AP600 containment compartments is characterized by stratification within compartments and by circulation between compartments. This section presents the relevant, dimensionless parameters and their context for scaling LST stratification results to AP600. The application of stratification results to AP600 is documented in Reference 5, Section 9. Circulation between compartments is analyzed and applied to AP600 in Reference 5, Section 9.

The scaling of momentum from forced and buoyant jets in large stratified volumes, such as the compartments and above-deck volumes in AP600, has been addressed by Peterson[29, 30, 31]. Baines and Turner[32] presented scaled relationships for density gradients in a stratified volume as a function of dimensionless plume characteristics. These references provide analytical bases for evaluating the effect of jets and plumes on enclosed volumes, and present equations for scaling the effects. Those references provide the analytical basis for scaling momentum in AP600 as it affects stratification and heat sink utilization during DBA.

Table 6-3 Reference Values for Containment Gas Scaling

Parameter	DECLG LOCA				MSLB
	Blowdown	Refill	Peak Pressure	Long Term	Blowdown
Containment gas temperature, °F	240	252	244	268	252
Total Pressure, psia, P_o	44	50	46	60	50
Saturation Temp, °F	273	281	276	293	281
Bulk air pressure, psia, $P_{air,o}$	18.9	19.3	19.0	19.7	19.3
Bulk steam pressure, psia, $P_{stm,o}$	25.0	30.7	26.9	40.3	30.7
Bulk stm density, lbm/ft.^{3}, $\rho_{stm,o}$	0.0587	0.0705	0.0627	0.0901	0.0705
Bulk air density, lbm/ft.^{3}, $\rho_{air,o}$	0.0732	0.0732	0.0732	0.0732	0.0732
Total density, lbm/ft.^{3}, ρ_o	0.1319	0.1437	0.1358	0.1632	0.1437
Liquid density, lbm/ft.^{3}, $\rho_{f,o}$	60.0	60.0	60.0	60.0	60.0
Break steam density, lbm/ft.^{3}, $\rho_{g,brk,o}$	0.1007	0.1132	0.1049	0.1337	0.1132
Specific heat ratio, γ_0	1.34	1.33	1.33	1.33	1.33
Enthalpy diff, B/lbm, $\Delta h_{g,brk,o}$	1084	1086	1084	1090	1086
Excess enthalpy, B/lbm, $h_{g,brk,o}$-$h_{stm,o}$	11.0	9.4	10.4	7.7	9.4
Internal energy diff, B/lbm, Δu_o	453.5	500.3	470.1	562.5	500.3
Break work, B/lbm	328.4	350.6	344.4	371.1	350.6
Compressibility Function, $(1+Z^T)_o$	1.065	1.080	1.074	1.103	1.080
Break stm flow, lbm/sec, $\dot{m}_{g,brk,o}$	4,444	200	200	45	367
Break pool flow, lbm/sec, $\dot{m}_{f,brk,p,o}$	5,555	0	200	200	0
Break drop flow, lbm/sec, $\dot{m}_{f,brk,d,o}$	2,222	0	0	0	0
IRWST liq flow, lbm/sec, $\dot{m}_{IR,o}$	0	0	0	245	0

Definitions

Stratification exists when horizontal layers overlie one another. A stably stratified gas volume has a vertical density distribution due to concentration and/or temperature in which the density decreases with elevation. The density gradient may change with time and must be considered, along with the vertical distribution of heat sinks in the volume, to calculate the heat and mass transfer rate histories. A stratified volume requires analytical methods with finer resolution than a single lumped volume. "Stably stratified" is not related to whether the gradient is weak or strong, only that it is stable over time.

An unstable containment atmosphere has no long-term, persistent temperature or concentration gradients, and requires such a high Froude number break source to disrupt stability that the resulting containment is well-mixed. In terms of the peak containment pressure, well-mixed is not necessarily good or bad, but produces well-defined boundary conditions for calculating heat and mass transfer rates between the atmosphere and the heat sinks. A well-mixed gas volume can be represented as a single lumped volume.

"Weakly stratified" is used as a qualitative measure of the vertical density gradient observed in the LST data for the LOCA configurations. "Weakly stratified" implies little vertical variation in the air/steam concentration, while "strongly stratified" implies nearly pure air at the deck elevation and nearly pure steam at the dome, which was never observed in the LST. If the jet entrainment is high enough, the resulting fluid circulation can nearly eliminate vertical concentration gradients, resulting in a weakly stratified atmosphere.

6.5.1 Froude Number Relationships

The internal mixing and stratification phenomena relative to the steam jet can be represented by the jet Froude number, or the Richardson number which is 1/Froude. The Froude number can be considered as a ratio of kinetic energy to potential energy, or $\rho U^2/\Delta\rho gH$. The Froude number is sometimes defined as the ratio Re^2/Gr. In AP600, interest is focused on the extent that the jet kinetic energy enhances mixing inside containment. During a design basis transient, the jet potential energy varies by a factor of 2 to 3, while the kinetic energy varies by many orders of magnitude. The Froude number is a more direct measure of the kinetic energy than its inverse, the Richardson number, and thus, the Froude number is used for scaling the AP600 internal phenomena.

The internal containment phenomena that are of interest for AP600 scaling are:

- The jet type, whether predominantly forced or buoyant, is important because it determines the rate at which the jet entrains and otherwise interacts with the containment volume.

- If the jet kinetic energy is high enough it may eliminate vertical gradients in the upper containment volume and to also induce mixing between the above-deck and below-deck regions as observed in some of the LST.

It is desired to use Froude number formulations that represent these phenomena in both AP600 and the LST to permit scaled inferences regarding mixing and stratification within a volume or compartment.

6.5.1.1 Forced/Buoyant Jet

Peterson recommended the following equation to determine the elevation where a forced jet transitions to a buoyant jet:

$$\left(\frac{\rho_0 U_o^2}{(\rho_a - \rho_0) g d_0}\right)^{-1/4}\left(\frac{\rho_0}{\rho_a}\right)^{-1/4}\left(\frac{z_{trans}}{d_0}\right) = 1 \qquad (84)$$

A jet Froude number can be defined, based on the jet source velocity, density, and diameter, and the ambient containment density:

$$Fr_{j,0} = \frac{\rho_0 U_0^2}{g(\rho_a - \rho_0) d_0} \qquad (85)$$

Rewriting Equation (84) in terms of the jet Froude number gives:

$$Fr_{j,0}\frac{\rho_0}{\rho_a} = \left(\frac{z_{trans}}{d_0}\right)^{-1} \quad \text{or} \quad \frac{z_{trans}}{d_0} = Fr_{j,0}^{1/4}\left(\frac{\rho_0}{\rho_a}\right)^{1/4} \qquad (86)$$

According to Equation (86), jet transition is not a function of the containment height or volume; the transition elevation only depends upon the jet source characteristics. Equation (86) is equally valid for predicting forced-to-buoyant jet transitions in AP600 and the LST.

6.5.1.2 Containment Stability

Peterson also presented equations for jets in large stratified fluid volumes. Peterson defined a stably stratified fluid as one in which the horizontal gradients of temperature, density, and concentration are negligible everywhere except at the boundaries of jets and wall boundary layers. Vertical gradients of temperature, density, and concentration remain, although their magnitude may be very small. His equation for a stably stratified volume is:

$$\left(\frac{(\rho_a - \rho_0) g d_0}{\rho_a U_0^2}\right)^{1/3}\frac{H}{d_0}\left(1 + \frac{d_0}{4\sqrt{2}\,\alpha H}\right)^{2/3} > 1 \qquad (87)$$

Taylor's jet entrainment parameter, α, can be assumed to be a constant with a value of 0.05 for this analysis.

A volumetric Froude number can be defined that is the square of the jet Reynolds number, divided by the containment Grashof number:

$$Fr_v = \frac{\rho_a U_0^2 d_0^2}{g(\rho_a - \rho_0) H^3} \qquad (88)$$

Rewriting Equation (87) for stable stratification in terms of the volumetric Froude number gives:

$$Fr_v < \left(1 + \frac{d_0}{4\sqrt{2}\,\alpha H}\right)^2 \tag{89}$$

As a measure of stability, or lack thereof, the volumetric Froude number can also be used to correlate vertical density gradients. It is shown in Table 6-4 that stability corresponds to a volumetric Froude number on the order of unity. Volumetric Froude values orders of magnitude greater than unity imply Reynolds number (or kinetic energy) dominated phenomena, while Froude numbers much less than unity imply that the Reynolds number is not an important parameter for mixing inside containment. Equation (89) is equally valid for AP600 and the LST with jets that are forced over most of the containment height.

6.5.2 Froude Numbers in AP600

The transient jet and volumetric Froude numbers for the AP600 DECLG and MSLB transients were calculated and presented in Figure 6-2 and Figure 6-3. The calculation assumes the typical transient pressure, mass, and enthalpy inputs from Section 3.

Values of the geometric parameters used to evaluate the jet and volumetric Froude numbers for AP600 and the LST are presented in Table 6-4. The values of the Froude numbers at the stability limit and for the jet transition elevation are summarized in Table 6-4 and compared to the AP600 transient Froude numbers in Figure 6-2 and Figure 6-3. The stability criterion shows the containment atmosphere is stably stratified during most of the transient (after approximately 3 sec during a DECLG and 50 sec for the MSLB). It is considered unlikely that a more rigorously applicable stability criteria would permit the conclusion that the atmosphere is unstable during the majority of the transient time. Therefore it is necessary to address the consequences of stratified gas volumes in the AP600 evaluation model. The consequences of stratification within regions or compartments are addressed in Reference 5 Section 9.

Equation (89) was derived from Peterson's equations for entrainment into a forced jet, so for Equation (89) to be applicable, it is necessary that the jet be predominantly forced, or $Z_{trans} \approx H$. Peterson also examined a stability criterion for buoyant jets, and concluded that buoyant jets almost never break up stably stratified fluid volumes. Thus, the criteria for instability are a predominantly forced jet, and violation of Equation (89).

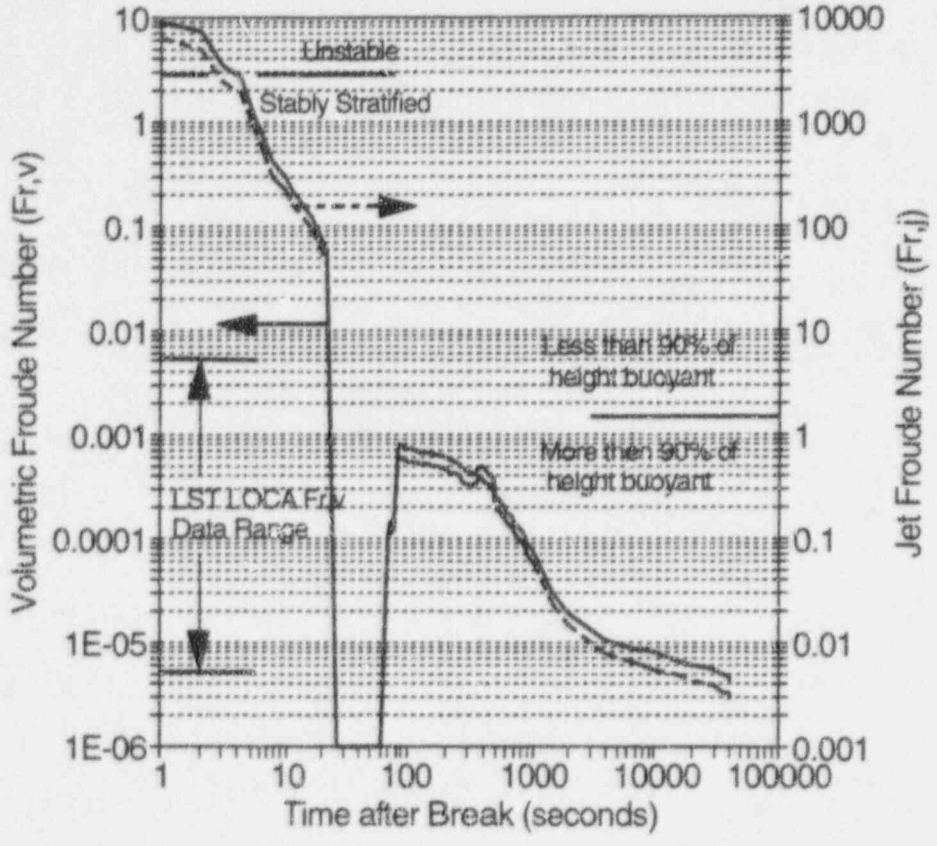

Figure 6-2 Froude Numbers Inside Containment for the AP600 DECLG

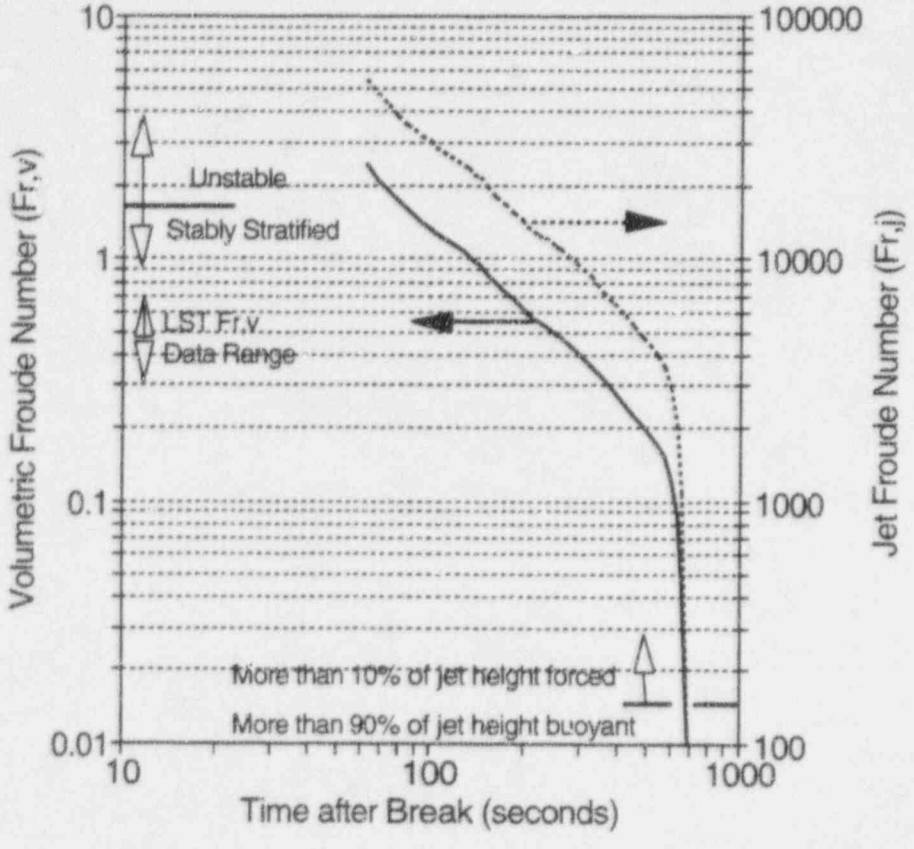

Figure 6-3 Main Steamline Break Jet and Volumetric Froude Numbers

Table 6-4 Geometric Parameters and Critical Froude Numbers for AP600 and LST LOCA and MSLB			
	AP600	LST	LST/AP600
LOCA:			
Height, H (ft.)	[redacted] a,b	13.2	1/8.26
Source Diameter, d_0, (ft.)	[redacted]	1.66	1/6.69
Fr_v at Stability Limit	2.96	3.57	1.21
$Fr_{j,0}$ at z_{trans} = 0.1H	1.46	0.62	0.42
$Fr_{j,0}$ at z_{trans} = H	1.46×10^4	0.62×10^4	0.42
MSLB:			
Height, H, (ft.)	[redacted] a,b	9.01	1/8.30
Source Diameter, d_0, (ft.)	[redacted]	0.256	1/9.61
Fr_v at Stability Limit	1.52	1.44	0.95
$Fr_{j,0}$ at ztrans = 0.1H	138	227	1.64
$Fr_{j,0}$ at ztrans = H	138×10^4	227×10^4	1.64

Stable/unstable regions are distinguished by the AP600 values of Fr_v presented in Table 6-4 calculated from Equation (89). Figure 6-2 and Figure 6-3 show the AP600 transients are expected to operate predominantly in the stably stratified regime.

For entrainment calculations it is important to know whether the jet is buoyant or forced, since buoyant and forced jets entrain the surrounding fluid at different rates. A forced jet transitions to a buoyant plume after traveling some distance and dissipating some of its kinetic energy. Thus, the first criterion to examine is whether the jet remains forced over the full height of containment, that is, what is the jet Froude number for Z_{trans} = H? The values were calculated for AP600 with Equation (86) and are presented in Table 6-4. Comparison to the transient Froude numbers in Figure 6-2 and Figure 6-3 show this criteria is never satisfied. So the jet always transitions to a plume before reaching the top of containment. The buoyant height of the jet is H - Z_{trans}, where H is the containment height above the source, and Z_{trans} is the height of the forced jet calculated from Equation (86).

The second criterion to consider is, since the jets cannot always be modeled as forced, can the jets be modeled as always buoyant? The strict answer is no, since Equation 86 always gives a finite value of Z_{trans}. However, if the jet is predominantly buoyant, say over 90 percent of the containment height, then it is reasonable to model the jet as buoyant over its full height. The value for Z_{trans} then is 10 percent of the height, and the corresponding jet Froude numbers are presented in Table 6-4. When compared to the AP600 jet Froude numbers, Figure 6-2 shows the DECLG jet height is 90 percent buoyant for the entire post-blowdown

time. Figure 6-3 shows the MSLB jet height does not become 90 percent buoyant until the end of the transient. Thus, prior to the end of the MSLB, the jet transition height must be calculated as a function of the jet Froude number and modeled as mixed (that is, part forced and the remainder buoyant) to accurately calculate entrainment.

6.5.2.1 Loss of Coolant Accident (LOCA)

The volumetric and jet Froude numbers were calculated for the AP600 DECLG, with the assumption of a well-mixed containment. The results are presented in Figure 6-2.

The fact that the jet and volumetric Froude numbers differ by a factor of 1000 simply results from the fact that $(H/d_0)^3 = 1000$, approximately. The jet Froude numbers show that the jet is mixed forced and buoyant over the first 27 sec. of the transient, and is buoyant over 90 percent or more of its height after 27 sec. The volumetric Froude numbers indicate that the containment is stably stratified after 4 sec. into the DECLG. The jet flow rate can cause the density gradients to increase or decrease, even while the containment atmosphere remains stably stratified. After approximately 1000 seconds, the time when external cooling becomes important, the volumetric Froude number is less than 1×10^{-4}. This is four orders of magnitude less than the stability limit. Consequently, it is expected that mixing between elevations above and below the jet source and above and below the operating deck, is limited to that induced by the large-scale circulation due to the rising buoyant jet. Furthermore, the very small magnitude of the volumetric Froude numbers (after 1000 sec.) indicates that the jet Reynolds number is not a factor in containment mixing during a LOCA.

6.5.2.2 Main Steamline Break (MSLB)

The volumetric and jet Froude numbers were calculated for an MSLB, with the assumption of a well-mixed containment. The results are presented in Figure 6-3. The jet Froude number indicates that the jet is mixed throughout the entire transient. The volumetric Froude number indicates that the containment volume is unstable over the first 40 seconds of the 700-second transient, and stable thereafter. It can be anticipated that this instability has the potential to induce a well-mixed state inside containment, both above and below the jet source elevation, and if the Froude number is high enough the vigorous mixing may even penetrate into the below-deck elevation. Comparison to the LST will indicate the effectiveness of mixing.

6.5.3 Froude Numbers in the Large-Scale Tests (LSTs)

The LSTs were conducted in several different internal configurations. The LST configuration with the steam source exiting from a diffuser located under the simulated steam generator approximates the geometric configuration of a LOCA, and the LST configuration with the steam source elevated 6 feet above the deck and exiting from a 3-inch ID pipe approximates

the geometric configuration of an MSLB. The mixing and stratification report, Ref. 5, Section 9, contains more description and discussion of these tests. Also the test data reports[10,17] and test drawings[18] describe the tests and hardware configurations.

6.5.3.1 LOCA Configuration

Twenty-five LSTs were conducted in the LOCA configuration, that is, with the diffuser located under the steam generator model. The jet Froude numbers ranged from 0.0016 to 0.231 and the volumetric Froude numbers ranged from $5x10^{-6}$ to $6x10^{-4}$. The LST Froude number ranges are compared to the AP600 DECLG Froude numbers in Figure 6-2. The figure shows that the LST data span the range of AP600 post-wetting operation. The jet Froude numbers indicate that over 92 percent of the LST jet height is buoyant, consistent with the post-blowdown buoyant height of 90 percent or more in AP600. The volumetric Froude numbers indicate that the LST containment atmosphere, like the post-blowdown AP600, is stably stratified with negligible momentum.

It is concluded that both the LST and AP600 LOCA jets are predominantly buoyant plumes, and the internal jet-induced mixing phenomena in the post-blowdown AP600 lies within the range of the LST.

As a further measure of mixing in the LST, steam concentrations just above the deck but below the jet source elevation (Elevation E) and below the deck in a dead-ended compartment near the bottom of the vessel (Elevation F) are presented in Figure 6-4. The plotted values are the ratio of the measured local steam partial pressure to the partial pressure of steam assuming perfect mixing. A value of 1.0 indicates perfect mixing. The values show the above-deck ratios generally range from 0.6 to 1.0 and the dead-ended compartment values range from 0.1 to 0.4. The data show no significant trend with the Froude number, as expected at these very low values of volumetric Froude number. These data support the fact that the jet Reynolds number is not a significant factor in containment mixing during the post-wetting phase of the DECLG.

6.5.3.2 MSLB Configuration

Four LSTs were conducted in the MSLB configuration, two with the steam jet directed horizontally and two with the jet directed upward. The jet Froude numbers ranged from 7,900 to 22,000 and the volumetric Froude numbers ranged from 0.286 to 0.695. The jet transitions from forced to buoyant in the LST at 25 to 35 percent of the containment height, compared to 40 to 71 percent in AP600. The greater forced height in AP600 will cause better mixing. The comparison of LST to AP600 volumetric Froude numbers in Figure 6-3 shows the LSTs lie at the minimum AP600 values and hence, confirm the least mixing to be expected in AP600. The mixing data measured in the LST and presented in Figure 6-4 show

that even at low volumetric Froude numbers mixing is nearly ideal, even in the bottom of the dead-ended compartment (MSLB-F in Figure 6-4).

These results are valid for both horizontally and vertically directed jet sources. It is expected that the high jet momentum during an MSLB will produce very effective mixing throughout the above-deck region of AP600, and some penetration through openings into the below-deck compartments.

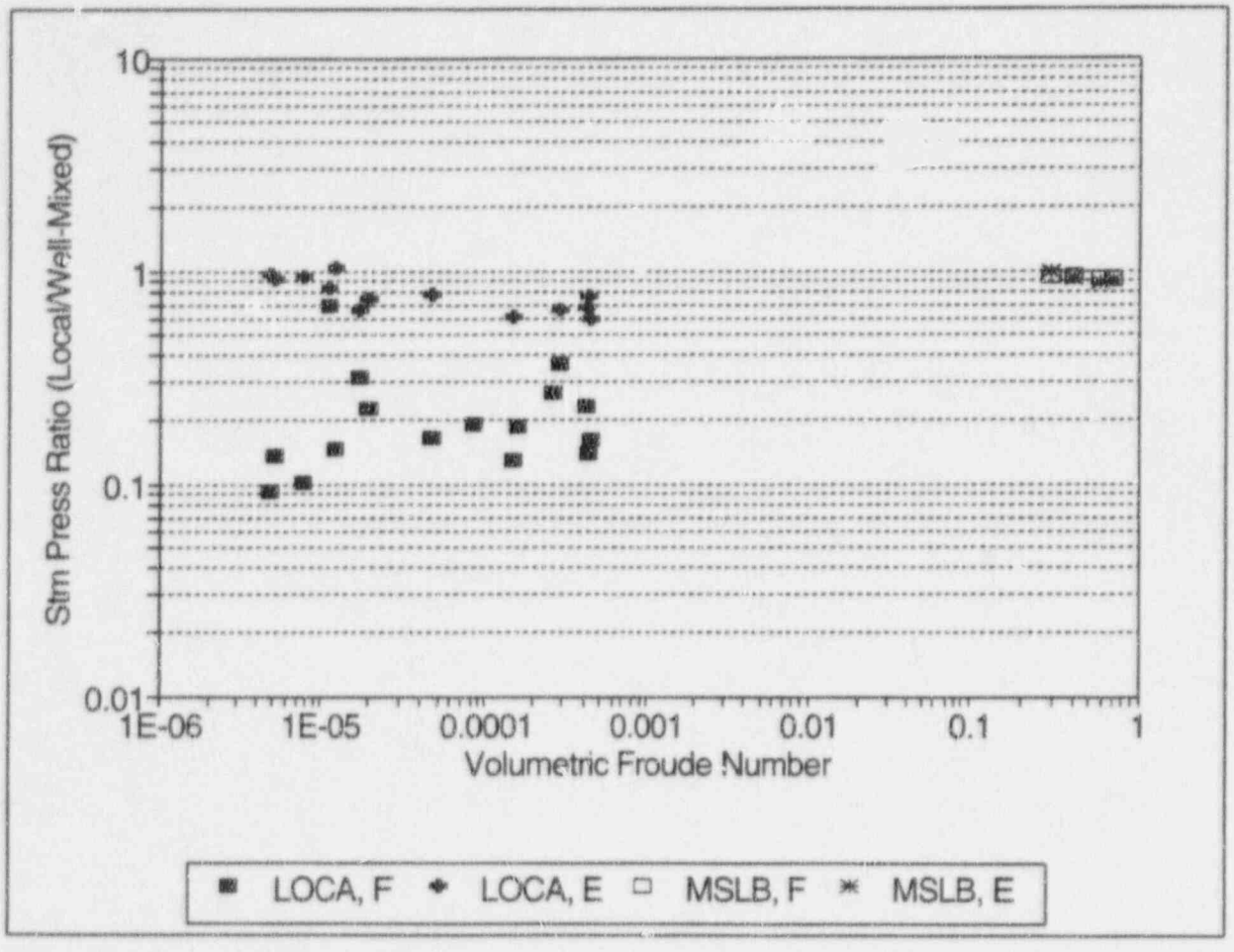

Figure 6-4 Steam Mixing Data Above and Below the Operating Deck from the LST

7 HEAT SINK ANALYSIS AND EQUATIONS FOR SCALING

Energy equations are required for each heat sink to track the temperature-time history that determines the heat and mass transfer rates between the atmosphere and the heat sink. As the heat sink temperature changes, the boundary layer and surface properties that appear in the transport equations also change. Consequently, for each heat sink, several properties must be determined.

The boundary condition for the heat sink energy interaction with the containment gas is the containment gas temperature and pressure history from WGOTHIC. This boundary condition is used to define the initial condition for each of the time phases shown in Figure 3-4. The containment gas energy interaction with the heat sinks is modeled using integral equations and other techniques to simplify the otherwise complicated time integration for each heat sink. The modeling method for each heat sink type is summarized in Table 7-1.

Table 7-1 Method Used to Model the Energy Absorbed by Heat Sinks

Heat Sink	Method
Drops, d	Exponential Approximation
Break Pool, p	Evap from a spreading layer
Internal Film, if	Steady-state conduction
Internal Steel, st	Lumped parameter
Internal Concrete, cc	Integral equation
Jacketed Concrete, jc	Bounded
Shell, sh	Integral equation
Baffle, bf	Lumped parameter
Chimney Concrete, ch	Integral equation

The state of the heat sinks are determined by tracking the heat sink heat and mass transfer interactions with the bulk gas from the beginning of the transient. The bulk gas properties are modeled as simple functions (either constant or linearly changing with time) during a time phase. The heat sinks are modeled using solutions that provide the heat sink surface temperature, which is needed to calculate the heat and mass fluxes, and the heat sink bulk, or average temperature that is needed to track the energy stored in the heat sink.

Heat sinks reduce containment pressure by absorbing energy that reduces the mass and energy stored in the gas atmosphere. Heat sinks are both solid and liquid. Solid heat sinks are

composed of steel and/or concrete and include walls, floors, ceilings, exposed structural steel, equipment, and the containment shell. Liquid heat sinks include drops, pools, and films.

Solid heat sinks include steel, concrete, and steel-jacketed concrete. These are treated as distinct heat sinks because each has different thermal conduction characteristics. Heat transfer to steel heat sinks is limited by the heat and mass transfer coefficient, whereas heat transfer to concrete is limited by internal conduction resistance.

Solid heat sinks are affected by condensation, radiation, and convection heat transfer. Evaporation from solid heat sinks requires a continuous liquid source which is not present inside containment. Consequently, internal solid heat sinks only reject heat by radiation and convection.

The shell is a solid heat sink with a surface that is subdivided into three regions, each with a distinctly different external energy transfer resistance. The three regions are subcooled, evaporating, and dry, corresponding to the dominant processes on the outside of the shell. In the subcooled region, the external liquid film is the heat sink. Evaporation, radiation, and convection from the subcooled film are neglected. In the evaporating region all of the energy is transferred to the riser by evaporation and convection, and to the baffle by radiation. In this scaling analysis, the evaporating film is assumed to have no sensible heat capacity, consistent with the classic Nusselt film solution. In the dry region, there is no external liquid film; heat is rejected by convection heat transfer to the riser gas and by radiation to the baffle.

Liquid heat sinks include drops, the break pool, the IRWST, and films. Liquid heat sinks can interact with the containment gas both by evaporation and condensation, as well as by radiation and convection heat transfer.

A general form of the energy conservation equation for liquid and solid heat sinks is:

$$mc_v\frac{dT}{dt} = \dot{m}_{in}c_v(T_{in}-T) - \dot{m}_{out}c_v(T_{out}-T) + \dot{q}_{in} - \dot{q}_{out} \qquad (90)$$

where the convective flow terms may be present for liquid heat sinks, but are absent for solid heat sinks. Equation (90) is modified as necessary for each of the heat sinks. Each of the $\dot{q}$ terms in Equation (90) may include the three parallel energy transfer components: mass transfer, convection heat transfer, and radiation heat transfer. Using the subscripts c, r, and m to denote convection heat transfer, radiation heat transfer, and condensation/evaporation mass transfer, and adding an x for the outside of the containment shell or the outside of the baffle:

$$\dot{q}''_{in} = \dot{q}''_m + \dot{q}''_c + \dot{q}''_r \quad \text{and} \quad \dot{q}''_{out} = \dot{q}''_{mx} + \dot{q}''_{cx} + \dot{q}''_{rx} \qquad (91)$$

Each of these energy transfer terms can be written as the product of a conductance and a temperature difference, $\dot{q}'' = h\Delta T$. In addition, the mass flux is written in terms of mass conductance, temperature difference, and enthalpy change, $\dot{m}'' = h_m\Delta T/(h_g-h_f)$. The subscript e is used to denote an equivalent heat transfer coefficient, h_e, when conductances are combined in series and/or parallel.

In general only three of the terms in Equation (90) are of interest for scaling AP600. The three terms include the two heat flux terms (in most cases there is only one of these two) that are normalized by the break enthalpy flow rate and define the $\pi_{e,i}$ groups in Equation (69), and the transient term that is normalized by the heat flux to define the heat sink time constant. The heat sink time constant provides valuable information on the time period when the heat sink is effective.

7.1 DROP ANALYSIS AND SCALING EQUATIONS

Drops, or fog particles, are created when the blowdown break source steam disperses a fraction of the break liquid along with the gas. After blowdown, the gas velocities in the break are too low to entrain a significant quantity of drops from the break liquid. The MSLB break flow does not include liquid until near the end of the blowdown when the drops have little or no effect on pressurization. Consequently, drops are created only during the blowdown phase of the DECLG.

Well-accepted phenomenological models are not available to predict the mass of drops created during blowdown, so an upper-limit entrainment rate equal to 1/2 the gas mass flow rate is assumed for the full blowdown period. It is assumed that the entire mass of drops are created with a diameter of 0.001 inch, which provides a sufficiently large surface area to strongly, thermally couple the drops to the containment atmosphere. In addition, at 0.001 in diameter, drops are strongly coupled by shear to the moving gas, even at low velocities, and persist for an extended period of time. (Since both couplings are strong, a smaller drop diameter has no effect, but a significantly larger diameter will reduce the coupling and further decrease the effect of drops). Ultimately, coalescence or other processes cause the drops to be removed from the atmosphere. The drops are assumed to enter containment at the saturation temperature based on the total gas pressure. The scaling calculations presented later show that even with assumptions that maximize the effect of drops, the effect of drops is small during blowdown and refill, and negligible thereafter.

The assumption that the drops remain at a constant diameter throughout the transient can be checked against the maximum evaporation fraction that results from reducing the drop temperature to the minimum system temperature of 120 F, $f = c_v \Delta T/h_{fg}$ =1(273-120)/1000 = 15 percent. Since the volume is proportional to d^3, the diameter change, Δd, will be approximately 1/3 of ΔVol, or only 5 percent.

The assumption that the drop surface area remains constant throughout the transient maximizes the surface area and consequently, the effect of the drops on containment pressure. However, it is clear the drops will agglomerate and fall out, thereby reducing the available surface area during the transient. The assumption of constant area can be justified by showing that even when maximized, the drops have a negligible effect on containment pressure. Examination of the magnitude of the post-refill pressure pi groups in Table 8-5 shows the effect of drops on containment pressure is less than 1 percent of the source pressurization, and consequently can be neglected with no significant effect on pressure.

The drops affect the containment atmosphere in three ways. First, a fraction of the drop flashes to steam when the drops enter containment. Second, the drops remain strongly coupled to the temperature of the atmosphere, so as the atmospheric temperature changes throughout the transient, the drop temperature closely follows the atmospheric temperature changes. The strong temperature coupling maintains the containment gas at or very near saturation. Third, the small diameter drops are strongly coupled to the moving convective gas flows, which effectively increases the gas density and affects circulation and potentially, heat sink utilization. The first and second of these effects are evaluated in this scaling analysis and the third is evaluated in Ref. 5, Section 9.

The following calculations show how strongly the drops are coupled to the atmosphere, by showing the effective time constant for the flashing drop is very small.

Drop Surface Area Calculation

The major parameter involved in drop-atmospheric interactions is the large surface area of the drops. That area is calculated as follows:

- The drop specific length, $L^s = V_{drop}/A_{drop} = D/6 = 0.001$ in $/(6x12$ in/ft.$) = 1.39x10^{-5}$ ft.
- At 50 percent of the gas mass the drop mass is $\dot{m}_{g,brk,o}\Delta t/2 =$ ~~4444~~ lbm/sec*27 sec / 2 = 60,000 lbm.
- The drop total volume is $m/\rho =$ 60,000 lbm / 60 lbm/ft^3 = 1000 ft^3.
- The total drop surface area is the number of drops times the area of a single drop, $A_{tot} = nA_{drop}$, and $n = V_{tot}/V_{drop}$, so $A_{tot} = A_{drop}\ V_{tot}/V_{drop} = V_{tot}/L^s = 1000$ ft$^3/1.39x10^{-5}$ ft. $= 7.2x10^7$ ft^2.
- The drop characteristic length is $L = V_{ct}/A_{tot} = 1.74x10^6/7.2x10^7 = 0.0242$ ft.

Time Constant Calculation

The "flashing and following" evaporation processes occur on two different time scales. Flashing occurs almost instantaneously as saturated drops are introduced to a containment atmosphere at a lower steam partial pressure, while following occurs on a time scale equal to the duration of the time phase.

Drops are assumed to enter containment saturated at the containment total pressure. Since $P_{stm,srf} = P_{tot}$ it must be the case that $P_{air,srf} = 0$ so the log-mean air pressure in the denominator of the mass transfer rate equation approaches 0 and the mass transfer rate is unbounded. More realistically, the initial evaporation rate from the surface is very high, but bounded, due to the presence of dissolved gasses that are released along with the vapor. Furthermore, the liquid surface temperature must change continuously and remain bounded: the high initial mass transfer rate occurs over a very small time period so the product of mass transfer rate and Δtime is finite, as is the internal energy change of the drop or surface layer. The initial high evaporation rate quickly cools the liquid and produces a value of $P_{stm,srf}$ less than P_{tot}. Then the air partial pressure is greater than zero, so the mass transfer rate equation is valid.

The small drop can be modeled as a lumped mass, and the mass and energy equations for the initial drop flashing can be approximated by neglecting the sensible heat transfer terms, so:

$$\frac{dm_d}{dt} = \dot{m}_{d,flash} \quad \text{and} \quad m_d c_v \frac{dT_d}{dt} = \dot{m}_{d,flash} h_{fg} \tag{92}$$

From this, a finite difference equation relating the evaporation rate to the drop temperature change can be written:

$$\Delta T_d = \frac{\dot{m}_{d,flash} h_{fg} \Delta t}{m_d c_v} \tag{93}$$

and integrated (or summed) to generate a time-temperature history. This was done for a drop during blowdown and the results are shown in Figure 7-1. The singularity in the mass flux equation was avoided by starting with an initial temperature 0.05°F cooler than the saturation temperature. A 0.05°F difference requires a negligible mass of evaporation and avoids the zero air partial pressure singularity. The calculated drop temperature is compared to an exponential temperature change and shows the calculated curve is steeper than the exponential initially, as expected since the slope is unbounded as t approaches zero. Later in the transient the exponential approximation decays faster than the calculated curve. Although a time constant cannot be defined based on dT/dt at t = 0, the time constant for the exponential curve shown in Figure 7-1 was determined by forcing the exponential to coincide with the calculated curve at 68 percent (one exponential time constant) of the

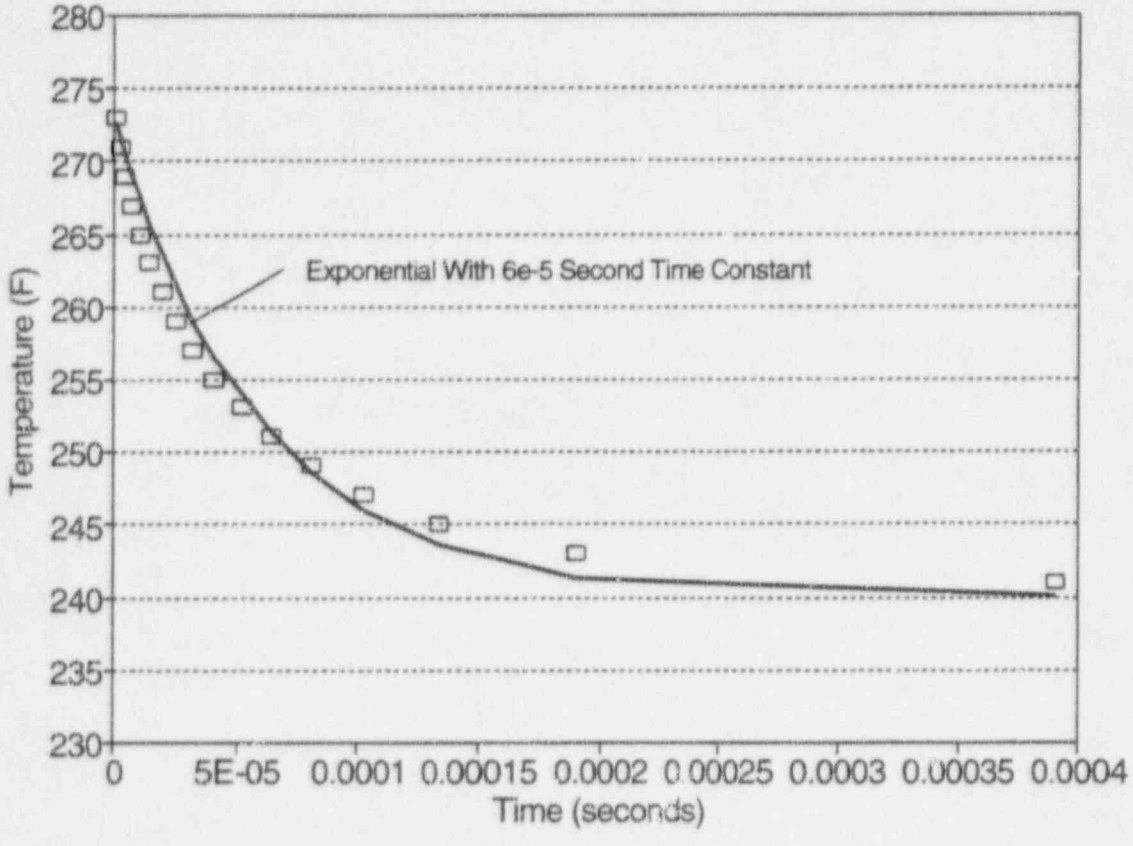

Figure 7-1 Exponential Approximation to the Cool-Down of Saturated Drops Injected into Containment

temperature change. The resulting time constant is $6x10^{-5}$ sec. and can be used to approximate the behavior of drops. The time constant for drops beyond blowdown changes less than a factor of 2, so the drops remain in thermal equilibrium with the atmosphere as long as they persist.

Since flashing is effectively instantaneous, relative to the other time constants for the system, the flashing will occur independent of other phenomena. The fraction of the drop that flashes can be estimated by relating the energy released by flashing to the sensible temperature change of the drop:

$$\dot{m}_{d,flash} h_{fg} = \dot{m}_d c_V (T_{in} - T) \quad \text{or} \quad f = \frac{\dot{m}_{d,flash}}{\dot{m}_d} = \frac{c_V (T_{in} - T)}{h_{fg}} \tag{94}$$

Calculations for the conditions during blowdown give f = 0.035, so 3.5 percent of the drop flashes to steam upon entering containment. The rate at which drops enter containment is 2222 lbm/sec during blowdown and zero thereafter, so the value for $\dot{m}_{d,flash}$ = 0.035 (2222 lbm/sec) = 77.7 lbm/sec during blowdown and zero thereafter.

7.1.1 Drop Conductance

The individual conductance terms for mass evaporation, heat convection, and radiation from the drop to the containment atmosphere are:

$$h_m = \frac{2(h_g - h_f)\rho_{stm} D_v}{(T_d - T)d} \frac{\Delta P_{stm}}{P_{lm,air}} \left(\frac{Sc}{Pr}\right)^{1/3} \quad h_c = \frac{2k}{d} \quad h_r = \sigma \varepsilon f(T_d, T)$$
$$h_m = \frac{2(h_g - h_f)\rho_{stm} D_v}{d} \left(\frac{Sc}{Pr}\right)^{1/3} \frac{dP_{sat}}{dT} \frac{\Delta T}{P_{air}} \quad (\text{for } \Delta T = 0) \quad \text{and} \quad h_e = h_m + h_c + h_r \tag{95}$$

The first definition of h_m is used to calculate the drop flashing mass transfer rate in Section 7.1, and the second, containing dP_{sat}/dt is used to calculate the evaporation rate as the drops follow the containment temperature throughout the transient. The individual conductances are scaled by dividing each term by the shell conductance, that includes the shell and coating, $h_{sh,o} = (\delta_{sh,o}/k_{sh,o} + 2\delta_{coat}/k_{coat})^{-1}$ so that:

$$\pi_{c,m,d} = h_{m,d,o}/h_{sh,o} \quad \pi_{c,c,d} = h_{c,d,o}/h_{sh,o} \quad \pi_{c,r,d} = h_{r,d,o}/h_{sh,o} \quad \pi_{c,e,d} = h_{e,d,o}/h_{sh,o} \tag{96}$$

7.1.2 Drop Mass Transfer

The mass rate of change equation includes terms for the drop source flow rate, the flashing rate, and the evaporation rate due to the atmospheric rate of temperature change. Because

the drops are assumed to persist for some time, the equation does not include a convective outflow mass term. The drop mass conservation equation is:

$$\frac{dm_d}{dt} = \dot{m}_{d,in} - \dot{m}_{d,flash} - \dot{m}_{d,evap} \tag{97}$$

The drop flashing and evaporation rate terms affect pressurization, so they are the terms of interest for scaling. The flashing and evaporation rates are normalized by the break source steam mass flow rate and made dimensionless with the constant $\dot{m}_{d,flash} = \dot{m}_{d,flash,o}$ and the variable $\dot{m}_{d,evap} = \dot{m}_{d,evap,o}\dot{m}^*_{d,evap}$.

$$\frac{\dot{m}_{d,flash}}{\dot{m}_{g,brk,o}} = \frac{\dot{m}_{d,flash,o}\dot{m}^*_{d,flash}}{\dot{m}_{g,brk,o}} = \pi_{m,flash,d}\dot{m}^*_{d,flash} \qquad \frac{\dot{m}_{d,evap}}{\dot{m}_{g,brk,o}} = \frac{\dot{m}_{d,evap,o}\dot{m}^*_{d,evap}}{\dot{m}_{g,brk,o}} = \pi_{m,evap,d}\dot{m}^*_{d,evap} \tag{98}$$

$$\text{where} \quad \pi_{m,flash,d} = f\frac{\dot{m}_{f,brk,d}}{\dot{m}_{g,brk,o}} \quad \text{and} \quad \pi_{m,evap,d} = \frac{2\rho_{stm}D_v}{d}\frac{dP_{sat}}{dT}\frac{\Delta T}{P_{air}}\left(\frac{Sc}{Pr}\right)^{1/3}\frac{A}{\dot{m}_{g,brk,o}}$$

The two drop mass pi groups are added to get the single mass pi group defined for transfer to a heat sink in Equation (59).

The values of the flashing and evaporating mass flow rates were calculated and scaled in Section 7.1.

7.1.3 Drop Energy Transfer

The drops are assumed to enter containment as saturated liquid at the containment total pressure. This introduces saturated drops with a temperature and steam partial pressure higher than the containment temperature and steam partial pressure. Consequently, the liquid drops evaporate to the containment gas and also transfer heat to the gas by convection and radiation. Drop removal is neglected. The energy equation for the drop is:

$$m_d c_{v,f}\frac{dT_d}{dt} = \dot{m}_{d,in}c_{v,f}(T_{in} - T_d) - \dot{m}_{d,flash}h_{fg} - \dot{m}_{d,evap}h_{fg} - h_{q,d}A_d(T - T_d) \tag{99}$$

Since the drop source is zero after blowdown, the flashing term is also zero after blowdown.

The dimensionless variables needed to make the flashing, evaporating, and heat transfer terms in the drop energy equation dimensionless are:

$$\dot{m}_{flash,d} = \dot{m}_{flash,d,o}$$
$$\dot{m}_{evap,d} = \dot{m}_{evap,d,o}\dot{m}^*_{evap,d}$$
$$h_{fg} = h_{fg,o}h^*_{fg}$$
$$h_{q,d} = h_{q,d,o}h^*_{q,d}$$
$$A_d = A_{d,o}$$
$$(T-T_d) = (T-T_d)_o\,\Delta T_d^*$$

The energy transfer rate from containment to the drops is scaled to the containment gas energy equation, using the break source enthalpy flow rate, $\dot{m}_{g,brk,o}\Delta h_{g,brk,o}$ and the dimensionless variables defined above:

$$\frac{\dot{m}_{flash,d}h_{fg}}{\dot{m}_{g,brk,o}\Delta h_{g,brk,o}} = \frac{\dot{m}_{flash,d,o}h_{fg,o}}{\dot{m}_{g,brk,o}\Delta h_{g,brk,o}}\dot{m}^*_{flash,d}h^*_{fg} = \pi_{e,fg,f}\dot{m}^*_{flash,d}h^*_{fg}$$
$$\frac{\dot{m}_{evap,d}h_{fg}}{\dot{m}_{g,brk,o}\Delta h_{g,brk,o}} = \frac{\dot{m}_{evap,d,o}h_{fg,o}}{\dot{m}_{g,brk,o}\Delta h_{g,brk,o}}\dot{m}^*_{evap,d}h^*_{fg} = \pi_{e,fg,f}\dot{m}^*_{evap,d}h^*_{fg} \qquad (100)$$
$$\frac{h_{q,d}A_d(T-T_d)}{\dot{m}_{g,brk,o}\Delta h_{g,brk,o}} = \frac{h_{q,d,o}h^*_{q,d}A_{d,o}(T-T_d)_o\Delta T_d^*}{\dot{m}_{g,brk,o}\Delta h_{g,brk,o}} = \pi_{e,q,d}h^*_{q,d}\Delta T_d^*$$

where the pi groups are defined:

$$\pi_{e,fg,d,flash} = \pi_{m,flash,d}\frac{h_{fg,o}}{\Delta h_{g,brk,o}} \qquad \pi_{e,fg,d,evap} = \pi_{m,evap,d}\frac{h_{fg,o}}{\Delta h_{g,brk,o}}$$
$$\pi_{e,q,d} = \frac{h_{q,d,o}A_o(T-T_d)_o}{\dot{m}_{g,brk,o}\Delta h_{g,brk,o}} = \left[\frac{2k}{d} + \sigma\varepsilon f(T_d,T)\right]\frac{A_o(T-T_d)_o}{\dot{m}_{g,brk,o}\Delta h_{g,brk,o}} \qquad (101)$$

This heat transfer pi group is the same ratio of terms as defined in Equation (70) for containment heat sinks. The flashing and evaporating groups are added to get the single phase change pi group, $\pi_{e,fg,f}$, defined in Equation (70). The liquid pi group is zero because the liquid film is part of the drop mass.

After a drop is created and flashes to near-equilibrium with the containment atmosphere, its temperature remains strongly coupled to the containment temperature and follows containment temperature changes at the same rate dT/dt. The energy equation for the drop can then be written in terms of the equivalent heat transfer coefficient (that includes mass, convection, and radiation heat transfer) as:

$$m_d c_v \frac{dT}{dt} + h_{e,d}A_d(T_d - T) \qquad (102)$$

7.1.4 Drop Effect on Pressure

The pressure scaling for the drops uses the pi group definitions of Equations (81) for each of the flashing and evaporating mass transfer pi groups. The single heat transfer pressure pi group, $\pi_{p,q,d}$, is defined in Equation (83). The drop pressure pi groups are:

$$\pi_{p,enth,flash,d} = \pi_{m,flash,d}\frac{(\gamma-1)_o}{\gamma_o(1+Z^T)_o}\frac{\rho_{stm,o}}{P_{stm,o}}(h_{stm,d}-h_{stm})_o \qquad \pi_{p,work,flash,d} = \pi_{m,flash,d}$$

$$\pi_{p,enth,evap,d} = \pi_{m,evap,d}\frac{(\gamma-1)_o}{\gamma_o(1+Z^T)_o}\frac{\rho_{stm,o}}{P_{stm,o}}(h_{stm,d}-h_{stm})_o \qquad \pi_{p,work,evap,d} = \pi_{m,evap,d} \qquad (103)$$

$$\pi_{p,q,d} = \frac{(\gamma-1)_o}{\gamma_o(1+Z^T)_o}\frac{\rho_{stm,o}}{P_{stm,o}}\frac{h_{q,d,o}A_{d,o}(T-T_d)_o}{\dot{m}_{g,brk,o}}$$

7.2 BREAK POOL ANALYSIS AND SCALING EQUATIONS

The break liquid is assumed to enter containment as saturated liquid at the containment total pressure. This is likely the case during the DECLG blowdown, whereas post-blowdown the liquid may be somewhat subcooled, depending on emergency core cooling system (ECCS) injection rates and mixing. The maximum containment pressure would result if all of the stored and decay heat produced steam with the liquid remaining at its initial temperature of 120°F. However, this would give the trivial case of no pool vaporization and maximum condensation on the pool. On the other hand, assuming the break liquid exits the break as saturated at containment total pressure will maximize the evaporation rate from the break liquid. The latter case of saturated break flow is assumed to permit calculations that show pool evaporation is never very large.

During blowdown the break liquid flow rate is approximately 1.75 times the gas flow rate. This liquid flow rate splits into two fractions, 0.5 times the gas flow rate is atomized to drops (Section 7.1), and the remainder is liquid flow rate to the pool. However, the vigor of blowdown causes extensive liquid splashing that wets most of the surface area in the break steam generator and the stairwell. This surface area, along with that of the blobs and large drops produce a large surface for mass transfer. In lieu of a mechanistic calculation of these complicated phenomena, an upper bound on the evaporation rate can be estimated by assuming that as much liquid evaporates as possible. This upper bound is calculated the same way as the flashing fraction of drops in Section 7.1:

$$\dot{m}_{flash,p}h_{fg} = \dot{m}_{in,p}c_V(T_{sat}(P_{tot})-T_{sat}(P_{stm})) \qquad \text{and} \qquad f=\frac{\dot{m}_{flash,p}}{\dot{m}_{in,p}} \qquad (104)$$

For a total pressure of 44 psia, steam partial pressure of 25 psia, c_V = 1 B/lbm-F, and h_{fg} = 918.6 B/lbm, f = 0.036. That is, 3.6 percent of the pool flow flashes to achieve thermal

and mechanical equilibrium with the bulk containment gas. Since the break gas mass flow rate and pool flow rates are equal, the pool flashing pi group (Section 7.2) has the value 0.036.

The total blowdown liquid mass is used as the reference value. The total blowdown liquid mass is approximately 210,000 lbm, so the bounding break pool mass (total minus drops) is 150,000 lbm. The corresponding break pool volume is 2500 ft^3.

At the initial containment pressure of 15.7 psia the initial liquid temperature is 215°F. The liquid is surrounded by the containment air at 120°F and bounded by concrete heat sinks initially at 120°F. Consequently, the liquid evaporates to the containment gas, transfers heat to the gas by convection and radiation, and transfers heat by convection and conduction heat transfer to the concrete walls. The energy transfer rate to the solid heat sinks will likely be greater than to the atmosphere. However, an upper limit estimate is desired for the evaporation to the atmosphere. Consequently, to maximize the evaporation rate, the maximum pool temperature should be used. Assuming the pool stratifies strongly, which to some extent will be the case, the pool surface temperature is the same as that of the incoming liquid through the time of the peak containment pressure. This provides the surface temperature and saturation pressure needed to calculate heat and mass transfer to the gas.

At some time, well beyond the time of the peak containment pressure, the containment saturation temperature may be reduced to a value less than the pool temperature. The large heat capacity of the pool causes it to remain hot after containment temperature begins to drop. When the break liquid is no longer hotter than the pool, a lumped-mass calculation of the pool temperature, assuming only heat interactions with the atmosphere, can give a conservatively high pool surface temperature for evaporation calculations. However, this is beyond the time under consideration for this scaling analysis, so only the stratified approximation is considered.

7.2.1 Pool Conductance

The individual conductance terms for mass evaporation, heat convection, and radiation from the pool to the containment atmosphere are:

$$h_m = \frac{0.13(h_g - h_f)\rho_{stm} D_v}{(T - T_{srf})(\nu^2/g)^{1/3}} \frac{\Delta P_{stm}}{P_{lm,air}} \left(\frac{\Delta\rho}{\rho} Sc\right)^{1/3} \qquad h_c = \frac{0.13k}{(\nu^2/g)^{1/3}} \left(\frac{\Delta\rho}{\rho} Pr\right)^{1/3} \qquad (105)$$

$$h_r = \sigma \varepsilon f(T, T_{srf}) \qquad h_e = h_m + h_c + h_r$$

The individual conductance terms are normalized by dividing each term by the shell conductance, $h_{sh,o} = k_{sh,o}/\delta_{sh,o}$ so that:

$$\pi_{c,m,p} = h_{m,p,o}/h_{sh,o} \quad \pi_{c,c,p} = h_{c,p,o}/h_{sh,o} \quad \pi_{c,r,p} = h_{r,p,o}/h_{sh,o} \quad \pi_{c,e,p} = h_{e,p,o}/h_{sh,o} \tag{106}$$

7.2.2 Pool Mass Transfer

The break pool is created from the blowdown break liquid that is not dispersed along with the gas but pours into the bottom of the steam generator and reactor cavities. Liquid from drop fallout and condensation below the operating deck also drain into the break pool. Liquid that condenses and falls out above the operating deck drains into the IRWST. The pool mass rate equation is:

$$\frac{dm_p}{dt} = \dot{m}_{f,brk,p} + \dot{m}_{in,p} - \dot{m}_{evap,p} \tag{107}$$

The term that is of interest for scaling is the pool evaporation rate term. That term is normalized by the break steam flow rate and made dimensionless with the variable $\dot{m}_{evap,p} = \dot{m}_{evap,p,o}\dot{m}^*_{evap,p}$:

$$\frac{\dot{m}_{evap,p,o}}{\dot{m}_{g,brk,o}} = \frac{\dot{m}_{evap,p,o}\dot{m}^*_{evap,p}}{\dot{m}_{g,brk,o}} = \pi_{m,evap,p}\dot{m}^*_{evap,p} \tag{108}$$

The effect of the pool on containment pressure is maximized by assuming the liquid enters at the containment saturation temperature, similar to drops. The saturated break liquid is assumed to flow across the top of the pool and to cool as it spreads. The net evaporation rate is the integrated evaporation flux over the surface area. The pool surface temperature was assumed to be at a steady-state with the spreading layer evaporating to the atmosphere, but not mixing or conducting to the cooler layer below. This maximizes the evaporation rate, resulting in the maximum pressure effect. The resulting evaporation rates are presented in Table 7-2 for each time phase.

The break pool surface area changes with time as the pool level rises. Since the analysis shows the evaporation rate is a small fraction of the flow into the pool, the pool liquid volume can be estimated as the integral of the flow rate over time. Using the flow rates and times of each phase from Table 7-3, the pool volume at the start of each time phase was calculated and the pool surface area was determined from the relationship between break pool volume and surface area shown in Figure 3-8. The results are summarized in Table 7-3.

Since the break flow rate drops to essentially zero during the refill time phase, the break pool evaporation rate during refill is assumed to be zero.

Table 7-2 Pool Evaporation Rate for a Saturated Liquid Break Source						
	Boundary Conditions			Calculated Pool Values		
Time Phase	P total psia	T sat °F	T bulk °F	Pool Area ft²	Evap Rate lbm/sec	$\dot{m}_{evap}/\dot{m}_{g,brk,c}$
Blowdown	44	273.1	240.2	420	7.1	0.0359[1]
Refill	50	281.0	252.0	533	0	0
Peak Pressure	46	275.8	244.2	1933	5.20	0.0260[2]
Long Term	60	292.7	267.7	1933	4.60	0.0657[2]

1. Calculated by flashing to equilibrium, Equation (104).
2. Calculated from spreading layer model.

Table 7-3 Break Pool Surface Area During DECLG Transient				
Phase	ΔTime sec	Break Flow Rate lbm/sec	Pool Volume ft³	Surf Area ft²
Blowdown	27	4,444	2500	420
Refill	60	0	2500	555
Peak Pressure	1,500	200	7200	1933

7.2.3 Pool Energy Transfer

The break liquid is assumed to leave the break saturated at the containment total pressure. The resulting temperature is always greater than the containment gas temperature, since the containment temperature remains approximately at the saturation temperature corresponding to the steam partial pressure. The energy equation for the pool is:

$$m_p c_{v,f} \frac{dT_p}{dt} = \dot{m}_{brk,f} c_{v,f} (T_{brk} - T) + \dot{m}_{in,p} c_{v,f} (T_{drain} - T) - \dot{m}_{evap,p} h_{fg,p} - h_{q,p} A_p (T - T_p) \quad \textbf{(109)}$$

The pi groups for scaling pool energy were defined in containment Equation (70) for the heat sinks, with the exception that the liquid film is part of the pool, so is not separately evaluated. The equations are:

$$\pi_{e,fg,p} = \pi_{m,p}\frac{h_{fg,p,o}}{\Delta h_{g,brk,o}}$$

$$\pi_{e,q,p} = \frac{h_{q,p,o}A_{p,o}(T-T_p)_o}{\dot{m}_{g,brk,o}\Delta h_{g,brk,o}} = \left[\frac{0.13k}{(\nu^2/g)^{1/3}}\left(\frac{\Delta\rho}{\rho}Pr\right)^{1/3} + \sigma\varepsilon f(T,T_p)\right]\frac{A_{p,o}(T-T_p)_o}{\dot{m}_{g,brk,o}\Delta h_{g,brk,o}} \quad (110)$$

7.2.4 Pool Effect on Pressure

The pressure scaling for the break pool uses the pi group definitions of Equations (81) for the evaporating mass transfer pi groups and Equation (83) for the heat transfer pi group:

$$\pi_{p,enth,p} = \pi_{m,p}\frac{(\gamma-1)_o}{\gamma_o(1+Z^T)_o}\frac{\rho_{stm,o}}{P_{stm,o}}(h_{stm,p}-h_{stm})_o \qquad \pi_{p,work,p} = \pi_{m,p}$$

$$\pi_{p,q,p} = \frac{(\gamma-1)_o}{\gamma_o(1+Z^T)_o}\frac{\rho_{stm,o}}{P_{stm,o}}\frac{h_{q,p,o}A_{p,o}(T-T_p)_o}{\dot{m}_{g,brk,o}} \quad (111)$$

7.3 IRWST ANALYSIS

The IRWST collects the condensate from above-deck, and after the primary system depressurizes, provides a gravity flow of borated water into the reactor. The gas space above the water level is dead-ended and does not circulate because the gas above-deck is less dense than that in the IRWST gas volume. The above-deck gas is less dense because the initial temperature of the IRWST water is 120°F or less, and the saturation temperature of the warmer condensate liquid that drains into the tank is less than that of the atmosphere, otherwise it would not have condensed. While flowing across the floor to the tank the water may heat, but at most it can only heat until the saturation pressure of the water reaches the steam partial pressure of the atmosphere at the operating deck. Consequently, it cannot become a vapor source by heating from the atmosphere, either while above-deck or after draining into the tank. (The draining fluid is assumed to stratify and spread across the surface without mixing with the cooler, deeper water). Consequently, the water in the IRWST, and the gas in the space above the water level both remain stably stratified relative to the atmosphere in the above-deck volume above the tank.

As a stably stratified, dead-ended volume, only the small volume of steam forced into the IRWST gas volume by containment pressurization will condense. With only 0.7 percent of the containment volume, the net effect of the small, stably stratified IRWST gas volume and its interactions with the IRWST water and the containment atmosphere is negligible. Thus, it is not necessary to perform scaling calculations for the IRWST as a heat sink that interacts with the atmosphere. However, other aspects of the IRWST, such as its supply of cooling water to the reactor vessel, are considered.

7.4 LIQUID FILM ANALYSIS

For containment analysis, liquid films can be categorized as draining films or stagnant films. Films that form on structures with slopes greater than 1° drain and remain thin. The film on the shell was determined to be less than approximately 0.005 inches thick and have a heat transfer coefficient of approximately 900 B/hr-ft^2-°F[27]. Horizontal surfaces facing downward show similarly high heat transfer coefficients.

The following two calculations help put the liquid film heat capacity and time constant in perspective:

Heat Capacity: The ratio of the heat capacity of a draining film less than 0.005 in. thick to the heat capacity of the average steel heat sink can be expressed as:

$$\frac{(\rho \delta c_v)_{film}}{(\rho \delta c_v)_{sink}} = \frac{60}{490}\,\frac{0.005}{0.5}\,\frac{1}{0.11} = 0.012 \qquad (112)$$

Since the film heat capacity is only 1 percent of the heat sink heat capacity, the film absorbs so little heat that its mass can be neglected relative to the mass of the heat sink in terms of energy storage.

Transient Response: The average heat flux to the shell at the time of peak containment pressure is approximately 5000 B/hr-ft^2-F. The heat flux to the inner shell surface and heat sinks during blowdown and prior to the peak pressure is even higher. Since the heat flux is predominantly due to condensation, and h_{fg} is approximately 1000 B/lbm, the condensation rate that produces the average heat flux is 5 lbm/hr-ft^2, or at 60 lbm/ft^3, 0.083 ft/hr of liquid. This corresponds to a film thickness buildup rate, neglecting drainage, of 0.00028 in/sec. At this rate the time constant for a typical 0.005 inch film thickness is 18 sec. Thus, the film will be approximately fully formed by the end of the 27 sec blowdown, and transient film effects will be negligible thereafter.

If it is assumed that the liquid film forms to an average thickness of 0.005 in. in 18 sec. during blowdown, without draining, the maximum values of $\pi_{m,f,if}$ and $\pi_{e,f,if}$ can be estimated. A total heat sink surface area of 250,000 ft^2 is used, rather than calculating the pi groups for each heat sink. As the calculation shows, the magnitude of the combined heat sink liquid mass pi group is small so further breakdown into individual heat sinks would not be informative.

$$\pi_{m,if} = \frac{\dot{m}_{if,o}}{\dot{m}_{g,brk,o}} = \frac{\rho_{if,o} A_{if,o} \delta_{if,o} / \Delta t}{\dot{m}_{g,brk,o}} = \frac{60\,\text{lbm/ft}^3\ 250{,}000\,\text{ft}^2\ (0.005/12)\text{ft}\ /18\text{sec}}{4444\text{lbm/sec}} = 0.078 \qquad (113)$$

Evaluation of the energy pi group requires the term $\Delta h_{if,o}$, which is the difference between the film internal energy and the reference water internal energy at 120°F. Since the difference is zero at the beginning of blowdown, the blowdown time-average provides a rational approach that is used elsewhere. The area-weighted average film temperature on the steel, shell, and concrete at the end of blowdown is 165°F. With T_{min} = 120°F:

$$\pi_{e,f,if} = \pi_{m,if}\frac{\Delta h_{if,o}}{\Delta h_{g,brk,o}} = \pi_{m,f,if}\frac{c_V(T_{if}-T_{min})}{\Delta h_{g,brk,o}} = 0.078\frac{1\ B/lbm\text{-}F\ (165-120)\ F)}{1084\ B/lbm} = 0.003219 \quad (114)$$

Consequently, the transient energy storage rate in the film is negligible during blowdown, and even less thereafter. During blowdown the film drainage is neglected, and after blowdown the transient film mass storage is neglected, so the draining mass flow rate is equal to the condensation mass flow rate. That is:

$$\frac{dm_{if,j}}{dt} = \dot{m}_{stm,j} - \dot{m}_{drain,j} = 0 \quad so \quad \dot{m}_{stm,j} = \dot{m}_{drain,j} \quad (115)$$

The conductance of draining films is included in the conductance term that couples the gas to the heat sink, as described in Sections 7.5 to 7.9. All draining films are assumed to have a thickness of 0.005 inches. The conductance pi groups show the film conductance is high enough that this assumption is a reasonable simplification and is a small conservatism that maximizes containment pressure.

Stagnant films are those that do not drain effectively and consequently build up sufficient thickness to lead to a significant heat transfer resistance to the surfaces on which they form. They also present large surface areas for evaporation/condensation mass transfer interactions. That is, they behave as a large shallow pool. However, having formed by condensation on cooler surfaces, the film is cooler than the atmosphere and behaves as a heat sink until reheated by the atmosphere. The sensible heating can only progress to the point that the film partial pressure is equal to that of the atmosphere. After condensing, the films can have little net effect on containment heat removal or addition. Consequently, horizontal liquid film energy transport is neglected and only their thermal conductance is considered.

Liquid films can form to a sufficient depth on nearly horizontal surfaces that their conductance becomes significant in limiting heat transfer. However, rather than tracking draining film flow rates, estimating the flow paths, and calculating film conductances, a more conservative approach of eliminating heat transfer surface area is used in the scaling analysis. That is, the upward facing horizontal surfaces are assumed to be adiabatic. For concrete floors this effectively eliminates the heat capacity of the floor.

The only steel structures of any size with upward facing horizontal surfaces are the crane rail, stiffener ring, and hatch covers. These are modeled by eliminating the upward facing surface area, while retaining the mass, since the downward facing surface area is still active.

Summarizing for liquid films, the heat capacity of draining film is negligible relative to the heat capacity of the surface they form on, and the conductance is included in the heat transfer coefficient. The heat capacity of stagnant films constitutes a heat sink for the gas, so is conservatively neglected, and the conductance to the horizontal surface is assumed to be so poor that the horizontal surface heat capacity is neglected.

7.5 INTERNAL SOLID HEAT SINKS ANALYSIS AND SCALING EQUATIONS

Internal solid heat sinks include steel, concrete, and steel-jacketed concrete. The conduction terms necessary to couple the containment atmosphere to the heat sink surface are defined using the one-dimensional energy balance from the containment atmosphere to a heat sink shown in Figure 7-2. The energy balance shown assumes the total energy flux out of the containment gas is reduced by the liquid enthalpy of the condensed film prior to entering the liquid film, rather than conducting some of the film energy partway through the film. Because the conductance of the film is more than 10 times that of the conductance from the atmosphere to the film, and the energy carried away by the liquid is only 1/10 that of the condensing gas energy, the error introduced by not conducting the liquid film energy partway through the liquid film is negligibly small. This assumption greatly simplifies the resulting mathematics.

The energy fluxes can be related to the series temperature drops by assuming thermal conduction through the liquid film, and condensation, convection, and radiation heat transfer to the liquid surface. For time greater than zero, the heat conducted into the solid and the solid surface temperature can be calculated by various analytical models. The analytical models depend on whether the solid is modeled as a lumped mass, a thick wall, or a semi-infinite conductor, such as concrete.

The temperature drop relationships to the heat fluxes are developed from Figure 7-2 for the containment to inner film surface, and inner film surface to solid heat sink surface:

$$T - T_{if,s} = \dot{q}''_{in}\left(h_m + h_c + h_r\right)^{-1} \quad \text{and} \quad T_{if,s} - T_{srf} = \dot{q}''_{in}\,(h_{if})^{-1} \tag{116}$$

These two equations are added, so $T - T_{srf}$ remains on the left side of the equation, and only multipliers on $\dot{q}_{in}''$ remain on the right side of the equation:

$$(T - T_{srf}) = \dot{q}''_{in}\left[(h_m + h_c + h_r)^{-1} + (h_{if})^{-1}\right] \tag{117}$$

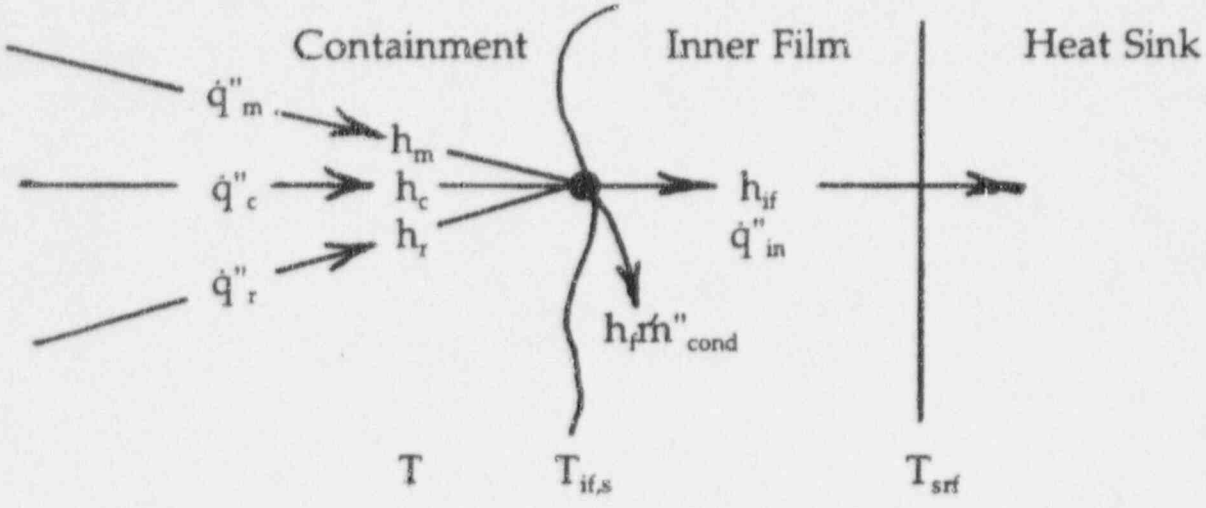

Figure 7-2 One-Dimensional Energy Balance and Temperatures for Energy Transfer Resistance to Solid Heat Sinks

The term in brackets defines the inverse conductance from the inside of containment to the solid heat sink surface. The effective heat sink conductance is defined $h_e = [(h_m + h_c + h_r)^{-1} + h_{if}^{-1}]^{-1}$ and is combined with the energy equation to give:

$$m_{hs} c_{v,hs} \frac{dT_{hs}}{dt} = h_e A (T - T_{srf}) \tag{118}$$

7.5.1 Heat Sink Conductance

The individual heat sink conductances are defined from the constitutive equations in Section 4:

$$h_m = \frac{0.13(h_g - h_f)\rho_{stm} D_v}{(T - T_{if,s})(\nu^2/g)^{1/3}} \frac{\Delta P_{stm}}{P_{lm,air}} \left(\frac{\Delta\rho}{\rho} Sc\right)^{1/3} \qquad h_c = \frac{0.13k}{(\nu^2/g)^{1/3}} \left(\frac{\Delta\rho}{\rho} Pr\right)^{1/3}$$
$$h_r = \sigma \varepsilon f(T, T_{if,s}) \qquad h_{if} = k_{if}/\delta_{if} \qquad h_e = [(h_m + h_c + h_r)^{-1} + h_{if}^{-1}]^{-1} \tag{119}$$

The individual conductance terms are normalized to the shell conductance, $h_{sh,o}$, to produce the pi groups for scaling the heat sink conductances:

$$\pi_{c,m} = h_{m,o}/h_{sh,o} \quad \pi_{c,c} = h_{c,o}/h_{sh,o} \quad \pi_{c,r} = h_{m,o}/h_{sh,o} \quad \pi_{c,if} = h_{if,o}/h_{sh,o} \quad \pi_{c,e} = h_{e,o}/h_{sh,o} \tag{120}$$

Expressions are needed to relate the heat transfer coefficients relative to $(T-T_{srf})$ to heat transfer coefficients relative to $(T-T_{if,s})$. Combining Equations (116) and (117), the ratio of temperature differences is:

$$\frac{T - T_{if,s}}{T - T_{srf}} = \frac{h_{if}}{h_r + h_c + h_m + h_{if}} = f_T \tag{121}$$

As the liquid film gets thinner and vanishes, the ratio represented by f_T approaches 1.0. Note that the heat transfer to heat sinks with liquid films, Equation (118), is written in terms of $(T-T_{srf})$, while the evaluation of the individual heat transfer coefficients, Equation (119), is in terms of $(T-T_{if,s})$, the liquid film surface temperature.

7.5.2 Heat Sink Mass Transfer

The mass condensation rate from containment to heat sink j is scaled to the containment mass equation according to Equation (59) where all the properties in the pi expression are

evaluated at their initial conditions for each time phase, using the bulk and liquid film surface conditions (not heat sink surface).

$$\pi_{m,j} = \frac{\dot{m}_{stm,j,o}}{\dot{m}_{g,brk,o}} = \frac{0.13 A \rho_{stm} D_v}{\dot{m}_{g,brk,o}(\nu^2/g)^{1/3}} \frac{\Delta P_{stm}}{P_{lm,air}} \left(\frac{\Delta\rho}{\rho} Sc\right)^{1/3} \quad (122)$$

7.5.3 Heat Sink Energy Transfer

The energy transfer rate terms defined in Equation (70) scale the energy transfer to the heat sinks. The properties in the pi expressions are evaluated at their initial conditions for each time phase, using the bulk and liquid film surface conditions (not heat sink surface).

$$\pi_{e,fg,j} = \pi_{m,j} \frac{(h_{g,j,o} - h_{if,j,o})}{\Delta h_{g,brk,o}} \qquad \pi_{e,f,j} = \pi_{m,j} \frac{(h_{if,j,o} - h_{f,To})}{\Delta h_{g,brk,o}}$$

$$\pi_{e,q,j} = \frac{h_{q,j,o} A_{j,o} (T - T_{if,j})_o}{\dot{m}_{g,brk,o} \Delta h_{g,brk,o}} = \left[\frac{0.13k}{(\nu^2/g)^{1/3}} \left(\frac{\Delta\rho}{\rho} Pr\right)^{1/3} + \sigma \varepsilon f(T, T_{if,j})\right] \frac{A_{j,o} (T - T_{if,j})_o}{\dot{m}_{g,brk,o} \Delta h_{g,brk,o}} \quad (123)$$

Heat Sink Time Constant

The time constant for a steel heat sink is the energy storage capacity of the heat sink divided by the energy transfer rate to the heat sink:

$$\tau_{hs} = \frac{m_{hs,o} c_{v,o} (T_{srf} - T)_o}{h_{hs,o} A_o (T_{srf} - T)_o} = \frac{\rho_{hs,o} c_{v,o} L^s}{h_{hs,o}} \quad (124)$$

where the specific length $L^s = V_{hs,o}/A_o$

The specific frequency is not defined for concrete and steel-jacketed concrete since the concrete thickness is not a valid measure of the useful heat capacity on a time scale less than a few days.

7.5.4 Heat Sink Effect on Pressure

The pressure scaling for the internal solid heat sinks uses the pi groups defined in Equation (81) for enthalpy and work, and Equation (83) for the heat transfer energy pi group:

$$\pi_{p,enth,j} = \pi_{m,j}\frac{(\gamma-1)_o}{\gamma_o(1+Z^T)_o}\frac{\rho_{stm,o}}{P_{stm,o}}(h_{stm,j}-h_{stm})_o \qquad \pi_{p,work,j} = \pi_{m,j}$$

$$\pi_{p,q,j} = \frac{(\gamma-1)_o}{\gamma_o(1+Z^T)_o}\frac{\rho_{stm,o}}{P_{stm,o}}\frac{h_{q,j,o}A_{j,o}(T-T_j)_o}{\dot{m}_{g,brk,o}} \qquad (125)$$

7.5.5 Steel Thermal Model

The average steel thickness, calculated from the steel volume/area is 0.5 inches. The Biot number for the average steel is Bi = 0.08, so it is clear that the steel can be modeled as a lumped mass. With this assumption, the surface heat flux and total stored energy in the heat sink can be related to the heat sink surface temperature and average temperature.

Each time phase is modeled by a linear change in the containment gas temperature from the beginning temperature to the end temperature. The heat transfer coefficient is assumed to be constant over the time phase at the beginning value. The surface and average temperature are tracked by integrating Equation (118) forward in time, subject to the boundary condition that at the beginning of the first time phase, t = 0, $T_{hs} = T_i = 120°F$, and T_i at the beginning of each subsequent time phase is equal to the value of T_{hs} at the end of the previous time step. By differentiation it can be shown that the solution to the differential equation and boundary condition is:

$$T_{hs} = T_1 + C_1(t-\tau) + [T_i - T_1 - C_1(t_1-\tau)]e^{-(t-t_1)/\tau} \qquad C_1 = \frac{T_2-T_1}{t_2-t_1} \qquad \tau = \frac{\rho c_V L^s}{h_e} \qquad (126)$$

7.5.6 Concrete Thermal Model

The thermal boundary layer cannot penetrate the thickness of the concrete during the 24-hour period of interest, so the concrete can be modeled as always thermally thick. Its surface temperature and surface heat flux can be calculated by coupling the time history of steam and air partial pressures and temperature to the surface, using the integral equations 28, 29, and 30 from Wulff [33] for thermally thick structures.

The containment boundary condition was modeled as a step function over each time phase, with initial conditions equal to the final surface and average temperature from the prior time phase. Wulff Equation (31) relates the Biot number, based on thermal penetration depth, to the time. The resulting equation:

$$t = \frac{\left(\frac{Bi_\delta + 2}{2}\right)^2 - 1 - 2\ln\left(\frac{Bi_\delta + 2}{2}\right)}{3\alpha_s (h_c / k_s)^2} \quad (127)$$

is evaluated for values of Bi_δ until the desired value of t results. The desired values of t correspond to the initial time of each time phase: 0, 27, 85, 1500 sec. The value of h_c is the time-weighted average of the heat transfer coefficients for each phase included by t.

The surface temperature of the concrete is determined from Wulff Equation (29) with x = 0. That is:

$$T_{surf} = T_o + (T_\infty - T_o)\frac{Bi_\delta}{Bi_\delta + 2} \quad (128)$$

The value of Bi_δ is from Equation (127) corresponding to t at each time phase. T_o is the initial temperature, 120°F inside containment, and 115°F outside. T_∞ is the peak containment gas temperature during the transient. This gives moderately high heat fluxes earlier in the LOCA, when containment temperatures are less than peak.

The average temperature of the structure can be calculated from Wulff Equation (30). Although (30) is the heat-absorbed division by mc_V and addition of T_o gives the average temperature:

$$T = T_o + \frac{(T_\infty - T_o)}{3}\frac{Bi_\delta^2}{Bi_\delta + 2}\frac{A\rho c_V}{mc_V}\frac{\delta}{\delta}\frac{k}{h} = T_o + \frac{(T_\infty - T_o)}{3}\frac{Bi_\delta}{Bi_\delta + 2} \quad (129)$$

The use of time-weighted average temperature and heat transfer coefficients compensates for the small variations in temperature and heat transfer coefficient relative to the model that assumes both are constant after a step change at time zero.

7.5.7 Steel-Jacketed Concrete Thermal Model

A large portion of the concrete is jacketed by 0.5-inch thick steel plate. Initially, the composite behaves like steel, and later as concrete. The composite is conservatively modeled (conservative in terms of underestimating heat flux and total heat storage) by modeling the two structures in parallel and taking the larger of the two as the instantaneous heat flux. This neglects the concrete heat capacity during the early part of the transient, when the steel absorbs fastest, and neglects the steel heat capacity later in the transient when the concrete absorbs fastest. In the long term, the conductance of the jacket is 624 B/hr-ft^2-F, so its

conductance is not significant in comparison to that of the gas conductance (50 to 100 B/hr-ft^2-F).

7.6 SHELL ANALYSIS AND SCALING EQUATIONS

The conduction terms necessary to couple the containment atmosphere to the shell, and the shell to the riser are defined from the one-dimensional energy balance shown in Figure 7-3. As was done for the heat sinks (Section 7.5) the total energy flux out of the containment gas is first reduced by the liquid enthalpy of the condensed film. The shell has such a high heat capacity that its heat capacity cannot be neglected until several thousand seconds into the transient. The energy fluxes in and out of the shell can be related to the series temperature drops by assuming thermal conduction through the film, condensation and evaporation mass transfer, and convection and radiation heat transfer. The temperature drop relationships to the heat fluxes are presented in the following equations.

The temperature drops through each of the conductances into the shell are shown in Figure 7-3 and are the same as for energy transfer into the heat sink developed in Section 7.5. That is:

$$(T - T_{sff}) = \dot{q}''_{in}\left[(h_m + h_c + h_r)^{-1} + (h_{if})^{-1}\right] \tag{130}$$

where the inverse of the term in brackets is the conductance from the containment atmosphere to the shell inner surface, $h_e = [(h_m + h_c + h_r)^{-1} + h_{if}^{-1}]^{-1}$

Energy transfer out of the shell through each of the conductances to the riser and baffle are also shown in Figure 7-3. The shell outer surface to external film outer surface temperature drop is:

$$T_{sh,o} - T_{xf,s} = \dot{q}''_{out}(h_{xf})^{-1} \tag{131}$$

and the external film outer surface with convection heat transfer and evaporation to the riser bulk flow, and radiation to the baffle is:

$$T_{xf,s} - T_{ri} = \dot{q}''_{out}\left(h_{mx} + h_{cx} + h_{rx}\frac{(T_{xf,s} - T_{bf})}{(T_{xf,s} - T_{ri})}\right)^{-1} \tag{132}$$

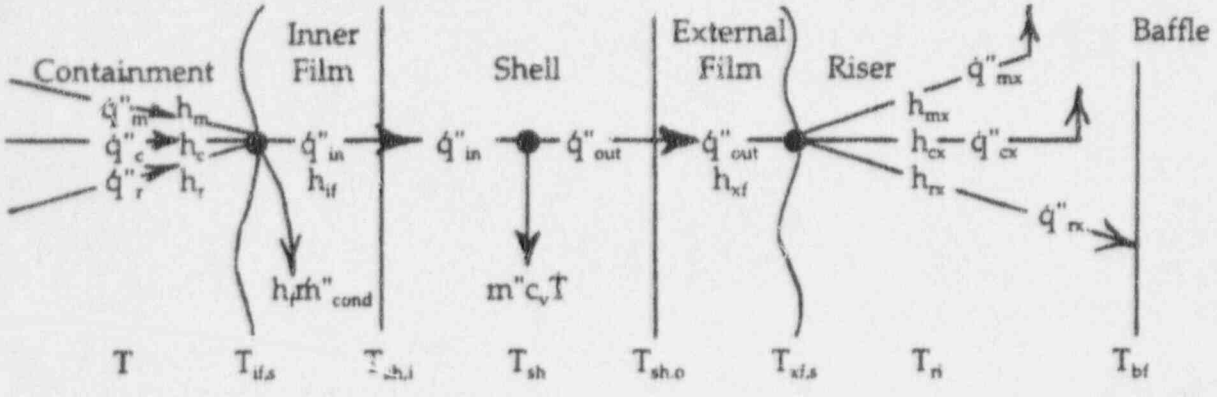

Figure 7-3 **One-Dimensional Energy Balance and Temperatures for Energy Transfer Conductance through the Containment Shell**

These two equations are added, resulting in the equation:

$$(T_{sh,o} - T_{ri}) = \dot{q}''_{out}\left[(h_{xf})^{-1} + \left(h_{mx} + h_{cx} + h_{rx}\frac{(T_{xf,s} - T_{bf})}{(T_{xf,s} - T_{ri})}\right)^{-1}\right] \quad (133)$$

The term in brackets is the inverse conductance for the outside of the shell, where the conductance is $h_{ex,o}$. Equations (130) and (133) can be combined with the general energy equation for a heat sink, Equation (90), to give:

$$m_{sh}c_{sh}\frac{dT_{sh}}{dt} = h_e A(T - T_{sh}) - h_{ex}A(T_{shx} - T_{ri}) \quad (134)$$

Equation (134) was written for the evaporating portion of the shell, but is also valid for the subcooled and dry portions of the external shell, with substitutions for the subcooled region $h_{mx} = h_{cx} = h_{rx} = 0$, and for the dry portion $h_{xf} = h_{mx} = 0$.

The areas of the subcooled and evaporating regions can vary with time, so a basis for calculation is required. The area of the subcooled region is determined from an energy balance on the subcooled liquid in which the heat conducted from the shell heats the liquid from its source temperature to the temperature of the evaporating film, T_{xf}. The subcooled film is assumed to have no evaporation, radiation, or convection from its surface. The bases for this assumption are

- The subcooled water exists at the top of the shell where the riser temperature is at its maximum. When compared to the average subcooled film temperature, $T_{xf,avg} = (T_{in} + T_{xf})/2$, the difference $(T_{xf,avg} - T_{ri})$ is a small positive value at peak pressure, and a small negative difference at long-term pressurization.

- The subcooled surface area is relatively small, only a few percent of the total, so errors have little effect on the evaporating region where most of the shell heat is removed.

The calculation proceeds by calculating the temperature of the evaporating film independently of the subcooled or dry regions. The film energy equation is then applied to estimate the area covered by the subcooled film:

$$A_{sc} = \frac{\dot{m}_{xf}c_V(T_{xf,s} - T_{in})}{h_{xf,ss}(T_{xf,avg} - T_{ssx})} \quad (135)$$

The liquid film wetted surface area is then estimated as discussed in Section 7.6.6, and the evaporating area is the difference between the wet area and the subcooled area, $A_{evap} = A_{wet} - A_{sc}$. The dry area is the difference between the total area and the wet area, $A_{dry} = 52662\ ft.^2 - A_{wet}$.

7.6.1 Shell Conductance

The individual conductance terms inside the shell are free convection heat and mass transfer, radiation, and liquid film conduction. These are evaluated independently for the internal portions of the shell that correspond to the subcooled, evaporating, and dry portions of the external shell.

$$h_m = \frac{0.13(h_g - h_f)\rho_{stm} D_v}{(T - T_{if})(\nu^2/g)^{1/3}} \frac{\Delta P_{stm}}{P_{lm,air}} \left(\frac{\Delta\rho}{\rho} Sc\right)^{1/3} \quad h_c = \frac{0.13k}{(\nu^2/g)^{1/3}} \left(\frac{\Delta\rho}{\rho} Pr\right)^{1/3}$$
$$h_r = \sigma\varepsilon f(T, T_{if}) \quad h_{if} = k_{if}/\delta_{if} \quad h_e = [(h_m + h_c + h_r)^{-1} + h_{if}^{-1}]^{-1} \qquad (136)$$

The conductance pi groups are each of these values divided by the reference shell conductance for each of the three shell portions. The fifteen pi groups result:

$$\pi_{c,e,sc} = \frac{h_{e,sc,o}}{h_{sh,o}} \quad \pi_{c,m,sc} = \frac{h_{m,sc,o}}{h_{sh,o}} \quad \pi_{c,c,sc} = \frac{h_{c,sc,o}}{h_{sh,o}} \quad \pi_{c,r,sc} = \frac{h_{r,sc,o}}{h_{sh,o}} \quad \pi_{c,if,sc} = \frac{h_{if,sc,o}}{h_{sh,o}}$$
$$\pi_{c,e,es} = \frac{h_{e,es,o}}{h_{sh,o}} \quad \pi_{c,m,es} = \frac{h_{m,es,o}}{h_{sh,o}} \quad \pi_{c,c,es} = \frac{h_{c,es,o}}{h_{sh,o}} \quad \pi_{c,r,es} = \frac{h_{r,es,o}}{h_{sh,o}} \quad \pi_{c,if,es} = \frac{h_{if,es,o}}{h_{sh,o}} \qquad (137)$$
$$\pi_{c,e,ds} = \frac{h_{e,ds,o}}{h_{sh,o}} \quad \pi_{c,m,ds} = \frac{h_{m,ds,o}}{h_{sh,o}} \quad \pi_{c,c,ds} = \frac{h_{c,ds,o}}{h_{sh,o}} \quad \pi_{c,r,ds} = \frac{h_{r,ds,o}}{h_{sh,o}} \quad \pi_{c,if,ds} = \frac{h_{if,ds,o}}{h_{sh,o}}$$

The evaporating portion of the shell outside operates with forced convection heat and mass transfer, radiation, and liquid film conductance:

$$h_{mx} = \frac{0.023 h_{fg} \rho_{stm} D_v}{(T - T_{xf}) D_h} \frac{\Delta P_{stm}}{P_{lm,air}} Re_D^{0.8} Sc^{1/3} \quad h_{cx} = \frac{0.023k}{D_h} Re_D^{0.8} Pr^{1/3}$$
$$h_{rx} = \sigma\varepsilon f(T_{xf}, T_{bf}) \quad h_{xf} = k_{xf}/\delta_{xf} \quad h_{ex} = \left[\left(h_{mx} + h_{cx} + h_{rx} \frac{(T_{dsx} - T_{bf})}{(T_{dsx} - T_{ri})}\right)^{-1} + h_{xf}^{-1}\right] \qquad (138)$$

The conductance pi groups for the external surface of the evaporating portion of the shell are each of these values, divided by the reference shell conductance:

$$\pi_{c,e,esx} = \frac{h_{e,esx,o}}{h_{sh,o}} \quad \pi_{c,m,esx} = \frac{h_{m,esx,o}}{h_{sh,o}} \quad \pi_{c,c,esx} = \frac{h_{c,esx,o}}{h_{sh,o}} \quad \pi_{c,r,esx} = \frac{h_{r,esx,o}}{h_{sh,o}} \quad \pi_{c,xf,es} = \frac{h_{xf,es,o}}{h_{sh,o}} \quad (139)$$

The dry portion of the shell outside operates with forced convection heat transfer and radiation:

$$h_{c,dsx} = \frac{0.023k}{d_h} Re_D^{0.8} Pr^{1/3} \quad h_{r,dsx} = \sigma \varepsilon f(T_{dsx}, T_{bf}) \quad h_{e,dsx} = h_{c,dsx} + h_{r,dsx} \frac{(T_{dsx} - T_{bf})}{(T_{dsx} - T_n)} \quad (140)$$

The conductance pi groups for the external surface of the dry portion of the shell are each of these values, divided by the reference shell conductance:

$$\pi_{c,e,dsx} = h_{e,dsx,o} / h_{sh,o} \quad \pi_{c,c,dsx} = h_{c,dsx,o} / h_{sh,o} \quad \pi_{c,r,dsx} = h_{r,dsx,o} / h_{sh,o} \quad (141)$$

The subcooled portion of the shell outside has only conduction to the film with the pi group defined:

$$h_{xf,scx} = 2k_{xf} / \delta_{xf} \quad \pi_{c,scx} = h_{xf,scx,o} / h_{sh,o} \quad (142)$$

7.6.2 Shell Mass Transfer

The mass condensation rate from containment for each portion, j, of the shell (evaporating, dry, and subcooled) is scaled according to Equation (59) where all the properties in the pi expression are evaluated at their initial conditions for each time phase, using the bulk and liquid film surface conditions (not heat sink surface).

$$\pi_{m,j} = \frac{\dot{m}_{stm,j,o}}{\dot{m}_{g,brk,o}} = \frac{0.13 A \rho_{stm} D_v}{\dot{m}_{g,brk,o} (v^2/g)^{1/3}} \frac{\Delta P_{stm}}{P_{lm,air}} \left(\frac{\Delta \rho}{\rho} Sc \right)^{1/3} \quad (143)$$

The mass evaporation rate from the shell to the riser for the evaporating portion of the shell is also scaled according to Equation (59) where all the properties in the pi expression are evaluated at their initial conditions for each time phase, using the external film surface (not shell surface) and bulk riser gas properties.

$$\pi_{m,esx} = \frac{\dot{m}_{stm,xf,o}}{\dot{m}_{g,brk,o}} = \frac{0.023 A \rho_{stm} D_v}{\dot{m}_{g,brk,o} D_h} \frac{\Delta P_{stm}}{P_{lm,air}} Re_D^{0.8} Sc^{1/3} \quad (144)$$

The external surface of the subcooled and dry shell portions do not evaporate, so there is no evaporating/condensing mass transfer.

7.6.3 Shell Energy Transfer

The energy transfer rate terms defined in Equation (70) scale the energy transfer to the inner surface of the evaporating, subcooled, and dry shell portions. The properties in the pi expressions are evaluated at their initial conditions for each time phase, using the bulk and liquid film surface conditions (not heat sink surface). In general conditions differ on each of the three portions.

$$\pi_{e,fg,j} = \pi_{m,j} \frac{(h_{g,j,o} - h_{if,j,o})}{\Delta h_{g,brk,o}} \qquad \pi_{e,f,j} = \pi_{m,j} \frac{(h_{if,j,o} - h_{f,To})}{\Delta h_{g,brk,o}}$$

$$\pi_{e,q,j} = \frac{h_{q,j,o} A_{j,o} (T - T_{if,j})_o}{\dot{m}_{g,brk,o} \Delta h_{g,brk,o}} = \left[\frac{0.13 k}{(\nu^2/g)^{1/3}} \left(\frac{\Delta\rho}{\rho} Pr \right)^{1/3} + \sigma \varepsilon f(T, T_{if,j}) \right] \frac{A_{j,o} (T - T_{if,j})_o}{\dot{m}_{g,brk,o} \Delta h_{g,brk,o}} \quad (145)$$

The energy transfer rate from the shell to the riser for the evaporating portion of the shell is also scaled according to Equation (70) where all the properties in the pi expression are evaluated at their initial conditions for each time-phase, using the external film surface (not shell surface) and bulk riser gas properties.

$$\pi_{e,fg,esx} = \pi_{m,esx} \frac{h_{fg,esx,o}}{\Delta h_{g,brk,o}} \qquad \pi_{e,f,esx} = 0 \qquad \pi_{e,q,esx} = \frac{h_{g,xf,o} A_{esx,o} (T_{xf,o} - T_{ri,o})}{\dot{m}_{g,brk,o} \Delta h_{g,brk,o}}$$

$$= \left[\frac{0.023 k}{D_h} Re_D^{0.8} Pr^{1/3} + \sigma \varepsilon f(T_{xf}, T_{bf}) \frac{(T_{xf} - T_{bf})}{(T_{xf} - T_{ri})} \right] \frac{A_{esx,o} (T_{xf,o} - T_{ri,o})}{\dot{m}_{g,brk,o} \Delta h_{g,brk,o}} \quad (146)$$

The energy transfer rate from the shell to the riser for the dry portion of the shell is scaled according to Equation (70) where all the properties in the pi expression are evaluated at their initial conditions for each time phase, using the shell surface temperature (since there is no external film) and bulk riser gas properties.

$$\pi_{e,g,dsx} = \frac{h_{g,dsx,o} A_{ds,o} (T_{dsx,o} - T_{ri,o})}{\dot{m}_{g,brk,o} \Delta h_{g,brk,o}}$$

$$= \left[\frac{0.023k}{D_h} Re_D^{0.8} Pr^{1/3} + \sigma \varepsilon f(T_{dsx}, T_{bf}) \frac{(T_{dsx} - T_{bf})}{(T_{dsx} - T_{ri})} \right] \frac{A_{esx,o} (T_{xf,o} - T_{ri,o})}{\dot{m}_{g,brk,o} \Delta h_{g,brk,o}} \quad (147)$$

The energy transfer rate from the shell to the subcooled liquid is scaled according to Equation (70) where all the properties in the pi expression are evaluated at their initial conditions for each time phase, using the shell surface temperature and average subcooled film temperature and properties.

$$\pi_{e,g,scx} = \frac{h_{g,scx,o} A_{sc,o} (T_{scx,o} - T_{f,sc,o})}{\dot{m}_{g,brk,o} \Delta h_{g,brk,o}} = \frac{k_{f,o}}{2\delta_{sc}} \frac{A_{sc,o} (T_{scx,o} - T_{f,sc,o})}{\dot{m}_{g,brk,o} \Delta h_{g,brk,o}} \quad (148)$$

Shell Time Constant

The shell time constant is the energy storage capacity of the shell divided by the heat transfer rate to the shell. A time constant can be defined for each of the three evaporating, subcooled, and dry portions, and for the inside and external heat transfer rates. Thus, the six time constants:

$$\tau_{es} = \frac{\rho_{sh,o} c_{v,o} L^s}{h_{e,es,o}} \quad \tau_{ds} = \frac{\rho_{sh,o} c_{v,o} L^s}{h_{e,ds,o}} \quad \tau_{sc} = \frac{\rho_{sh,o} c_{v,o} L^s}{h_{e,sc,o}}$$

$$\tau_{esx} = \frac{\rho_{sh,o} c_{v,o} L^s}{h_{e,esx,o}} \quad \tau_{dsx} = \frac{\rho_{sh,o} c_{v,o} L^s}{h_{e,dsx,o}} \quad \tau_{scx} = \frac{\rho_{sh,o} c_{v,o} L^s}{h_{e,scx,o}} \quad (149)$$

where the specific length $L^s = V_{sh,o}/A_o = \delta_{sh}$.

The time constant for the external heat transfer to the subcooled shell is much smaller than the time constant for the inner surface, indicating that heat transfer to the subcooled water is limited by the shell heat capacity and/or heat transfer to the inside.

7.6.4 Shell Effect on Pressure

The pressure scaling for the internal surfaces of the evaporating, subcooled, and dry portions of the shell uses the pi groups defined in Equations (81) and (83):

$$\pi_{p,enth,j} = \pi_{m,j}\frac{(\gamma-1)_o}{\gamma_o(1+Z^T)_o}\frac{\rho_{stm,o}}{P_{stm,o}}(h_{stm,j}-h_{stm})_o \qquad \pi_{p,work,j} = \pi_{m,j}$$

$$\pi_{p,q,j} = \frac{(\gamma-1)_o}{\gamma_o(1+Z^T)_o}\frac{\rho_{stm,o}}{P_{stm,o}}\frac{h_{q,j,o}A_{j,o}(T-T_j)_o}{\dot{m}_{g,brk,o}} \qquad (150)$$

The properties are based on initial conditions for each time phase and on the bulk and liquid film free surface conditions, not on the shell surface temperature.

7.6.5 Shell Thermal Model

As time progresses, the thermal boundary layer advances through the thickness of the shell and eventually reaches the (nearly) adiabatic outer surface of the shell (thermal penetration). The time of thermal penetration is an important characteristic time for modeling energy transfer into the shell. Internal processes are not coupled to the riser until the thermal boundary layer reaches the outside of the shell. Using the correlation developed by Wulff[33], the thermal boundary layer reaches the outside of the shell in 22 seconds. Thus, the steel shell is modeled as a thermally thick structure during blowdown and as a thermally thin structure thereafter. Because the energy transfer from the shell outer surface is very low until it wets sometime after 300 seconds, the shell can be modeled with an adiabatic outer surface to 300 sec. and with evaporation heat transfer thereafter.

The shell energy equation was formulated in terms of the shell inner and outer surface temperatures. The integral relationships developed by Wulff [13,33] for thermally thick structures are used to track the shell surface and average temperatures for appropriately short values of time, and Wulff[33] for thermally thin structures with heat transfer from two sides. Both the thermally thick and thin regimes are modeled assuming the environment changes as a step function over the time phase of interest.

The shell is modeled considering three independent regions defined by the external film: the relatively small area covered by subcooled liquid, the area covered by evaporating liquid, and the dry area. The integral relationships are applied separately to each of the three regions.

The thermally thick solution is first applied to determine the time when the thermal boundary layer penetrates to the shell outer surface. Wulff gives the time in terms of the Fourier number for a plane-parallel slab, which is the geometry characterizing nearly all the surfaces of interest in AP600. For curved structures, such as the shell, the approximation is valid as long as the radius of curvature is much greater than the thickness. The thermal penetration time is:

$$Fo = \frac{1}{12} + \frac{1}{3Bi} + \frac{2}{3Bi^2}\ln\left(\frac{2}{2+Bi}\right) \qquad (151)$$

where $Fo = \alpha t/\delta^2$

α is the structure thermal diffusivity

t is time

δ is the structure thickness

$Bi = h\delta/k$

h is the surface heat transfer coefficient

k is the structure thermal conductivity

Condensation on the inner shell surface produces a penetration time of 18.4 sec. With this time, Equation (127) is solved for the Biot number, then Equation (129) is solved for the average structure temperature.

The solution to the temperature in a thermally thin structure uses as input an initial average temperature, gas boundary temperatures, and the Biot number (which is the dimensionless heat transfer coefficient) for each surface. The output is the temperature of each surface and the average temperature after some time increment. Thus, it is possible to do a series of calculations to sequentially calculate the average and surface temperatures at the end of each time phase, given the initial conditions for the time phase. The equations used are Wulff Equations (14) - (18), and for the plane-parallel slab can be written:

$$\frac{d\bar{T}}{dt} = \frac{\alpha}{\delta^2}[B_1(T_i - T_1) - B_2(T_2 - T_o)] \qquad \bar{B} = \frac{2B_1}{3} + \frac{B_1 B_2}{6} + \frac{2B_2}{3}$$

$$\frac{T_i - T_1}{T_i - \bar{T}} = \frac{2}{2+\bar{B}} + \frac{B_2}{2+\bar{B}}\left(1 - \frac{1}{2}\frac{T_i - T_o}{T_i - \bar{T}}\right) \qquad \frac{T_2 - T_o}{\bar{T} - T_o} + \frac{2}{2+\bar{B}} + \frac{B_1}{2+\bar{B}}\left(1 - \frac{1}{2}\frac{T_i - T_o}{\bar{T} - T_o}\right) \tag{152}$$

This is a system of 4 equations with the four unknowns:

$\bar{T}$ the average structure temperature

T_1 the inside surface temperature

T_2 the outside surface temperature

$\bar{B}$ the combined Biot number

The input values are:

T_i the inside gas temperature

T_o the outside gas temperature

B_1 the inside Biot number

B_2 the outside Biot number

α the thermal diffusivity, and

δ the plate thickness.

By substitution, T_1, T_2, and $\bar{B}$ can be eliminated and the rate of change of average temperature can be expressed in terms of known quantities:

$$\frac{d\bar{T}}{dt} = \frac{\alpha}{\delta^2}[B_1(2+B_2) + B_2(2+B_1) - 2(B_1+B_1B_2+B_2)\bar{T}] \quad (153)$$

Since this equation is of the form $d\bar{T}/dt = C_1 - C_2\bar{T}$ with boundary conditions $\bar{T} = \bar{T}_o$ at $t = t_o$ it has the solution:

$$\bar{T} = (\bar{T}_o - C_1/C_2)e^{-C_2(t-t_o)} + C_1/C_2 \quad (154)$$

where:

$$C_1 = \frac{\alpha}{\delta^2}\left(B_1T_i\frac{2+B_2}{2+\bar{B}} + B_2T_o\frac{2+B_1}{2+\bar{B}}\right) \quad \text{and} \quad C_2 = \frac{\alpha}{\delta^2}\frac{2(B_1+B_1B_2+B_2)}{2+\bar{B}} \quad (155)$$

After Equation (154) is solved for $\bar{T}$ Equations (152) are solved for surface temperatures T_1 and T_2 to get the initial conditions for the next time phase.

7.6.6 Weir and Water Coverage Timing

The containment shell is assumed to be dry at the initiation of an overpressure signal that starts the external water flow. The time from signal actuation includes valve opening, pipe filling, and the center bucket filling and overflowing. The water flows and fills the first weir, then the second weir, and then flows down the side wall. The growth of initial coverage is a combination of two processes: the increasing flow rate, and the advancing contact line.

The flow rate out of each weir increases with time because the outflow increases with the elevation of the water backed up behind the weir. The greater the volume of water stored in the weir, the longer it takes to approach a steady-state where the outflow equals the inflow. The weir outflow rates were calculated for the 440 gpm PCS water flow rate and the results are shown in Figure 7-4). The time for significant occurrences are presented in Table 7-4. The steady-state time is assumed to be when the outflow has reached 90 percent of 440 gpm.

Observations of the LST wetting, both on hot and cold vessel surfaces show, after achieving an initial constant water flow rate, the width of the wet stripe may grow for a few seconds and is essentially static within 10 sec. Since the time constants for flow rate are much greater than the few-second time constant for contact line motion, the times considering only flow coverage will be used for scaling. The resulting elapsed time of 245 sec for steady-state coverage below the second weir is a nominal approximation to the more conservative 353 sec value quoted in Reference 5.

Table 7-4 Calculated Time Sequence of Weir Flow Events for AP600	
Event	**Elapsed Time, sec**
Initiate Flow	0
Bucket Spills	37
First Weir Spills	110
First Weir Steady	145
Second Weir Spills	205
Second Weir Steady	245

Using the times presented in Table 7-4 from this model, heat input to the subcooled liquid is assumed to start at 105 sec from an initially dry vessel, and evaporation to start at 245 sec from an initially dry vessel. Consequently, the subcooled liquid scaling and evaporating scaling begin at the beginning of the peak pressure phase (85 sec). The fact that the time phase boundary does not coincide exactly with the 105 and 245 sec times is of little concern, since conditions at the beginning of the peak pressure phase (85 sec) and long-term phase (1500 sec) bound conditions for times between.

[

]^{a,b}

The method used to calculated the evaporating, subcooled and dry areas is:

- Calculate the subcooled area as described in Section 7.6 and Equation (135).
- Subtract the subcooled area from the maximum wet area (49,062 ft^2 - A_{sc}) to get the maximum evaporating area.
- Use the maximum evaporating area to calculate the total evaporation. If the total evaporation is greater than 40 lbm/sec (Reference 5, Table 7-9, peak heat flux) then reduce the evaporating area until the evaporation rate is 40 lbm/sec.

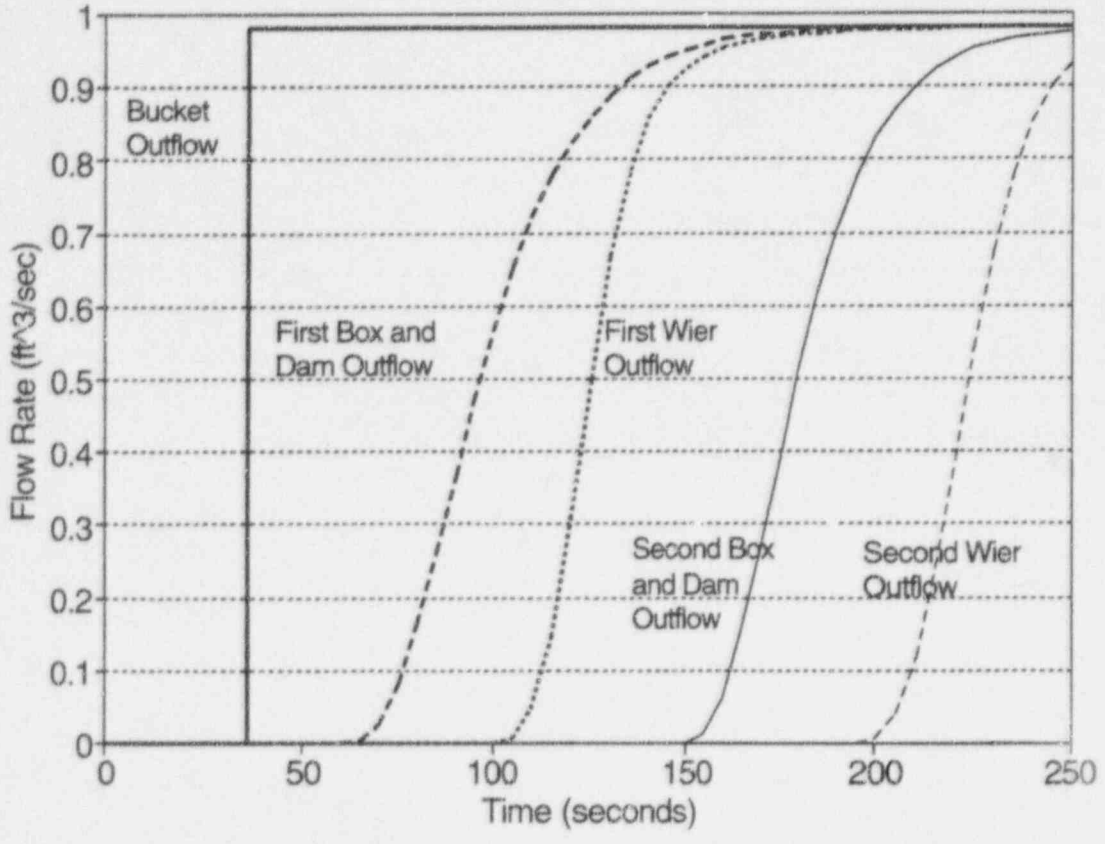

Figure 7-4 Weir Outflow

- Subtract the evaporating area and the subcooled area from the total area to get the dry area A_{dry} = 52,662 ft^2 - A_{sc} - A_{evap}.

7.7 BAFFLE ANALYSIS AND SCALING EQUATIONS

The baffle receives heat by radiation from the shell and loses heat by radiation to the shield building and by convection to the riser and downcomer. The energy equation for the baffle is formulated accordingly, assuming radiation heat transfer from both wet and dry portions of the shell that are generally at different temperatures. Examination of when the shell becomes wetted, and the temperatures calculated for the wet and dry portions of the shell shows that through the beginning of the post-refill time phase, the outer shell temperatures for wet and dry portions are sufficiently close in temperature that wet or dry does not matter. Furthermore, once wetting is well along, the shell heat rejection to the baffle can be minimized by assuming 100 percent of the shell is wet (although for shell evaporative heat losses to the riser a lesser fraction is assumed wet). For the scaling analysis the baffle was forced by the dry shell during blowdown and refill, and by the wet shell from the beginning of the peak pressure period and beyond.

The baffle is a thin steel member with such a small Biot number that it is well-represented as a lumped mass with identical bulk and surface temperatures. Both sides of the baffle are subject to forced convection and radiation. The downcomer side of the baffle is always dry. The riser side of the baffle may be wet or dry, depending upon the radiation heat transfer rate to the baffle and the convection heat transfer from the baffle to the riser and downcomer. The energy equation for the baffle is:

$$m_{bf} c_v \frac{dT_{bf}}{dt} = h_{r,shx-bf} A (T_{shx} - T_{bf}) + h_{c,ri-bf} A (T_{ri} - T_{bf}) - h_{r,bf-dc} A (T_{bf} - T_{dc}) - h_{c,bf-dc} A (T_{bf} - T_{dc}) + \dot{m}_{stm,bf} h_{fg} \quad (156)$$

In terms of inside and outside equivalent conductances, the baffle equation is:

$$m_{bf} c_v \frac{dT_{bf}}{dt} = h_e A_{bf} (T_{ri} - T_{bf}) - h_{ex} A_{bf} (T_{bf} - T_{dc}) \quad (157)$$

7.7.1 Baffle Conductance

The individual baffle conductance terms are:

$$h_{r,shx-bf} = \sigma\varepsilon f(T_{shx}, T_{bf}) \quad h_{r,bf-dc} = \sigma\varepsilon f(T_{bf}, T_{dc}) \quad h_{m,ri-bf} = \frac{h_{fg}\rho_{stm}D_v}{(T_{ri}-T_{bf})d_h}\frac{\Delta P_{stm}}{P_{lm,air}}0.023\,Re_d^{0.8}Sc^{1/3}$$

$$h_{c,ri-bf} = \frac{k}{D_h}0.023\,Re_d^{0.8}Pr^{1/3} \quad h_{c,bf-dc} = \frac{k_o}{d_h}0.023\,Re_{d,o}^{0.8}Pr_o^{1/3} \qquad (158)$$

$$h_e = h_{m,ri} + h_{c,ri} + h_{r,ri}\frac{(T_{shx}-T_{bf})}{(T_{ri}-T_{bf})} \quad h_{ex} = h_{c,dc} + h_{r,dc}$$

The riser operates in forced convection and the downcomer in opposed mixed convection. The liquid film conductance on the baffle is neglected.

The individual conductance terms are normalized to the shell conductance, $h_{sh,o}$, to produce the pi groups for scaling the heat sink conductances:

$$\pi_{c,r,shx-bf} = \frac{h_{r,shx-bf,o}}{h_{sh,o}} \quad \pi_{c,c,ri-bf} = \frac{h_{c,ri-bf,o}}{h_{sh,o}} \quad \pi_{c,r,bf-dc} = \frac{h_{r,bf-dc,o}}{h_{sh,o}} \quad \pi_{c,c,bf-dc} = \frac{h_{c,bf-dc,o}}{h_{sh,o}} \qquad (159)$$

$$\pi_{c,m,ri-bf} = \frac{h_{m,ri-bf,o}}{h_{sh,o}} \quad \pi_{c,e,bf} = \frac{h_{e,bf,o}}{h_{sh,o}} \quad \pi_{c,ex,bf} = \frac{h_{ex,bf,o}}{h_{sh,o}}$$

7.7.2 Baffle Mass Transfer

The riser side of the baffle may experience condensation mass transfer if the baffle is colder than the riser gas saturation temperature. The mass transfer rate and pi group are:

$$\dot{m}_{stm,bf} = \frac{\rho_{stm}D_v}{d_h}\frac{\Delta P_{stm}}{P_{lm,air}}0.023\,Re_d^{0.8}Sc^{1/3} \quad \pi_{m,bf} = \frac{\rho_{stm}D_v}{\dot{m}_{g,brk,o}d_h}\frac{\Delta P_{stm}}{P_{lm,air}}0.023\,Re_d^{0.8}Sc^{1/3} \qquad (160)$$

7.7.3 Baffle Energy Transfer

Each term of the right-hand side of Equation (156) represents energy transfer processes that are of interest to scale. The terms are normalized by the break source enthalpy flow rate and are made dimensionless with the substitutions defined above:

$$\frac{h_{r,shx-bf}A(T_{shx}-T_{bf})}{\dot{m}_{g,brk,o}\Delta h_{g,brk,o}} + \frac{h_{c,ri-bf}A(T_{ri}-T_{bf})}{\dot{m}_{g,brk,o}\Delta h_{g,brk,o}} - \frac{h_{r,bf-dc}A(T_{bf}-T_{dc})}{\dot{m}_{g,brk,o}\Delta h_{g,brk,o}} - \frac{h_{c,bf-dc}A(T_{bf}-T_{dc})}{\dot{m}_{g,brk,o}\Delta h_{g,brk,o}}$$
$$+ \frac{\dot{m}_{stm,bf}h_{fg}}{\dot{m}_{g,brk,o}\Delta h_{g,brk,o}} = \frac{h_{r,shx-bf,o}h^{*}_{r,shx-bf}A_{o}\Delta T_{shx-bf,o}\Delta T^{*}_{shx-bf}}{\dot{m}_{g,brk,o}\Delta h_{g,brk,o}} + \frac{h_{c,ri-bf,o}h^{*}_{c,ri-bf}A_{o}\Delta T_{ri-bf,o}\Delta T^{*}_{ri-bf}}{\dot{m}_{g,brk,o}\Delta h_{g,brk,o}} \quad (161)$$
$$- \frac{h_{r,bf-dc,o}h^{*}_{r,bf-dc}A_{o}\Delta T_{bf-dc,o}\Delta T^{*}_{bf-dc}}{\dot{m}_{g,brk,o}\Delta h_{g,brk,o}} - \frac{h_{c,bf-dc,o}h^{*}_{c,bf-dc}A_{o}\Delta T_{bf-dc,o}\Delta T^{*}_{bf-dc}}{\dot{m}_{g,brk,o}\Delta h_{g,brk,o}} + \frac{\dot{m}_{stm,bf,o}\dot{m}^{*}_{stm,bf}h_{fg,o}h^{*}_{fg}}{\dot{m}_{g,brk,o}\Delta h_{g,brk,o}}$$
$$= \pi_{e,r,shx-bf}h^{*}_{r,shx-bf}\Delta T^{*}_{shx-bf} + \pi_{e,c,ri-bf}h^{*}_{c,ri-bf}\Delta T^{*}_{ri-bf} - \pi_{e,r,bf-dc}h^{*}_{r,bf-dc}\Delta T^{*}_{bf-dc}$$
$$- \pi_{e,c,bf-dc}h^{*}_{c,bf-dc}\Delta T^{*}_{bf-dc} + \pi_{e,fg,bf}\dot{m}^{*}_{stm,bf}h^{*}_{fg}$$

where the pi groups are defined:

$$\pi_{e,r,shx-bf} = \frac{h_{r,shx-bf,o}A_{o}\Delta T_{shx-bf,o}}{\dot{m}_{g,brk,o}\Delta h_{g,brk,o}} \quad \pi_{e,c,ri-bf} = \frac{h_{c,ri-bf,o}A_{o}\Delta T_{ri-bf,o}}{\dot{m}_{g,brk,o}\Delta h_{g,brk,o}} \quad \pi_{e,r,bf-dc} = \frac{h_{r,bf-dc,o}A_{o}\Delta T_{bf-dc,o}}{\dot{m}_{g,brk,o}\Delta h_{g,brk,o}} \quad (162)$$
$$\pi_{e,c,bf-dc} = \frac{h_{c,bf-dc,o}A_{o}\Delta T_{bf-dc,o}}{\dot{m}_{g,brk,o}\Delta h_{g,brk,o}} \quad \pi_{e,fg,bf} = \pi_{m,bf}\frac{h_{fg,o}}{\Delta h_{g,brk,o}}$$

Baffle Time Constant

The baffle time constant is defined in Section 7.7.4.

7.7.4 Baffle Thermal Model

For scaling, it is of interest to determine the rate of change of baffle temperature, assuming other parameters are constants. Under this assumption and assuming the baffle can be modeled as a lumped mass, the baffle energy equation can be written as:

$$\frac{dT_{bf}}{dt} = a - bT_{bf} \quad (163)$$

where:

$$a = \frac{h_{r,shx-ri}T_{shx} + h_{c,ri-bf}T_{ri} + h_{r,bf-dc}T_{dc} + h_{c,bf-dc}T_{dc} + h_{m,ri-bf}T_{ri}}{\rho_{bf}c_{v}\delta_{bf}} \quad b = \frac{h_{r,shx-bf} + h_{c,ri-bf} + h_{r,bf-dc} + h_{c,bf-dc} + h_{m,ri-bf}}{\rho_{bf}c_{v}\delta_{bf}} \quad (164)$$

With boundary condition $T = T_{o}$ at $t = t_{o}$, the solution to Equation (163) can be shown to be:

$$T_{bf} = a/b - (a/b - T_o)e^{-b(t-t_o)} \quad \text{for} \quad t \geq t_o \tag{165}$$

The ratio a/b can be set equal to $\bar{T}$, then the solution to the energy equation is:

$$T = \bar{T} - (\bar{T} - T_o)e^{-(t-t_o)/\tau} \tag{166}$$

where $\tau = 1/b$. This is the thermal model that is used to calculate the baffle temperature at the end of each time phase, given the values for t_o and T_o, and with all the parameters in Equation (164) evaluated at t_o and T_o.

The baffle Biot number, $h\delta/k$, is on the order of 0.04 for high condensation mass transfer rates, and less without mass transfer. Therefore, using the criterion Bi < 0.1, the baffle can be modeled as a lumped mass with little loss of accuracy.

7.8 SHIELD BUILDING ANALYSIS AND SCALING EQUATIONS

The shield building is a concrete heat sink with dry forced convection to the downcomer and radiation heat transfer from the baffle. Because it is so thick it behaves as a semi-infinite solid.

The shield building can potentially affect the downcomer air flow rate by heating the downcomer air, thereby inducing buoyancy that counteracts the riser and chimney buoyancy. The maximum effect results if all the radiation from the baffle is assumed to be deposited into the downcomer, rather than some being absorbed in the concrete. It is shown in Section 8.4 that the energy transfer to the downcomer is small, and in Section 9.4 that the counterflow buoyancy is small, so it is reasonable to simplify the analysis by neglecting the shield energy interaction and allow the baffle radiation to be deposited directly into the downcomer air.

7.9 CHIMNEY ANALYSIS AND SCALING EQUATIONS

The chimney and upper part of the shield building are large concrete structures that can cool the PCS air flow before it exits from the chimney, and thereby reduce the natural circulation buoyancy force. Section 4.2 shows the chimney operates in opposed mixed convection heat and mass transfer. The concrete was modeled with the same equation used for the internal heat sinks, except that radiation from the top of the shell to the concrete is neglected. Neglecting radiation reduces the heating rate and overpredicts the heat removal from the air flow path, thereby minimizing the air flow rate.

The effective heat sink conductance is defined $h_e = [(h_m + h_c)^{-1} + h_{if}^{-1}]^{-1}$ and is combined with the general energy equation for a heat sink to give:

$$m_{ch} c_v \frac{dT_{ch}}{dt} = h_e A (T_{ch} - T_{ch,srf}) \tag{167}$$

The right-hand side of Equation (167) is normalized by the break enthalpy flow rate and made dimensionless with the substitutions above.

$$\frac{h_{e,ch} A_{ch} (T_{ch} - T_{srf})}{\dot{m}_{g,brk,o} h_{g,brk,o}} = \frac{h_{e,ch,o} h^*_{e,ch} A_{ch,o} \Delta T_{ch,o} \Delta T^*_{ch}}{\dot{m}_{g,brk,o} h_{g,brk,o}} = \pi_{e,ch} h^*_{e,ch} \Delta T^*_{ch} \tag{168}$$

$$\text{where} \quad \pi_{e,ch} = \frac{h_{e,ch,o} A_{ch,o} \Delta T_{ch,o}}{\dot{m}_{g,brk,o} h_{g,brk,o}}$$

7.9.1 Chimney Conductance

The individual conductance terms are:

$$h_c = \frac{k}{d_h} \left(\frac{(0.13 d_h)^3}{(\nu^2 \quad g)} \frac{\Delta\rho}{\rho} + (0.023)^3 Re_d^{2.4} \right)^{1/3} Pr^{1/3} \qquad h_{if} = k_{if} / \delta_{if} \tag{169}$$

$$h_m = \frac{(h_g - h_f) \rho_{stm} D_v}{(T - T_{srf}) d_h} \frac{\Delta P_{stm}}{P_{lm,air}} \left(\frac{(0.13 d_h)^3}{(\nu^2 / g)} \frac{\Delta\rho}{\rho} + 0.023^3 Re_d^{2.4} \right)^{1/3} Sc^{1/3} \qquad h_e = [(h_m + h_c)^{-1} + h_{if}^{-1}]^{-1}$$

The individual conductance terms are normalized to the shell conductance, $h_{sh,o}$, to produce the pi groups for scaling the heat sink conductances. Radiation to the concrete is neglected, resulting in more heat transfer from the gas to the chimney, and consequently, less buoyancy to drive the natural circulation air flow. The liquid film is assumed to be 0.005 inches thick.

$$\pi_{c,m,ch} = \frac{h_{m,ch,o}}{h_{sh,o}} \qquad \pi_{c,c,ch} = \frac{h_{c,ch,o}}{h_{sh,o}} \qquad \pi_{c,if,ch} = \frac{h_{if,ch,o}}{h_{sh,o}} \qquad \pi_{c,e,ch} = \frac{h_{e,ch,o}}{h_{sh,o}} \tag{170}$$

7.9.2 Chimney Mass Transfer

The opposed mixed convection condensation mass transfer to the chimney is calculated and scaled:

$$\pi_{m,ch} = \frac{\dot{m}_{stm,ch,o}}{\dot{m}_{g,brk,o}} = \frac{\rho_{stm} D_v A_{ch}}{\dot{m}_{g,brk,o} d_h} \frac{\Delta P_{stm}}{P_{lm,air}} \left(\frac{(0.13 d_h)^3}{(\nu^2/g)} \frac{\Delta\rho}{\rho} + (0.023)^3 Re_d^{2.4} \right)^{1/3} Sc^{1/3} \qquad (171)$$

where the parameters are evaluated at initial conditions at the bulk and condensed film free surface.

7.9.3 Chimney Energy Transfer

Energy transfer terms similar to those for the internal heat sinks are defined and scaled. Those are the energy change from the gas to the condensed film, the energy of the film above the minimum energy (here h_f at 115°F) and the heat transfer to the film:

$$\pi_{e,fg,ch} = \pi_{m,ch} \frac{(h_{g,ri} - h_f)}{\Delta h_{g,brk,o}} \qquad \pi_{e,f,ch} = \pi_{m,ch} \frac{(h_f - h_{f,To})}{\Delta h_{g,brk,o}}$$

$$\pi_{e,q,ch} = \frac{h_{q,ch} A_{ch} (T_{ri} - T_{f,ch})}{\dot{m}_{g,brk,o} \Delta h_{g,brk,o}} = \frac{k}{d_h} \left(\frac{(0.13 d_h)^3}{(\nu^2/g)} \frac{\Delta\rho}{\rho} + (0.023)^3 Re_d^{2.4} \right)^{1/3} Pr^{1/3} \frac{A_{ch} (T_{ri} - T_{f,ch})}{\dot{m}_{g,brk,o} \Delta h_{g,brk,o}} \qquad (172)$$

where the parameters are evaluated at initial conditions at the bulk and condensed film free surface, and $h_q = h_c$.

7.9.4 Chimney Thermal Model

The time history of the chimney and shield building concrete surface temperature is predicted using the same integral methods for thermally thick structures as used for the internal concrete in Section 7.5.6.

8 EVALUATION OF CONTAINMENT AND HEAT SINK PI GROUPS

8.1 HEAT SINK SURFACE AREAS DURING TRANSIENTS

Surface area is a very important parameter for calculating the heat and mass transfer to the heat sinks. The surface area of some heat sinks change over time: the break pool volume and surface area increase with time, and the wetted area of the external shell initially increases, then varies with time as the source flow rate changes and the containment pressure causes the shell heat flux to change. The pool areas were discussed in Section 7.2.2 and the shell surface areas were discussed in Section 7.6.6. All other areas are assumed constant over the time covered by the scaling analysis. The areas of all heat sinks used in the calculations are summarized in Table 8-1.

Table 8-1 Heat Sink Areas During DECLG and MSLB Transients (Units are ft^2)

Heat Sink	DECLG LOCA				MSLB
	Blowdown	Refill	Peak Press	Long Term	Blowdown
Drops	$7.2x10^7$	$7.2x10^7$	$7.2x10^7$	$7.2x10^7$	0
Break Pool	420	555	1933	1933	0
Steel	142,700	142,700	142,700	142,700	73,800
Concrete	22,600	22,600	22,600	22,600	22,600
Jacketed Concrete	46,500	46,500	46,500	46,500	12,600
Evaporating Shell	0	0	47,613	27,000	0
Dry Shell	52,662	52,662	3,600	24,077	52,662
Subcooled Shell	0	0	1449	1586	0

8.2 CONDUCTANCE PI GROUP VALUES

Table 8-2 presents the energy transfer conductance pi values for each heat sink and shell region during each time phase. The conductance pi values are defined in Section 7 as the ratio of the equivalent conductance (that combines for radiation, convection, mass transfer, and the liquid film) to the shell conductance, that is, $\pi_c = h_e/h_{sh}$. Since the normalizing value is the same for all values in Table 8-2, the values can be compared both horizontally and vertically.

Table 8-2 Heat Sink Energy Transfer Conductances Scaled to Shell Conductance						
Heat Sink		**Blowdown**	**Refill**	**Peak Press**	**Long Term**	**MSLB**
Drops	$\pi_{c,d}$	141	165	149	202	--
Pool	$\pi_{c,p}$	184	0.02	1.38	0.98	--
Steel	$\pi_{c,st}$	0.31	0.40	0.42	0.45	0.37
Concrete	$\pi_{c,cc}$	0.25	0.41	0.35	0.50	0.29
Jacketed	$\pi_{c,jc}$	0.31	0.40	0.42	0.50	0.37
Dry Shell	$\pi_{c,ds}$	0.33	0.39	0.37	0.54	0.37
	$\pi_{c,dsx}$	0.01	0.01	0.01	0.02	--
Subcooled Shell	$\pi_{c,sc}$	--	--	0.39	0.58	--
	$\pi_{c,scx}$	--	--	3.88	3.88	--
Evaporating Shell	$\pi_{c,es}$	--	--	0.37	0.60	--
	$\pi_{c,esx}$	--	--	0.10	0.52	--
Baffle	$\pi_{c,bf}$	0.03	0.03	0.05	-7.6	--
	$\pi_{c,bfx}$	0.01	0.01	0.01	0.02	--
Chimney	$\pi_{c,ch}$	0.03	0.03	0.02	0.07	--

All the conductance values have been normalized to the coated shell conductance, h_{sh} = 216.58 B/hr-ft^2-F. The coated shell conductance is the shell plus the inner and outer inorganic zinc coatings. The coating conductance is 4840 B/hr-ft^2-F, so has little effect on the shell conductance.

Table 8-2 shows the conductances for the drops are extremely high, so the drops quickly reach thermal equilibrium with the gas and subsequently follow changes in the gas temperature with no significant lag. The conductance to the pool during blowdown is very high because it is assumed to flash to thermal and mechanical equilibrium with the average containment, as was assumed for the drops. After refill the assumption of a saturated source causes the pool evaporation conductance to remain high. During refill the pool condensation conductance is low.

The conductance of the outside surface of the subcooled shell is very high because heat is conducted directly from the shell to the subcooled liquid through the thin film thickness.

Since the film is the heat sink, there is no additional evaporation, radiation, or convection conductance.

The conductances for the solid heat sinks, shell inside and evaporating shell outside all are high, in the range of 0.10 to 0.62, due to the high mass transfer conductance. The external conductance on the evaporating shell at the time of peak containment pressure is nearly equal to the internal conductance, and both are approximately 1/2 the shell conductance.

The remaining conductances range from 0.01 to 0.05 and are low mainly because mass transfer is not involved. The chimney operates with low conductances, even when condensate forms, due to the high noncondensible concentration. The dry shell external conductance is 1 to 2 orders of magnitude less than the internal conductance. The baffle inside and outside both operate dry and have low conductances. The anomalously high negative baffle conductance resulted from a reversal of the baffle-riser temperature difference that was coincidentally small. The energy transfer is low, similar to the value during the preceding time phase.

8.3 MASS TRANSFER PI GROUP VALUES

The containment mass flux pi groups discussed in Section 6.1, and the heat sink mass flux pi groups defined in Section 7 are presented in Table 8-3. The values greater than 10 percent are shaded.

Conclusions of the mass flow rate scaling are:

- The mass flow pi groups show the break liquid mass flow rate is high, and the steel, concrete, jacketed concrete, dry shell, and evaporating shell have high-scaled mass flow rates during some time phases.

- The pool, drops, subcooled shell, baffle, and chimney always have small-scaled mass flow rates.

- During blowdown the break source flow rate is so high that even with significant energy absorption, none of the heat sinks have high-scaled mass flow rates.

8.4 ENERGY TRANSFER PI GROUP VALUES

The containment energy flux pi groups discussed in Section 6.2, and the heat sink energy flux pi groups defined in Section 7 are presented in Table 8-4. Values greater than 10 percent are shaded.

Table 8-3 Containment and Heat Sink Mass Scaling Pi Group Values						
Pi Group		Blowdown	Refill	Peak Press	Long Term	MSLB
Containment	τ_o (sec)	39	985	913	5173	537
	$\pi_{m,\tau}$	1.31	1.27	1.30	1.22	1.27
	$\pi_{m,brk}$	1.00	0.00*	1.00*	1.00	1.00
	$\pi_{m,f}$	1.75	0.00	2.00	0.00	0.00
Drops	$\pi_{m,flash,d}$	0.02	0.00	0.00	0.00	--
	$\pi_{m,evap,d}$	0.03	-0.04	0.01	0.00	--
Pool	$\pi_{m,p}$	0.04	0.00	0.03	0.07	--
Steel	$\pi_{m,st}$	-0.05	-1.41	-0.69	-0.02	-0.44
Concrete	$\pi_{m,cc}$	-0.01	-0.08	-0.02	-0.09	-0.12
Jacketed	$\pi_{m,jc}$	-0.02	-0.46	-0.23	-0.18	-0.08
Sc Shell	$\pi_{m,sc}$	--	--	-0.01	-0.06	--
Evap Shell	$\pi_{m,es}$	--	--	-0.43	-0.90	--
	$\pi_{m,esx}$	--	--	-0.02	-0.89	--
Dry Shell	$\pi_{m,ds}$	-0.02	-0.61	-0.03	-0.08	-0.37
Baffle	$\pi_{m,bf}$	0.00	0.00	0.00	0.00	--
Chimney	$\pi_{m,ch}$	0.00	0.00	0.00	0.05	--

* Refill was scaled with the same 200 lbm/sec flow rate used to normalize peak pressure.

Pi groups are normalized to different energy flow rates in each time phase, so cannot be compared between different time phases — only comparisons within the same column are meaningful.

The sensible heat transfer terms (q subscripted) are always small. The energy carried away by the liquid film (f subscripted) is generally 10 percent or less of the energy transferred into the heat sink by condensation (fg subscripted).

The inside of the dry shell during refill, and the inside of the evaporating shell during the peak pressure phase have large values of scaled energy transfer, while the outside is small, indicating the significance of the shell heat capacity. Energy interactions with the baffle and chimney are always small.

Table 8-4 Containment and Heat Sink Energy Scaling Pi Group Values

Pi Group		Blowdown	Refill	Peak Press	Long Term	MSLB
Containment	$\pi_{e,t}$	0.55	0.58	0.56	0.63	0.58
	$\pi_{e,brk}$	1.00	0.00*	1.00*	1.00	1.00
	$\pi_{e,f,work}$	0.00	0.00	0.00	0.00	0.00
Drops	$\pi_{e,q,d}$	0.00	0.00	0.00	0.00	--
	$\pi_{e,fg,d}$	0.05	-0.04	0.00	0.00	--
Pool	$\pi_{e,q,p}$	0.00	0.00	0.00	0.00	--
	$\pi_{e,fg,p}$	0.03	0.00	0.02	0.06	--
Steel	$\pi_{e,q,st}$	0.00	-0.08	-0.03	0.00	-0.03
	$\pi_{e,fg,st}$	-0.05	-1.35	-0.64	- 0.02	-0.44
	$\pi_{e,f,st}$	0.00	-0.05	-0.05	0.00	-0.01
Concrete	$\pi_{e,q,cc}$	0.00	0.00	0.00	0.00	-0.01
	$\pi_{e,fg,cc}$	-0.01	-0.07	-0.02	-0.08	-0.12
	$\pi_{e,f,cc}$	0.00	-0.01	0.00	-0.01	0.00
Jacketed Concrete	$\pi_{e,q,jc}$	0.00	-0.03	-0.01	0.00	-0.01
	$\pi_{e,fg,jc}$	-0.02	-0.44	-0.21	-0.16	-0.07
	$\pi_{e,f,jc}$	0.00	-0.02	-0.02	-0.02	0.00
Subcooled Shell	$\pi_{e,q,ss}$	--	--	0.00	0.00	--
	$\pi_{e,fg,ss}$	--	--	-0.01	-0.06	--
	$\pi_{e,f,ss}$	--	--	0.00	-0.01	--
	$\pi_{e,q,ssx}$	--	--	-0.01	-0.08	--
Evaporating Shell	$\pi_{e,q,es}$	--	--	-0.02	-0.03	--
	$\pi_{e,fg,es}$	--	--	-0.41	-0.81	--
	$\pi_{e,f,es}$	--	--	-0.02	-0.09	--
	$\pi_{e,q,esx}$	--	--	0.00	-0.03	--
	$\pi_{e,fg,esx}$	--	--	-0.02	-0.81	--
Dry Shell	$\pi_{e,q,ds}$	0.00	-0.03	0.00	0.00	-0.02
	$\pi_{e,fg,ds}$	-0.02	-0.59	-0.03	-0.07	-0.36
	$\pi_{e,f,ds}$	0.00	-0.02	0.00	-0.01	0.00
	$\pi_{e,q,dsx}$	0.00	0.00	0.00	-0.03	--

* Refill was scaled with the same pressure normalization used for peak pressure.

Table 8-4 Containment and Heat Sink Pressure Scaling Pi Group Values (cont.)						
Pi Group		Blowdown	Refill	Peak Press	Long Term	MSLB
Chimney	$\pi_{e,q,ch}$	0.00	0.00	0.00	0.00	--
	$\pi_{e,fg,ch}$	0.00	0.00	0.00	-0.05	--
	$\pi_{e,f,ch}$	0.00	0.00	0.00	0.00	--
Baffle	$\pi_{e,q,bf}$	0.00	0.00	0.00	-0.02	--
	$\pi_{e,q,btx}$	0.00	0.00	0.00	-0.02	--

* Refill was scaled with the same pressure normalization used for peak pressure.

8.5 PRESSURE PI GROUP VALUES

The containment pressure pi groups discussed in Section 6.3, and the heat sink pressure pi groups defined in Section 7 are presented in Table 8-5. Values greater than 10 percent are shaded.

The negative signs in Table 8-5 indicate pressure decreases, while all others are pressure increases. The drops produce a small pressure increase during blowdown, and thereafter are either a pressure sink, or at worst, a negligible pressure source. The pool is always a small pressure source that increases to 7 percent at the time of peak containment pressure. The remaining heat sinks reduce pressure during the time phases considered.

The pi groups in Table 8-5 show the work due to mass removal is the most significant pressure reduction process: heat transfer (radiation plus convection) are typically less than 20 percent of the flow work. The enthalpy pi groups for both the source and heat sinks are always small. The pi groups clearly show the importance of mass transfer as the process that dominates the rate of pressure change after blowdown.

Volumetric compliance, $\pi_{p,v}$ is always a significant factor that mitigates the rate of pressure rise.

Table 8-5 Containment and Heat Sink Pressure Scaling Pi Group Values

Pi Group		Blowdown	Refill	Peak Press	Long Term	MSLB
Containment	$\pi_{p,t}$	0.76	0.76	0.77	0.76	0.76
	$\pi_{p,g,brk,work}$	1.00	0.00*	1.00*	1.00	1.00
	$\pi_{p,g,brk,enth}$	0.03	0.00	0.03	0.02	0.03
	$\pi_{p,f,work}$	0.00	0.00	0.00	0.00	0.00
Drops	$\pi_{p,q,d}$	0.00	0.00	0.00	0.00	–
	$\pi_{p,enth,d}$	0.00	0.00	0.00	0.00	–
	$\pi_{p,work,d}$	0.05	-0.04	0.01	0.00	–
Pool	$\pi_{p,q,p}$	0.00	0.00	0.00	0.00	–
	$\pi_{p,enth,p}$	0.00	0.00	0.00	0.00	–
	$\pi_{p,work,p}$	0.04	0.00	0.03	0.07	–
Steel	$\pi_{p,q,st}$	-0.01	-0.24	-0.09	-0.00	-0.0[illegible]
	$\pi_{p,enth,st}$	0.00	0.00	0.00	0.00	0.00
	$\pi_{p,work,st}$	-0.05	-1.41	-0.69	-0.02	-0.44
Concrete	$\pi_{p,q,cc}$	0.00	-0.01	0.00	-0.01	-0.02
	$\pi_{p,enth,cc}$	0.00	0.00	0.00	0.00	0.00
	$\pi_{p,work,cc}$	-0.01	-0.08	-0.02	-0.09	-0.12
Jacketed Concrete	$\pi_{p,q,jc}$	0.00	-0.08	-0.03	-0.01	-0.02
	$\pi_{p,enth,jc}$	0.00	0.00	0.00	0.00	0.00
	$\pi_{p,work,jc}$	-0.02	-0.46	-0.23	-0.18	-0.08
Evaporating Shell	$\pi_{p,q,es}$	–	–	-0.07	-0.08	–
	$\pi_{p,enth,es}$	–	–	0.00	0.00	–
	$\pi_{p,work,es}$	–	–	-0.43	-0.90	–
Subcooled Shell	$\pi_{p,q,ss}$	–	–	0.00	0.01	–
	$\pi_{p,enth,ss}$	–	–	0.00	0.00	–
	$\pi_{p,work,ss}$	–	–	-0.01	-0.06	–
Dry Shell	$\pi_{p,q,ds}$	0.00	-0.10	-0.01	-0.01	-0.07
	$\pi_{p,enth,ds}$	0.00	0.00	0.00	0.00	0.00
	$\pi_{p,work,ds}$	-0.02	-0.61	-0.03	-0.08	-0.37

* Refill was scaled with the same pressure normalization used for peak pressure.

9 PCS AIR FLOW PATH SCALING

Outside containment, the PCS air flow path, consisting of the downcomer, riser, and chimney, has one inlet to the downcomer, one outlet from the chimney, a source of steam that evaporates from the shell, and a steam sink for condensation on the chimney concrete and baffle. It is necessary to write the conservation equations separately for the downcomer, riser, and chimney, so the changes from the inlet to outlet of each can be tracked and factored into the buoyancy calculation in Section 9.3.

9.1 PCS AIR FLOW PATH MASS TRANSFER

The three mass equations can be written:

$$\frac{dm_{dc}}{dt} = \dot{m}_{in} - \dot{m}_{dc} \qquad \frac{dm_{ri}}{dt} = \dot{m}_{dc} - \dot{m}_{ri} + \dot{m}_{stm,xf} - \dot{m}_{stm,bf}$$

$$\frac{dm_{ch}}{dt} = \dot{m}_{ri} - \dot{m}_{ch} - \dot{m}_{stm,ch} \qquad (173)$$

The condensation and evaporation rates and the time constants are the variables of interest for scaling. The pi groups were defined, respectively, for the shell evaporation, baffle condensation, and chimney condensation in Sections 7.6, 7.7, and 7.9. The necessary flow rate variables are defined:

Time	t	=	$\tau\, t^*$
Volume	V	=	V_o
Inlet air flow rate	$\dot{m}_{in}$	=	$\dot{m}_{in,o}\dot{m}^*_{in}$
Downcomer density	ρ_{dc}	=	$\rho_{dc,o}\rho_{dc}^*$
Riser density	ρ_{ri}	=	$\rho_{ri,o}\rho_{ri}^*$
Chimney density	ρ_{ch}	=	$\rho_{ch,o}\rho_{ch}^*$

The downcomer, riser, and chimney time constants are defined as the mass of gas in each region divided by the air mass flow rate through the entire flow path. The steam evaporation and condensation flow rates are an order of magnitude smaller than the air flow rate, so contribute little to the time constants:

$$\tau_{dc} = \frac{V_{dc}\rho_{dc,o}}{\dot{m}_{in,o}} \qquad \tau_{ri} = \frac{V_{ri}\rho_{ri,o}}{\dot{m}_{in,o}} \qquad \tau_{ch} = \frac{V_{ch}\rho_{ch,o}}{\dot{m}_{in,o}} \qquad (174)$$

9.2 PCS AIR FLOW PATH ENERGY TRANSFER

The energy transfer terms fo. the PCS air flow path include the mass transfer terms discussed in Section 9.1, with their respective enthalpies, plus convective heat transfer between the gas and surfaces. Although there is radiation from the shell to the baffle and baffle to the shield, the beam length and steam partial pressure are too small to allow the gas to absorb significant radiation. Hence gas absorption is neglected. The one potential exception is if fog appears in the riser. Although the conditions assumed for safety analyses preclude fog formation, due to the rather high saturation temperature of the gas, it is important to evaluate what happens if other ambient conditions are assumed. Such an evaluation is presented in the PIRT, where it was concluded that the heat released to the gas by condensation increases the buoyancy, resulting in a net improvement in heat removal from containment.

Because the steam partial pressure in the PCS air flow path remains low, less than approximately 2 psi, steam can be approximated as an ideal gas. This permits the energy equations to be written in terms of specific heats and temperature differences:

$$\frac{d(mu)_{dc}}{dt} = \dot{m}_{air}(h_{air,in}-h_{air,dc}) + \dot{q}_{dc} = \dot{m}_{air}c_{P,air}(T_{in}-T_{dc}) + \dot{q}_{dc}$$

$$\frac{d(mu)_{ri}}{dt} = \dot{m}_{air}(h_{air,dc}-h_{air,ri}) + \dot{m}_{stm,xf}(h_{stm,xf}-h_{stm,ri}) - \dot{m}_{stm,bf}(h_{stm}-h_{stm,ri}) + \dot{q}_{ri} \qquad (175)$$

$$= \dot{m}_{air}c_{P,air}(T_{dc}-T_{ri}) + \dot{m}_{stm,xf}c_{P,stm}(T_{xf}-T_{ri}) - \dot{m}_{stm,bf}c_{P,stm}(T-T_{ri}) + \dot{q}_{ri}$$

$$\frac{d(mu)_{ch}}{dt} = \dot{m}_{air}(h_{air,ri}-h_{air,ch}) + (\dot{m}_{stm,xf}-\dot{m}_{stm,bf})(h_{stm,ri}-h_{stm,ch}) - \dot{m}_{stm,ch}(h_{stm}-h_{stm,ch}) + \dot{q}_{ch}$$

$$= \dot{m}_{air}c_{P,air}(T_{ri}-T_{ch}) + (\dot{m}_{stm,xf}+\dot{m}_{stm,bf})c_{P,stm}(T_{ri}-T_{ch}) - \dot{m}_{stm,ch}c_{P,stm}(T-T_{ch}) + \dot{q}_{ri}$$

where the dc, ri, and ch subscripts on temperature, enthalpy, (and later) molecular weight, and density imply the value at the outlet of that region. T is the bulk temperature of the region, or the average of the inlet and outlet temperatures.

The evaporation, condensation, and heat transfer are the energy transfer rates of interest for scaling. These terms were defined for the shell, baffle, and chimney in Sections 7.6, 7.8, and 7.9, respectively.

9.3 PCS AIR FLOW PATH MOMENTUM EQUATION

The wind-positive character of the PCS air flow path is neglected and the PCS air flow is modeled as entirely buoyancy-driven (Ref. 5, Section 6). The positive buoyancy is provided by air heating and the evaporation of low density steam into the riser and chimney. A small amount of negative buoyancy is provided by heating from the baffle and shield walls in the

downcomer, and heat and mass transfer to the cool shield building and chimney at the outlet. Wind-induced recirculation was shown to have a negligible impact on containment pressure (Ref. 5, Section 6).

The PCS air flow path consists of the downcomer, riser, and chimney, which are modeled as distinct, series-connected flow paths. The PCS air flow path, with elevations of important features, are shown in Figure 9-1. It is assumed that the heat and mass are added to, or removed from, each leg of the path at thermal centers that are located to minimize the PCS air flow rate.

Following the example of Wulff [13], the system of momentum equations for a single loop can be written in vector form where the overline indicates vectors:

$$\bar{I} \cdot \frac{d\bar{\dot{m}}}{dt} = G - \bar{R} \cdot \overline{(KE)} \tag{176}$$

$\bar{I}$ is the geometry dependent inertia vector:

$$\bar{I} = \left((L/A)_{dc} , (L/A)_{ri} , (L/A)_{ch} \right) \tag{177}$$

$\bar{\dot{m}}$ is the mass flow rate vector:

$$\bar{\dot{m}} = \left(\dot{m}_{dc} , \dot{m}_{ri} , \dot{m}_{ch} \right) \tag{178}$$

G is the buoyancy defined by integrating the density times the dot product of the gravity and displacement vectors around a closed path:

$$G = \oint_S \rho \bar{g} \cdot d\bar{s} = \int_{dc} \rho g dz + \int_{ri} \rho g dz + \int_{ch} \rho g dz + \int_{env} \rho g dz \tag{179}$$

$\bar{R}$ is the impedance vector and R_i is the sum of the form and friction resistance for each segment determined from the 1/6 scale pressure drop test[34]:

$$\bar{R} = \frac{1}{2\rho_o A_{ri}^2} \left(R_{dc} , R_{ri} , R_{ch} \right) \text{ where } R_i = \frac{K_i + f_i L_i / d_{h,i}}{(A_i / A_{ri})^2} \tag{180}$$

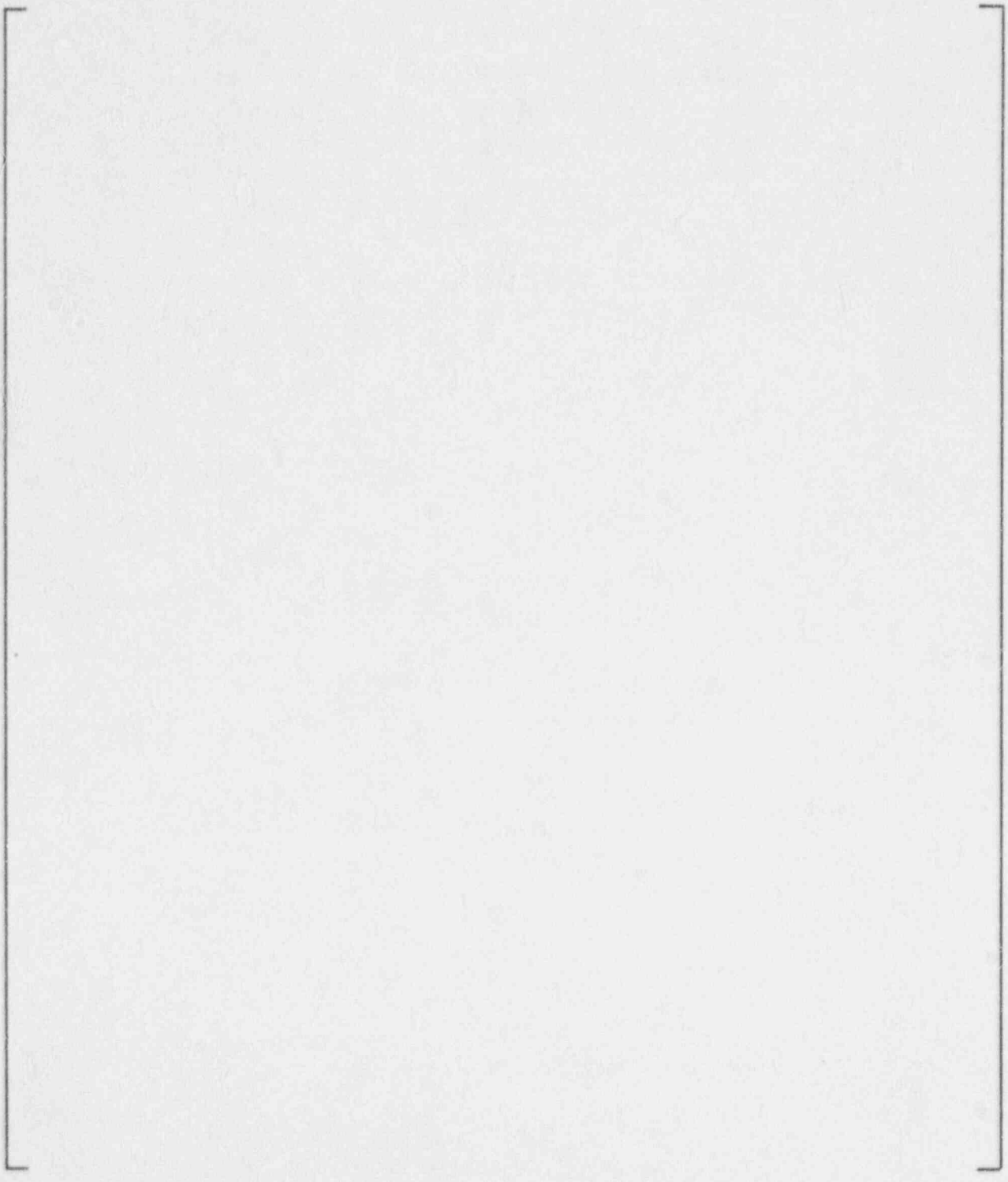

a,b

Figure 9-1 Passive Cooling System Air Flow Path Momentum Parameters

KE is the vector of kinetic energies:

$$\overline{(KE)} = \left(\dot{m}_{dc}^2 \, , \, \dot{m}_{ri}^2 \, , \, \dot{m}_{ch}^2\right) \tag{181}$$

where

$$\dot{m}_{dc} = \dot{m}_{air}, \; \dot{m}_{air} + \dot{m}_{stm,xf} - \dot{m}_{stm,bf} = \dot{m}_{ri}, \text{ and } \dot{m}_{air} + \dot{m}_{stm,xf} - \dot{m}_{stm,bf} - \dot{m}_{stm,ch} = \dot{m}_{ch}.$$

9.3.1 Dimensionless PCS Momentum Equations

The matrix elements are made dimensionless by setting each equal to the product of a reference value and a dimensionless value:

Inertia	$I_i = I_o I_i^*$	where $I_o = \Sigma I_{i,o}$
Mass flow rate	$\dot{m}_i = \dot{m}_o \dot{m}_i^*$	
Buoyancy	$G = G_o G^*$	
Density	$\rho_i = \rho_o \rho_i^*$	where $\rho_o = \rho_{air}$ th. ambient air density
Flow resistance	$R_i = R_o R_i^*$	where R_o = the total PCS loss

The reference mass flow rate comes from the reference buoyancy term, which is used to normalize the inertia and resistance terms. The reference buoyancy is the steady-state solution to the momentum equation, that is, the solution to the momentum equation without the inertial term. The buoyancy term is defined, in terms of thermal center differences shown in Figure 9-1. The thermal center values, H_1, H_2, H_3, and H_4 are [

]^{a,c} ft. respectively for the downcomer, riser, chimney, and outlet. The thermal center approach assumes the density changes step-wise at the thermal center. The buoyancy is:

[a,b

(182)

]

where the last three bracketed terms represent, respectively, the downcomer, riser, and chimney buoyancy contributions. The density used in Equation (182) is defined from the ideal gas law, which is sufficiently accurate for air and steam at atmospheric pressure. The molecular weight is defined for the air-steam mixture and the temperature is defined by the steady-state portions of the PCS air flow path energy equations (175).

$$\rho_{dc} = \frac{PM_{dc}}{RT_{dc}} \quad M_{dc} = M_{air} \quad T_{dc} = T_{in} + \frac{\dot{q}_{dc}}{\dot{m}_{air} c_{p,air}} \tag{183}$$

$$\rho_{ri} = \frac{PM_{ri}}{RT_{ri}} \quad M_{ri} = \frac{\dot{m}_{air} + \dot{m}_{stm,xf} - 0.5\dot{m}_{stm,bf}}{\frac{\dot{m}_{air}}{M_{air}} + \frac{\dot{m}_{stm,xf} - 0.5\dot{m}_{stm,bf}}{M_{stm}}} \quad T_{ri} = \frac{\dot{m}_{air} c_{P,air} T_{dc} + \dot{m}_{stm,xf} c_{P,stm} T_{xf} - 0.5\dot{m}_{stm,bf} c_{P,stm} T_{dc} + \dot{q}_{ri}}{\dot{m}_{air} c_{P,air} + \dot{m}_{stm,xf} c_{P,stm} - 0.5\dot{m}_{stm,bf} c_{P,stm}} \tag{184}$$

$$\rho_{ch} = \frac{PM_{ch}}{RT_{ch}} \quad M_{ch} = \frac{\dot{m}_{air} + \dot{m}_{stm,xf} - \dot{m}_{stm,bf} - 0.5\dot{m}_{stm,ch}}{\frac{\dot{m}_{air}}{M_{air}} + \frac{\dot{m}_{stm,xf} - \dot{m}_{stm,bf} - 0.5\dot{m}_{stm,ch}}{M_{stm}}} \tag{185}$$

$$T_{ch} = T_{ri} + \frac{\dot{q}_{ch}}{\dot{m}_{air} c_{p,air} + (\dot{m}_{stm,xf} - \dot{m}_{stm,bf} - 0.5\dot{m}_{stm,ch}) c_{p,stm}}$$

The q terms represent the net heat transfer into the gas, $\dot{m}_{air}$ is the same in all terms, and P is one atmosphere. The evaporation was assumed to enter at the temperature of the evaporating surface, $T_{sat,xf}$ and the condensation was assumed to leave at the average of the (riser or chimney) inlet and outlet temperatures. A simultaneous solution was used to calculate the temperatures (T_{dc}, T_{ri}, T_{ch}), flow rates ($\dot{m}_{air}$, $\dot{m}_{stm,xf}$, $\dot{m}_{stm,bf}$, $\dot{m}_{stm,ch}$), and buoyancy (G_o). The calculated results are conservative in terms of minimizing air flow, because the thermal center of the riser and downcomer were both selected high up [ ]^{a,c} elevation in Figure 9-1), rather than at the geometric center (approximately at [ ]^{a,c} ft. elevation).

The areas, lengths, and loss coefficients for the AP600 air flow path are shown in Figure 9-1. From these values the $\bar{R}$ and $\bar{I}$ vectors are:

[ ]^{a,b}

(186)

(187)

[a,b]

Figure 9-2 shows an example of a simplified PCS buoyancy calculation using density values calculated with the scaling equations for AP600, and assuming the density variations are linear. The net buoyancy is represented by the enclosed area. The buoyancy calculated using the thermal center approach is shown for comparison. For this case both the distributed density and thermal center approaches give the same result. Note that for this assumed case, the net buoyancy is not affected by the amount of heat transferred from the riser to the downcomer. (Moving point 2 along the horizontal axis does not change the area within triangle 1-2-3). However, moving point 2 does change the relative ratio of negative downcomer buoyancy to positive riser buoyancy.

9.3.2 Normalized PCS Momentum Equations

The dimensionless and reference variables defined in Section 9.3.1 are substituted into Equation (176), and each term is normalized by the reference buoyancy. The result is:

$$\frac{I_o \dot{m}_o}{G_o \tau}\bar{i}\cdot\frac{d\overline{\dot{m}^*}}{dt^*} = \frac{G_o}{G_o}G^* - \frac{R_o \dot{m}_o^2}{2\rho_o G_o}\bar{r}\cdot\overline{KE^*} \quad \text{or} \quad \pi_{mv,in}\bar{i}\cdot\frac{d\overline{\dot{m}^*}}{dt^*} = \pi_{mv,buoy}G^* - \pi_{mv,res}\bar{r}\cdot\overline{KE^*} \tag{188}$$

$$\text{where} \quad \tau = \frac{V_o}{Q_o} \quad \pi_{mv,in} = \frac{I_o \dot{m}_o}{G_o \tau} \quad \pi_{mv,buoy} = 1 \quad \pi_{mv,res} = \frac{R_o \dot{m}_o^2}{G_o}$$

The three components of the buoyancy equation (182) are defined as pi groups:

[a,b]

(189)

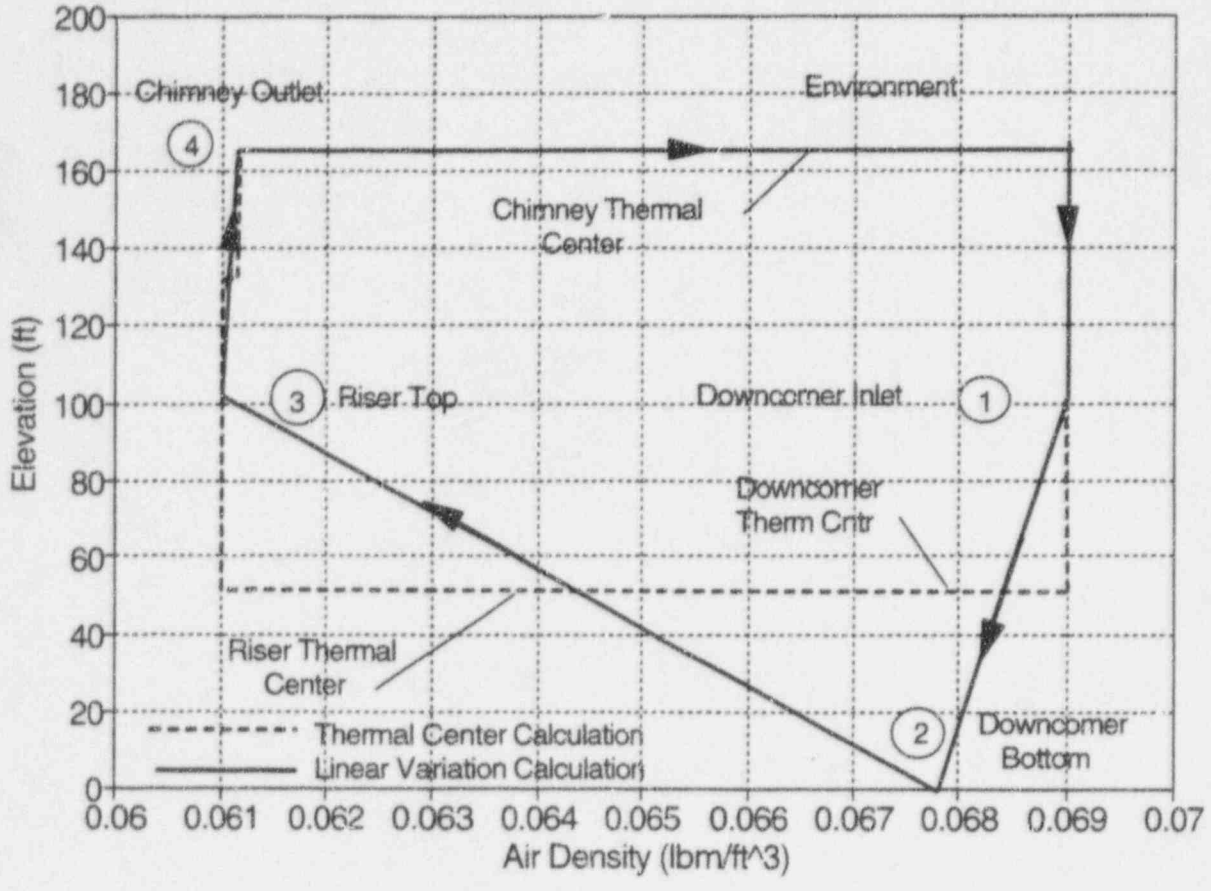

Figure 9-2 Buoyancy Calculation for the AP600 PCS Air Flow Path Comparing Distributed and Thermal Center Approaches

9.4 VALUES FOR PCS AIR FLOW PATH MOMENTUM PI GROUPS

The reference PCS air flow path buoyancy is calculated using heat fluxes calculated from the equations presented in Section 9.2, and the reference mass flow rate is determined from the buoyancy. The time constant and pi groups are then calculated for each time phase and are presented in Table 9-1. The ratio of the branch buoyancy to the total buoyancy, G/G_o is presented to show the relative contribution of the downcomer, riser, and chimney to the total buoyancy. The PCS is not considered for the MSLB, due to relatively short duration of the transient.

Table 9-1 PCS Air Flow Path Momentum Scaling Groups

	Blowdown	Refill	Peak Press	Long Term
τ_{ri}	70	61	15	7.0
$\pi_{mv,in}$	0.13	0.13	0.13	0.11
$\pi_{mv,buoy}$	1.00	1.00	1.00	1.00
$\pi_{mv,res}$	1.00	1.00	0.97	0.86
$\pi_{mv,dc}$	0.00	-0.05	-0.03	-0.16
$\pi_{mv,ri}$	0.48	0.52	0.46	0.58
$\pi_{mv,ch}$	0.52	0.53	0.58	0.58
$Ra_dD/L)_{dc}$	--	247,000	$7.6x10^6$	$2.2x10^8$
$Re_{d,dc}$	16,100	18,500	74,000	151,000
$Ra_dD/L)_{ri}$	7,600	19,800	333,000	270,000
$Re_{d,ri}$	16,600	19,000	77,000	163,000
$Ra_dD/L)_{ch}$	$3.3x10^{11}$	$3.2x10^{11}$	$1.3x10^{11}$	$4.5x10^{11}$
$Re_{d,ch}$	27,400	31,400	128,000	282,000

The pi groups show the inertial effect is relatively small, and the effect of the downcomer on the net buoyancy is relatively small. The air flow Reynolds number is high even during blowdown due to the assumed initial condition of 120°F shell temperature and 115°F riser air. The free/mixed/forced convection regime of the flow in the downcomer, riser, and chimney is determined from the Reynolds and Rayleigh (RaD/L) numbers as shown in Section 4.2.

At the time of the peak containment pressure, the shell temperature and evaporation rate are higher than during other time phases, so the buoyancy-induced volumetric air flow rate is

highest. The riser Reynolds number is proportional to the riser volumetric flow rate so is highest at the time of the peak containment pressure. The PCS air flow path time constant is the ratio of the air flow path volume to the volumetric flow rate so is lowest at the time of peak containment pressure.

10 EVALUATION OF SCALED TESTS

This section evaluates the effects of scale for the separate effects tests (SET) and the integral effects tests (IET) relative to AP600. The SET and some IET data are used to validate constitutive models for some of the dominant transport processes and phenomena in AP600. The IET are used to validate the dimensionless rate of pressure change equation, and pi groups for the LST and AP600 are compared.

The rather detailed breakdown of heat sinks presented in Section 7 is useful for clarifying the effect of the several distinct heat sinks. However, the rate of change equations show the same transient response results from considering a net source and a net sink. The scaled rate of change equations for, respectively, mass, energy, and pressure are:

$$\pi_{m,\tau}\frac{dm^*}{dt^*} = \pi_{m,brk}\dot{m}^*_{g,brk} + \sum_j \pi_{m,j}\dot{m}^*_{stm,j} \tag{190}$$

$$\pi_{e,\tau}\frac{d(mu)^*}{dt^*} = \pi_{e,brk}\dot{m}^*_{g,brk}\Delta h^*_{brk} - \sum_j\left(\pi_{e,fg,j}\dot{m}^*_{stm,j}\Delta h^*_{stm,j} + \pi_{e,if,j}\dot{m}^*_{stm,j}\Delta h^*_{if,j} + \pi_{e,q,j}h^*_{q,j}A^*_j\Delta T^*_{if,j}\right) \tag{191}$$

$$\pi_{p,\tau}\frac{Z^{T*}V^*}{\gamma^*_m}\frac{dP^*}{dt^*} = \pi_{p,g,brk,enth}\Delta h^*_{g,brk}\dot{m}^*_{g,brk} + \pi_{p,g,brk,work}\frac{\gamma^*Z^{T*}}{\gamma^*_m}\frac{P^*_{stm}}{\rho^*_{stm}}\dot{m}^*_{g,brk} + \pi_{p,f,work}\frac{\gamma^*Z^{T*}}{\gamma^*_m}\dot{m}^*_f P^* + \sum_j\left(\pi_{p,enth,j}\frac{\dot{m}^*_{stm,j}}{\dot{m}^*_{g,brk}}\Delta h^*_{stm,j} + \pi_{p,work,j}\frac{\dot{m}^*_{stm,j}}{\dot{m}^*_{g,brk}}\frac{\gamma^*Z^{T*}}{\gamma^*_m}\frac{P^*_{stm}}{\rho^*_{stm}} + \pi_{p,q,j}h^*_{q,j}A^*_j\Delta T^*_{if,j}\right) \tag{192}$$

The pi groups for the composite heat sink approach are defined by adding the values for heat sinks within the summation terms. It is useful to approach the simplification in two steps: the first produces a set of combined internal heat sink pi values and a set of combined shell pi values, while the second combines the internal heat sinks and shell into a single set of pi values. The results are presented in the following six tables for mass, energy, and pressure.

In addition to the composite pi groups, the rate of change terms for each of the scaled parameters, dm^*/dt^*, $d(mu)^*/dt^*$, and dP^*/dt^* are calculated from the above rate of change equations and included in the following tables.

Table 10-1 Containment and Heat Sink/Shell Mass Pi Group Values

Pi Group		LOCA				MSLB
		Blowdown	Refill	Peak Press	Long Term	
Containment	τ_o (sec)	31	980	913	5173	537
	$\pi_{m,\tau}$	1.31	1.27	1.30	1.22	1.27
	$\pi_{m,brk}$	1.00	0.00*	1.00*	1.00	1.00
	$\pi_{m,f}$	1.75	0.00	2.00	0.00	0.00
Internal Heat Sink	$\pi_{m,hs}$	0.01	-1.99	-0.90	-0.22	-0.64
Shell	$\pi_{m,sh}$	-0.02	-0.61	-0.47	-1.04	-0.37
	$\pi_{m,shx}$	--	--	-0.02	-0.89	--

* Refill was scaled with the same 200 lbm/sec flow rate used to normalize peak pressure.

Table 10-2 Containment and Net Heat Sink Mass Pi Group Values

Pi Group		LOCA				MSLB
		Blowdown	Refill	Peak Press	Long Term	
Containment	$\pi_{m,\tau}$	1.31	1.27	1.30	1.22	1.27
	$\pi_{m,brk}$	1.00	0.00*	1.00*	1.00	1.00
	$\pi_{m,f}$	1.75	0.00	2.00	0.00	0.00
Net Heat Sink	$\pi_{m,ns}$	-0.01	-2.60	-1.37	-1.26	-1.01
	$\pi_{m,esx}$	--	--	-0.02	-0.57	--
dm^*/dt^*		0.76	-2.05	-0.30	-0.68	-0.01

* Refill was scaled with the same 200 lbm/sec flow rate used to normalize peak pressure.

Table 10-3 Containment and Heat Sink/Shell Energy Pi Group Values

Pi Group		LOCA				MSLB
		Blowdown	Refill	Peak Press	Long Term	
Containment	$\pi_{e,t}$	0.55	0.58	0.56	0.63	0.58
	$\pi_{e,brk}$	1.00	0.00*	1.00*	1.00	1.00
	$\pi_{e,f,work}$	0.00	0.00	0.00	0.00	0.00
Internal Heat Sink	$\pi_{e,q,hs}$	0.00	-0.11	-0.04	0.00	-0.05
	$\pi_{e,fg,hs}$	0.00	-1.90	-0.85	-0.20	-0.63
	$\pi_{e,f,hs}$	0.00	-0.08	-0.07	-0.03	-0.01
Shell	$\pi_{e,q,es}$	0.00	-0.03	-0.02	-0.03	-0.02
	$\pi_{e,fg,es}$	-0.02	-0.59	-0.45	-0.94	-0.36
	$\pi_{e,f,es}$	0.00	-0.02	-0.02	-0.11	0.00
	$\pi_{e,q,esx}$	0.00	0.00	-0.00	-0.06	--
	$\pi_{e,q,ssx}$	--	--	-0.01	-0.08	--
	$\pi_{e,fg,esx}$	--	--	-0.02	-0.81	--

* Refill was scaled with the same energy normalization used for peak pressure.

Table 10-4 Containment and Net Heat Sink Energy Pi Group Values

Pi Group		LOCA				MSLB
		Blowdown	Refill	Peak Press	Long Term	
Containment	$\pi_{e,t}$	0.55	0.58	0.56	0.63	0.58
	$\pi_{e,brk}$	1.00	0.00*	1.00*	1.00	1.00
	$\pi_{e,f,work}$	0.00	0.00	0.00	0.00	0.00
Net Heat Sink	$\pi_{e,q,ns}$	0.00	-0.14	-0.06	-0.03	-0.07
	$\pi_{e,fg,ns}$	-0.02	-2.49	-1.30	-1.14	-0.99
	$\pi_{e,f,ns}$	0.00	-0.10	-0.09	-0.14	-0.01
	$\pi_{e,q,nsx}$	0.00	0.00	0.00	-0.06	--
	$\pi_{e,q,ssx}$	--	--	-0.01	-0.08	--
	$\pi_{e,fg,esx}$	--	--	-0.02	-0.81	--
d(mu)*/dt*		1.78	-4.71	-0.80	-0.49	-0.12

* Refill was scaled with the same energy normalization used for peak pressure.

Table 10-5 Containment and Heat Sink/Shell Pressure Pi Group Values

Pi Group		LOCA				MSLB
		Blowdown	Refill	Peak Press	Long Term	
Containment	$\pi_{p,t}$	0.76	0.76	0.77	0.76	0.76
	$\pi_{p,g,brk,work}$	1.00	0.00*	1.00*	1.00	1.00
	$\pi_{p,g,brk,enth}$	0.03	0.00	0.03	0.02	0.03
	$\pi_{p,f,work}$	0.00	0.00	0.00	0.00	0.00
Internal Heat Sinks	$\pi_{p,q,hs}$	-0.01	-0.33	-0.12	-0.02	-0.13
	$\pi_{p,enth,hs}$	0.00	0.00	0.00	0.00	0.00
	$\pi_{p,work,hs}$	0.01	-1.99	-0.90	-0.22	-0.64
Shell	$\pi_{p,q,sh}$	0.00	-0.10	-0.08	-0.10	-0.07
	$\pi_{p,enth,sh}$	0.00	0.00	0.00	0.00	0.00
	$\pi_{p,work,sh}$	-0.02	-0.61	-0.47	-1.04	-0.37

* Refill was scaled with the same pressure normalization used for peak pressure.

Table 10-6 Containment and Net Heat Sink Pressure Pi Group Values

Pi Group		LOCA				MSLB
		Blowdown	Refill	Peak Press	Long Term	
Containment	$\pi_{p,t}$	0.76	0.76	0.77	0.76	0.76
	$\pi_{p,g,brk,work}$	1.00	0.00*	1.00*	1.00	1.00
	$\pi_{p,g,brk,enth}$	0.03	0.00	0.03	0.02	0.03
	$\pi_{p,f,work}$	0.00	0.00	0.00	0.00	0.00
Net Heat Sinks	$\pi_{p,q,ns}$	-0.01	-0.43	-0.20	-0.12	-0.20
	$\pi_{p,enth,ns}$	0.00	0.00	0.00	0.00	0.00
	$\pi_{p,work,ns}$	-0.01	-2.60	-1.37	-1.26	-1.01
dP*/dt*		1.33	-3.99	-0.70	-0.47	-0.24

* Refill was scaled with the same pressure normalization used for peak pressure.

The scaled rate of change values show mass, energy and pressure increase during blowdown, then drop rapidly during refill. Since refill has no source, each is expected to drop. However, the scaled rates of change for the peak pressure phase are also negative, indicating a decrease in mass, energy, and pressure at the beginning of the peak pressure time phase. This is contrary to the pressure history presented in Figure 3-4 that shows pressure increasing at the beginning of the peak pressure time phase. The explanation is that the model that generated the "typical" pressure transient in Figure 3-4 included several conservative assumptions, including:

- The shell heat and mass transfer correlations are biased approximately 25 percent low
- The internal solid heat sinks are modeled using Uchida, which produces approximately 1/2 the energy transfer as McAdams free convection

A 50 percent reduction in the heat and mass transfer rate to the internal heat sinks and a 25 percent decrease in the shell heat and mass transfer rate is estimated to change dP^*/dt^* from -0.70 to +0.14, which is at least consistent with the expected sign of the pressure rate of change.

The value of dP^*/dt^* for the long-term time phase is also inconsistent with Figure 3-4 at the start of the long-term time phase. The same reasons for the inconsistency apply, and in addition, the pressure assumed for the start of the long-term time phase was 60 psia (approximately the containment design limit), which is even higher than the model predicted in Figure 3-4. The higher pressure produces higher energy transfer rates, resulting in an even higher rate of pressure decrease.

10.1 SEPARATE EFFECTS TESTS (SETs) AND CONSTITUTIVE RELATIONSHIP SCALING

Examination of the containment and net heat sink energy pi groups summarized in Table 10-4 shows the largest pi group values for the gas compliance ($\pi_{e,\tau}$), break source ($\pi_{e,brk}$), energy absorbed by the shell and heat sinks by condensation ($\pi_{e,fg,ns}$), and energy removed from the shell by evaporation ($\pi_{e,fg,nsx}$) are of order 1.0. The pi groups for displacement work ($\pi_{e,f,work}$), energy absorbed by the subcooled liquid ($\pi_{e,q,ssx}$), energy transferred to the inside surface by sensible heat transfer ($\pi_{e,q,ns}$), energy carried off the internal condensing surfaces by the liquid film ($\pi_{e,f,ns}$), and energy rejected from the shell by sensible heat transfer ($\pi_{e,q,nsx}$) are of order 0.1.

Examination of the containment and net heat sink pressure pi groups summarized in Table 10-6 shows the gas compliance ($\pi_{p,\tau}$), break work ($\pi_{p,g,brk,work}$), and condensation work ($\pi_{p,work,ns}$) are order 1.0 terms; internal sensible heat transfer ($\pi_{p,q,ns}$) is intermediate order; and

break enthalpy ($\pi_{p,g,brk,enth}$), break liquid displacement work ($\pi_{p,f,work}$), and condensation enthalpy ($\pi_{p,enth,ns}$) are order 0.1 or less.

Combining the results of the energy and pressure pi values shows the gas compliance, break source, condensation, and evaporation are the dominant order 1.0 terms. Internal sensible heat transfer is intermediate order, and external sensible heat transfer, liquid displacement, energy to the external subcooled film, energy carried by the condensed liquid, and enthalpy (of break and condensate) are order 0.1 or less terms.

From this the very important conclusions are drawn that condensation and evaporation mass transfer are the dominant transport processes for containment pressurization. Consequently, the constitutive relationships for condensation and evaporation mass transfer are examined in detail[9] and the results of the dimensionless correlations for AP600 are summarized in subsections 10.1.1 and 10.1.2. Since sensible heat transfer is of intermediate importance, its modeling is discussed in subsection 10.1.3. The constitutive relationships used in the scaling analysis for convective heat and mass transfer are compared to the test data and to the range of operation of the important dimensionless groups. The comparisons show the selected correlations represent the test data and the range of AP600 operation is adequately covered by the test data.

The scaling of additional phenomenological data to AP600 is discussed in the following subsections.

10.1.1 Condensation Mass Transfer

Condensation mass transfer was identified as a high importance phenomena in the PIRT, and as discussed in Section 10. The dimensionless relationship for free convection condensation mass transfer, represent . by the Sherwood number, was developed in subsection 4.3.1, Equation (16). The Sherwood number correlation is presented in Figure 10-1. Figure 10-1 shows the range of parameters covered by the LST envelopes the operating range of AP600 and shows the test data agree well with the free convection mass transfer correlation. The data and correlation are discussed in more detail in Reference 9.

10.1.2 Evaporation Mass Transfer

Evaporation mass transfer was identified in the PIRT as a high importance phenomena, and was verified by the discussion in Section 10 as a dominant phenomenon. The mass transfer correlation for forced convection evaporation mass transfer was developed in Section 4.3.1 and presented in Equation (18). The forced convection evaporation mass transfer, as represented by the Sherwood number correlation, is presented in Figure 10-2. The range of

Sherwood and Reynolds numbers for AP600 operation is shown in Figure 10-2 to be within the range covered by the LST and Gilliland and Sherwood test data. The figure also shows the data agree well with the forced convection mass transfer correlation. Note that although the Gilliland and Sherwood data range is shown on the figure, the actual data were not local, so are not included on the plot. The data and correlation are discussed in more detail in Reference 9.

10.1.3 Convection Heat Transfer

Heat transfer to surfaces inside containment was ranked medium in the PIRT. The scaling discussion in Section 10 shows heat transfer to be of intermediate magnitude: it accounts for approximately 10 percent as much energy and 10 to 20 percent as much dP/dt as condensation mass transfer. Heat transfer inside containment is the sum of radiation and free convection; the calculations show that radiation and free convection are approximately equal in magnitude. As a second order energy transfer phenomena, heat transfer inside containment is modeled using the conventional correlations for radiation and free convection presented in Sections 4.1 and 4.2. Although the SETs and IETs included these phenomena, they were always present with condensation mass transfer, which dominated the energy transfer and prevented measuring the second order phenomena.

It is significant that the condensation mass transfer correlation discussed in subsection 10.1.1 is derived from the heat and mass transfer analogy. Since mass transfer is well modeled by the free convection mass transfer correlation, by the heat and mass transfer analogy it can be argued that heat transfer is equally well modeled.

The PIRT ranked heat transfer from the shell to the riser as medium importance, and the scaling analysis presented in Section 10 showed it to be a second order phenomenon. Heat transfer from the shell to the riser in AP600 is modeled using the Colburn forced convection heat transfer correlation:

$$Nu = 0.023 Re_D^{0.8} Pr^{1/3} \quad \text{where} \quad Nu = \frac{hD_h}{k} \tag{193}$$

where the length parameter is the annulus hydraulic diameter, D_h. Incropera and DeWitt[35], Table 8.4, suggest the use of Colburn, Dittus-Boelter, and Seider-Tate correlations for internal flows.

a,b

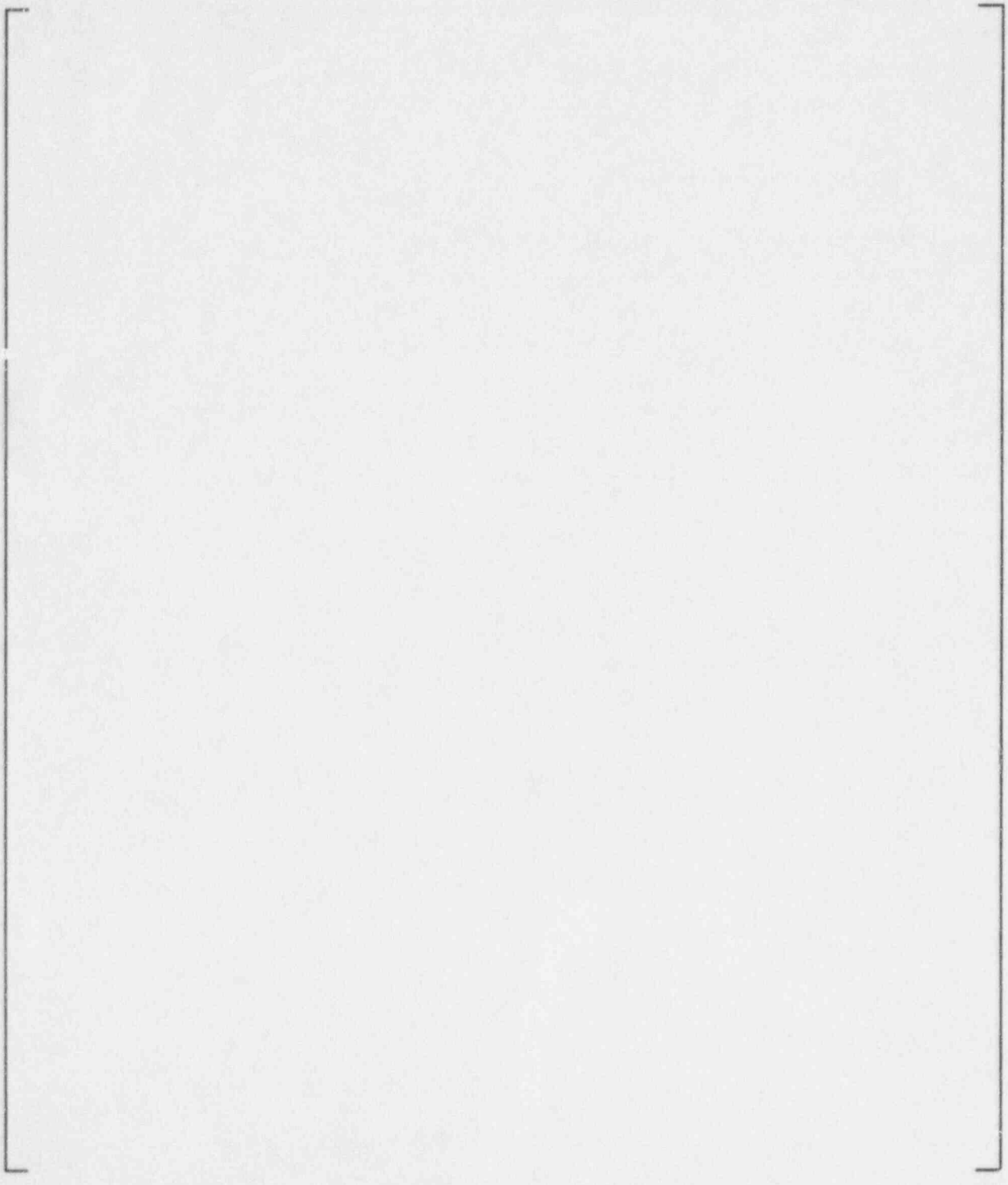

Figure 10-1 Free Convection Condensation Data from the Large-Scale Test Compared to the Correlation and the AP600 Operating Range

a,b

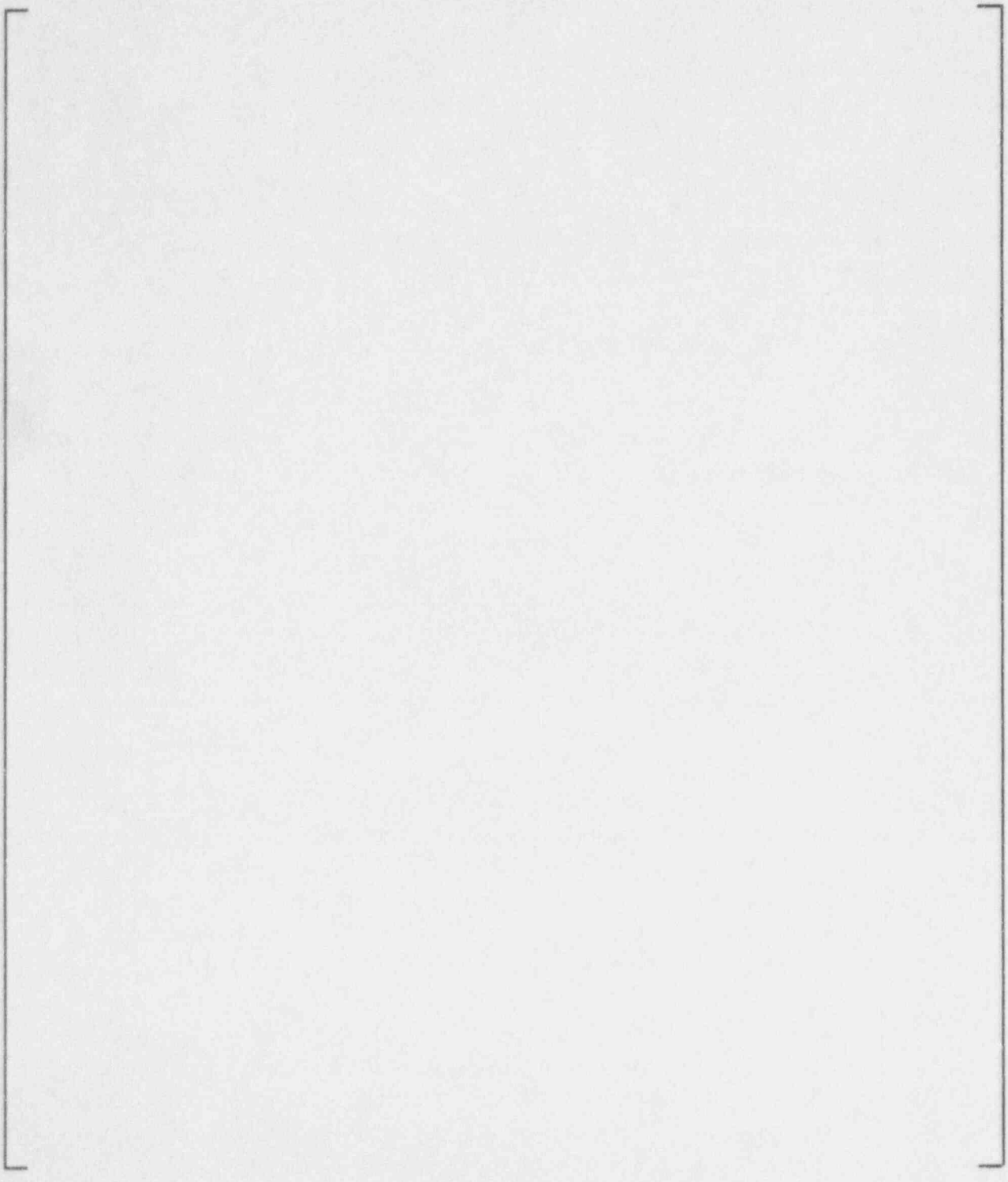

Figure 10-2 Forced Convection Evaporation Data from the STC Flat Plate Test Compared to the Correlation and the AP600 Range of Operation

- The Dittus-Boelter correlation differs from Colburn by a Prandtl number exponent of 0.4 instead of 1/3. For the predominantly air flows in the PCS Dittus-Boelter gives results that are 2 percent less than Colburn.

- The Seider-Tate correlation adds a multiplier of $(\mu/\mu_s)^{0.14}$ to the Colburn correlation. For the PCS with air and bulk-to-surface temperature differences less than 100°F, Seider-Tate also gives results 2 percent less than Colburn.

All of these correlations are recommended for Re > 10,000, L/D > 10, and .7 < Pr < 160. The corresponding AP600 parameters are 16,100 < Re < 163,000, Pr ≈ 0.72, and L/D ≈ 60 which satisfy the criteria for use of the Colburn correlation.

10.1.4 PCS Air Flow Path Flow Resistance

The natural circulation air flow rate in the PCS air flow path determines the riser Reynolds number, an important parameter in the evaporation mass transfer correlation. The PCS flow resistance is one of the dominant terms in the PCS momentum equation presented in Section 9. The form loss coefficient measurements from a geometrically scaled model of the AP600 PCS air flow path are presented and extrapolated to AP600.

The flow resistance in the PCS air flow path was measured in the 1/6 scale air flow test[34]. Although AP600 operates in natural circulation and the test was fan forced, the buoyant pressure, G_o and the forced pressure drop, ΔP are interchangeable in the pi groups. Consequently, a fan forced test produces a flow resistance that is equally valid for a buoyancy driven system.

The overall pressure loss coefficient for the system is a combination of form losses and friction losses. It is known from the test that the form and friction losses are approximately equal. Thus it is expected that the resistance should be a weak function of the Reynolds number, with an exponent on the Reynolds number approximately 1/2 the Reynolds number exponent for pure friction at the same Reynolds number. This can be demonstrated as follows.

Since form losses are known to be independent of Reynolds number at high Reynolds numbers ($K = C_1Re^0$), and since the frictional losses are known to have only a weak dependence on Reynolds number at high Reynolds numbers ($fL/d = C_2Re^n$, where n = -0.20), it is reasonable to expect the sum of the form and friction losses can also be approximated by a function of the form $K_{tot} = C_3Re^m$. An approximating function can be defined as the tangent to the approximated function at some Reynolds number, R_o. The values of C_3 and m in the approximating function can be determined as follows with the assumption:

1. The form, K, and friction losses, fL/d, are equal in magnitude at $Re = R_0$, so $C_1 = C_2 Re^n$,

and with the definition of the tangent:

2. The magnitudes of the approximated function, (K+fL/d), and the approximating function, K_{tot} are equal at $Re = R_0$, so $K_{tot} = K + fL/d$, and

3. The slope of the approximating function dK_{tot}/dRe is equal to the slope of the approximated function $d(K+fL/d)/dRe$, at $Re = R_0$.

From assumption (1): $C_2 = C_1/R_0^n$; from assumption (1) and definition (2): $C_3 = 2C_1/R_0^m$; and from definition (3): $nC_2R_0^{n-1} = mC_3R_0^{m-1}$. Substituting the first and second expressions into the third to eliminate C_2 and C_3 results in the equation $m = n/2$.

The root mean square roughness of the inorganic zinc coating on three Westinghouse Science & Technology Center (STC) tests ranged from 150 to 250 micro inches, and the roughness of the commercial steel baffle is estimated to be no rougher than the shell. Consequently, $\varepsilon/d_h = 0.00012$ in the riser where most of the friction occurs. At this relative roughness and the riser Reynolds number at the time of peak containment pressure, 163,000 from Table 9-1, the tangent to the $\varepsilon/d = 0.0001$ curve on the Moody friction factor chart has a slope of -0.20, hence the value used in the calculations. Although the Blassius friction factor correlation, with its exponent of -0.25, is a reasonable approximation for turbulent Reynolds numbers less than 100,000, it is not quite correct for the higher Reynolds numbers of the PCS. Thus, the loss coefficient is expected to be of the form $C\ Re^{-0.10}$.

The loss coefficient is defined by setting $\pi_{res} = 1$ and expressing the loss coefficient as the ratio of pressure drop to stagnation pressure:

$$\Sigma R_i = C Re_o^{-0.10} = \frac{\Delta P_o}{\dot{m}_o^2/(2\rho_v A_o^2)} \qquad (194)$$

[ ] a,b

(195)

10.1.5 Wind Effects

An aspect of the AP600 design is its sensitivity to external wind. The external conditions affect the performance of the PCS air flow path, due to high wind speeds and turbulence induced by upwind structures or terrain.

A series of tests were conducted in wind tunnels to characterize the effect on the AP600 PCS air flow of environmental wind speeds up to the AP600 design limit of 214 mph. The particular concern was the effect of upwind terrain and obstructions that could subject the PCS air flow path to pressure fluctuations that induce reversed flow in the riser. Such fluctuations have been evaluated relative to the assumed zero wind effect. The test evaluation (Ref. 5, Section 6) considered the effects of wind tunnel model scale and showed the wind-positive characteristic of AP600 more than offset the effect of fluctuations.

The recirculation of the chimney outflow (warmer and more humid than the environment) to the downcomer inlets was evaluated (Ref. 5, Section 6) and determined to have an insignificant effect.

10.1.6 Wetting Stability

Liquid film stability is an important parameter in the external evaporation calculation. This was identified in the PIRT and is included in the important phenomena listed in Section 2. The film stability is discussed in detail in Reference 5 and the results are summarized in the following.

Heated and unheated water distribution measurements were made on tests to support the modeling of water coverage on the external shell of AP600. The model and its application to AP600 is presented in Reference 5. The dimensionless groups appropriate for scaling water coverage are defined in the literature and those that are most significant for AP600 are the film Reynolds number, Marangoni number, and Bond number, defined respectively as:

$$Re = \frac{4\Gamma}{\mu} \qquad Ma = \frac{d\sigma}{dT}\frac{\dot{q}''\delta^2\rho c_p}{2k^2\mu} \qquad B = \frac{\rho g \delta^2}{\sigma} \tag{196}$$

The range of these groups for AP600 and two of the tests are presented in Table 10-7. The comparisons show the range of AP600 operation is adequately covered by the test data.

Table 10-7 Comparison of AP600 Operating Range to Tests for Liquid Film Stability (February 24, 1997)

	AP600	Large-Scale Test	Water Distribution Test
Film Reynolds Number:		[	] a,b
Upper Sidewall	2900		
Bottom of PCS surface	600		
Marangoni Number:			
Upper Sidewall	2600		
Bottom of PCS surface	720		
Bond Number:			
Upper Sidewall	0.009		
Bottom of PCS surface	0.005		

10.1.7 Liquid Film Model Validation

Heat transfer through the draining liquid film on the inside and outside surfaces of the shell and heat sinks was ranked low importance in the PIRT. The film conductance calculated with the scaling equations is 840 B/hr-ft^2-F. This makes the conductance approximately an order of magnitude greater than that of mass transfer, so film conductance scales low importance.

The Chun and Seban[36] correlation was selected to model the film heat transfer. The validity of the Chun and Seban correlation for evaporating turbulent and wavy laminar films on vertical surfaces was demonstrated in the original paper. Data from tests at the University of Wisconsin[37] are added to extend the validity of the Chun and Seban correlation to condensing wavy laminar flow and to surfaces which are inclined, as in the dome region of the AP600.

Five of the Wisconsin Tests were conducted without a noncondensible gas present. Without a noncondensible gas, the gas-to-liquid heat transfer coefficient is so high that the gas-to-liquid temperature drop is negligible compared to the temperature drop across the liquid film. Consequently, the temperature of the liquid film surface may be assumed equal to the gas temperature and the liquid film heat transfer coefficient is heat flux divided by the liquid film temperature drop. Since the heat flux, solid surface temperature, and gas temperature are measured, the liquid film heat transfer coefficient may be derived directly from the measurements. The Wisconsin tests thus provided a relatively direct measurement of the liquid film heat transfer coefficient for a range of surface inclinations from vertical to horizontal.

The Wisconsin and Chun and Seban data are compared to the Chun and Seban laminar and turbulent correlations in Figure 10-3. The correlation seems to predict nearly best-estimate values over the full Reynolds number range of data. The range of film Reynolds numbers on the outside of AP600 is also shown in the figure, and falls well within the range of the test data. Reynolds numbers on the inside of containment are less than outside due to film removal at the crane rail and stiffener ring, and the fact that the inside film flow rate starts at zero at the top of the dome and increases as the film flows down. The AP600 liquid film Prandtl number range is approximately $1.5 < Pr < 3.0$, whereas the range of the Chun and Seban data Prandtl numbers is $1.77 < Pr < 5.9$, which adequately covers the AP600 range. Comparison of the correlation to the test data show that the Chun and Seban correlation is a good representation of the data, so the Chun and Seban model is sufficiently accurate for this low importance phenomena. Uncertainties in the small fraction of the total conductance due to the liquid film does not significantly affect the containment pressure.

10.2 INTEGRAL EFFECTS TESTS (IETs) AND AP600 SCALING

This section presents a scaled comparison between the LST[10] (integral test) and the AP600 plant, and validates the scaling equations by comparison to the LST. The purpose of the comparison is to show the scaled LST captures the high ranked phenomena associated with the AP600 containment and therefore the data obtained from the test can be used for correlation and code validation.

The scaled comparison between the LST and AP600 focuses on the phenomena associated with the containment features that are unique to AP600, that is, the PCS. Phenomena associated with the PCS become significant during the refill phase of a DECLG LOCA, and remain dominant into the long-term phase of the transient. This is shown in Figure 10-4 which shows heat sink energy removal rates for AP600. Referring to the figure, the energy transfer from the gas to the shell becomes important during the refill time phase and is dominant by about 200 sec (i.e., during the peak pressure phase).

Phenomena associated with the blowdown and refill phase of a DECLG LOCA are not unique to AP600. Those phenomena exist in current pressurized water reactors (PWRs). These scaling comparisons focus on test validation to represent the peak pressure and long-term time phases, the time when the AP600 PCS performance validation requires unique test results.

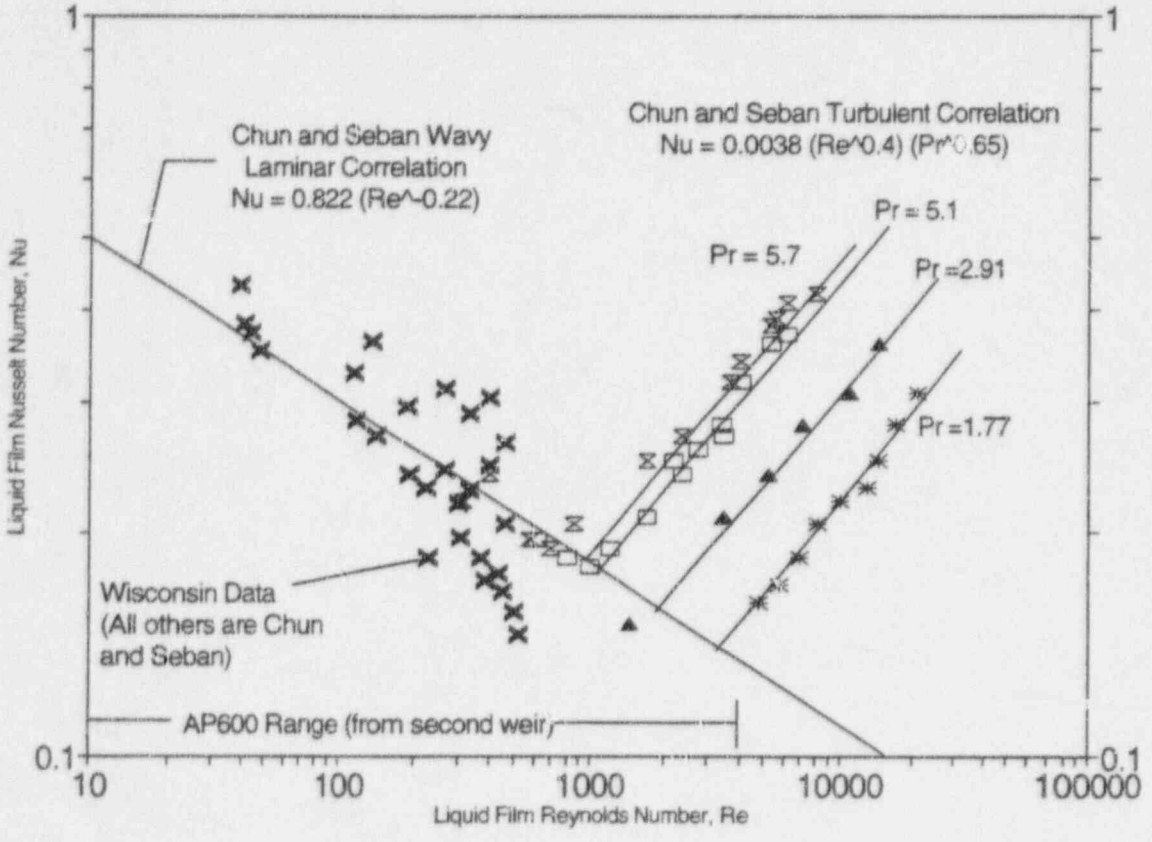

Figure 10-3 Chun and Seban Liquid Film Nusselt Number Correlation Comparison to Condensation and Evaporation Test Data

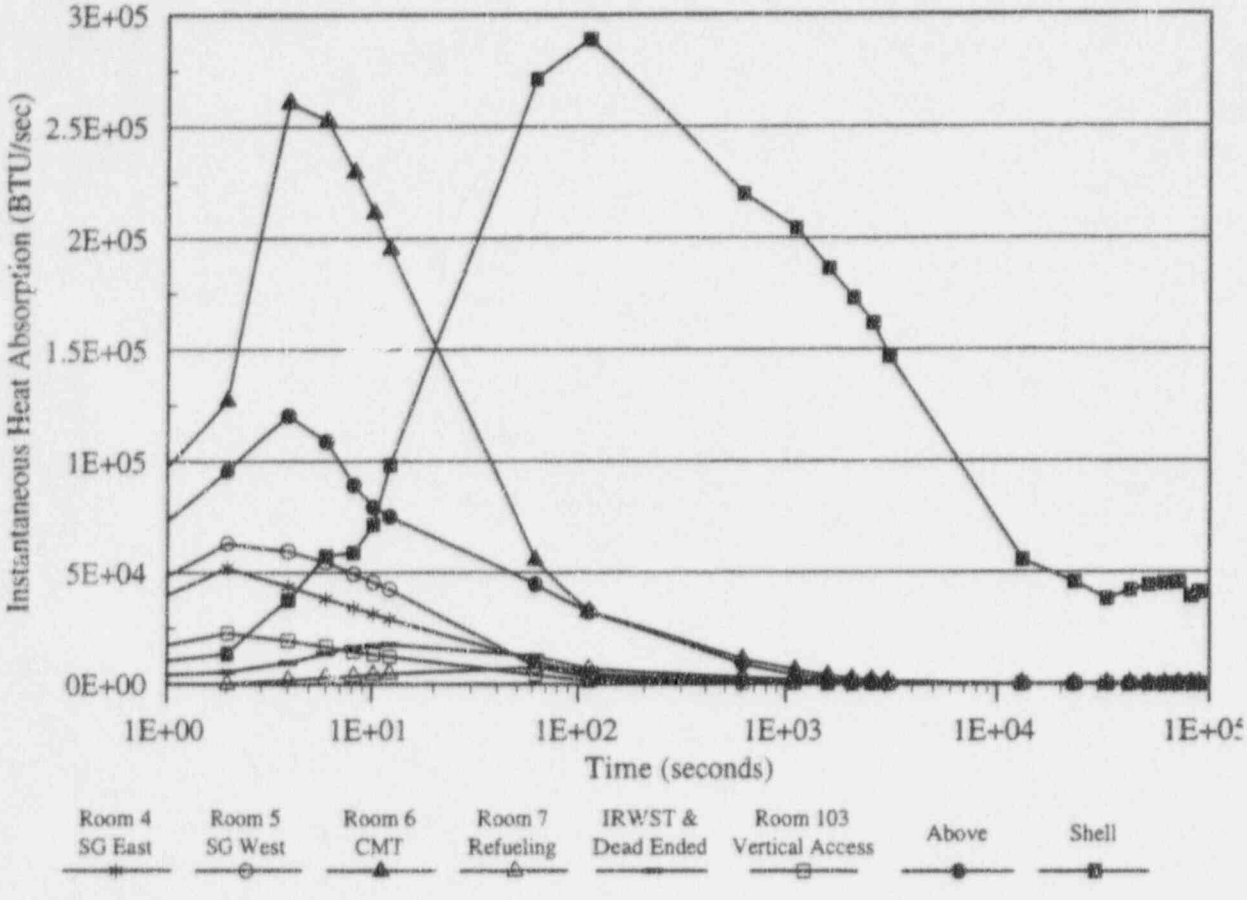

Figure 10-4 Heat Sink and Shell Inner Surface Energy Partitioning in AP600 from WGOTHIC

10.2.1 Governing Scaling Equations

The general form of the governing equations and their normalized form have been previously derived in Section 6.2 for the AP600 plant. The normalized form of the energy equation for the containment gas is:

$$\pi_{e,\tau}\frac{d(mu)^*}{dt^*} = \pi_{e,brk}\dot{m}^*_{g,brk}\Delta h^*_{brk} - \sum_j\left(\pi_{e,fg,j}\dot{m}^*_{stm,j}\Delta h^*_{stm,j} + \pi_{e,if,j}\dot{m}^*_{stm,j}\Delta h^*_{if,j} + \pi_{e,q,j}h^*_{q,j}A^*_j\Delta T^*_{if,j}\right) \quad (197)$$

For a defined initial condition, all the * terms have unit values so:

$$\pi_{e,\tau}\frac{d(mu)^*}{dt^*} = \pi_{e,brk} - \sum_j\left(\pi_{e,fg,j} + \pi_{e,if,j} + \pi_{e,q,j}\right) \quad (198)$$

Since the containment gas is in a quasi steady-state during the long-term portion of the DECLG LOCA transient, $d(mu)^*/dt^* = 0$. By normalization, $\pi_{e,brk} = 1$, so Equation (198) can be simplified to:

$$0 = 1 - \sum_j\left(\pi_{e,fg,j} + \pi_{e,if,j} + \pi_{e,q,j}\right) \quad (199)$$

The mass rate of change equation can be similarly reduced, for steady state, to:

$$0 = 1 - \sum_j \pi_{n,j} \quad (200)$$

These mass and energy equations are valid for both AP600 and the LST. A comparison of test measurements to predictions of Equations (199) and (200) will validate the rate of change equations for mass and energy. Since the RPC equation is the result of combining the mass and energy rate equations, with the equation of state, validation of the mass and energy equations also validate the RPC equation. These comparisons are provided in the following two subsections.

10.2.1.1 Validation of Steady-State Mass and Energy Transfer Equations

The constitutive equations for steady-state heat and mass transfer inside and outside the LST were coupled and solved using properties measured on the LST as boundary conditions. The containment total pressure, steam pressure, and bulk temperature defined the state inside the LST. The riser gas velocity, bulk riser gas temperature, wetted fraction, and the external water flow rate and temperature define the state outside the vessel. The heat and mass

transfer rates inside and outside were calculated for the subcooled, evaporating and dry regions.

The measured values for $\dot{m}_{g,brk,o}$ and $\dot{m}_{g,brk,o}\Delta h_{g,brk,o}$ were used to normalize the predicted values, respectively, for mass and for energy that define the pi values in Equations (199). The results are summarized in Table 10-8 for 21 LST cases. All tests are included that had measured steam concentrations and the steam source located under the steam generator model. The results show the average quasi steady-state mass and energy transfer rates are very close to zero, with a standard deviation of 0.13. Such agreement is considered good for such a simple model. These results verify that the mass and energy equations used in the scaling analysis accurately predict the transfer rates, thereby validating the equations. Verification of the transient pressure predictions are presented in subsection 10.2.1.2.

10.2.1.2 Transient Validation of dP/dt Equation

A comparison is made between the RPC equation and the startup of LST 221.1 (for which dP/dt data are available at t=0). At startup there is no heat or mass transfer to the internal heat sinks or shell since there is initially no temperature or steam partial pressure differences to drive transport processes. The initial pressurization is adiabatic compression which is described by the RPC equation without heat sinks or a break liquid source:

$$\frac{(1+Z^T)}{(\gamma-1)} V \frac{dP}{dt} = \dot{m}_{g,brk}\left(h_{g,brk} - h_{stm} + \frac{\gamma(1+Z^T)}{(\gamma-1)}\frac{P_{stm}}{\rho_{stm}}\right) \qquad (201)$$

Since the initial state of the LST is isothermal, full of air at 75°F and 14.2 psia, $Z^T = 0$ and $P_{stm}/\rho_{stm} = R_{stm}\,T$, the simplified RPC equation is:

$$\frac{dP}{dt} = \dot{m}_{g,brk}\left[(\gamma-1)(h_{g,brk} - h_{stm}) + \gamma R_{stm} T\right] \qquad (202)$$

The values for the parameters in Equation 201 are listed in Table 10-9. The values, when input to the dP/dt equation give dP/dt = 0.38 psi/sec, whereas the measured transient pressure shows dP/dt = 0.29. The difference is likely due to the fact that the hot steam jet, as it enters the LST, immediately encounters the diffuser and the simulated steam generator model, and in 2 to 3 sec encounters the dome. The "adiabatic" assumption is not strictly satisfied, and consequently, the source is not quite so effective. The agreement is considered to be sufficiently close to provide validation of the transient capability of the RPC equation. When combined with the steady-state validation in subsection 10.2.1.1, this transient comparison shows the RPC equation is valid.

Table 10-8 Energy Rate of Change Equation Comparison to Steady-State LST					
Large-Scale Test	Pressure psia	Temperature °F	$\dot{m}_{g,brk,o}\Delta h_{g,brk,o}$ BTU/sec	$1-\Sigma(\pi_{e,fg,j}+\pi_{e,if,j}+\pi_{e,q,j})$	$1-\Sigma\ \pi_{m,j}$
212.1A	23.77	334.3	427.2	-0.167	-0.197
212.1B	29.36	317.8	667.8	-0.058	-0.076
212.1C	36.93	317.7	963.4	-0.036	-0.948
213.1A	23.5	334.3	398.2	-0.185	-0.213
213.1B	28.83	327.0	642.1	0.039	0.022
213.1C	40.29	319.6	980.6	0.324	0.321
216.1A	32.44	326.5	706.7	-0.173	-0.206
216.1B	50.18	329.1	711.7	0.092	0.068
217.1A	42.37	314.9	1320.7	0.142	0.141
217.1B	50.86	319.7	1303.9	0.116	0.115
218.1A	42.44	314.0	1329.4	0.051	0.047
218.1B	50.05	317.6	1250.3	-0.001	-0.001
219.1A	34.97	343.0	145.9	0.082	0.088
219.1B	41.89	343.8	148.1	0.086	0.102
219.1C	23.24	340.2	143.8	-0.001	0.016
221.1A	19.36	339.6	185.7	-0.117	-0.132
221.1B	26.02	333.2	189.5	0.089	0.080
221.1C	63.36	336.7	186.0	0.098	0.106
222.1	99.66	331.1	719.1	-0.158	-0.167
224.1	45.51	298.9	309.5	-0.118	-0.064
224.2	55.54	310.4	712.2	-0.106	-0.087
			Average =	-0.00001	-0.004
			Standard Deviation	0.128	0.133

Table 10-9 Parameters for LST Transient 221.1		
Parameter	**Value**	
$\dot{m}_{g,brk}$	[	] a,b
V		
γ		
$h_{g,brk}$		
h_{stm}		
R_{stm}		
T		

10.2.2 Steady-State Validation of the LST

Pi groups for both the LST and AP600 were calculated using a solution to the equations developed for scaling AP600. The calculations correspond to conditions expected in AP600 at 4000 to 5000 sec. into the transient.

Inspection of the detailed energy pi groups in Table 7-8 shows that during all the phases of a DECLG LOCA, phenomena associated with the drops, pools, chimney, and baffle are not important and can therefore be neglected since the pi group numerical values are of order less than 0.1. The only pi groups of any significance are those associated with the solid internal heat sinks and the shell. However, the solid heat sinks become saturated prior to the time when the peak pressure occurs. Therefore, only the pi groups identified as containment or shell were calculated for the AP600 plant and the LST.

The results of the energy scaling comparison between the LST and AP600 are summarized in Table 10-10. The transient pi group $\pi_{e,t}$ is not applicable since d(mu)*/dt* = 0, that is, the containment atmosphere is in a quasi steady-state condition. Since the pi groups are normalized on break energy, $\pi_{e,brk}$ = 1.0. The table shows the dominant phenomena are condensation on the inside of the shell, $\pi_{e,fg,ns}$, and evaporation on the exterior of the shell, $\pi_{e,fg,esx}$. The values for $\pi_{e,fg,ns}$ and $\pi_{e,fg,esx}$ in Table 10-10 show the dominant phenomena (condensation and evaporation) compare favorably. The shell energy phenomena for the subcooled and dry shell, $\pi_{e,q,ns}$ and $\pi_{e,q,sex}$ are shown to be second order phenomena. Although the pi values for subcooled and dry energy do not compare quite as well as those for condensation and evaporation, the former are second order phenomena in both the plant and test, so do not invalidate the use of the test data.

Table 10-10 Energy Pi Group Comparison for AP600 and the LST

Pi Group	Predicted at 41.0 psia		LST Measured
	AP600	LST	
$\pi_{e,\tau}$	1.24	1.24	1.22
$\pi_{e,brk}$	1.00	1.00	1.00
$\pi_{e,f,wrk}$	0.00	0.00	0.00
$\pi_{e,q,ns}$	0.02	0.02	0.03
$\pi_{e,fg,ns}$	0.91	0.93	0.90
$\pi_{e,if,ns}$	0.08	0.06	0.08
$\pi_{e,q,nsx}$	0.13	0.18	0.09
$\pi_{e,q,ssx}$	0.13	0.15	0.09
$\pi_{e,fg,esx}$	0.67	0.62	0.74

* Not measured in LST

The scaling comparison permits the conclusion that the scaled LST represents the dominant internal and external phenomena in AP600 with sufficient accuracy that the tests can be used to validate computer codes during quasi-steady (long-term) operation.

11 DIFFERENCES AND DISTORTIONS BETWEEN THE TESTS AND AP600

Certain features of the design and operation of the LST prevent the use of the LST to represent specific duty cycle transients in AP600. However, the LST was not designed and operated as a conventional integral test to represent specific AP600 transients. Rather, the LST was designed and operated to characterize the internal velocity, temperature, and concentration fields, the shell temperature and heat flux distributions, and the air flow path and baffle temperatures under the effects of:

- Break source mass flow rate, elevation, direction, and velocity
- Noncondensibles
- External air flow rate
- External water flow rate and fractional coverage

The results of the LST were used to help resolve high and medium ranked phenomena in AP600:

- The measurements of the steady-state condensation mass transfer inside the shell are used to validate the phenomenological correlations for condensation mass transfer used in the scaling calculations and in the evaluation model.

- The external evaporating liquid film water coverage data are used to validate the liquid film stability models used in the evaluation model.

- Stratified temperature and air/steam concentration distributions measured inside the LST are used to address stratification for the evaluation model.

- Heat transfer measurements from tests with no external water provided data to validate dry heat transfer to the riser.

In addition, the steady-state and transient LST are used to validate predictions of the scaling equations and the computer code and selected segments of the LST are scaled to represent the dP/dt behavior of AP600.

Although the LST provided data to support the resolution of the most important phenomena in AP600, the test did not provide a transient simulation of specific duty cycle transient. It is therefore helpful to discuss differences between the test and AP600 that have been identified as concerns, and to consider whether those differences constitute *distortions* that must be considered when the LST data is applied to AP600. Features of the LST that differ from AP600, with the concern for each, are listed in Table 11-1. Each feature is discussed in the following text.

Table 11-1 LST Features That Differ from AP600

Feature	Potential Concern	Distortion
Break Source Superheat	Condensation correlation and pressurization are not prototypic because more thermal energy was input.	No
Diffuser used for break source	The actual break is a pipe break with a high velocity jet.	No
No Downcomer	Flow instability in the downcomer may limit the PCS air flow rate.	No
Riser Scaled 1/4	The riser heat and evaporation mass transfer are biased because the 3-inch riser width is 1/4 scale rather then 1/8 scale, as is the remainder of the test.	Yes
Fan Forced Riser Air Flow	The fan provides a forced air flow instead of the natural circulation air flow.	Yes
No Circulation Below Deck	The above/below-deck noncondensible distribution makes the test results inapplicable.	Yes
External Water Flow too High for some tests	The external water flow rate removes too much energy by its subcooled heat capacity.	No
External Water Coverage was too high	The water coverage was controlled artificially, rather than according to stability. The excess flow rate made the water more stable than it should have been.	No
External water flow was established before break	Cold water was not applied to a hot surface.	No
Internal heat sinks not prototypic	The internal concrete, steel, and pools are not represented.	Yes
External water flow oscillation	Oscillations in the external water flow rate affected the cooling and water coverage	Yes
Crane rails not the same	Internal liquid film is different	No
External water not applied by weirs	External water coverage and stability are different	Yes
Condensate drained out	There was no break pool to interact with the atmosphere in the test	No

Break Source Superheat – The phenomenological correlations used to predict pressurization due to heat transfer and mass transfer to the AP600 shell are independent. Sensible heat transfer is calculated using conventional radiation and free convection heat transfer relationships in which the heat transfer rate is proportional to the temperature difference between the bulk gas and the liquid (film or pool) surface. Condensation mass transfer is calculated from the free convection heat transfer correlation, modified according to the heat and mass transfer analogy, in which the mass transfer rate is proportional to the steam partial pressure difference between the bulk gas and the liquid surface.

To achieve a steady-state, the net condensation rate from the containment gas must equal the steam source mass flow rate, and the net sensible heat transfer from the containment gas must equal the break source energy addition by superheat. This phenomenological independence was used in the mass transfer correlation validation, using LST data, to derive mass transfer data for evaluating the internal condensation correlation.

Consequently, although the LST was forced with a steam source with more superheat than expected for an AP600 LOCA, the independence of the heat and mass transfer permits the use of the LST mass transfer data to validate the AP600 mass transfer correlation. The scaling analysis shows the pressure scaling pi group for superheat is approximately 0.03 in AP600 and 0.10 in the LST. Although the ratio is approximately 1/3, since the scaling analysis shows superheat is small relative to the source work term and superheat is accommodated by the pressurization model, the difference is not a distortion.

Diffuser used for break source – The diffuser located below the steam generator model produced a relatively low velocity steam source where the steam exited the steam generator compartment into the large above-deck volume. This approximated conditions for a LOCA where the high velocity break is expected to dissipate and entrain, and exit the steam generator compartment at a relatively low velocity. The steam source into the above-deck region is a buoyant plume rather than a forced jet in both AP600 and the LST conducted in this configuration. The buoyant plume-driven tests produced a state of free convection heat and mass transfer above-deck in the LST, as is expected in AP600 after blowdown. The diffuser does not constitute a distortion in applying the LST results to AP600 LOCA modeling.

No Downcomer – The scaling analysis shows both the energy and momentum contributions from the downcomer are sufficiently small that the downcomer does not have a significant effect on the PCS performance, and consequently, cannot induce instability. Consequently the downcomer is adequately treated by including it as a flow path with thermal and hydraulic interactions with the baffle and shield building. Based on scaling results this difference was not a distortion.

Riser Scaled 1/4 – The riser removed sufficient energy from the test to achieve the necessary internal and wall heat flux conditions to validate the condensation mass transfer model and the liquid film stability and wetted coverage model. However, the maximum Reynolds numbers achieved in the LST riser was approximately 1/2 that in AP600. AP600 is adequately covered by data from other tests. It was more important to achieve internal conditions for prototypic condensation mass transfer than to achieve scaled external conditions. Since other data are required to supplement the LST data for riser heat and mass transfer modeling, the difference is a distortion. Because of this distortion, other data were used to supplement the LST data for riser heat and mass transfer modeling.

Fan Forced Riser Air Flow – The lack of a downcomer, less height, and significantly different air flow loss coefficients prevent the use of the LST to simulate the natural circulation air flow in the AP600 PCS air flow path. This is a distortion. However, the natural circulation air flow in the PCS was never intended to be verified by the LST due to the inherent difficulty of simulating natural circulation phenomena with a 1/8 vertical scale model. Although a fan was generally used to increase the riser Reynolds number, tests without the fan provide data to validate natural circulation models. The AP600 natural circulation air flow rate is determined from an analysis that uses a conservative upper bound on the PCS form and friction loss coefficient. Natural circulation LST data are not used to represent AP600 natural circulation performance.

No Circulation Below-Deck – The lack of an opening between the simulated steam generator compartment and the other below-deck compartment that was open to the above-deck region prevented the above/below-deck circulation that would otherwise have developed. It also caused excessive air concentration below-deck and a steam-rich atmosphere above-deck. This is a distortion that prevents the use of the LST as a direct simulation of circulation during AP600 transients. However, the range of above-deck air/steam concentrations and mass transfer rates achieved in the tests was more than sufficient to span the range of AP600 operating parameters, so the condensation mass transfer data are not distorted.

External Water Flow too High – The scaled external cooling water flow rates in the LST spanned the range of AP600 operation. Since the flow rates were not too high, the effect is that of a ranged parameter, and is neither a difference nor a distortion. The magnitude of the external cooling water flow rates did not compromise the use of the data to validate the condensation mass transfer correlation or the external film stability and coverage model.

External water flow was established before break – LST 219.1 operated at a dry steady-state with a shell temperature of 240°F, then water was applied. Video tapes were taken of a test with cold water applied to a hot shell at 250°F to provide data for assessing the transient shell wetting influence. Tests that started wet cannot be used to validate AP600 performance during the initial wetting portion of the transient. This has no effect on the steady-state condensation mass transfer data validity.

Internal heat sinks not prototypic – The heat sinks in the LST have significantly less scaled heat capacity than those in AP600, so the transient test heat sink behavior cannot generally represent that of AP600. The lack of internal circulation prevents access of steam to the available below-deck heat sinks, further increasing the performance discrepancy between the test and AP600 internal heat sinks. This difference is a distortion. However, the steady-state condensation mass transfer and external film stability and coverage remain valid for application to AP600, and the stratification data are useful for understanding and bounding behavior in AP600.

External water flow oscillations – The external water supply rate oscillated. The flow rate dropped when the boiler feed-water level initiated refill of the feedwater tank, temporarily reducing the external water flow rate. The cycling rate was proportional to the steam flow rate, and was typically on the order of a few minutes. The reduced flow portion of the cycle was only a fraction of the total cycle, with the majority of the cycle operating at the set flow rate. The flow cycling may have affected the vessel cooling and water coverage.

The test data were used to validate the heat and mass transfer models used time and spatial-averaged temperatures, flow rates, and fluxes. The averaging time period was long enough to include several cycles, so fluctuations are averaged out. Furthermore, the transport models include data from other tests that did not experience such fluctuations. The fluctuations are not believed to have affected vessel cooling in a way that could compromise the use of the LST for pressure, temperature, or transport predictions.

The external water flow rate is a relatively steady flow, interrupted by a periodic drop and recovery. Since the water coverage grows with time, the state of coverage was continually recovering from a flow reduction. Consequently, the wetted coverage never reached its maximum possible at steady flow, although it may have been very close. The data were evaluated using both the maximum and minimum flow rates, so a conservative approach was used for the data evaluation. However, the flow oscillations are considered a distortion.

Crane rails are not the same – The LST lacked an internal structure to simulate the stiffener ring located part-way up the vessel side wall. The crane rail and stiffener ring strip the liquid film flowing down the inside surface. The film redevelops below these structures. The thinner film has a higher conductance than would an unstripped film, but both conductances are so high they have little effect on AP600 performance. Since the scaling analysis showed the film conductance was less than second order, relative to the other conductances, incomplete simulation in the test has an insignificant effect on the results so is not a distortion.

External water not applied by weirs – Both the weir slots on AP600 and the J-tubes used on the LST apply water to the surface as a free-falling stream that impacts the shell surface and spreads radially outward. The difference is not considered a distortion. Data from the Water

distribution tests, that include a prototypic weir design and application are included in the water coverage model database. These latter data insure that the effect of application is represented by the model.

Condensate drained out – The condensate was drained from the LST to prevent the vessel from filling during long test times, in contrast to the break pool that floods up from the reactor cavity and sump in AP600. Since the scaling analysis showed the pool has a less than second order effect on containment pressure, the difference is not a distortion. The pool is included in the evaluation model.

12 CONCLUSIONS

The scaling analysis satisfies the five stated needs for AP600 containment pressure scaling. The five needs and the conclusions are:

1. Quantatively evaluate the relative magnitude of transport processes and physical components as they affect energy, pressure, and momentum inside containment and in the PCS air flow path.

   - The pi groups for the detailed component and transport process scaling is presented in Table 8-5, Table 8-6, and Table 9-1. From these details the important components are identified as the break, atmosphere, steel heat sinks, concrete heat sinks, jacketed concrete heat sinks, evaporating shell, and dry shell. The dominant transport processes are condensation and evaporation mass transfer. In the PCS air flow path, the riser and chimney are important components, and the buoyancy and flow resistance dominate the air flow rate.

2. Use the quantitative evaluation to confirm the importance ranking of components and transport processes in the PIRT.

   - The conclusions of item 1 are consistent with the rankings in the PIRT.

3. Identify the important dimensionless groups and their range needed to scale test results to AP600.

   - The scaled comparisons between the SETs and AP600 show that the important phenomena are well modeled by the selected correlations, and the data cover the range important for AP600 operation.

4. Validate the use of the SETs and IETs to validate phenomenological models and the WGOTHIC computer code for use on AP600.

   - Predictions of the scaling equations were compared to steady-state and transient LSTs. The agreement is sufficiently close to provide validation of the RPC equation.

   - The scaling comparison permits the conclusion that the scaled LST represents the dominant internal and external phenomena in AP600 with sufficient accuracy that the tests can be used to validate phenomenological models and the AP600 evaluation model during quasi-steady (long-term) operation.

5. Identify test distortions that limit the applicability of the tests to AP600.

   - There are several distortions between the design and operation of the LST and AP600. Those distortions are recognized and various analytical and experimental results are used to account for those distortions. The distortions do not prevent the use of the LST results to validate the high-ranked phenomena of condensation mass transfer and liquid film stability and coverage. In addition, the temperature and concentration measurements from the LST provide data to understand and bound stratification in the AP600 evaluation model.

13 NOMENCLATURE

Symbol	Quantity
	Letters
A	Area
C	Steam concentration, and arbitrary constants or coefficients
c_p	Constant pressure specific heat
c_v	Constant volume specific heat
d	Hydraulic diameter, drop diameter
d_0	Hydraulic diameter of jet at source
D_v	Gas phase diffusion coefficient
f	Friction factor, or a fraction defined in text
g	Gravitational acceleration
h	Convective heat transfer coefficient
h_g	Gas phase enthalpy
h_f	Liquid phase enthalpy
h_{fg}	Liquid-to-gas enthalpy
H	Height, height of containment above steam source
k	Thermal conductivity
k_g	Gas phase mass transfer coefficient
L	Length
L^s	Specific length
m	Mass
$\dot{m}$	Mass flow rate
$\dot{m}''$	Mass flux
M	Molecular weight
n	number of drops, number of moles,
P	Pressure or partial pressure
P_{lm}	Log mean pressure difference = $(P_2-P_1)/\ln(P_2/P_1)$
$\dot{q}$	Heat flow rate
$\dot{q}''$	Heat flux
Q	Volumetric flow rate
R	Gas constant for specific species
$\bar{R}$	Universal gas constant
t	time
T	Temperature
u_f	Liquid phase internal energy
u_g	Gas phase internal energy
u_{fg}	Liquid-to-gas internal energy
U_0	Velocity of jet at source
v	Specific volume, or velocity as defined in text

V	Volume
z_{trans}	Elevation for jet transition from forced to buoyant
Z	Gas compressibility $Z = P/\rho RT$
Z^T	a normalized partial derivative of compressibility $Z^T = (T/Z)(\partial Z/\partial T)$

Subscripts

a	Ambient containment
air	Air
bf	Baffle
brk	Break source
buoy	Buoyancy pi group
c	Convection heat transfer, or conductance pi group
cc	Concrete
ch	Chimney
cond	Condensation
ct	Containment gas
cx	External convection
d	hydraulic diameter, or droplet value
dc	Downcomer
ds	Dry shell inside
dsx	Dry shell outside
e	Equivalent heat transfer coefficient, or energy pi group
enth	Enthalpy pi group
es	Evaporating shell inside
esx	External evaporating shell
evap	Evaporation
ex	External equivalent heat transfer coefficient
f	Fluid (or liquid) property value, fluid pi group
fg	Fluid-to-gas phase change property value, phase change pi group
g	Gas property value
hs	Heat sink, composite of all internal heat sinks (excluding shell)
if	Internal liquid film
in	Inertial pi group
in	Inlet value
j	Jet value
m	Mass transfer, mass transfer pi group
mv	Momentum pi group
mx	External mass transfer
ns	Net sink - combination of all internal shell and heat sinks
out	Outlet value
p	Pressure pi group

pi	Pool
q	Sensible heat transfer pi group
r	Radiation
res	Resistance pi group
rx	External radiation
ri	Riser
IR	IRWST water
ss	Subcooled shell inside
ssx	Subcooled shell external
sd	Shield building
sh	Containment shell
sat	Saturated
srf	Surface
st	Steel
stm	Steam
v	A volumetric parameter
work	Work pi group
x	A suffix that means external, or outside
xf	External liquid film
o	Initial or boundary value for nondimensionalizing
0	Value at jet nozzle exit
∞	A reference value defined in text

Superscripts

*	Dimensionless value
+	A ratio of LST to AP600 pi values

Greek Letters

α	Taylor's jet entrainment constant, value is 0.05
γ	Gas constant c_p/c_v
δ	Thickness, subscript on Biot number indicating variable thickness
Δ	Difference
ε	Product of emissivity and beam length in radiation heat transfer
ρ	Density
σ	Radiation constant
ν	Kinematic viscosity
τ	Time constant, pi group associated with scaled rate of change term

Dimensionless Groups

Bi	Biot number	=	hL/k (gas h and solid conductivity)
B	Bond number	=	$\rho g \delta^2/\sigma$
Fr	Froude number	=	$\rho_0^2 U_0^2/g(\rho_a-\rho_0)d_0$ or $\rho_0^2 U_0^2 d_0^2/g(\rho_a-\rho_0)H^3$
Ma	Marangoni number	=	$d\sigma/dT(\dot{q}''\delta^2\rho\, c_p)/\,(2\, k^2\mu)$
Gr	Grashof number	=	$g(\rho_a-\rho_0)H^3/\rho_a\nu^2$ or $g(\rho_a-\rho_0)d_0^3/\rho_a\nu^2$ or $g(\rho_2-\rho_1)L^3/\rho_2\nu^2$
Nu	Nusselt number	=	hL/k (gas h and gas conductivity)
Pr	Prandtl number	=	$\mu c_p/k$
Re	Reynolds number	=	$U_0 d_0/\nu$ or $4\Gamma/\mu$, or $\rho v d/\mu$
Sc	Schmidt number	=	$\mu/\rho D_v$
Sh	Sherwood number	=	$k_g RTP_{Bm}L/D_v P$
π	Dimensionless Scaling Group. Initial subscripts m, e, p, c are respectively mass, energy, pressure, and conductance.		

14 REFERENCES

*1. NSD-NRC-97-4968, *AP600 Passive Containment Cooling System Design Basis Analysis Reports*, January 31, 1997.

2. "AP600 Standard Safety Analysis Report," June 26, 1992, Westinghouse Electric Corporation.

3. M. J. Loftus, D. R. Spencer, J. Woodcock, "Accident Specification and Phenomena Evaluation for AP600 Passive Containment Cooling System," WCAP-14811, Westinghouse Electric Corporation.

4. D. L. Paulsen, et al., "WGOTHIC Code Description and Validation," WCAP-14382, May 1995, Westinghouse Electric Corporation.

*5. D. L. Paulsen, et al., "WGOTHIC Application to AP600," WCAP-14407, September 1996, Westinghouse Electric Corporation.

6. NTD-NRC-95-4563, "GOTHIC Version 4.0 Documentation," September 21, 1995, Westinghouse Electric Corporation.

7. NTD-NRC-95-4577, "Updated GOTHIC Documentation," October 12, 1995, Westinghouse Electric Corporation.

8. NTD-NRC-95-4595, "AP600 WGOTHIC Comparison to GOTHIC," November 13, 1995, Westinghouse Electric Corporation.

9. R. P. Ofstun, "Experimental Basis for the AP600 Containment Vessel Heat and Mass Transfer Correlations," WCAP-14326, March 31, 1995, Westinghouse Electric Corporation.

10. F. E. Peters, "Final Data Report for PCS Large-Scale Tests, Phase 2 and Phase 3," WCAP-14135, July 1994, Westinghouse Electric Corporation.

11. NTD-NRC-94-4138, *AP600 Design Certification Test Program Overview*, Rev. 6, May 17, 1994.

12. NUREG/CR-5809 EGG-2659, "An Integrated Structure and Scaling Methodology for Severe Accident Technical Issue Resolution," INEL, EG&G Idaho, Inc.

13. W. Wulff, "Scaling of Thermohydraulic Systems," BNL-62325, May 1995, Brookhaven National Laboratory.

14. Letter, N. J. Liparulo (Westinghouse) to R. W. Borchardt (US NRC), "AP600 Passive Containment Cooling System Preliminary Scaling Report," NTD-NRC-94-4246, July 28, 1994. (Superseded by WCAP-14845).

15. D. R. Spencer, "Scaling Analysis for AP600 Passive Containment Cooling System," WCAP-14190, October 1994, Westinghouse Electric Corporation. (Superseded by WCAP-14845).

16. Letter, B. A. McIntyre (Westinghouse) to T. R. Quay (US NRC), NSD-NRC-96-4762, July 1, 1996, D. R. Spencer, "Scaling Analysis for AP600 Containment Pressure During Design Basis Accidents," (Superseded by WCAP-14845).

17. F. E. Peters, "AP600 1/8th Large-Scale Passive Containment Cooling System Heat Transfer Test Baseline Data Report," December 1992, Westinghouse Electric Corporation.

18. Letter, N. J. Liparulo (Westinghouse) to R. W. Borchardt (US NRC), "Facility As-Built' Drawings for AP600 PCS Large (1/8th) Scale Test Facility," ET-NRC-93-3983, October 6, 1993, Westinghouse Electric Corporation.

19. F. E. Peters, "Thermal Conductivity Tests," DCP/WMS0574, January 16, 1995: Transmittal of TRL 1455, R. E. Taylor, H. Groot, J. Ferrier, "Thermophysical Properties of ASME SA516 GR70 Steel – A Report to Westinghouse Electric Corporation," December 1994, Purdue University, West Lafayette, Indiana.

20. B. Metais and E. R. G. Eckert, *Journal of Heat Transfer*, 86:295 (1964).

*21. Letter, N. J. Liparulo (Westinghouse) to R. W. Borchardt (US NRC), "Supporting Information for the Use of Forced Convection in the AP600 PCS Annulus," NTD-NRC-95-4397, February 16, 1995.

22. F. Kreith, *Principles of Heat Transfer*, 1965, International Textbook Company.

23. S. W. Churchill, "Combined Free and Forced Convection in Channels," Section 2.5.10 in E. U. Schlunder, *Heat Exchanger Design Handbook*, Hemisphere, 1983.

24. E. R. G. Eckert and R. M. Drake, Jr., *Analysis of Heat and Mass Transfer*, 1972, McGraw-Hill.

25. C. R. Wilke, *J. Chem. Phys.*, 18, 517-519 (1950).

26. R. B. Bird, W. E. Stewart, and E. N. Lightfoot, *Transport Phenomena*, 1960, John Wiley & Sons.

*27. Letter, N. J. Liparulo (Westinghouse) to R. W. Borchardt (US NRC), AP600 Passive Containment Cooling System Letter Reports: "Liquid Film Model Validation," by D. R. Spencer, NTD-NRC-94-4100.

28. G. J. Van Wylen and R. E. Sonntag, *Fundamentals of Classical Thermodynamics*, 1965, John Wiley & Sons, p334.

29. E. Hihara and P. F. Peterson, "Mixing in Thermally Stratified Fluid Volumes by Buoyant Jets," ASME/JSME Thermal Engineering Conference: Volume 1, ASME 1995.

30. P. F. Peterson, "Scaling and Analysis of Mixing in Large Stratified Volumes," *International Journal of Heat and Mass Transfer*, Vol. 37, Supplement 1, pp 97-106, 1994.

31. P. F. Peterson, V. E. Schrock, and R. Grief, "Scaling for Integral Simulation of Mixing in Large, Stratified Volumes," Sixth International Topical Meeting on Nuclear Thermal Hydraulics, October 5-8, 1993, Grenoble, France.

32. W. D. Baines and J. S. Turner, "Turbulent Buoyant Convection from a Source in a Confined Region," *Journal of Fluid Mechanics*, Vol. 37, Part 1, pp 51-58, (1969).

33. W. Wulff, "Integral Methods for Simulating Transient Conduction in Nuclear Reactor Components," *Nuclear Engineering and Design* 151 (1994) 113-129.

34. W. A. Stewart and A. T. Pieczynski, "Tests of Air Flow Path for Cooling the AP600 Reactor Containment," WCAP-13328, 1992, Westinghouse Electric Company.

35. F. P. Incropera and D. P. DeWitt, *Fundamentals of Heat and Mass Transfer*, Second Edition, John Wiley & Sons.

36. K. R. Chun and R. A. Seban, "Heat Transfer to Evaporating Liquid Films," *Journal of Heat Transfer*, November 1971.

37. WCAP-13307, "Condensation in the Presence of a Noncondensable Gas-Experimental Investigation," Westinghouse Electric Corporation.

* One or more sections of these reports will be revised as a result of outstanding NRC open items.